Disaster Management

Editors
N C Mahanti
S K Samal
P Datta
N K Nag

Narosa

Disaster Management

Alpha Science

Disaster Management

Editors
N C Mahanti
S K Samal
P Datta
N K Nag

Narosa Publishing House
New Delhi Chennai Mumbai Kolkata

Editors
N C Mahanti
S K Samal
P Datta
N K Nag
Department of Applied Mathematics
Birla Institute of Technology, Mesra
Ranchi, India

NAROSA PUBLISHING HOUSE PVT. LTD.

22 Daryaganj, Delhi Medical Association Road, New Delhi 110 002
35-36 Greams Road, Thousand Lights, Chennai 600 006
306 Shiv Centre, D.B.C. Sector 17, K.U. Bazar P.O., Navi Mumbai 400 703
2F-2G Shivam Chambers, 53 Syed Amir Ali Avenue, Kolkata 700 019

www.narosa.com

Printed from the camera-ready copy provided by the Editors.

ISBN 81-7319-727-X
E-ISBN 978-81-8487-296-5
Published by N.K. Mehra for Narosa Publishing House Pvt. Ltd.,
22 Daryaganj, Delhi Medical Association Road, New Delhi 110 002
and printed at Rajkamal Electric Press, New Delhi 110 033, India

FOREWORD

India, due to its spatial location, suffers often from disasters arising out of natural calamities like flood, draught, earthquake, cyclone and tsunami. The tsunami which struck Southern Indian coast on December 26, 2004 created havoc and enormous number of life and property was lost and thousands of people became homeless and jobless. As prediction of these events often fails, it is the management of disasters, which helps the affected people in terms of evacuation and rehabilitation. Keeping these in mind, the Department of Applied Mathematics of the Institute organised a National Seminar on Disaster Management as a part of Golden Jubliee Celebration of the Institute.

I am pleased to note that the Department is bringing out the reviewed proceedings of the seminar in a very short time. Several eminent speakers from SAC, Ahmadabad; CAS, IIT Delhi; Andhra University, Waltair; IITM, Pune; IMD, Calcutta; Jadavpur University, Calcutta delivered lectures and took part in the deliberations for proper management of disaster. I am sure that this book will be useful to the Scientists, Engineers, Government agencies and NGOs dealing with different aspects of disaster management. I am thankful to the reviewers, members of editorial board, organiser of the seminar, learned speakers and funding agencies like CSIR, Indian Overseas Bank and Punjab National Bank for their support in bringing out the proceedings in book form.

S K Mukherjee
Vice Chancellor
Chairman of Organising Committee

Alpha Science

PREFACE

The word disaster is now well known to every Indian after the occurrence of tsunami on 26th December 2004. Due to its devesting effect, many people died and equal number of people lost their homes and jobs when it struck coastal areas of Tamil Nadu, Andhra Pradesh and Kerala to some extent. Disasters are of two types: (i) man made and (ii) natural. Man made disasters can be prevented but not the natural one. Therefore, important thing for us is to manage disaster for proper rehabilitation of the affected people. With this in mind, the national seminar on disaster management was organised as a part of Golden Jubliee Celebration of the institute to create a common platform wherein experts would interact with each other for different issues and policies relating to the disaster management.

The book based on this seminar contains two different kinds of papers: (i) the papers directly related to the disaster including recently occurred tsunami and (ii) the papers dealing with sources of disasters. This must be an important document for the agencies dealing with the management and its control.

We express our sincere thanks to Dr. H.C. Pande, Vice Chancellor Emeritus and Dr. S.K. Mukherjee, Vice Chancellor, Birla Institute of Technology, for help and guidance to organise the seminar. We are also thankful to the funding agencies like CSIR, New Delhi, Indian Overseas Bank and Punjab National Bank, Ranchi branch for support to organise the event. We are also grateful to Narosa Publishing House, New Delhi for publishing the proceedings in a very short time. We also thank Sri R. Chattaraj and Sri Pramod Kumar for helping us in editing the manuscript. We further acknowledge advice and help of Prof. S.K. Dube, Director, IIT Kharagpur; Prof. U.C. Mohanty and Prof. S.K. Dash, Centre for Atmospheric Sciences, IIT Delhi; Dr. D.R. Sikka and Dr. P. Sanjeeva Rao of DST New Delhi and Dr. G.B. Panth, Director, IITM Pune.

N C Mahanti
Chief Editor

Alpha Science

CONTENTS

Disaster Management
Editors: N.C. Mahanti et al.

Simulation of a Recent Nor'Wester Over Kolkata Using a Mesoscale Model and Verification by Doppler Radar

P. Mukhopadhyay[1] and H.A.K. Singh

[1]Indian Institute of Tropical Meteorology, Pune-411 008, India
India Meteorological Department, Kolkata, India

Abstract

On 22 May 2003 Kolkata city experienced very severe Nor'wester. The storm was reported to strike the city at 1800 hours (local time) and cause heavy rain along with huge damages. 71 mm of rain was reported to occur in just 90 minutes. An attempt is made to simulate this severe Nor'wester using Regional Atmospheric Modelling System (RAMS) and further the simulation is verified with the Doppler radar observation. The analyses of upper air observation of 22 may 2003 over Kolkata station suggest that the atmosphere was unstable even at the 0000 UTC and the extent of instability increases further at 1200 UTC. In one of the experiment (EXP-1), six hourly NCEP/NCAR reanalyses data is used to initialize the model at 0000 UTC of 22 may 2003. The model is initially run in FDDA (Four Dimensional Data Assimilation) nudging mode till 0600 UTC and integrated for 12 hours till 1800 UTC in forecasting mode. The model is run with two nested domain (two way interactive) of horizontal resolution 16 and 4 km respectively. EXP-1 could not simulate the storm with reasonable accuracy. The main reason appears to be the inability of the coarse (2.5 x 2.5 deg) initial analyses to resolve the prevailing instability over the region. In another experiment (EXP-2), the upper air data from three stations, Ranchi, Patna and Kolkata are blended with NCEP/NCAR reanalyses to prepare mesoscale analyses of the region which better represents the prevailing instability of the region. The model is run in the similar fashion as that of EXP-1. Comparison of the results of the two experiments and with the Doppler radar observation, clearly reveal that EXP-2 has significantly better simulated the formation, maturity and dissipation of the storm. The time, location and movement also are better simulated by EXP-2. However the amount of rainfall in 12 hour forecast appears to be largely underestimated which could be due to the very coarse resolution of the initial analyses. The experiments conclusively show that the mesoscale forecast of the Nor'wester has been significantly improved by assimilating data over the region.

Introduction

The thunderstorms of the Gangetic West Bengal (Fig. 1) region appear frequently during the pre-monsoon (March, April and May) summer months. These storms cause havoc every year over the different districts of West Bengal (Fig. 1) including the city of Kolkata. The fury of these storms causes damage to aviation, rail, traffic, power supply, agriculture, mango groves along with the loss of precious lives. Nor'westers generally originate over the Bihar and Jharkhand regions (blue dots in Fig. 2) and strike the State of West Bengal from the north-west and hence are called Nor'westers (Desai, 1950). Desai (1950) mentioned that the formation of Nor'westers is attributed to the lower level warm, moist southerly flow from Bay of Bengal and upper level dry, cool westerly or north-westerly flow giving rise to an atmosphere with high latent instability. The 22 May 2003 Nor'wester was the last of 2003 pre-monsoon season. Due to the small spatio-temporal scale, dynamic forecast of Nor'westers remained a challenge to meteorologists. As such here an attempt is made to make a real data simulation of the event using RAMS. The model simulation is objectively verified with the Doppler radar and Meteosat imageries.

Data and Methodology

For the present study, the six hourly NCEP/NCAR reanalyses data of 22 May 2003 at 17 pressure levels and of horizontal resolution of 2.5° x 2.5° (Lat-Lon) is used. In EXP-1, the model is initialized with the NCEP analysis at 00 UTC of 22 May and further run in Four Dimensional Data Assimilation (FDDA) nudging mode till 06 UTC and thereafter the model is run in forecast mode for 12 hours ending at 18 UTC of 22 May. In another experiment (EXP-2) the upper air data from Ranchi, Patna and Kolkata (Fig. 3) are merged

with the 00 UTC NCEP analysis to prepare an enhanced analysis. Subsequently the model is initialized with the 00 UTC enhanced analysis and run in similar fashion as in EXP-1. The model forecast produced at every hour for a period of 12 hour is compared with hourly satellite imageries and Doppler radar hourly observations.

Model configuration

The simulations are performed using the compressible, nonhydrostatic modelling system RAMS version 4.30. Details about RAMS can be found in Pielke et al. (1992) and Cotton et al. (2003). For the present study the model is used with two nested domains of horizontal resolutions16 and 4 km (Fig. 3) with 36 vertically stretched terrain following levels. The levels are stretched at a ratio of 1.1:100;2000 implying the first level will have a thickness of 100 m, the next level will be of thickness 110 m and so on till the level reaches the thickness of 2000 m. When thickness will be 2000 m, it will remain fixed for rest of the levels. Modified Kuo cumulus parameterization (Tremback et al. 1990) is used for large scale convection. Explicit cloud microphysics by Walko et al. (1995) is used with prognostic equations for mixing ratios of rain, pristine ice, snow, aggregates, graupel and hail. A two-stream radiation scheme developed by Harrington (1997) and Harrington et al. (1999) is used. It allows interaction of three solar and five infrared bands with model gas constituents and cloud hydrometeors (Cotton et al., 2002). In RAMS, gridded data are used to provide initial conditions, lateral and top boundary conditions throughout the simulation using nudging technique (Davies, 1983). Klemp and Wilhelmson (1978a, 1978b) radiative boundary condition is applied at the lateral boundary. The land-surface model known as Land Ecosystem-Atmosphere Feedback model (LEAF-2) developed by Walko et al. (2000) is used for the present study. LEAF-2 is a prognostic model for the temperature and water content of soil, snow cover, vegetation and canopy air. It includes turbulent and radiative exchanges between these components and with the atmosphere. Eddy diffusion is parameterized using Smagorinsky (1963) deformation-K scheme with modifications for the influence of Brunt-Vaisala frequency by Hill (1974) and that for Richardson number by Lilly (1962). The model is run with Silhouette averaged USGS 30 arc sec topography data.

Results and Discussions

Figure 3 shows the surface chart plot of IMD at 03 UTC of 22 May 2003. According to IMD report a shallow trough was passing from Bihar to Tamilnadu through Jharkhand, Orissa and coastal Andhra Pradesh (A. P.) on 21 May and the same was reported to be passing from east Uttar Pradesh (U. P.) to coastal A. P. through Jharkhand and Orissa on 22 May. The weather report of 22 May 2003 suggests that the eastern part and some part of east coast of India were under the influence of a shallow trough. The low pressure area (denoted as L in Fig. 4) over Orissa and the associated wind field and isobars do suggest existence of a trough. The nor'wester was reported to have struck the city of Kolkata at 1800 hours (local time) and caused heavy rain and damages. 71 mm of rainfall was reported to have occurred in just 90 minutes due to this storm. To estimate the extent of instability over Kolkata, the thermodynamic parameters such as CAPE, CINE, TT index, K index, Shawalter index, Humidity index (HI), LCL and LFC for 0000 and 1200 UTC are computed. The values are shown in Table 1.

Table 1: Thermodynamic parameters based on 0000 and 1200 UTC sounding of 22 May 2003 over Kolkata station

Parameters	0000 UTC	1200 UTC
CAPE	1952.00 Jkg^{-1}	6540.00 Jkg^{-1}
CINE	-166.5 Jkg^{-1}	-21.5 Jkg^{-1}
TT	49.7° C	55.6° C
K	36.0° C	44.5° C
Showalter index	-1.50	-7.85
HI	33.5	18.3
LFC Pressure	722hPa	890 hPa
LCL Pressure	948 hPa	934 hPa

It may be noted from the values of thermodynamic indices of Table 1 that the atmosphere was having significant instability even at the early hours (0000 UTC) of 22 May 2003. At 1200 UTC the increase of CAPE, TT, K and decrease of Showalter index and HI further indicates that the atmosphere became more unstable. This is also reflected by the LFC value which is found to have come down from 722 to 890 hPa. The parameters at 1200 UTC further suggests that the atmosphere did not start releasing the available potential energy to kinetic energy, in other words it can be said that at 1200 UTC the storm was about to start over Kolkata.

The comparison of relative humidity (RH) analysis at 850 hPa without upper air and with upper air data at 0000 UTC of 22 May 2003 are shown in Fig. 5(a) and 5(b) respectively. It can be seen from Fig. 5(a) that the isolines of analysed RH is ranging from 30% to 80% and most of the 16 km grid domain is covered by very low RH value (30~60%). This lower value of RH may cause less conditional instability which is not conducive for storm initiation. Fig. 5(b) on the contrary shows higher values of RH. Particularly the north-west corner of the domain shows significant increase of the level of RH (80~90%) as compared to the other Fig. Thus it appears that assimilation of upper air data may have improved the level of RH over the coarse domain. Figure 6a shows the contour of HI estimated from the 00 UTC NCEP analysis and 6b shows the same estimated from the enhanced NCEP analysis. These two figures clearly bring out the improvement of the initial analysis that has been achieved by incorporating the upper air data of three stations. Figures 7 (a) and (b) show the streamline analyses at 850 hPa without and with upper air data respectively. A cyclonic circulation is found to be located on the extreme north-west corner of the coarse domain (Fig. 7a). Figure 7b also shows the circulation but it is found to be centered south of the location of circulation seen in Fig. 7a. The cyclonic circulation (Fig. 7b) is seen to generate wind flow from the Bay of Bengal to the Gangetic plains. The increased RH distribution over Gangetic plains could be attributed to this wind flow. The model after being initialized with these analyses are run in nudging mode for initial 6 hours and followed by run in forecast mode for 12 hours.

The hourly forecast of wind barb at 850 hPa as obtained from the 16 km grid domain by EXP-1 is shown in Fig 8. At the 6 hour forecast (Fig. 8), a cyclonic circulation is found to develop east of 88° E and south of 24° N. In the subsequent forecast hours (7 - 12) the center of circulation is found to have moved southward to the Bay. Due to this circulation, wind speed over Kolkata and surrounding has increased from 5 knot to 10-15 knot at six hour forecast. Northesterly wind is found to increase further in the following forecast hours (7-12). The circulation is found to move southward to the bay by 10 hour forecast (1600 UTC). However the Doppler radar estimated horizontal wind field suggests a cyclonic circulation at 11 UTC (Fig. 10) with wind barb of 5 Kt in and around Kolkata. Fig. 9 shows the hourly forecast of 850 hPa wind barb in the coarse domain as obtained by EXP-2 and here the cyclonic circulation is formed at 7 hour forecast (13 UTC) and persisted for following 5 hour. Comparing these three figures (Figs. 8, 9 and 10), it can be said that the EXP-2 has simulated the time and location of the circulation better compared to the EXP-1 and with respect to Doppler radar observation. The accuracy of model simulation is further investigated by comparing the total cloud condensate (gm kg^{-1}) at 850 hPa level by EXP-1 and 2. The hourly forecasts of 850 hPa total cloud condensate in 16 km domain as obtained by EXP-1 and EXP-2 are shown in Figs. 11 and 12 respectively and compared with the cloud liquid water estimate of Doppler radar (Fig. 13).

Fig1.: State of West Bengal and its different districts

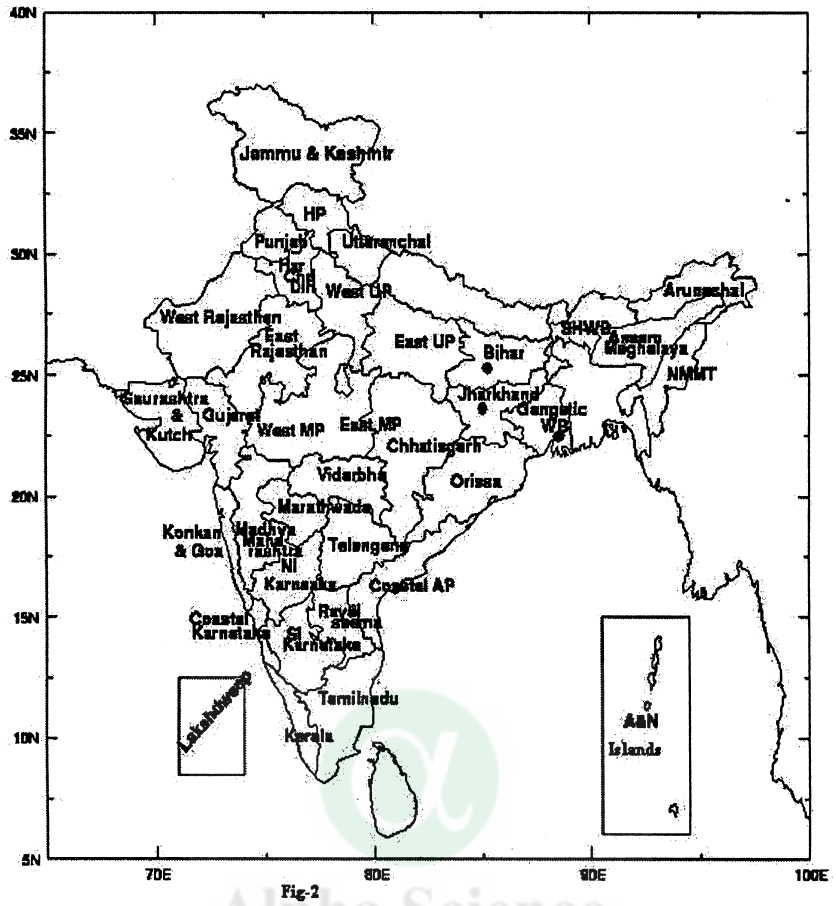

Fig. 2: Meteorological subdivisions of India

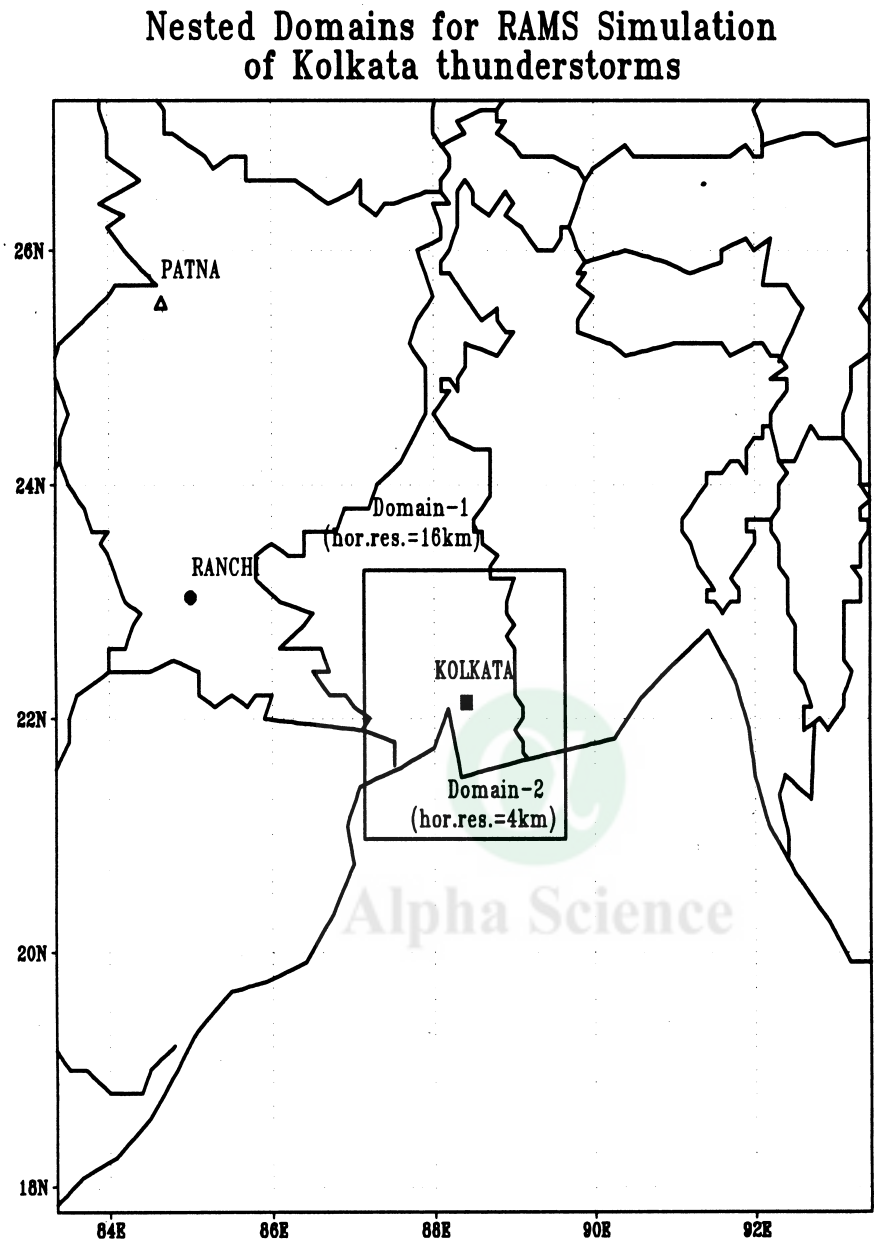

Fig. 3: Two nested domains and the location of three upper air stations

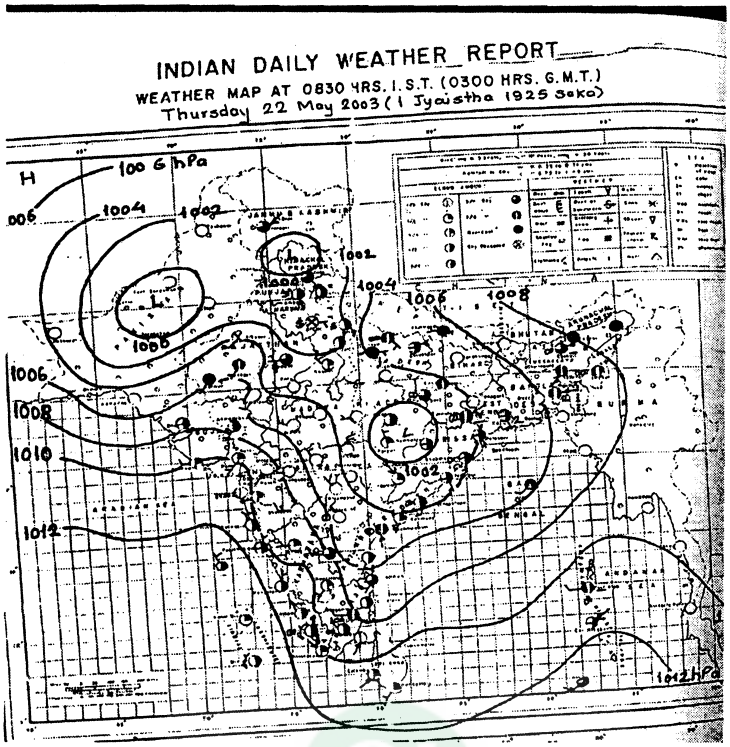

Fig. 4: Surface chart of 22 May 2003 03 UTC

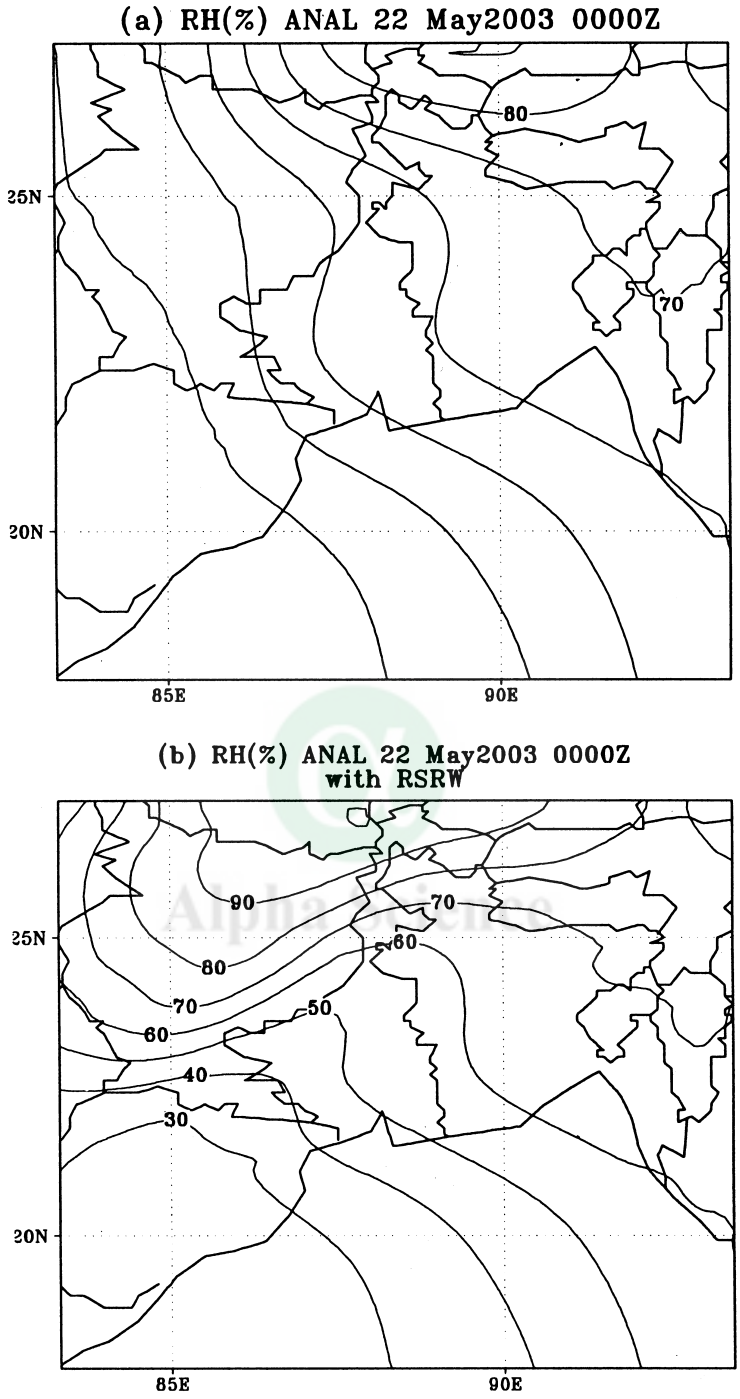

Fig. 5: Relative humidity (%) analyses a) without RSRW; b) with RSRW data for 16 km domain

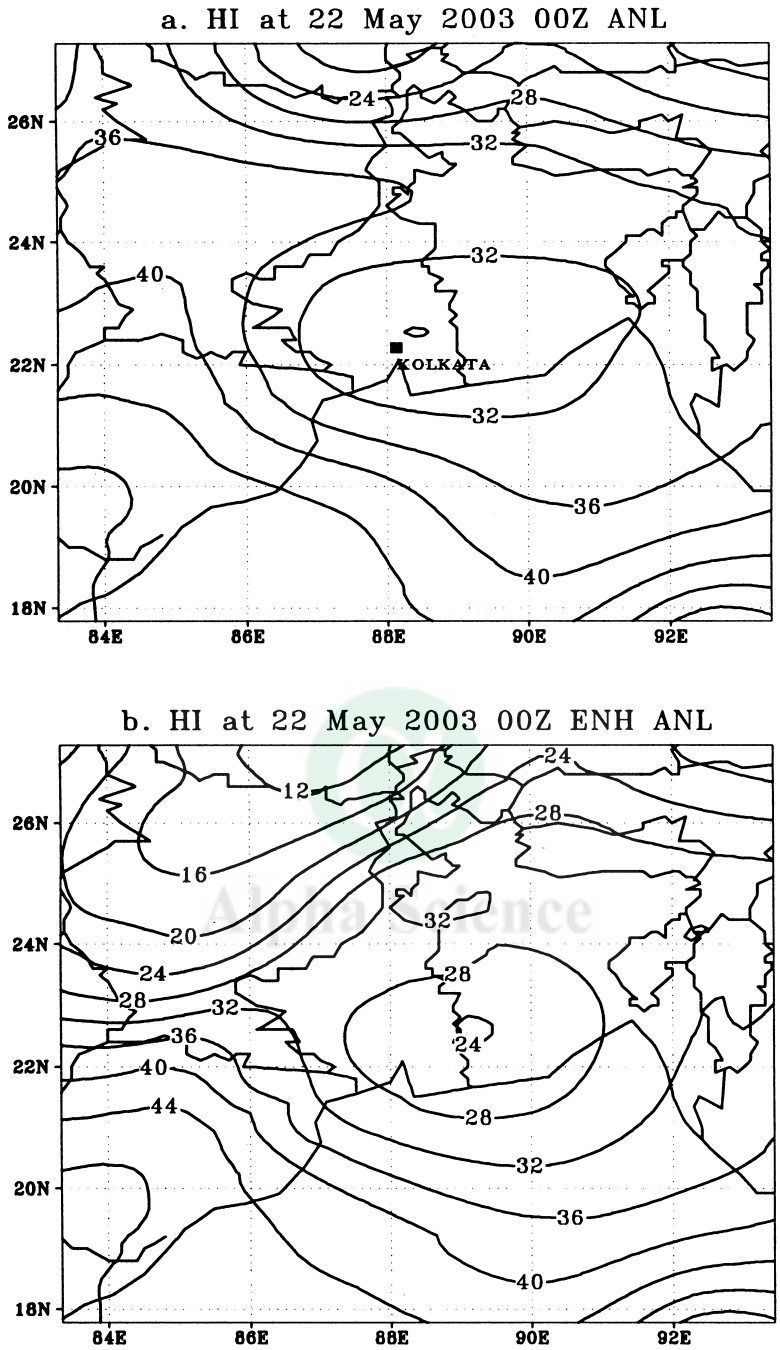

Fig. 6: Humidity index (HI) estimated a) from NCEP analyses; b) from enhanced analyses; c) after 6 hour nudging with NCEP analysis and d) after 6 hour udging with enhanced aalysis

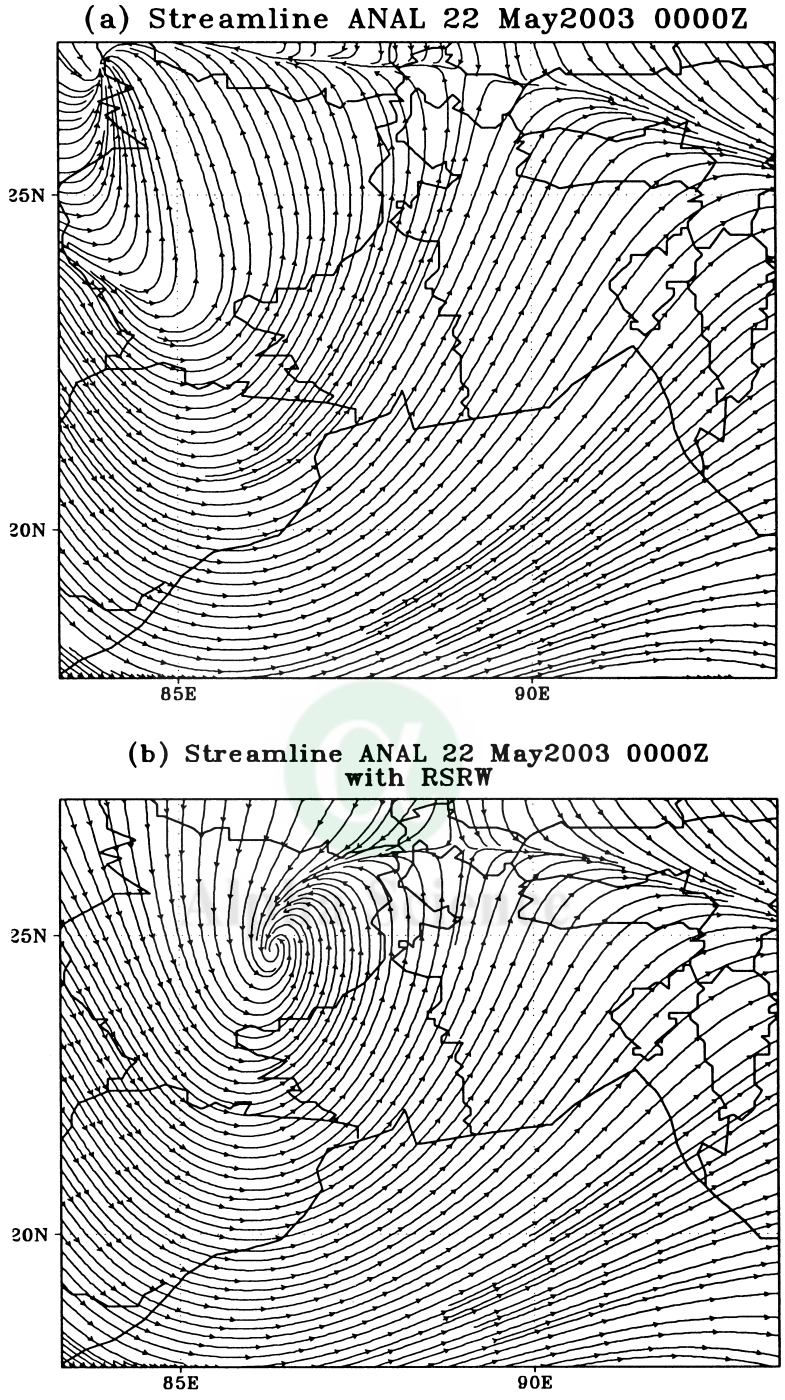

Fig. 7: Streamline at 850 analyses a) NCEP b) enhanced with RSRW

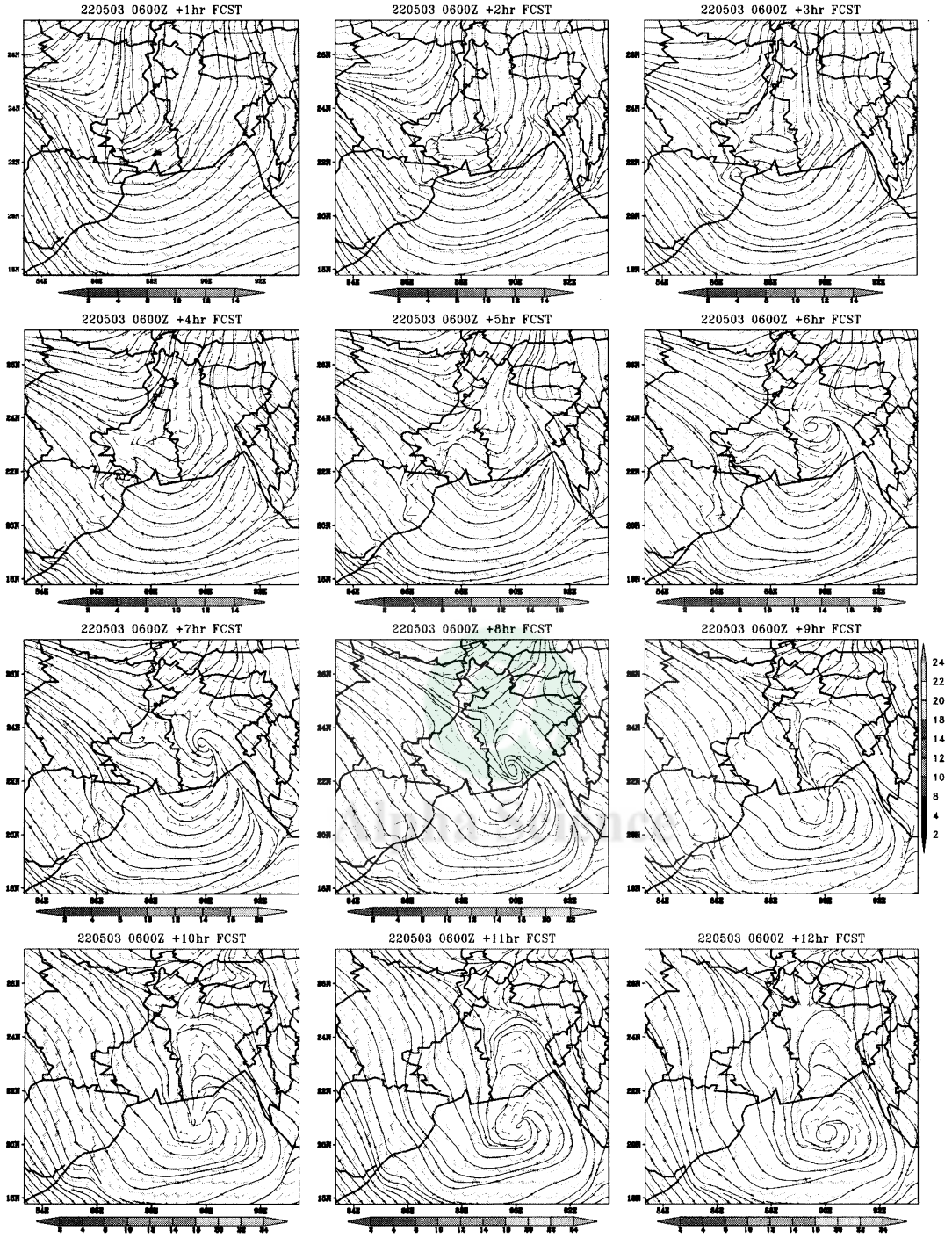

Fig. 8: Hourly forecast of wind barb at 850 hPa in coarse domain (16 km) in EXP-1

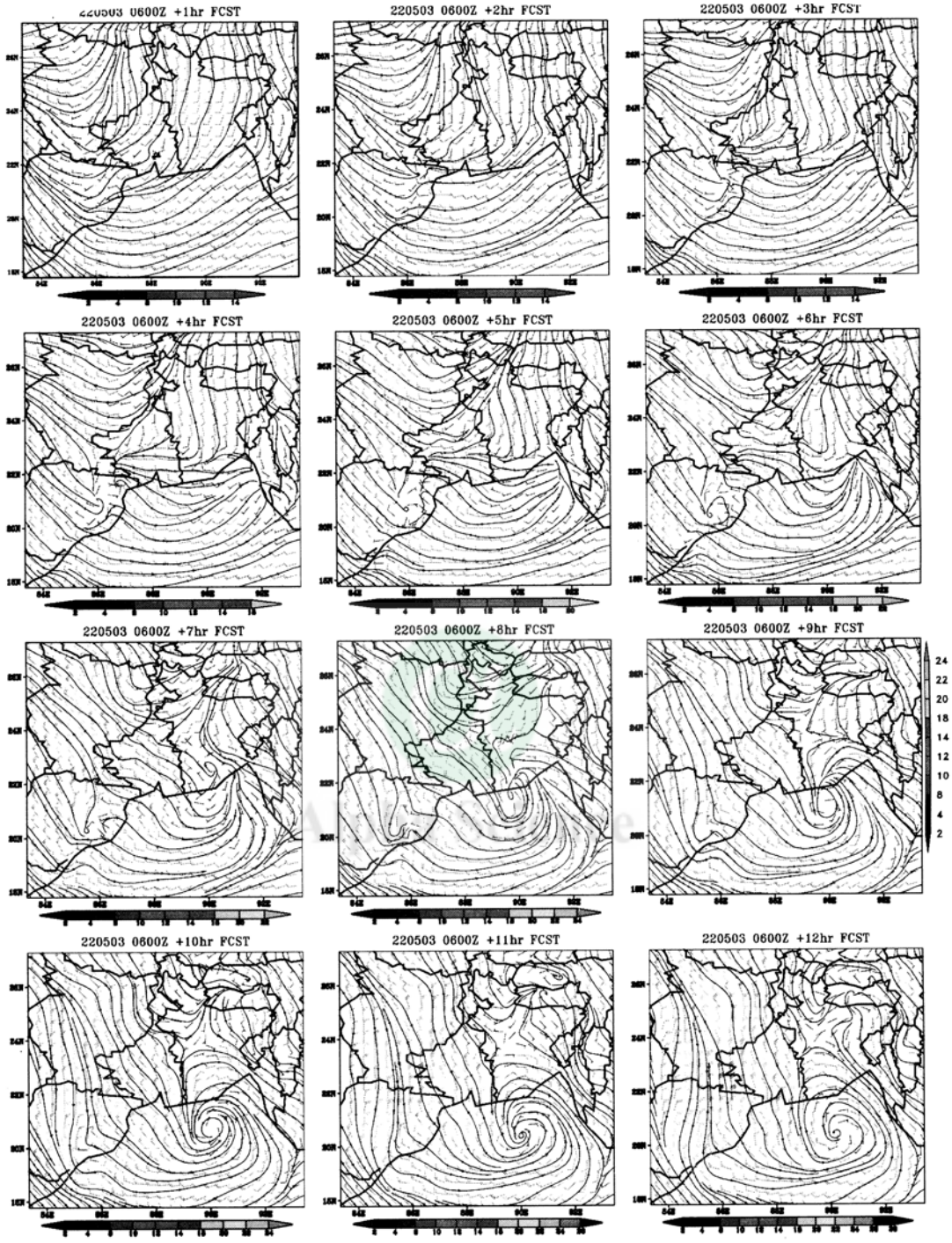

Fig. 9: Hourly forecast of wind barb in coarse domain in EXP-2

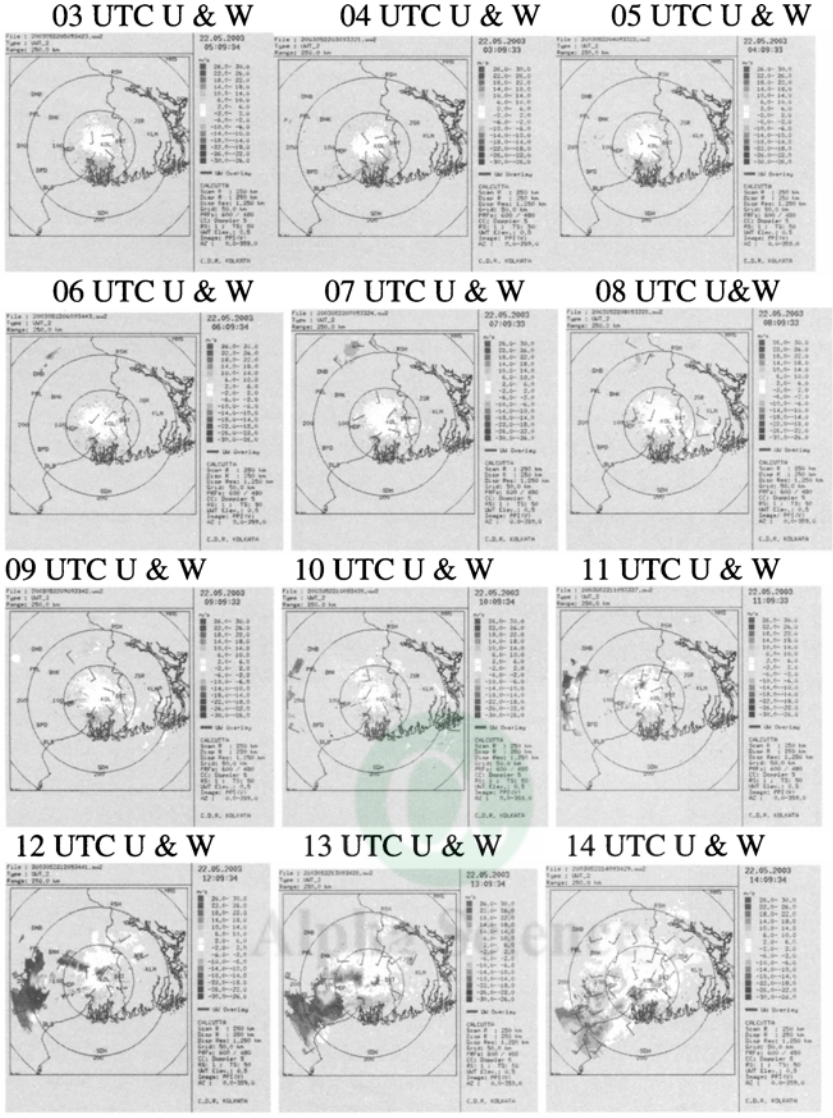

Fig. 10: Doppler radar estimated horizontal wind barb and vertical velocity (Shaded)

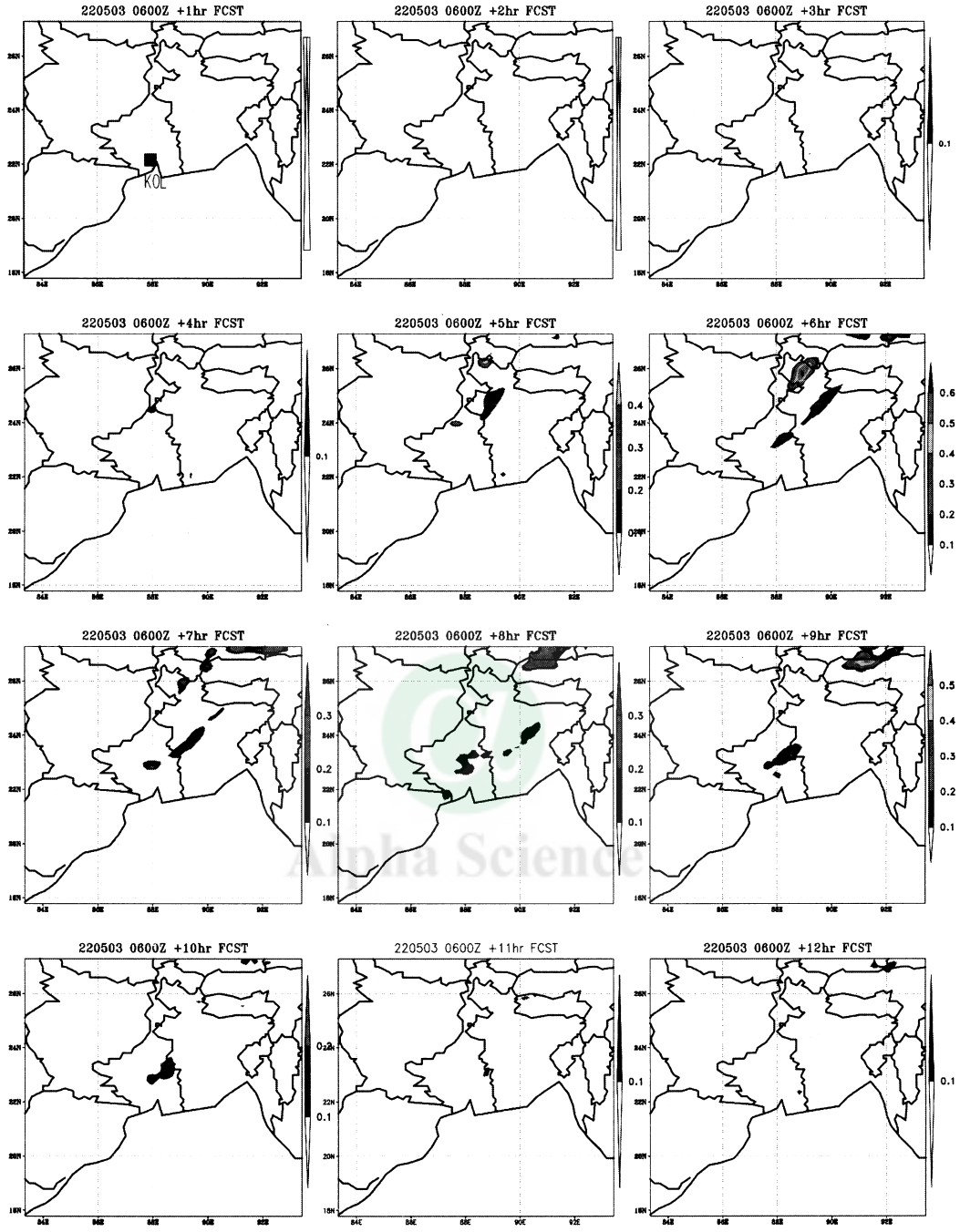

Fig. 11: Hourly forecast of total cloud condensate in coarse domain in EXP-1

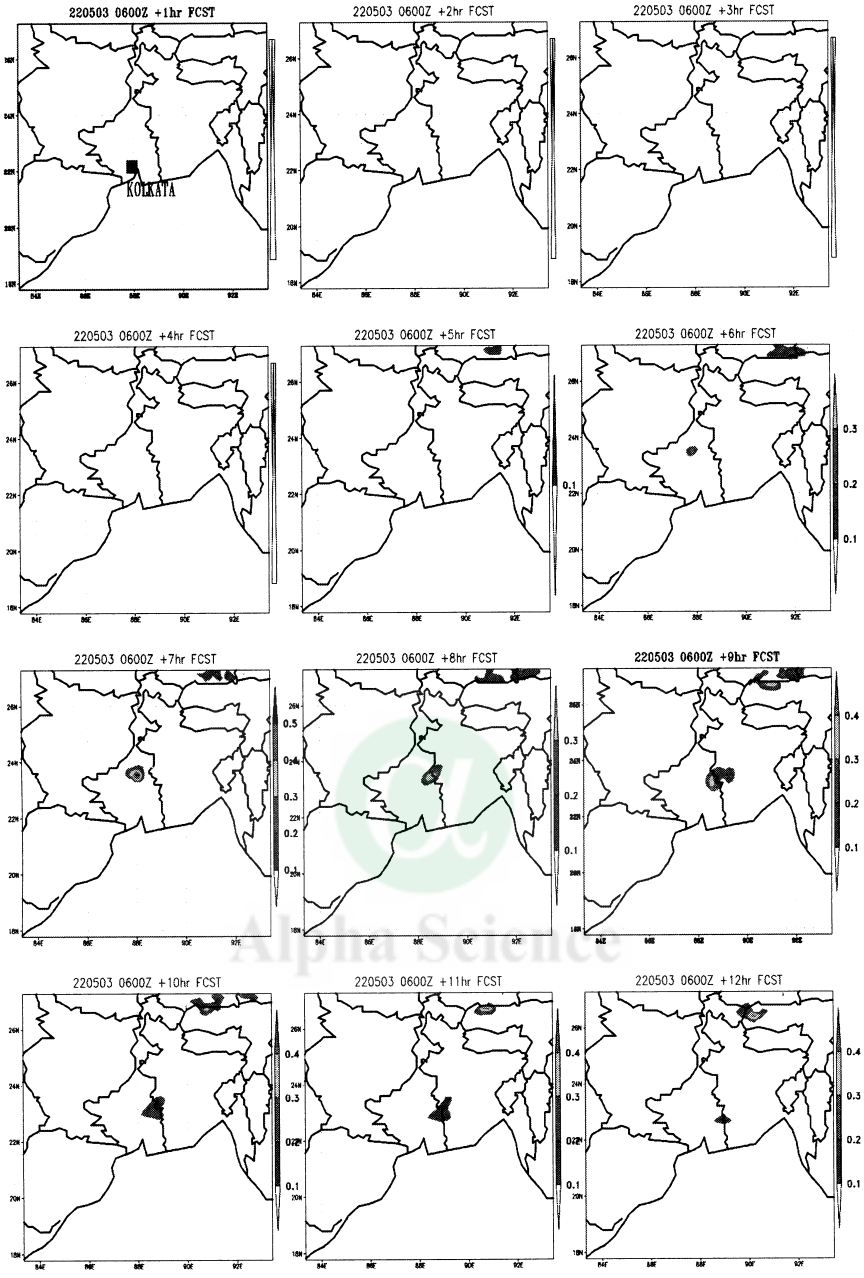

Fig. 12: Hourly forecast of total cloud condensate in coarse domain in EXP-2

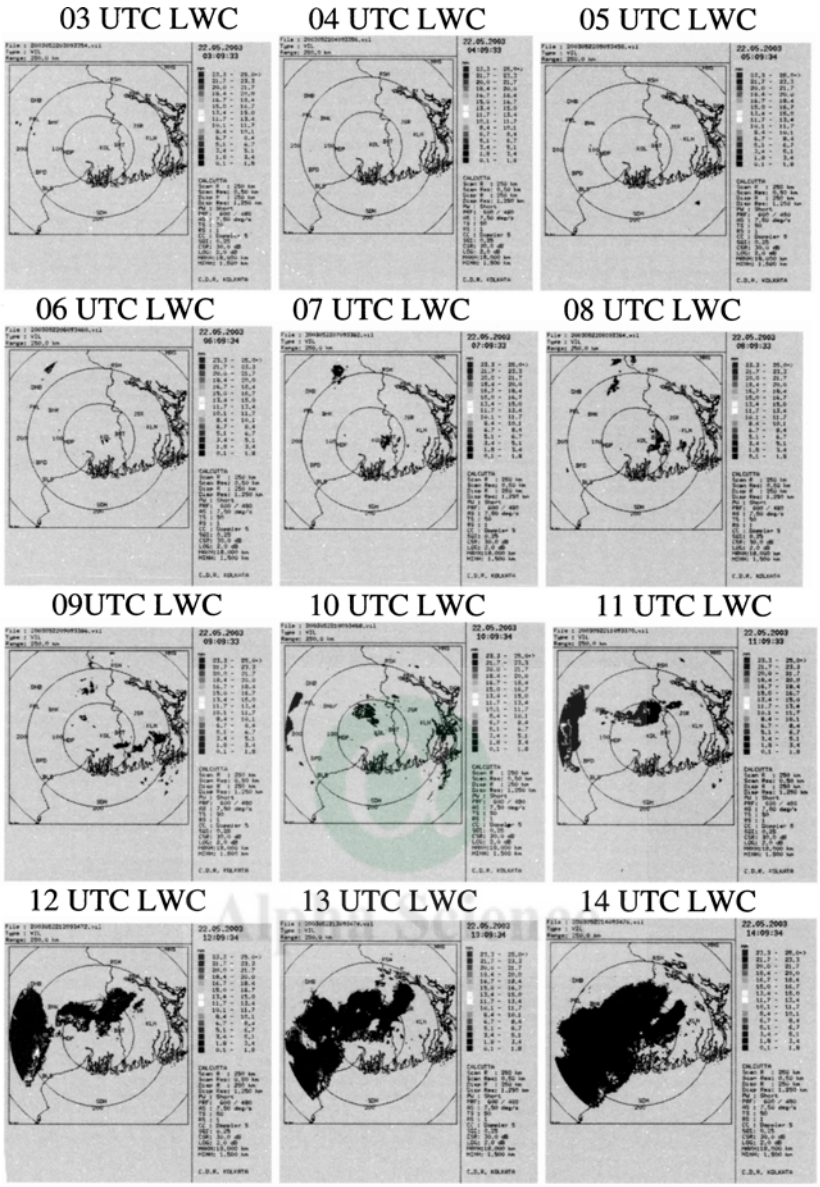

Fig. 13: Doppler radar estimate of cloud liquid water content (LWC)

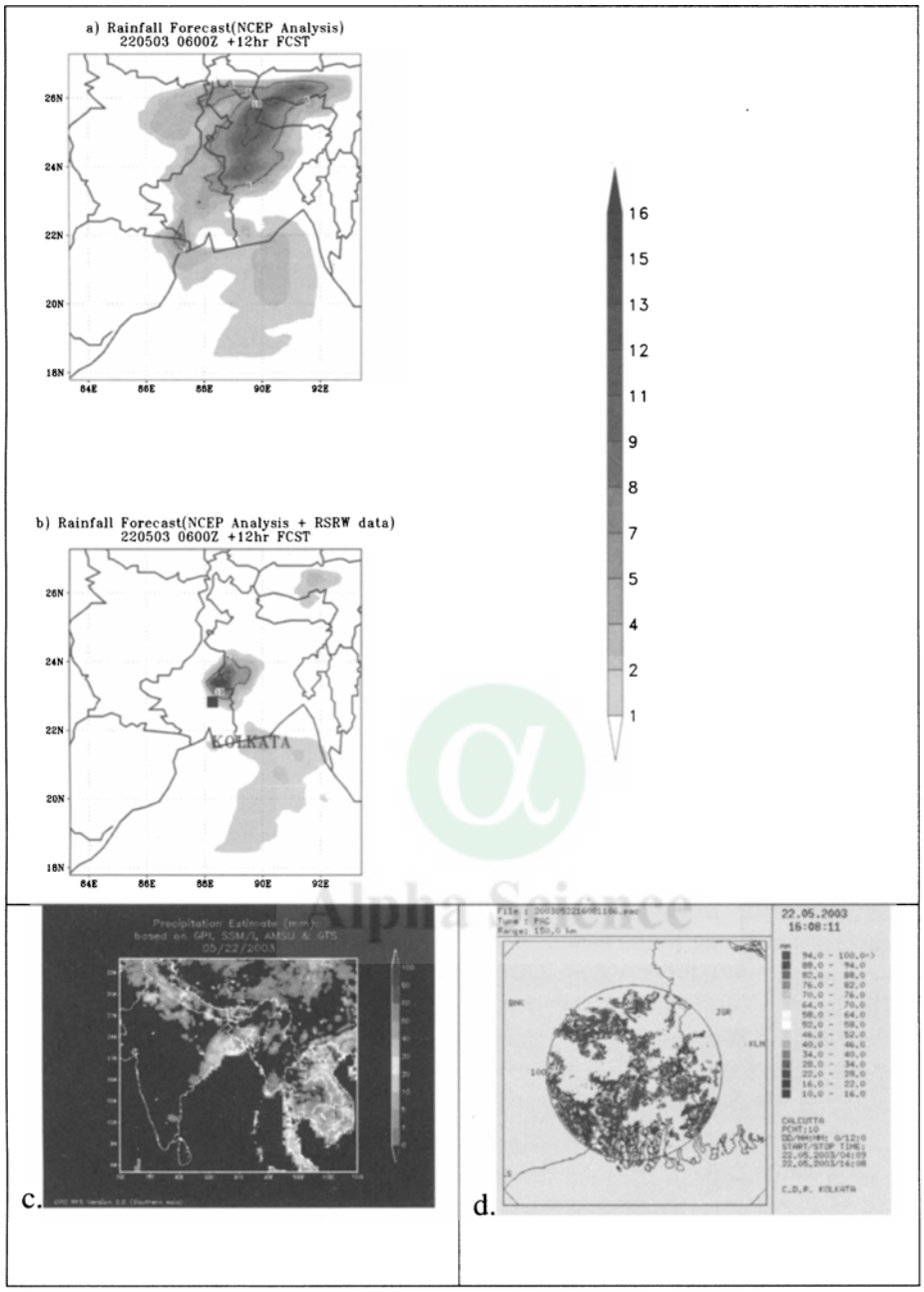

Fig. 14: 12 hourly accumulated forecast precipitation a) in EXP-1, b)in EXP-2; c) CPC 24 hour accumulated precipitation; d) Doppler radar estimated 12 hourly accumulated precipitation.

Comparison of Figs. 11 and 12 clearly suggest that the system is simulated much to the east and north of Kolkata by EXP-1 whereas the EXP-2 could reasonably well simulate the time and location of formation of the Nor'wester. The north-easterly propagation of the storm also is well brought out by the simulated total cloud condensate (Fig. 12) by EXP-2. The results of EXP-2 match reasonably well with the Doppler observation (Fig. 13). However the squall line structure seen in the Doppler radar observation at 11, 12 and 13 UTC could not be reproduced. The comparison of 12 hour accumulated forecast rain (cm) by EXP-1 (Fig. 14a), EXP-2 (Fig. 14b), Climate prediction centre (CPC) daily rain (Fig. 14c) and Doppler radar rainfall estimate (Fig. 14d) reveal that the EXP-2 could produce the location of rainfall close to the observation however the magnitude is significantly underestimated. On the other the EXP-1 could neither bring out the location nor the magnitude of the rainfall.

Conclusions

Two experiments are carried out using RAMS version 4.30 to simulate the Nor'wester of 22 May 2003. One of the experiment (EXP-1) is initialized with 00 UTC of 22 May NCP/NCAR reanalysis gridded data and the other EXP-2 is initialized with an enhanced NCEP analysis where the three stations upper air data are blended with the NCEP analyses to prepare a high resolution (16 km) mesoscale analysis as the input. The comparison of analyses of wind field and humidity index indicate that the mesoscale analysis is able to better resolve the prevalent instability of the region when the three stations upper air data are incorporated. The comparison of forecast fields namely wind barb, total cloud condensate and rainfall have clearly established the fact that the model is able to better simulate the storm in terms of its time of initiation, location and movement when initialized with the enhanced analyses as compared to the simulation with NCEP data only. However it may be noted that the squall lline structure of the storm as revealed by the Doppler radar observation at 11, 12 and 13 UTC could not be reproduced by the simulation experiments (1 or 2). Thus the above experiments show for the first time over Indian region a severe Nor'wester could be simulated using a mesoscale model initialized with gridded data of NCEP and available data over the region.

Acknowledgements

The author is thankful to Dr. G. B. Pant, Director, Indian Institute of Tropical Meteorology, Pune, India, for his keen interest in this study. First author thankfully acknowledges ATMET (ATmospheric Meteorological and Environmental Technologies) for providing RAMS code free of cost under the collaborative project and also thank Dr. William R. Cotton of Department of Atmospheric Sciences, Colorado State University for many fruitful discussions. Director General, Indian Meteorological Department is greatfully acknowledged for making the Doppler radar observations available for the study. Daily rainfall observation is taken from CPC, NOAA, USA. The figures are drawn using GrADS software developed by Brian Dotty and others of COLA, USA.

References

Bernardet, L. R., Grasso, L. D., Nachamkin, J. E., Finley, C. A., Cotton, W. R. (2000) Simulating convective events using a high-resolution mesoscale model. J. Geophys. Res., 105: 14963-14982

Cotton, W. R., Pielke R. A. Sr., Walko, R. L., Liston, G. E., Tremback, C. J., Jiang, H. McAnelly, R. L., Harrington, J. Y., Nicholls, M. E., Carrio, G. G., McFadden, J. P., (2002) RAMS 2001: Current status and future directions. Meteorol. Atmos. Phys., 82: 5-29

Davies, H. C., (1983) Limitations of some common lateral boundary schemes used in NWP models. Mon. Wea. Rev., 111: 1002-1012

Harrington, J. Y., (1997) The effects of radiative and micro-physical processes on simulated warm and transition season Arctic stratus. PhD Dissertation, Atmospheric Science Paper No 637, Colorado State University, Department of Atmospheric Science, Fort Collins, CO 80523, 289 pp

Harrington, J. Y., Reisin, T., Cotton, W. R., Hreidenweis, S. M., (1999) Cloud resolving simulations of Arctic stratus. Part II: Transition-season clouds. Atmos Res 55: 45-75

Hill, G. E., (1974) Factors controlling the size and spacing of cumulus clouds as revealed by numerical experiments. J. Atmos. Sci., 31: 646-673

Keshavamurty, R. N., Sankar Rao, M., (1992) The Physics of Monsoons. Allied Publishers Limited, pp 196

Klemp, J. B., Wilhelmson, R. B., (1978a) The simulation of three dimensional convective storm dynamics. J. Atmos. Sci., 35: 1070-1096

Klemp, J. B., Wilhelmson, R. B., (1978b) Simulations of right- and left- moving storms produced through storm splitting. J. Atmos. Sci., 35: 1097-1110

Lilly DK (1962) On the numerical simulation of buoyant convection. Tellus 2: 148-172

Mesinger, F., (1996) Improvements in quantitative precipitation forecasts with the Eta regional model at the National Centre for environmental Prediction: the 48 km upgrade. Bull. Amer. Meteor. Soc., 77: 2637-2649

Nachamkin, J. E., Cotton, W. R., (2000) Interaction between a developing mesoscale convective system and its environment. Part II: Numerical simulation. Mon. Wea. Rev., 128: 1225-1244

Pielke, R. A. Sr., Cotton, W. R., Walko, R. L., Tremback, C. J., Lyons, W. A., Grasso, L. D., Nicholls, M. E., Moran, M. D., Wesley, D. A., Lee, T. J., Copeland, J. H., (1992) A comprehensive meteorological modelling system-RAMS, Meteorol. Atmos. Phys., 49: 69-91

Smagorinsky, J., (1963) General circulation experiments with the primitive equations. Part I: The basic experiment. Mon. Wea. Rev., 91: 99-164

Tremback, C. J., (1990) Numerical simulation of a mesoscale convective complex: Model development and numerical results. PhD dissertation, Atmos. Sci. Paper No 465, Colorado State University, Department of Atmospheric Science, Fort Collins, CO 80523

Walko, R. L., Cotton, W. R., Meyers, M. P., Harrington, J. Y., (1995) New RAMS cloud microphysics parameterization part I: the single-moment scheme Atmos. Res., 38: 29-62

Walko, R. L., Band, L. E., Baron, J., Kittel, T. G. F., Lammers, R., Lee, T. J., Ojima, D., Pielke, R. A. Sr., Taylor, C., Tague, C., Tremback, C. J., Vidale, P. J., (2000) Coupled atmosphere-biophysics-hydrology models for environmental modeling. J. Appl. Meteor., 39: 931-944

Disaster Management
Editors: N.C. Mahanti et al.

Unsteady State Modeling on Convective Thunderstorm

Anil Kumar, P.N. Sen and K.C. Sharma

Department of Atmospheric and Space Sciences, University of Pune, India

Abstract

Any quantitative investigation of the formation of clouds and precipitation cannot avoid dealing with the complicated motion of particles such as cloud droplets and raindrops. These particles move in viscous medium of the air, thus creating complex flow fields around themselves. These fields have important effect on the growth of particles themselves. For example, due to existence of these flow fields collision efficiency is significantly different, since the collusional growth is very important mechanism responsible for precipitation particle formation, especially in the warm rain process; it goes without saying that the flow field has significant impact on both time and magnitude of precipitation development. (Georgakakos, 1998) worked on QPF modeling , inconsistency in QPF model is further improved by spatial variation, we have tried to develop such model and simulated state variables precipitation content , cloud water content and vertical velocity.

Keywords: Clouds, Convection, Downdraft, Precipitation, Rainfall.

Introduction

A set of ascending or descending parcel of air that conserve vertical momentum, mass and liquid water content. The model parametrizes mixing of mass and momentum with the environment surrounding of air parcel. Model is driver by forcing field such as acceleration due to thermal buoyancy, water vapor vertical gradient and environmental vapor saturation deficit. Finally, a microphysical parameterization is also involved that allows production of precipitation and estimation of heating (cooling) from condensation (evaporation). A great advantage of the model is that it is capable of generating rain field of high temporal resolution over extended period of time while preserving the stochastic nature of simulated precipitation. The basic partial differential equation assumes to govern the system, are due to Kessler (1969) with some modification. Three state variable are consider namely, w, M, m. 'w' represent the updraft (positive value) or downdraft (negative value) motion of the buoyant air parcel. The variable 'M' stand for the precipitation content of the air and it is always positive or zero. Finally 'm' represent the cloud water content, if it is positive (equal to saturation vapor density) or if it is negative, the vapor deficit (the amount of moisture required to saturate the air).

1.1 Formulation

The governing equation are in quasi-steady case; only time derivative term is included to describe atmospheric behaviour in time scale also.

1.2.1 Cloud microphysics Equations

Precipitation content conservation equation

$$\frac{\partial M}{\partial t} = -(V+w)\frac{\partial M}{\partial z} - M\frac{\partial V}{\partial z} + Mw\frac{\partial \ln \rho}{\partial z} + AC + CC - EP - k_{55}M \qquad (1)$$

Cloud water content Equation

$$\frac{\partial m}{\partial t} = -w\frac{\partial m}{\partial z} + wG + mw\frac{\partial \ln \rho}{\partial z} - AC - CC + EP - k_{55}(m - m_e) \qquad (2)$$

Vertical Velocity Equation

$$\frac{\partial w}{\partial t} = -w\frac{\partial w}{\partial z} + g\frac{\theta'}{\theta_{ve}} - k_8(M+m) - k_5|w|w \qquad (3)$$

Microphysical parameterization is also involved that allows production of precipitation, and estimation of heating (cooling) from condensation (evaporation). A great advantage of the model is that it is capable of generating rain fields of high temporal resolution over extended periods of time.

The basic partial differential equations, assumed to govern the system, are due to Kessler (1969) with some modifications. Three state variables are considered, namely w, M, and m. The first variable, w, represents the updraft (positive value) or downdraft (negative value) motion of the buoyant air parcel. The variable M stands for the precipitation content of the air and it is always positive or zero. Finally, m represents the cloud water content if it is positive (in which case the actual vapor density is taken to be equal to the saturation vapor density) or, if it is negative, the vapor deficit (the amount of moisture required for saturate the air)

The temporal and spatial coordinate are respectively, t and z. the first two equations describe the water substance distribution in a vertical column, where as the third one describes its motion. Here V represents the terminal velocity of precipitation relative to air, it is always a negative quantity, and it is given by

$$V = -38.3N_0^{\frac{1}{8}}M^{\frac{1}{8}}\exp(k_7\frac{z}{2}) \qquad (4)$$

Where N_0 is the number of raindrops per unit volume of air per unit raindrop diameter and k_7 is a constant that essentially describes the rate of change of air density with height. The basic assumption here is that all the droplets fall at the same speed, V, equal to the terminal velocity of the median droplet diameter.

The first term on the right-hand side of Eq. (1) describe gain or loss of rain water mass due to vertical gradients in rainwater and raindrop terminal velocity, and the third term stands for the effects of the vertical density ρ variation. The letters AC, CC, EP describes the microphysics. In Eq. (2) the first, third, fourth, fifth, and sixth term are analogous to their counterparts in the previous equation. Here G is the condensation function. The term that includes G describes the rate with which condensation and evaporation occur as the air parcels ascend or descend. It is a function of the vertical gradient of the water vapor saturation mixing ratio and it is one of the model forcing fields. The last term of Eq. (2) describes the depletion of cloud mass through mixing with the environment air of saturation deficit, m_e (a forcing variable).

The first term in Eq. (3) is the gain or loss of vertical momentum due to vertical advection in a momentum field with vertical gradients. The second term in right-hand side of Eq. (3) represents thermal acceleration (buoyancy) in the form of local convective available potential energy (CAPE). The acceleration due to gravity is given by g, θ_{ve} is the potential temperature of the environment surrounding the parcel, and $\theta' = \theta_v - \theta_{ve}$, with θ_v being the potential temperature of the air parcel. The next term describes the effect of negative acceleration due to the weight of the condensed mass (both cloud and precipitation). Conversion of mass to acceleration is achieved by k_8 and only positive value of m is considered. Finally last term describe the exchange of vertical momentum between the moving air parcel and the environment surrounding it.

1.2.2 Microphysics of cloud

The microphysics terms (AC, CC, and EP) constitute important component of the PDEs governing the generation and evolution of rain. The parameterization was devised by Kessler (1969).

- AC (Auto Conversion Threshold)
  Kessler assumed that the rate of auto conversion increases linearly with cloud liquid water content m but is zero for cloud liquid water contents below a threshold, a_{th}, and consequently

$$AC = -\frac{dm_{AC}}{dt} = \frac{dM_{AC}}{dt} = k_1(m - a_{th}) \qquad (5)$$

where k_1 is the auto conversion coefficient, different choices of k_1 and a_{th} can lead to rapid or slow generation or cloud seeding.

- CC (Collection of cloud droplet)

  In order to describe the collection of cloud droplet, Kessler assumed a Marshall-Palmer-type drop size distribution (DSD) for the rain throughout the entire vertical column as follows:

$$N(D_d) = N_0 e^{-\lambda D_d} \qquad (6)$$

  N(D) is number of raindrop per unit volume per unit diameter range of δD_d, N_0 is constant, λ is associated with the median volume diameter D_0 (D_0 separate the distribution in equal part of water content.

$$CC = -\frac{dm_{cc}}{dt} = \frac{dM_{cc}}{dt} = 2S_3K_2E_{col}\frac{N_0^{0.125}}{H}mM_0^{0.875} \qquad (7)$$

  E_{col} is collection efficiency with which big raindrop collects small raindrop as they fall freely. It is seen that CC increases linearly with cloud content 'm'.

- EP (Evaporation)

  Finally Kessler started from the rate of change of mass of a freely falling water drop to formulate EP

$$EP = \frac{dm_{EP}}{dt} = -\frac{dM_{EP}}{dt} = 0.826K_3N_0^{0.35}|m|M_0^{0.65} \qquad (8)$$

  Eq. (3) shows that evaporation depends more strongly on the number of particles N_0 and less strongly on the amount of precipitable water M_0 than CC. Also, EP depends linearly on cloud content m.

  The key parameters in Kessler's implementation are a_{th}, E_{col}, and N_0. it should be mentioned that implicit in the Kessler scheme is the fact that precipitation shares the horizontal motion of air. Kessler's microphysics scheme is rather simple and it does not represent to a high degree of accuracy the physical processes involved.

1.2.3 Large-scale forcing formulation

The forcing fields are presented through the terms containing $g\theta_v'/\theta_{ve}$, the condensation function G, and the environment vapor saturation deficit m_e. The first forcing field is attributed to the acceleration of an air parcel due to buoyancy. In other words, it is an indicator of CAPE. A parcel of air is freely accelerated upward by the density difference between the parcel and its environment when no vertical pressure gradient exists and no mass exchange between the parcel and the environment occurs. The environment is assumed in hydrostatic equilibrium the buoyancy factor B is given by

$$B = \frac{\theta_v - \theta_{ve}}{\theta_{ve}} \qquad (9)$$

Where θ_v and θ_{ve} are estimated according to Houze (1993), when the buoyancy factor is multiplied by the acceleration g due to gravity we obtain the acceleration due to thermal buoyancy $A(= gB)$ and its vertical average α is defined as

$$\alpha = \frac{1}{H}\int_{LFC}^{H}\{A\}dz \qquad (10)$$

where the integration take place from the level of free convection (parcel becomes warmer than the environment) to the maximum height of the convective column. It should be mentioned that even if the air

parcel and the environment air have the same temperature, a difference in their water vapor content results also in potential temperature difference between the moist air parcel and the environment air surrounding it. The next forcing field used in this study is attributed to water vapor gradients. As a saturated air parcel ascends, the effects of condensation and evaporation of the cloud occur at a rate.

$$G = -\rho \frac{\partial Q_s}{\partial z} \qquad (11)$$

where Q_s is the saturation water vapor mixing ratio and is given by

$$Q_s = 0.622 \frac{e_s}{P} \qquad (12)$$

with e_s being the saturation water vapor pressure and P the air pressure. The condensation function G pertains to the amount of the condensed (evaporated) moisture under saturated (Unsaturated) conditions per meter of ascent or descent. A good approximation of G in a real troposphere is a linear decline with height.

Finally, last forcing field provides an indication of how close to saturation the environment moisture is, or how conducive to rain the environment surrounding the cloud is. The field has a negative value and the less negative it is the easier it becomes to generate rain. When m_e is equal to zero the environment becomes saturated. The deficit m_e is given by (Wallace and Hobbs 1977)

$$m_e = Q_s \rho (RH - 1) \qquad (13)$$

Where RH is the relative humidity that varies between 0 and 1.

As can be seen, modeling the forcing fields represented by Eq (10), (11) and (13) requires a number of parameters. Depending on the goals if different studies the parameters can be provided either from theoretical considerations or actual measurements. In our case the parameters are based on observation of the forcing variables themselves during convection.

1.3 Precipitation Content

Precipitation forms from clouds that consist of droplets having different sizes and fall speed, where there is much variety in these quantities, some droplets tend to grow at the expense of others, which evaporate, and the relative motions of cloud droplets produce occasional contacts resulting in fusion. Somewhere near the dense middle of the cloud, precipitation forms first. Unless the updraft is faster than a few meters per second, the precipitation particles descend to the ground, while cloud is thinner than before. Development of precipitation depends not only on the rate at which vapor is transformed to condensate, but also on the time interval available for precipitation development during its descent to the ground. As long as updraft speeds are quite small (for example, less than 0.5 m s^{-1}) compared with precipitation fallspeed (about 6-8 m s^{-1}), time taken for precipitation to descent to the ground is only slightly affected by variation of updraft speed. But when the updraft speed is considerably faster than the fallspeed, more time passes during precipitation descent as the updraft increases. This means, for example, that a doubling of maximum updraft speed from 1 to 2 m s^{-1} may associate with increased precipitation rate at ground by a factor, for example, of about 2.5. in this case. Increased updraft speed contribution is significant to both the rate of development of a precipitation packet and the time interval available for its development before it reaches the ground. When updraft is strong, the cloud particles rise farther before they are converted to precipitation. This means that the cloud content tends to be greater as updraft increases, But when conversion to precipitation start, there is larger amount of cloud to change to precipitation, and hence a larger amount of precipitation in the upper part of column.

In a strong updraft, precipitation cannot descend to the ground through the rising current. In some cases, it may descend to the ground in adjacent descending currents, especially if there is substantial horizontal wind at altitude. Then the precipitation is subject to large losses by evaporation, because the distance to the ground may be far and descending currents are usually dry. In other cases, the upward transport of water vapor and condensate may be balanced for sometime by the horizontal spreading of a great storm anvil at high altitudes.

A given amount of condensation may be produced by a slow updraft operating over a long period of time or by a stronger updraft operating for a proportionately shorter period. The period of condensation is followed

or overlapped by a stage of cloud conversion and then by precipitation at the ground. The amount of condensate that arrives at the ground as precipitation beneath the updraft column depends on whether the vertical displacement of air is large enough and completed rapidly enough to carry cloud out of the updraft column before microphysical processes have time to change the cloud to precipitation. Thus precipitation at the ground is expected to be proportional to the amount of small vertical displacement and its velocity.

Transient vertical profile of precipitation for a case in which, precipitation gains near the middle of the cloud column.

Precipitation profile at initial stage of thunderstorm is consider from steady state as shown in figure

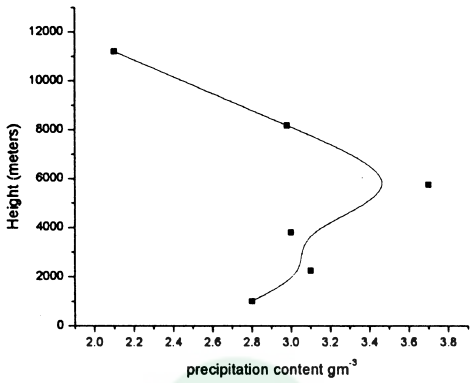

Figure 1

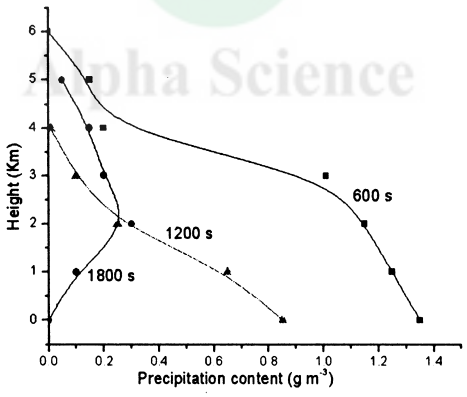

Figure 2

Simulation of precipitation content for 30 minutes duration of thunderstorm as shown in fig 2, at beginning of thunderstorm, the precipitation profile as shown in fig 1, precipitation content is found to me more at middle of cloud. As model runs for 30 minutes duration, a precipitation profile has been seen at 600 sec, 1200 sec, and 1800 sec.

Initially precipitation is parabolic in nature, but at time step 600 secs, precipitation is decreasing with height and amount of precipitation is found to be less than initial values. After 1200 sec, precipitation profile is linearly decreasing and precipitation content in cloud decreasing simultaneously. And at 1800 sec, we found precipitation content is very less in cloud as seen in fig 2. From this we concluded that, precipitation content decreases in thunderstorm cloud at different stage of thunderstorm. As shown in fig 2 precipitation content.

1.4 Cloud Water Content

It is in the form of small suspended liquid-phase droplets (i.e., drop that are too small to have any appreciable terminal fall speed constitute cloud liquid water and therefore are generally carried along by the air in which they are suspended.

Conversion of cloud water content to precipitation is involved in model by introducing auto-conversion rate, which is given by

$$AC = K_1(m - a_{th})$$

it is assumed to be proportional to the amount by which the cloud water mixing ratio exceeds a selected threshold. The rate of cloud auto conversion increases linearly with the cloud liquid water 'm' but is zero for cloud liquid water content below a threshold a_{th}.

Result obtained with a time dependent model of the type described above. The cloud was initiated by maintaining a vertical velocity forcing. It can be seen that the model cloud grew steadily and reaching a maximum altitude of 8km. during most of this growth period, the cloud consisted of updraft at all levels, with the strongest upward motion in the middle levels of cloud. In the growing updraft, the perturbations of potential temperature and water vapor mixing ratio were generally positive, contributing to positive buoyancy. As cloud water content increases, the buoyancy was weakened as a result of the weight of the hydrometeors. This negative buoyancy reversed the vertical velocity.

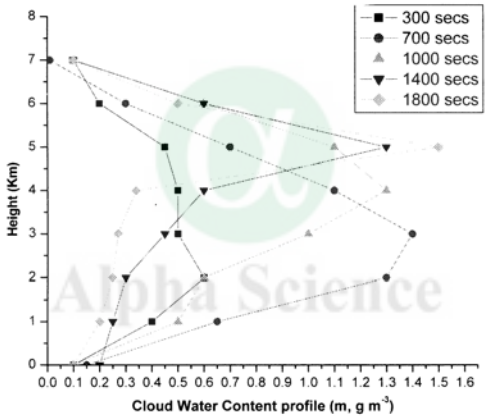

Figure 3

Model output at various times for cloud water content is shown in figure 3, after 300 seconds model shows that cloud water content is somewhat parabolic in nature, initially it start increasing, and after 2 km height, it is almost stable till 4 km then it start decreasing, after 700 seconds the cloud content profile is parabolic in nature, and cloud water is maximum at 3 km height, after that it gradually decreases and become very less almost negligible at height 7 km. At 1000 seconds amount of cloud water is decreases as compare to previous time but found maximum value at 4 km and then it start decreasing and reaching minimum value around 7 km. after further model run we found cloud water profile at 1400 seconds, which show that below 4 km we found amount is decreasing what we had earlier time step and found to be maximum at 5 km, at last 1800 second, the cloud water content decreases more and more till 4 km and then gradually increases to maximum value around 1-5 - 1-6 g m^{-3} at height 5 km and then decreases to minimum value at 7 km height. This variation in cloud water content through out 30 minutes simulation shows (fig 4) that at initial point, cloud water content increases till 4 km, as model runs further it start decreasing and above 4 km cloud water content amount increases with increasing time step and after 4 km it gradually decreases with height to it minimum value at 7 km. From this we may conclude that vertical velocity and entrainment will responsible cloud water profile, as we have seen in previous chapter that vertical velocity profile which gradually increase with height till 4-5 km height and if vertical velocity is higher than cloud water content density is shifted with height, as it is seen clearly that cloud water content maximum value is shifted with height on

increasing time step. As seen in precipitation content in fig 2, after 30 minutes simulation, precipitation is still there between 0 – 5 km range and in cloud water profile we can see that cloud water is present at 30 minutes time step.

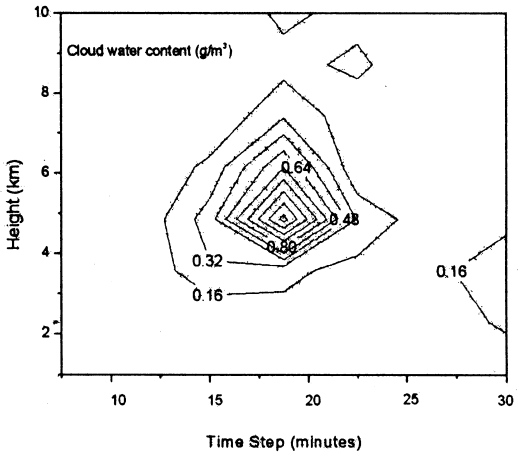

Figure 4

1.5 Vertical Velocity

The computation of vertical velocity in this model depends on following terms in Eq (3) as follows, the first term is the gain or loss of vertical momentum, the second term represent thermal buoyancy in the form of local convective available potential energy, water loading effects is achieved through k_8 and only positive values of m are considered. Last term describes the exchange of vertical momentum between parcel and environment.

The simulated vertical velocity at different time step of model is shown in fig 5

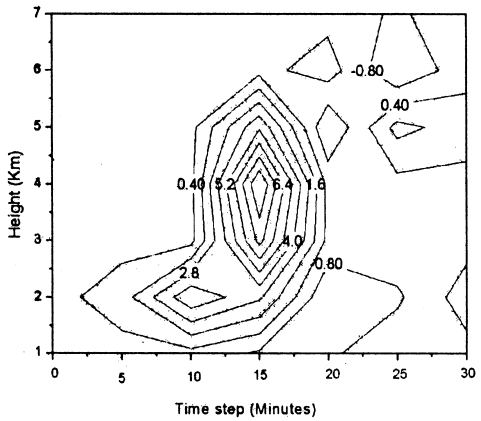

Figure 5

Simulated vertical velocity is shown in fig above. We found that vertical velocity is maximum after 15 minutes model run at 6 km height, prior to that model show, vertical velocity is developing slowly and found 10 m/s maximum value in 30 minutes simulation, , after 15-20 minutes simulation, model output shows that vertical velocity is gradually decreasing, as seen in fig 5, we can see that we found negative vertical velocity also, this shows that model is simulating downdrafts.

Buoyancy is also plotted and shown in fig 6 , buoyancy indicate the convective available potential

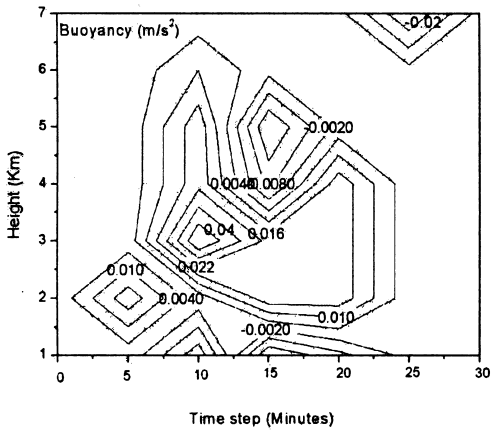

Figure 6

energy and we can match the buoyancy and vertical velocity profiles, buoyancy

patters reveal that CAPE is closely resemblance with vertical velocity, we found where there is high buoyancy, high vertical velocity is found. We have done analysis using potential temperature perturbation, potential temperature has been estimated from input parameters temperature and pressure, the observed potential temperature from station, we found perturbation in potential temperature and plotted as graph, shown in fig 7.

As seen in fig 7, potential temperature perturbation is parabolic in nature with height, which say that perturbation is high at 4 – 5 km range, and buoyancy and vertical

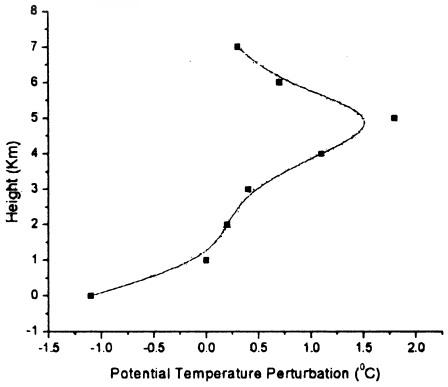

Figure 7

velocity is found high at 4 – 6 km range. From this we concluded that model is simulating transient state variable as with potential temperature perturbation.

1.6 Result and Conclusion

Station : Nagpur

Date (2003)	Sen et al Model (mm/hr)	Extended Model (mm/hr)	Complete Model (mm/hr)	Actual Rate of Precipitation mm/hr)

20 May	0.60	0.20	0.01	0.06
21 May	3.02	2.90	3.12	3.23
22 May	1.75	1.40	1.90	2.25
23 May	1.03	3.02	4.23	5.40
24 May	1.61	0.40	0.75	1.01
25 May	0.42	1.61	1.15	0.64

- Sen at all Model is based on Conservation of moisture (Humidity).
- Extended model is Sen at al model with thermodynamic term added.

We have seen behavior of state parameter which describes the convective cloud model, it is bit difficult to validate the behavior of state parameter with different time step, and we have seen the vertical velocity distribution, cloud water content and precipitation content. We have seen that vertical velocity is high at middle of cloud, vertical velocity is develop after 15 minutes simulation and similarly it cloud water content is developed after 15 minutes simulation, afterward all three state parameters start decaying, this may be because the convective system weakened and hence as cloud water and vertical velocity decay, precipitation also decreases. The faster rate at which latent heat is realized produces a more rapid recovery of thermal buoyancy, which now increases faster than the contrary tendency of the increasing water load. Therefore, the updraft continues to increase, precipitation is held aloft, and the high-speed steady updraft develops. The precipitation aloft diverges there, and descent toward the ground is implied in regions where the updraft is not so strong. One effect of hastened transformation of cloud to precipitation in the model is a reduction of the total amount of precipitation deposited on the ground. The reduction may be because the updraft, the ultimate source of precipitation in the model, suffers an earlier reduction of buoyancy owing to precipitation evaporating in the sub-cloud layer. We infer that stimulation of the cloud conversion process in an effort to increase rainfall might actually have the opposite effect unless the effort is carefully timed.

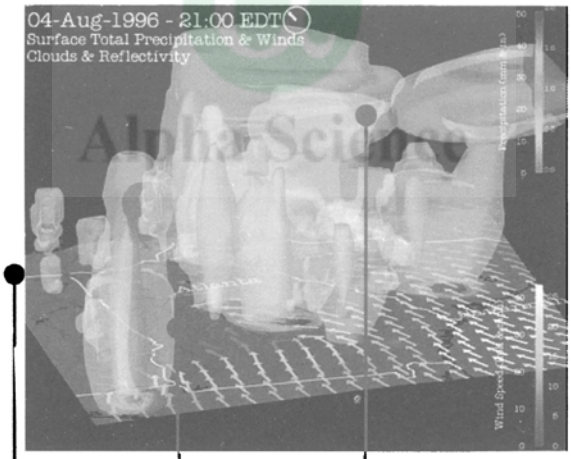

Fig 1.

In above figure, cloud water, precipitation content and rainwater is shown.

We can enhance in many ways, firstly physics of cloud is not understand fairly well till date, thermal buoyancy acceleration is important forcing term, which has to be studied deeply, thermal buoyancy should be studied by using heat equation. Secondly, input data which describes the initial state of atmosphere are of high resolution of 100-200 meters. Effects Gravity wave drag on distribution of water substance in atmosphere has to explore, which may enhanced QPF model.

We have simulated for 30 minutes only, there are many limitation for one hour simulation. Firstly we have taken care of boundary condition using extrapolation techniques, but still error propagates from boundary to center and generally after 30 minutes simulation, it effect values in large extent at 45 minute.
Another limitation is, lack of high resolution data, satellite data which is downloaded from NCEP-NCAR data center, generally this data is available in 2.5° x 2.5°, and then interpolated for fine resolution, but problem with this available resources is it may capture convective state, because of this reason we have seen two convective area, one is very weak and another which describe in this is moderate one.

APPENDIX

List of Symbols, Constants, Units, and Typical values

a_{th} Auto conversion threshold, g m^{-3}
AC Auto conversion of cloud, g m^{-3} s^{-1}
B Buoyancy factor (unit less)
CC Collection of cloud, g m^{-3} s^{-1}
$e_s(T)$ Saturation vapor pressure 1704.3 N
E_{col} Collection efficiency, unit less
EP Evaporation of cloud, g m^{-3} s^{-1}
G water vapor gradient g m^{-4}
k_1 Auto conversion coefficient, 10^{-3}
k_2 Constant associated with CC, 6.96×10^{-4} $m^{3.875}$ $g^{-0.875}$ s^{-1}
k_3 Constant associated with EP, 1.93×10^{-6} $m^{3.15}$ $g^{-0.65}$ s^{-1}
k_5 Momentum mixing coefficient, m^{-1}
k_{55} Mass mixing coefficient, s^{-1}
k_7 Constant associated with the existence of water vapor gradient, 1×10^{-4} m^{-1}
k_8 Constant associated with "weight" of M_0 and m, 10^{-2} m^4 g^{-1} s^{-2}
m Cloud density or deficit, g m^{-3}
m_e Environmental vapor saturation deficit, g m^{-3}
M Precipitation density or content, g m^{-3}
M_0 Maximum precipitation density or content g m^{-3}
N_0 Number of raindrops per unit volume per unit diameter, m^{-4}
Q_s Saturation water vapor mixing ratio g Kg^{-1}
P Air pressure N m^{-2}
S_1 5457 if updraft, 5901 if downdraft
S_2 4055 if updraft, 1503 if downdraft
S_3 4352 if updraft, 2040 if downdraft
T Air parcel temperature, 288 K
V Terminal fall velocity of raindrops, m s^{-1}
w Vertical velocity, m s^{-1}
w_{max} Maximum vertical velocity, m s^{-1}
z Vertical coordinate, m
Q_v Potential temperature of air parcel, K
Q_{ve} Potential temperature of environment surrounding air parcel, K
Q' Q_v - Q_{ve}, K

ρ Air density, 0.00128 g cm^{-3}

References

Georgakakos, K. P., Krajewski W F, 1997: "Statistical-microphysical causes of rainfall variability in the tropics." J. Geophys. Res, 101(D21), 26165-26180.

Gershenfeld, N., 1999: The Nature of Mathematical Modeling, , Cambridge University Press.

Houze, R.A., 1993: Cloud Dynamics. Thunderstorm, Academic Press, 268 pp.

Jain, M.K., 1992: Numerical Methods and analysis.

Kessler, R., 1969: On the Distribution and Continuity of Water Substance in Atmospheric Circulation Meteor, Monogr, No. 32, Amer Meteor. Soc., 84pp.

Sen., P. N., 1991: "Mathematical model for QPF for flood forecasting purposes", Mausam, 44, 19.

Tsintikidis D, and Georgakakos, K. P., 1999: "Microphysical and large-scale dependencies of temporal rainfall variability over a Tropical Ocean.", J. Atmos. Sc., 56, 724-748.

Tim H, Lee, and Georgakakos, K .P, 1996: "Operational prediction on meso-y scales for hydrologic applications", Water Resour. Res., 32, 987-1003.

Wallace, J.M., and P.V. Hobbs, 1997: Atmospheric Thermodynamics. Atmospheric Science: An Introductory Survey, Academic Press, 48-107.

Disaster Management
Editors: N.C. Mahanti et al.

Time Stability Criteria in a Convective Cloud Modeling for Rainfall Prediction

Anil Kumar, P.N. Sen and K.C. Sharma

Department of Atmospheric and Space Sciences, University of Pune, India

Abstract

Convective and other precipitation processes occur on scales much smaller that can be resolved by most operational models. Governing equations for convective thunderstorm is generally microphysical partial differential equations and solved by finite difference schemes. But still time step stability criteria are a challenging task in cloud modeling for rainfall forecast. In this paper we have estimated time step for cloud model using equation of microphysics. Kessler's microphysics equation for precipitation content, cloud water content and vertical velocity (Updraft and Downdraft) have been consider and appropriate time step is estimated for mechanism associated with thunderstorm.

Keywords: Clouds, Convection, Downdraft, Precipitation, Rainfall.

Introduction

Convection in the earth's atmosphere may be either shallow (restricted to the lowest 1-2 kilometers) or deep (extending all the way up to the tropopause). Deep convection is always of the moist kind and usually involves cumulonimbus clouds (accompanied by thunder and lightning when they form over land). Shallow convection may be either of the moist type or dry type. Shallow moist convection generally involves small, lumpy cumulus clouds or flatter stratocumulus clouds. Convection is usually made up of buoyant, rising plumes of warmer, more moist air known to glider pilots as 'thermals', separated by slowly sinking cooler, dryer air. Thermals start out as "hot spots" in the surface layer close to the ground and they rise until they eventually run out of buoyancy. They expand and cool as they rise, and if they rise high enough, the water vapor in them condenses to form clouds. The level at which condensation first occurs (i.e. the cloud base) is called the 'Lifting Condensation Level' (LCL). During their life cycle, thermals transport heat and moisture upward from the earth's surface, where they start out, up to the level where they run out of buoyancy. At intermediate levels, warm, moist thermals are going up and cooler, drier air is subsiding in between them. Thermals that rise all the way up to the upper tropopause lose nearly all their moisture on the way up. The latent heat released by the condensing moisture warms the atmosphere. This latent heat was taken up from the earth's surface wherever the moisture entered the atmosphere via evaporation. Time stability criterion $\frac{v\Delta t}{\Delta x} \leq 1$, this is the Courant-Friedrichs-Levy stability criterion (Neil Gershenfeld 1999), it says that the velocity at which information propagates within the numerical algorithm ($\Delta x/\Delta t$) must be faster than the velocity of the solution v. For space and time steps that satisfy this condition, otherwise there is a "numerical boom" as the real solution tries to out-run the rate at which the numerical solution can advance. Time step criteria for state parameters like precipitation content, cloud water content and vertical velocity are varying with heights as entrainment at different various level have different entrainment rate and have significant impact on other processes like cloud water content and vertical velocity, Similarly vertical velocity (updraft and downdraft) profile has strong variation in convective cloud model, vertical velocity increases up to mid-level of cloud then it start decreasing and in top of cloud layer, if latent heat is released due to phase change then it may increase further. Hence many process like melting can occur. So, the time step is not constant in convective cloud model at various cloud model heights like local thunderstorm, time step is changing with different entrainment rate, vertical velocity variation etc.

An attempt has been made to obtain the time stability criteria in convective systems, which occasionally lead to local thunderstorm and thus heavy rainfall associated with this system. The state parameters, which govern the convective system has much smaller time scale for microphysical processes.

Model Formulation

The basic partial differential equations, assumed to govern the system, are due to Kessler (1969) with some modifications. Three state variables are considered, namely w, M, and m. The first variable, w, represents the updraft (positive value) or downdraft (negative value) motion of the buoyant air parcel. The variable M stands for the precipitation content of the air and it is always positive or zero. Finally, m represents the cloud water content if it is positive (in which case the actual vapor density is taken to be equal to the saturation vapor density) or, if it is negative, the vapor deficit (the amount of moisture required for saturate the air)

Precipitation content conservation equation

$$\frac{\partial M}{\partial t} = -(V+w)\frac{\partial M}{\partial z} - M\frac{\partial V}{\partial z} + Mw\frac{\partial \ln \rho}{\partial z} + AC + CC - EP - k_{55}M \qquad (1)$$

Cloud water content Equation

$$\frac{\partial m}{\partial t} = -w\frac{\partial m}{\partial z} + wG + mw\frac{\partial \ln \rho}{\partial z} - AC - CC + EP - k_{55}(m - m_e) \qquad (2)$$

Vertical Velocity Equation

$$\frac{\partial w}{\partial t} = -w\frac{\partial w}{\partial z} + g\frac{\theta'}{\theta_{ve}} - k_8(M+m) - k_5|w|w \qquad (3)$$

Here V represents the terminal velocity of precipitation relative to air, it is always a negative quantity, and it is given by

$$V = -38.3 N_0^{\frac{1}{8}} M^{\frac{1}{8}} \exp(k_7 \frac{z}{2}) \qquad (4)$$

Where N_0 is the number of raindrops per unit volume of air per unit raindrop diameter and k_7 is a constant that essentially describes the rate of change of air density with height. The basic assumption here is that all the droplets fall at the same speed, V, equal to the terminal velocity of the median droplet diameter. This modeling approach was introduced by Georgakakos and Krajewski (1996) , Tsintikidis and Georgakakos (1999) and Lee and Georgakakos (1996).

Stability Analysis

Precipitation Content

We analyze first, the equation of precipitation content denoted by M . The behavior of this variable is set up over a benchmark value (generally obtained from some average) in its region. We denote it by M_s. If M' are the transient over M_s, we write

$$M = M_s + M'$$

The equation for M_s in precipitation content equation is

$$\frac{\partial M_s}{\partial t} = -V\frac{\partial M_s}{\partial z} - w_s\frac{\partial M_s}{\partial z} - M_s\frac{\partial V}{\partial z} + M_s w_s\frac{\partial \ln \rho}{\partial z} +$$

$$k_1 m_s - k_1 a_{th} + 2S_3 k_2 E_{col}\frac{N_0^{0.125}}{H} m_s M_0^{0.875} - \qquad (5)$$

$$0.826\, k_3 N_0^{0.35} |m_s| M_0^{0.65} - k_{55} M_s$$

Substitution of $M = M_s + M'$ in Eqn 1 results into

$$\frac{\partial\left(M_s + M'\right)}{\partial t} = -V\frac{\partial M_s}{\partial z} - w_s\frac{\partial M_s}{\partial z} - w'\frac{\partial M_s}{\partial z} - V\frac{\partial M'}{\partial z} - w_s\frac{\partial M'}{\partial z} -$$
$$w'\frac{\partial M'}{\partial z} - M_s\frac{\partial V}{\partial z} - M'\frac{\partial V}{\partial z} + M_s w_s\frac{\partial \ln\rho}{\partial z} + M_s w'\frac{\partial \ln\rho}{\partial z} + M'w'\frac{\partial \ln\rho}{\partial z}$$
$$+ k_1 m_s + k_1 m' - k_1 a_{th} + 2S_3 k_2 E_{col}\frac{N_0^{0.125}}{H} M_0^{0.875} m_s \qquad (6)$$
$$+ 2S_3 k_2 E_{col}\frac{N_0^{0.125}}{H} M_0^{0.875} m' - 0.826 k_3 N_0^{0.35}|m_s| M_0^{0.65}$$
$$- 0.826 k_3 N_0^{0.35}|m'| M_0^{0.65} - k_{55} M_s - k_{55} M'$$

The equation of transient behaviour then is obtained as

$$\frac{\partial M'}{\partial t} = -V\frac{\partial M'}{\partial z} - w_s\frac{\partial M'}{\partial z} - w'\frac{\partial M'}{\partial z} + M_s w'\frac{\partial \ln\rho}{\partial z} + M'w_s\frac{\partial \ln\rho}{\partial z} +$$
$$M'w'\frac{\partial \ln\rho}{\partial z} + k_1 m' + 2S_3 k_2 E_{col}\frac{N_0^{0.125}}{H} M_0^{0.875} m' -$$
$$0.826\, k_3 N_0^{0.35}|m'| M_0^{0.65} - k_{55} M'$$

We rewrite the above equation in forward difference equation to give

$$M_{i+1}^{n+1} - M_i^{n+1} = -V\frac{\left(M_{i+1}^{n+1} - M_i^{n+1}\right)}{\Delta z}\Delta t - w_s\frac{\left(M_{i+1}^{n+1} - M_i^{n+1}\right)}{\Delta z}\Delta t - w'\frac{\left(M_{i+1}^{n+1} - M_i^{n+1}\right)}{\Delta z}\Delta t$$
$$+ M_s w'\frac{\left(\ln\rho_{i+1}^{n+1} - \ln\rho_i^{n+1}\right)}{\Delta z}\Delta t + M'w_s\frac{\left(\ln\rho_{i+1}^{n+1} - \ln\rho_i^{n+1}\right)}{\Delta z}\Delta t \qquad (7)$$
$$+ k_1 m' + 2S_3 k_2 E_{col}\frac{N_0^{0.125}}{H} M_0^{0.875} m' - 0.826 k_3 N_0^{0.35}|m'| M_0^{0.65} - k_{55} M'$$

Cloud Water Content

Similarly for Cloud water content equation denoted by 'm' we write

$$m = m_s + m'$$

The transient behaviour equation works out to be

$$\frac{\partial\left(m'\right)}{\partial t} = -w_s\frac{\partial m'}{\partial z} - w'\frac{\partial m'}{\partial z} + w'G + m_s w'\frac{\partial \ln\rho}{\partial z}$$
$$+ m'w_s\frac{\partial \ln\rho}{\partial z} + m'w'\frac{\partial \ln\rho}{\partial z} - 2S_3 k_2 E_{col}\frac{N_0^{0.125}}{H} M_0^{0.875} m' \qquad (8)$$
$$+ 0.826\, k_3 N_0^{0.35}|m'| M_0^{0.65} - k_{55} m' - k_1 m'$$

$$m_{i+1}^{n+1} - m_i^{n+1} = -w_s\frac{\left(m_{i+1}^{n+1} - m_i^{n+1}\right)}{\Delta z}\Delta t - w'\frac{\left(m_{i+1}^{n+1} - m_i^{n+1}\right)}{\Delta z}\Delta t$$
$$+ m_s w'\frac{\left(\ln\rho_{i+1}^{n+1} - \ln\rho_i^{n+1}\right)}{\Delta z}\Delta t + m'w_s\frac{\left(\ln\rho_{i+1}^{n+1} - \ln\rho_i^{n+1}\right)}{\Delta z}\Delta t \qquad (9)$$
$$+ w'G - k_1 m' - 2S_3 k_2 E_{col}\frac{N_0^{0.125}}{H} M_0^{0.875} m' +$$
$$0.826\, k_3 N_0^{0.35}|m'| M_0^{0.65} - k_{55} m'$$

Vertical Velocity

The Vertical velocity equation denoted by 'w' gives equation of transient behaviour as

$$\frac{\partial w'}{\partial t} = -w_s\frac{\partial w'}{\partial z} - k_8 M' - k_8 m' - k_5 w_s|w'| - k_5 w'|w_s|$$

we can write above equation in forward difference scheme as

$$w_{i+1}^{'n} - w_i^{'n} = -w_s \frac{\left(w_{i+1}^{'n} - w_i^{'n}\right)}{\Delta z}\Delta t - k_8 M' \Delta t - k_8 m' \Delta t - k_5 w_s |w'| \Delta t - k_5 |w_s| w' \Delta t \quad (10)$$

Equation (7), (9), and (10) are now formatted into the form

$$\begin{bmatrix} M_i^{'n+1} \\ m_i^{'n+1} \\ w_i^{'n+1} \end{bmatrix} = \mathrm{A}^* \begin{bmatrix} M_i^{'n} \\ m_i^{'n} \\ w_i^{'n} \end{bmatrix} \quad (11)$$

Where $A = \begin{bmatrix} (AA+V)*k + BB*\Delta t & CC*\Delta t & DD*\Delta t \\ 0 & AA*k + EE*\Delta t & FF*\Delta t \\ GG*\Delta t & GG*\Delta t & AA*k - HH*\Delta t \end{bmatrix}$

Where $k = \dfrac{\Delta t}{\Delta z}$

In the above

$AA = w_s$

$BB = w_s \dfrac{\partial \ln \rho}{\partial z} - k_{55}$

$CC = k_1 - 2S_3 k_2 E_{col} \dfrac{N_0^{0.125}}{H} M_0^{0.875} - 0.826 k_3 N_0^{0.35} M_0^{0.65}$

$DD = M_s \dfrac{\partial \ln \rho}{\partial z}$

$EE = w_s \dfrac{\partial \ln \rho}{\partial z} - k_1 - k_{55} - 2S_3 k_2 E_{col} \dfrac{N_0^{0.125}}{H} M_0^{0.875} + 0.826 k_3 N_0^{0.35} M_0^{0.65}$

$FF = G - m_s \dfrac{\partial \ln \rho}{\partial z}$

$GG = -k_8$

$HH = k_5 w_s + k_5 |w_s|$

Determinant [A] in the expanded form is

$$(AA)^3\left(\frac{\Delta t}{\Delta z}\right)^3 + V(AA)^2\left(\frac{\Delta t}{\Delta z}\right)^3 - (AA)^2 * HH * \frac{(\Delta t)^3}{(\Delta z)^2} - V * AA * HH * \frac{(\Delta t)^3}{(\Delta z)^2}$$

$$+ (AA)^2 * EE * \frac{(\Delta t)^3}{(\Delta z)^2} + V * AA * EE * \frac{(\Delta t)^3}{(\Delta z)^2} - AA * EE * HH * \frac{(\Delta t)^3}{(\Delta z)} - V * EE * HH * \frac{(\Delta t)^3}{(\Delta z)}$$

$$- V * GG * FF * \frac{(\Delta t)^3}{(\Delta z)} - AA^{**} GG * FF * \frac{(\Delta t)^3}{(\Delta z)} + (AA)^2 * BB * \frac{(\Delta t)^3}{(\Delta z)^2}$$

$$- AA * BB * HH * \frac{(\Delta t)^3}{(\Delta z)} + AA * BB * EE * \frac{(\Delta t)^3}{(\Delta z)} - BB * EE * HH * (\Delta t)^3 - BB * GG * FF * (\Delta t)^3$$

$$+ CC * GG * FF * (\Delta t)^3 - AA * DD * GG * \frac{(\Delta t)^3}{(\Delta z)} - DD * GG * EE * (\Delta t)^3$$

The above expression of det [A] is cubic in Δt, hence we can write as

$$\det[A] \equiv \Delta t^3 \left(\begin{array}{l} \dfrac{(AA)^3 + V*(AA)^2}{\Delta z^3} + \\ \dfrac{(AA)^2*EE + V*AA*EE - (AA)^2*HH - V*AA*HH + (AA)^2*BB}{\Delta z^2} + \\ \dfrac{AA*BB*EE - DD*GG*AA - AA*BB*HH - AA*EE*HH - AA*GG*FF - V*EE*HH - V*GG*FF}{\Delta z} + \\ CC*GG*FF - DD*GG*EE - BB*EE*HH - BB*GG*FF \end{array} \right)$$

The coefficient of $1/\Delta z$ are simplified and denoted by

$$a_0 = (AA)^3 + V*(AA)^2 = w_s^3 + V*w_s^2$$

$$a_1 = (AA)^2 * EE + V*AA*EE - (AA)^2 * HH - V*AA*HH + (AA)^2 * BB$$

$$a_1 = -w_s^2\left(k_5 w_s + k_5|w_s|\right) + V*w_s*\left(k_5 w_s + k_5|w_s|\right) + w_s^2\left(w_s \frac{\partial \ln \rho}{\partial z} - k_{55}\right)$$

$$- V*w_s*\left(w_s \frac{\partial \ln \rho}{\partial z} - k_{55}\right) +$$

$$w_s^2\left[w_s \frac{\partial \ln \rho}{\partial z} - k_1 - k_{55} - 2S_3 k_2 E_{col} \frac{N_0^{0.125}}{H} M_0^{0.875} + 0.826 k_3 N_0^{0.35} M_0^{0.65}\right]$$

$$a_2 = AA*BB*EE - DD*GG*AA - AA*BB*HH - AA*EE*HH - AA*GG*FF - V*EE*HH - V*GG*FF$$

$$a_2 = w_s*\left(w_s \frac{\partial \ln \rho}{\partial z} - k_{55}\right)*\left(w_s \frac{\partial \ln \rho}{\partial z} - k_1 - k_{55} - 2S_3 k_2 E_{col} \frac{N_0^{0.125}}{H} M_0^{0.875} + 0.826 k_3 N_0^{0.35} M_0^{0.65}\right)$$

$$-\left(M_s \frac{\partial \ln \rho}{\partial z}\right)(-k_8)(w_s) - w_s*\left(w_s \frac{\partial \ln \rho}{\partial z} - k_{55}\right)*\left[k_5 w_s + k_5|w_s|\right]$$

$$- w_s\left[w_s \frac{\partial \ln \rho}{\partial z} - k_1 - k_{55} - 2S_3 k_2 E_{col} \frac{N_0^{0.125}}{H} M_0^{0.875} + 0.826 k_3 N_0^{0.35} M_0^{0.65}\right]*\left[k_5 w_s + k_5|w_s|\right]$$

$$- w_s(-k_8)\left(G - m_s \frac{\partial \ln \rho}{\partial z}\right)$$

$$- V*\left[w_s \frac{\partial \ln \rho}{\partial z} - k_1 - k_{55} - 2S_3 k_2 E_{col} \frac{N_0^{0.125}}{H} M_0^{0.875} + 0.826 k_3 N_0^{0.35} M_0^{0.65}\right]*\left[k_5 w_s + k_5|w_s|\right]$$

$$- V*(-k_8)\left(G - m_s \frac{\partial \ln \rho}{\partial z}\right)$$

$$a_3 = CC*GG*FF - DD*GG*EE - BB*EE*HH - BB*GG*FF$$

$$a_3 = \left(w_s \frac{\partial \ln \rho}{\partial z} - k_{55}\right)\left(w_s \frac{\partial \ln \rho}{\partial z} - k_1 - k_{55} - 2S_3 k_2 E_{col} \frac{N_0^{0.125}}{H} M_0^{0.875} + 0.826 k_3 N_0^{0.35} M_0^{0.65}\right)$$

$$\left[k_5 w_s + k_5|w_s|\right]\Delta t^3 - \left[w_s \frac{\partial \ln \rho}{\partial z} - k_{55}\right](-k_8)\left[k_5 w_s + k_5|w_s|\right]$$

$$- \left[k_1 + 2S_3 k_2 E_{col} \frac{N_0^{0.125}}{H} M_0^{0.875} - 0.826 k_3 N_0^{0.35} M_0^{0.65}\right](-k_8)\left[G - m_s \frac{\partial \ln \rho}{\partial z}\right]$$

$$- \left(M_s \frac{\partial \ln \rho}{\partial z}\right)(-k_8)\left(w_s \frac{\partial \ln \rho}{\partial z} - k_1 - k_{55} - 2S_3 k_2 E_{col} \frac{N_0^{0.125}}{H} M_0^{0.875} + 0.826 k_3 N_0^{0.35} M_0^{0.65}\right)$$

Hence, the determinant [A] is recasted in the form

$$\det[A] = \Delta t^3\left[\frac{a_0}{\Delta z^3} + \frac{a_1}{\Delta z^2} + \frac{a_2}{\Delta z} + a_3\right]$$

The stability theory of numerical solution states that the solution will be stable (Jain 1992), if the det[A] ≤

1. The relation det[A] ≤ 1 provides a map between Δt and Δz. One can then find out a range of Δt for a given domain of Δz. This has been worked out for a specified data as given in the table of content and average values as follows

$w_s = 15$

$M_s = 0.04$

$m_s = 0.45$

Where w_s is standard vertical velocity in m/sec in thunderstorm mechanism, M_s is standard precipitation content in g/m3 and m_s is standard water content in air g/m3.

We obtain

a_0=3375.0 , a_1=6744.7, a_2=3115.8, and a_3=0.67

Stability criteria then become

$$\det[A] \equiv \Delta t^3 \left[\frac{3375.0}{\Delta z^3} + \frac{6744.7}{\Delta z^2} + \frac{3115.8}{\Delta z} + 0.67 \right] \leq 1 \qquad (12)$$

Secondly the CFL stability criteria $c\frac{\Delta t}{\Delta z} < 1$, coupled with the above enable us to find the upper value of c for which the choice Δt and Δz is valid. We provide an example for the same. Let

$a = \frac{3375.0}{\Delta z^3}$ $b = \frac{6744.7}{\Delta z^2}$ $c = \frac{3115.8}{\Delta z}$ $d = 0.67$

The following table is developed for $100 \geq \Delta z \geq 2000$, v be the wave velocity for which the specific value of Δt and Δz confine the wave in Δz for motion.

Δz	A	b	c	d	Δt	$v = \frac{\Delta z}{\Delta t}$
25	0.216	10.79	124.6	0.67	0.22	113.6
50	0.027	2.69	62.31	0.67	0.28	178.5
75	0.008	1.19	41.54	0.67	0.32	234.3
85	0.005	0.93	36.65	0.67	0.33	257.5
100	0.003	0.67	31.15	0.67	0.35	285.7
125	0.0017	0.43	24.92	0.67	0.376	332.8
150	0.001	0.29	20.77	0.67	0.39	384.6
300	0.000125	0.0749	10.38	0.67	0.45	666.6
500	0.000027	0.0269	6.23	0.67	0.5	1000

Table 1.

From the above table, the temporal and spatial resolutions are to be chosen for accommodating wave velocity in CFL criterion. For acoustic velocity i.e. 330 m/sec, the spatial and temporal resolution are Δz =125 meters and Δt =0.3 seconds. From above table we can see that as Δt and Δz increases, then $v\frac{\Delta t}{\Delta z}$ is decreasing gradually.

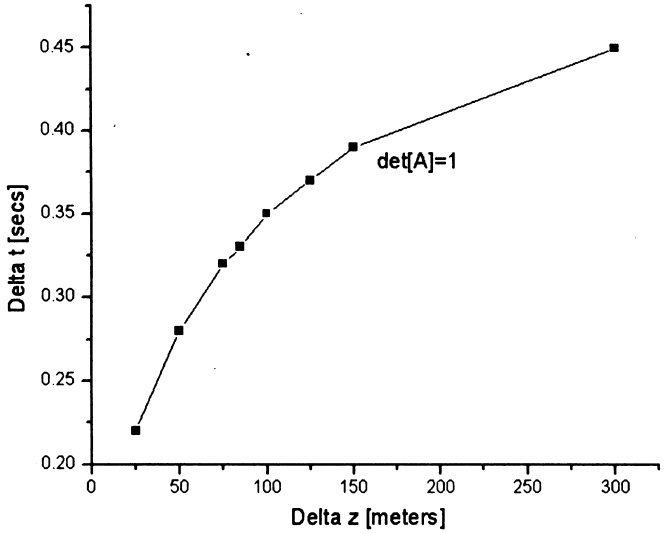

Fig 1.

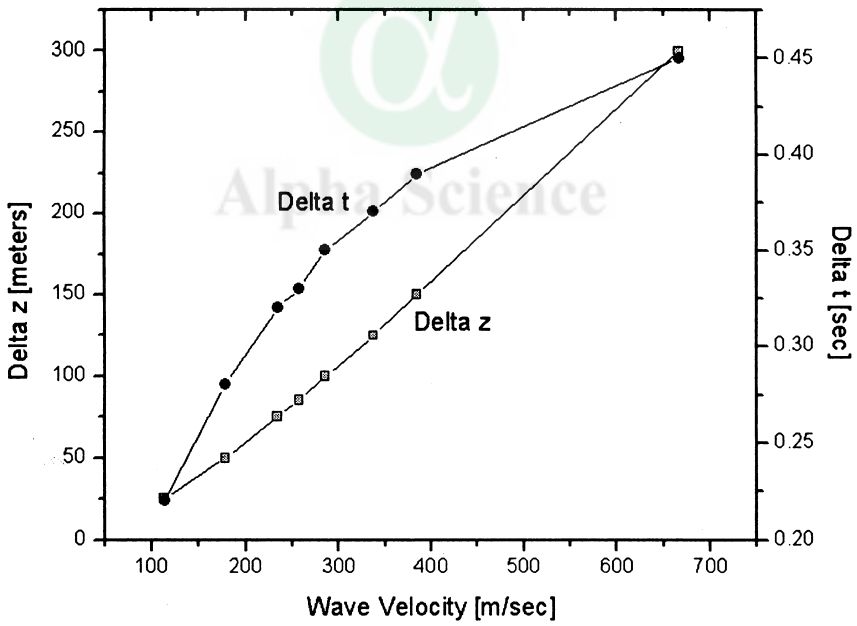

Fig 2.

Conclusion

The stability criteria Eqn [21] provides appropriate wave velocity for specific time and spatial domain Δt and Δz. From Table 1. We can chose wave velocity in CFL condition with specific choises of Δt and Δz. Fig 1. is plotted between Δt and Δz, and found that det[a]=1 increases with increase in both Δt and Δz values. From Fig 2 we can estimate the wave velocity for appropriate Δt and Δz, and hence appropriate

wave velocity should be chosen for thunderstorm mechanism for specific Δt and Δz. Average standard value for vertical velocity, cloud water content and precipitation content is chosen for tropical thunderstorm condition. The choice of Δz also depends upon the accuracy of initial condition for the solution of the problem.

APPENDIX

List of Symbols, Constants, Units, and Typical values

a_{th} Auto conversion threshold, g m^{-3}
AC Auto conversion of cloud, g m^{-3} s^{-1}
B Buoyancy factor (unit less)
CC Collection of cloud, g m^{-3} s^{-1}
$e_s(T)$ Saturation vapor pressure 1704.3 N
E_{col} Collection efficiency, unit less
EP Evaporation of cloud, g m^{-3} s^{-1}
G water vapor gradient g m^{-4}
k_1 Auto conversion coefficient, 10^{-3}
k_2 Constant associated with CC, 6.96×10^{-4} $m^{3.875}$ $g^{-0.875}$ s^{-1}
k_3 Constant associated with EP, 1.93×10^{-6} $m^{3.15}$ $g^{-0.65}$ s^{-1}
k_5 Momentum mixing coefficient, m^{-1}
k_{55} Mass mixing coefficient, s^{-1}
k_7 Constant associated with the existence of water vapor gradient, 1×10^{-4} m^{-1}
k_8 Constant associated with "weight" of M_0 and m, 10^{-2} m^4 g^{-1} s^{-2}
m Cloud density or deficit, g m^{-3}
m_e Environmental vapor saturation deficit, g m^{-3}
M Precipitation density or content, g m^{-3}
M_0 Maximum precipitation density or content g m^{-3}
N_0 Number of raindrops per unit volume per unit diameter, m^{-4}
Q_s Saturation water vapor mixing ratio g Kg^{-1}
P Air pressure N m^{-2}
S_1 5457 if updraft, 5901 if downdraft
S_2 4055 if updraft, 1503 if downdraft
S_3 4352 if updraft, 2040 if downdraft
T Air parcel temperature, 288 K
V Terminal fall velocity of raindrops, m s^{-1}
w Vertical velocity, m s^{-1}
w_{max} Maximum vertical velocity, m s^{-1}
z Vertical coordinate, m
Q_v Potential temperature of air parcel, K
Q_{ve} Potential temperature of environment surrounding air parcel, K
Q' $Q_v - Q_{ve}$, K
ρ Air density, 0.00128 g cm^{-3}

Parameter	Value and unit	Range (%) for sensitivity
k_5	1×10^{-4} m^{-1}	± 50
k_{55}	2×10^{-4} s^{-1}	± 50
a_{th}	1 g m^{-3}	± 50
N_0	9×10^{6} m^{-4}	± 50
E_{col}	0.63	± 50

Table 2. Nominal parameters (Tsintikidis and Georgakakos 1999)

Reference

Georgakakos, K. P., Krajewski W F, 1997: "Statistical-microphysical causes of rainfall variability in the tropics." J. Geophys. Res, 101(D21), 26165-26180.

Gershenfeld, N., 1999: The Nature of Mathematical Modeling, , Cambridge University Press.

Houze, R.A., 1993: Cloud Dynamics. Thunderstorm, Academic Press, 268 pp.

Jain, M.K., 1992: Numerical Methods and analysis.

Kessler, R., 1969: On the Distribution and Continuity of Water Substance in Atmospheric Circulation Meteor, Monogr, No. 32, Amer Meteor. Soc., 84pp.

Sen., P. N., 1991: "Mathematical model for QPF for flood forecasting purposes", Mausam, 44, 19.

Tsintikidis D, and Georgakakos, K. P., 1999: "Microphysical and large-scale dependencies of temporal rainfall variability over a Tropical Ocean.", J. Atmos. Sc., 56, 724-748.

Disaster Management
Editors: N.C. Mahanti et al.

Development of Site-Specific Design Response Spectra for Chennai City

K.Premalatha and R. Uma Maheswari

Division of Soil Mechanics, Anna University, Chennai-25, India

Abstract

Most of the natural disasters dampened the progress and development of infrastructural facilities. Source of these disasters are inevitable but the consequence can be minimized or prevented by proper engineering and adaptation of sustainable development. Bureau of Indian standards revised the earthquake codebook, in that the city Chennai is upgraded to zone III. So the development of Site-Specific Design Response Spectra for Chennai City is highly essential.

One of the most important and most commonly encountered problems in Geotechnical Earthquake Engineering is the evaluation of Ground response. Ground response analysis is used to predict ground surface motions for development of design response spectra. In order to safeguard the structures one should consider the local site conditions while designing earthquake resistant structures. For that we need site-specific response spectrum for a particular site is required. The design response spectrum given in IS code is general this study makes an attempt towards the development of site-specific design response spectra for Chennai city. To develop this design spectra, three analyses namely seismic hazard analysis, ground response analysis and site-specific design spectra are to be done. Seismic hazard analysis is done to calculate the likelihood magnitude from fault details and ground motion characteristics from attenuation relationships. The ground motion characteristics and soil properties are given as input in the ground response analysis. Finally site-specific design response spectra is obtained for a particular location and is compared with IS 1893 (part I) - 2002.

GENERAL

Ground response analyses are used to predict the ground surface motions for development of design response spectra, to determine the earthquake-induced forces that can lead to instability of earth and earth retaining structures. Despite of the fact that seismic waves may travel through tens of kilometers of rock and often less than 100m of soil, the soil plays a very major role in determining the characteristics of the ground surface motion.

Observations made after destructive earthquakes have shown a correlation between damage and local geology with destruction being in general larger on soft soil than hard soil or rock. The characteristics of the ground shaking (amplitude, frequency content, and duration) can be modified by local soils. Some recent earthquakes have dramatically illustrated this effect, through selective damage and collapse of long period buildings located in areas having softer or deeper soils.

Therefore, observed damage patterns and statistical analysis of recorded ground motions at well instrumented soil sites, suggest the seismic design of structures should taken into account the influence of local soils. Here local soils act as a filter and modify the ground motion characteristics.

Need for the study

There is a need to prepare seismic map and Site-Specific Design Spectra, which will enable urban planners to design earthquake resistant structures and strengthen existing unstable structures. Satellite images also showed fault lines running through Tamil Nadu and cracks under the tectonic plateau. As a result the status of Chennai along with major towns in the eastern coast, in terms of their vulnerability has been enhanced. Especially after Chennai experienced tremor on 26th September 2001, following a quake measuring 5.6 on the Richter scale, off the Pondicherry coast, Chennai was among the 28 centers classified under seismic zoneIII along with places like Ahemedabad, Vadodara, Mumbai and Pune. The epicenter of the earthquake

that was experienced on 26th September 2001 was located in the Bay of Bengal, about 50km off the Pondicherry coast. There was no report on the generation of giant sea waves, similar to Tsunamis in the Bay of Bengal, possibly because of the shallow depth of water in the epicentral region close to the coast. Such movement accounting for neotectonic activity in the coastal region may well be the root cause for the earth tremors of September 2001. There is a view that if the epicenter of the earthquake of 2001 had been greater on land and not in the offshore area, there would have been greater damage to structures. These observations show that cities along east coastal zone are moderately vulnerable to earthquake. In order to safeguard the existing structures and new structures, Site-Specific Design Response Spectrum is needed.

Objectives of the study

1. To compute the ground surface motion from bedrock motion for two areas of Chennai city.
2. To determine the response spectrum for that areas.
3. To determine the site-specific design spectrum for that areas and Comparison with IS code.

FAULT AND SOIL DETAILS OF CHENNAI CITY

Precambrian crystalline rocks, patches of gondwanas, Jurassic, cretacious, tertiary and quartenary sediments, largely cover Tamilnadu. The details of faults in and around Chennai are given table1. The thickness of the soil formation ranges from few meters in the south part to as much as 50m in the central and northern parts of Chennai city. This is made up of mainly clays, sand, sandy clays and occasionally gravel zone. Some of the alluvial clays particularly that of the Cooum basin is brownish black in color and very plastic in nature. This alluvium is underlined by the crystalline complex of Charnockite, granite gneiss suited of rock along the eastern and southern marine at depths ranging from 10 to 30m below ground level. In this study two areas in Chennai have been taken for analysis. Perungudi is at the bottom most southern part of Chennai and Adayar is in between center and southern part of Chennai.

TABLE.1 LENGTH, ORIENTATION AND DISTANCE OF FAULT LINES IN AND AROUND CHENNAI

Fault Name	Length (Km)	Orientation (deg)	Distance from Chennai (Kms)
Muttukadu Fault	11.58	55	43
Cheyyar Fault	24.45	59.79	48
Tambaram Fault	12.12	58.78	12
Palar river Fault	39.73	107	27
Kilcheri Fault	42.56	61.72	80
Kaliveli	31.25	55	51

SEISMIC HAZARD ANALYSIS

Deterministic seismic hazard analysis consist of following steps

1. Identification and characterization of all earthquake sources capable of producing significant ground motion at the site.
2. Selection of a source- to-site distance parameter for each source zone.
3. Selection of the controlling earthquake (i.e., the earthquake that is expected to produce the strongest level of shaking), generally expressed in terms of some ground motion parameter, at the site.
4. The hazard at the site is formally defined usually in terms of the ground motions produced at the site by the controlling earthquake. Its characteristics are usually described by one or more ground motion parameters obtained from predictive relationships peak acceleration, peak velocity, and response spectrum ordinates are commonly used to characterize the seismic hazard.

Based on the attenuation relationships moment magnitude, peak ground acceleration, predominant period and duration were calculated. The details of input parameters are shown in table2. The empirical relationships used are

$$M_W = 4.86 + 1.32 \log L$$

$$\text{Log PHA (g)} = b_1 + b_2 + b_2 (M_w - 6)^2 + b_4 R + b \log R + b_6 G_B + b_7 G_C$$

Where

$$R = \sqrt{d^2 + h^2}$$

d = closest distance to the surface projection of the fault in Km

G_B = 0 for site class A
= 1 for site class B
= 0 for site class C

G_C = 0 for site class A
= 0 for site class B
= 1 for site class C

TABLE2 DETAILS OF GROUND MOTION PARAMETERS TO BE DEVELOPED AT CHENNAI

Fault Name	Surface rupture length in km	Moment Magnitude (M_w)	Peak horizontal acceleration (g)	Predominant period (Sec)	Duration (Sec)
Muttukadu	11.58	6.30	0.088	0.33	15.20
Cheyyar	24.45	6.69	0.099		
Tambaram	12.12	6.29	0.235		
Palar river	39.73	6.97	0.179		
Kilcheri	42.56	7.00	0.078		
Kaliveli	31.25	6.83	0.102		

Procedure for parameter modification in order to account for the local Soil

Conditions

1. The seismic hazard analysis will produce parameters that describe a ground motion at the surface of a site with subsurface condition that corresponds to those of the sites in the database from which the predictive relationships was developed.
2. The motion then deconvolved through a soil profile corresponding to the predictive relationship to determine the time history of bedrock motion.
3. The corresponding rock at cropping motion produces the bedrock motion applied at the base of the soil profile at the site of interest.
4. A conventional ground response analysis is then performed to predict the motion at the surface of the soil profile of interest.

GROUND RESPONSE ANALYSIS

Ground response analysis is a one-dimensional analysis of vertically propagating shear waves. The input for this analysis is the time history of motion parameters at the bedrock and the appropriate soil parameters (shear modulus, damping, density and thickness of soil layers). The output includes time history of ground motion parameters at the ground surface, amplification ratio and response spectra. In this study the computer program SHAKE91 was used in the analysis. In shake91 equivalent linear analysis technique is used.

Acceleration Time History At the Bed Rock

Chennai is classified under IIIrd zone. In this study strong motion record such as Taft kern available in the literature was used. The peak ground acceleration (PGA) 0f Chennai city was used from seismic hazard analysis. Based on that analysis bedrock acceleration of 0.18g was used. Predominant period and bracketed duration was 0.33sec and 15.20sec respectively based on attenuation relationships.

Soil parameters

The soil parameters required for the site response analysis are shear modulus, damping characteristics and density. Extensive Geotechnical engineering data is available for soils in Chennai city. The SPT N values for different soil layers and the correlations are shown in table3 was used to estimate the initial shear modulus. Input details for Perungudi and Adayar are given in table4 and table5 respectively.

TABLE 3 EMPIRICAL CORRELATIONS FOR SOIL PROPERTIES

Parameter	Reference
$G=\rho V_S^2$ $V_S=100N^a$(m/sec) for clay and silt $V_S=80N^a$ (m/sec) for fine, med and coarse sand where a=0.33	JRA (1980)

TABLE.4 INPUT SOIL PARAMETERS DETAILS FOR PERUNGUDI

Layer	Material Name	Thickness (m)	Unit Weight KN/m^3	G_{max} Mpa	V_sm/sec
1.	Clayey silty sand	0.8	15	49	179
2.	Clayey silty sand	0.8	12	22.6	136
3.	Clayey sand	0.5	12	17.50	120
4.	Sandy silty clay	1	12	17.9	121
5.	Sandy silty clay	1	13	23.4	133
6.	Soft rock	1.5	19	385.5	450
7.	Hard rock	Infinite	20	1125	750

TABLE .5 INPUT DETAILS FOR ADYAR

Layer	Material Name	Thickness (m)	Unit weight (KN/m^3)	G_{max} Mpa	V_s m/sec
1	Clayey silty sand	0.4	14.8	86.9	240
2	Fine sand	0.9	15.2	93	245
3	Fine to medium sand	0.7	14.6	68.2	214
4	Fine to medium sand	1.0	15.2	84.2	233
5	Medium stiff clay	1.3	15.4	89	238
6	Medium sand	0.3	14.6	65.7	210
7	Stiff to medium stiff clay	1.7	13.8	40.2	169
8	Stiff clay	2.1	14.5	46.3	177
9	Soft sandy clay	0.8	14.5	22	122
10	Fine to medium sand	2.1	14	146	282
11	Soft rock	1.6	19	385	450
12	Hard rock	Infinite	20	1280	800

Results of site response analysis

The results of site response analysis for two areas, using the input from strong motion earthquake record are summarized in table6 and table7. The max acceleration at the ground surface has increased from 0.18g to 0.26g for Perungudi and 0.23g for Adayar. Output results of two areas are shown in table 6and 7 respectively.

Response spectra are a collection of charts depicting maximum response values for any single degree freedom system within the frequency or period range for particular frequency. The analysis has shown that the max spectral velocity for Perungudi is 0.55g and 0.9g for Adayar, indigating that the effect of earthquake characteristics is minimal on the response spectra.

TABLE.6OUTPUT DETAILS OF PERUNGUDI

Depth (m)	Peak Acceleration (g)	Peak Velocity m/sec	Peak Displacement (m)	Peak shear strain m x 10^{-3}	Peak Shear stress Psf
0	0.26	0.177	0.16	0.51	29.3
1.5	0.25	0.177	0.16	3.72	148.04
3	0.23	0.174	0.16	4.14	291.13
4.5	0.21	0.174	0.16	3.39	399.27
6	0.18	0.168	0.16	3.03	523.37

TABLE .7 OUTPUT DETAILS OF ADAYAR

Depth (m)	Acceleration (g)	Velocity (m/sec)	Displacement (m)	Peak shear stress (psf)	Peak shear strain (m)
0	0.23	0.25	0.06	14.71	0.207 (max)
3	0.22	0.25	0.06	100.2	
4.5	0.21	0.25	0.06	300.76	
6	0.19	0.22	0.06	558.31	
8.3	0.18	0.22	0.06	556.898	
9	0.17	0.22	0.06	552.65	
11.14	0.19	0.17	0.06	550.31	
12.68	0.18	0.17	0.06	633.85	

RESPONSE SPECTRA AND DESIGN RESPONSE SPECTRA

Response spectrum analysis became the method of choice for dynamic analysis of structures. It is necessary to define the design spectra where major structures are to be constructed. Chennai city is an area where high rise buildings are planned to be constructed and there is no information about the local site effect on the amplification of earthquake ground motion and the consequences it may has on buildings.

The variability in actual mass and stiffness of buildings from those of the design values, the variability of site parameters and their influence on magnification of earthquake motion and the continuous change in the building dynamic properties such as period due to inelastic response suggest the use of average, smooth and conservative response spectra curves that include local site effects which are known as design spectra. Response spectra for two areas are shown in fig 1 and fig2. Design response spectra for two areas and I.S code design response spectra are shown in fig3.

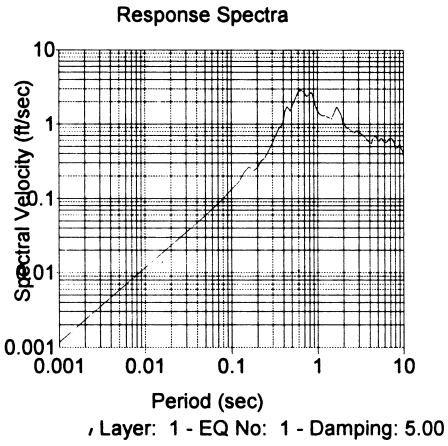

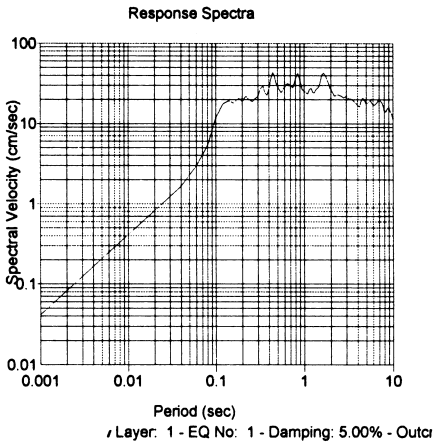

FIG1 SPECTRALVELOCITY FOR ADAYAR

FIG2 SPECTRAL VELOCITY FOR PERUNGUDI

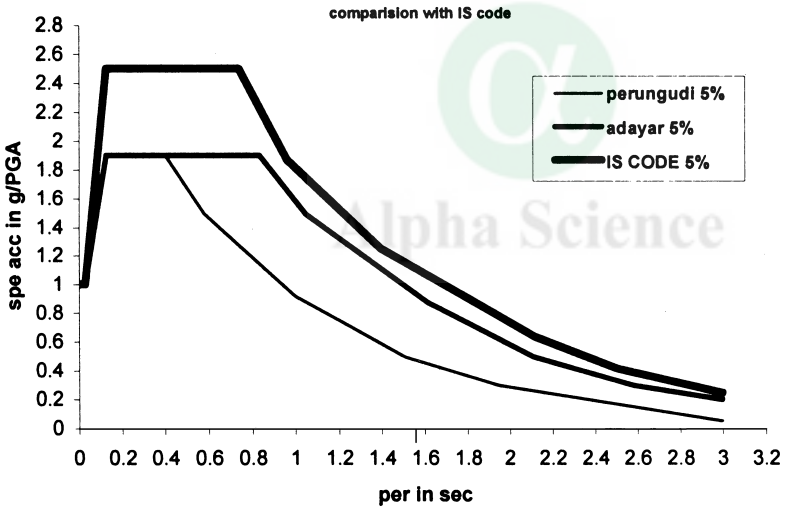

FIG3 DESIGN RESPONSE SPECTRA FOR TWO AREAS AND I.S CODE DESIGN SPECTRA

CONCLUSIONS

Data was collected from available Geotechnical investigations in Chennai to study the local soil conditions on the earthquake ground motion parameter. Soil details, fault details and seismic hazard analysis were outlined. Site response analysis was performed for Perungudi and Adayar areas in Chennai city using the program SHAKE91. The following conclusions are inferred from this study

1. The soft clay deposits over a thickness of 5m in perungudi area have the capability to increase the earthquake motion from 0.18g to 0.26g.

2. The fine to med sand deposits over a thickness of 11m in Adayar area have the capability to increase the earthquake motion from 0.18g to 0.23g
3. The maximum spectral acceleration for perungudi and Adayar is 0.55g and 0.9g respectively.
4. Natural period for Perungudi varies from 0.15 to 0.45sec and for Adayar varies largely from 0.15 sec to 0.9sec.For both the sites spectral acceleration/PGA is 1.9
5. In I.S 1893(PART1)-2002 Spectral acceleration/PGA is 2.5. It is in a higher side, which will increase the equivalent static force.

REFERENCES

Aki.K, (1933), "Local site effects on weak and strong ground motion"*Tectonophysics218*, pp 93-111.

Chen, D., (1984), "Some empirical formulae for hazard analysis in China" *Proceedings of 8th world conference on earthquake engineering*, San Francisco, vol pp 173-180.

Cluff, L.S and cluff, J.L (1984) "Importance of assessing degrees of fault activity for engineering decisions", *Proceedings of 8th world conference on Earthquake Engineering*, san Francisco, vol 2, pp 629-636.

Idriss I.M (1991), "Earthquake ground motions at soft soil sites" *Proceedings of 2nd international conference on recent advances in Geotechnical Earthquake Engineering and soil dynamics*, vol3, pp 2265-2271.

IdrissI.M (1990), "Response of soft soil during earthquakes", proceedings of Bolton seed memorial symposium, pp 273-290.

IS1893 (part1): 2002 "Criteria for earthquake resistant design of structure", *Bureau of Indian standards*, New Delhi.

Lausie,G., Basie, (2003) "Site response at treasure and Yerba Buena islands, California"*Journal of Geotechnical and Geoenvironmental Engineering* pp 415-426.

Newmark, N.M. and hall, W.J (1978)"Development of criteria for earthquake resistant design" *Building practices for disaster mitigation,* Washington, D.C building science series46 pp 209-231.

R.N. Iyengar and S.TG.Raghu ganth (2002) "Strong ground motion at Bhuj city during Kutch earthquake" *Research communications* vol8 pp1366-1372.

Reiter. L (1990) "Earthquake hazard analysis-issues and insights", *Columbia University press*, New York 254 pp.

Tian-Pan Chang and Guey-Kuen Yu (2002) "A study of strong motion response spectrum in west –central Taiwan-tao" vol13 no2 135-152.

R.Uma Maheswari (2003) "Development of Site-Specific Design Response Spectra for Chennai city" M.E. Thesis,Department of civil engineering,Anna university,Chennai

Wells and coppersmith K.J (1994) "New empirical relationships among magnitude, rupture length, rupture width, rupture area and surface displacement" *Bulletin of the seismological society of America* vol84, no4 pp 974-1002.

Yahia E.A mohamedzein, Jamal et.al (2004) "Development of design response spectral for central Khartoum, Sudan"*13th world International conference on Earthquake Engineering.*

Disaster Management
Editors: N.C. Mahanti et al.

Disaster Management and Mitigation by Mathematical Model

Smita Dey, Sutapa Chaudhuri[1] and Moutusi Dey[2]

Ranchi Women's College, Ranchi, India
[1]Department of Atmospheric Science Calcutta University, India
[2]F.M.S, B.H.U

Abstract

Disaster is a misfortune or a calamity which occurs suddenly. Its suddenness as well as its magnitude makes preventive action on large scale difficult. The only way out of this situation is to prepare us to face the disaster and mitigate its effects by timely rescue, relief and rehabilitation operations. In this context, disaster management assumes immense importance.

India is hit by at least one major disaster every year, not to mention the number of small once occurring every now and then. The recent devastating Tsunami has taken lakhs of precious life and loss of agriculture land.

Disaster therefore, needs to be analyzed in terms of the challenges they throw for transforming threats into opportunities. Here in this paper we will discuss whether there is any possibility to predict time and location and intensity of Tsunami to hit Indian Coast.

Introduction

The giant killer waves that swept the coasts of South and Southeast Asia, have added a new word to the global lexicon of disaster: tsunami.The toll of the disaster-which is still to be talled fully-is stupefying; over 300,000 people dead. The economic losses might take years to compute. The truly fearsome aspect of the disaster is that it was totally unpredictable. So little is known about catastrophic phenomena like tsunamis that is virtually impossible for government or populations to take precautionary action.

The 'Tsunami in Japanese, meaning "harbourwaves". But the term "harbor wave inaccurate. A tsunami may be defined as a wave train, or Series of waves of extremely long wavelength and period generated is a body of water by an impulsive disturbance that displaces the water. Tsunami is most often triggered by earthquakes, but they can also be produced by landslides, volcanic eruption, explosions. A suite of numerical simulation codes known collectively as the MOST (Method of splitting Tsunami) model has been implemented and tested. The evaluation of earthquake generated tsunami waves has three distinct stages: generated by earthquakes, transoceanic propagation, and inundation of dry Land. The MOST numerical models computes all three stages providing a complete solution. We shall also discuss project SIFT (Short term Inundation Forecasting For Tsunamis)

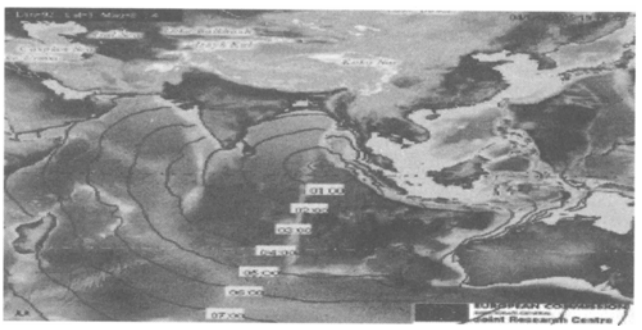

A tsunami is often invested with a great deal of energy by the earthquake or other disturbance that triggers it. The energy in a wave is proportional to the length and the square of the height. This means that high-energy tsunami in the deep ocean may have a height of less than a meter, but a wave length of up to 650 km-in effect, its energy is spread out across the ocean. So it is possible for it to travel vast distances and still wreak havoc when it hits a coast.

Tsunami are shallow-water waves, which means that the ratio between water depth and wavelength is very small. These shallow-water waves move at a speed equal to the square root of the product of the acceleration of gravity(9.8 m/sec/sec) and the water depth.

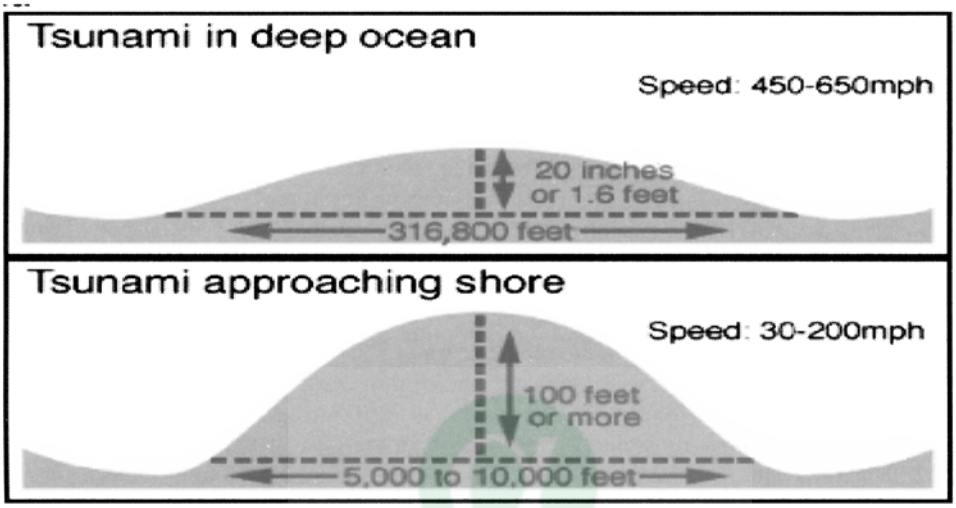

4: In deep water the Tsunami cannot be noticed, but in shallow water it rapidly increases in height as it slows.

The deeper the water ,the faster and shorter the wave is. For example, when the ocean is 20,000 feet deep, a tsunami travels at 550 miles per hour. Another important factor in considering tsunamis is the rate at which they lose energy. Because a wave loses energy at a rate inversely related to its wavelength, tsunamis can travel at high speeds for a long period of time and lose very little energy in the process.

The wave propagation shown in the accompanying map is rough estimation of the projection and radiation of a tsunami caused by earthquake. The wave energy radiates following by simple laws

Of fluid dynamics. The long waves radiate out from the epicenter, and as they approach the coastline, compress, and flatten out to follow the relief of the coast. Small island in the mouth of the delta would not receive as high a wave as the coast proper, as the transferal of energy is still being contained under the sealevel.There would be minor localized waves on shore as the shockwaves of the tsunami passed by. As Adams &Lewis (1979) have shown, these small islands have little modifying effect on the tsunami, they would rather contribute to some measure of noise in the shape of the long wave.

As the long waves bounce off the continental shelf back to sea, the tide appears to recede. Once the long wave reaches the coast and mouth of the delta, the shallows compress the water into a rising wall and the shockwave starts to cause water to move forward. The banks of the delta at the mouth of the estuary will then compress the wave inwards on a horizontal plane by reflection, much the same way normal beach waves break around rocky headlands, and curve inwards to the beach.

The sideways compress, combined with compressing from the decreasing estuary bottom, can only cause an increase in forward momentum and wave height, and thus the tsunami effect is under way. Bearing in mind that the 1998 PNG (Papua New Guinea) tsunami struck a 30 km stretch of coastline, the 40 km wide mouth

of the delta would absorb the entire force of such a wave. This huge body of water will then be compressed into a space only 18 kms wide, and less than 10m in depth. The inertia would carry the wave up several of the river mouths at the reach of the estuary, and would probably extend many kilometers up the river, much like a hurricane driven storm surge. Henry& Murty (1995) describe this effect, known as resonance amplification observation in the March 1964 Alaska Earthquake, where an earthquake generated wave traveled up Barkley Sound on Vancouver Island,65kms inlands to Port Alberni. This compression by the inlet caused a 3-fold amplification of the measured tsunami height at the head of the sound. Places that will receive full force of the tsunami are those areas that lie parallel to the face of the wave. Shorelines that run perpendicular to the face of the wave will experience a less destructive effect of the tsunami, which will have a "shearing" action as it moves along the banks of the rivers upstream.

Description of the Event

The earthquake off the Sumatra cast on 26th December 2004 measured 9.0 on the Richter scale. This is the world's largest earthquake in the last 40 years. Such violet earthquakes are usually of a type known as "megathurst", which are caused by the sinking of the Indian plate under the Burma plate. A megathurst is the name for a violet slippage, which occurs along the fault line. It is estimated that this earthquake caused a slip of 10-20 meters along a 1000 km fault between Sumatra and the Andaman Islands. The vertical displacement by several meters of 100s of cubic kilometers of water triggered a huge shock wave or Tsunami.

The energy released is quite staggering. It is estimated that an equivalent energy of 25,000 Hiroshima bombs was released (500 Megatons of TNT). Perhaps 20% of this energy was transferred to the Tsunami. The energy of the wave then dissipates as 1/R (R=distance) as the Tsunami travels. After 150 km(distance to Sumatra coast) the wave energy equivalent would be as high as 100 tons of TNT per meter. When the wave reaches Srilanka it's energy density would be 10 times lower at roughly 10 tons of TNT per meter of wave. The kinetic energy of the wave was then released through turbulence, friction losses and by sweeping masses of water, boats, vehicles and debris kms in-land.

Tsunami velocity

In deep water Tsunamis travel very fast, but their wavelength is long(some 200 km),and the amplitude is small (0.5 meter)The arrival time in Sri Lanka and India indicates that a large westward velocity should be in the order of 1000km/h. At this latitude the depth is about 6300m and the corresponding velocity is about 900 km/h.In the Bengali gulf the depth is lower, in the order of 2900 m and there the speed should be about 600 km/h After the Maldives islands the dept decreases to 5800 m and therefore the speed should be lower, about 800km/h.

PROPAGATION

A tsunami can propagate long distances before it strikes a shoreline hundreds or thousands of kilometers from the earthquake source. To accurately model tsunami propagation over such large distances, the Earth's curvature should be taken into account. Other factors, such as Carioles forces and dispersion may also be important.

Dispersion changes the wave shape due to slightly different propagation speeds of waves with different frequencies. This effect can be taken into account even without the explicit use of depressive terms in the governing equations; Shuto (1991) suggested that exploiting the numerical dispersion inherent in finite-difference algorithms could simulate this process. This method accounts for dispersive effects, but allows the use of non- dispersive linear or non-linear equations for wave propagation modeling. The MOST propagation model uses a numerical dispersion scheme and the non-linear shallow-water wave equations in spherical coordinates, with Coriolis terms (Murty,1984):

$$(uh)_\lambda + (vh\cos\varphi)_\varphi$$

$$h_t + \frac{(uh)_\lambda}{R\cos\varphi} + \frac{(vh\cos\varphi)_\varphi}{R\cos\varphi} = 0$$

$$u_t + \frac{u u_\lambda}{R\cos\varphi} + \frac{v u_\varphi}{R} + \frac{g h_\lambda}{R\cos\varphi} = \frac{g d_\lambda}{R\cos\varphi} + fv$$

$$v_t + \frac{u v_\lambda}{R\cos\varphi} + \frac{v v_\varphi}{R} + \frac{g h_\varphi}{R} = \frac{g d_\varphi}{R} - fu,$$

Where λ is longitude, φ is latitude, $h = h(\lambda, \varphi, t) + d(\lambda, \varphi, t)$, $h(\lambda, \varphi, t)$ is the amplitude, $d(\lambda, \varphi, t)$ is the undisturbed water depth, $u(\lambda, \varphi, t)$, $v(\lambda, \varphi, t)$ are the depth-averaged velocities in the longitude and latitude directions, respectively, g is the gravity acceleration, f is the Coriolis parameter ($f=2\omega \sin\varphi$), and R is the Earth radius. In the MOST model, these equations are solved numerically using a splitting method similar to that described by Titov (1997)

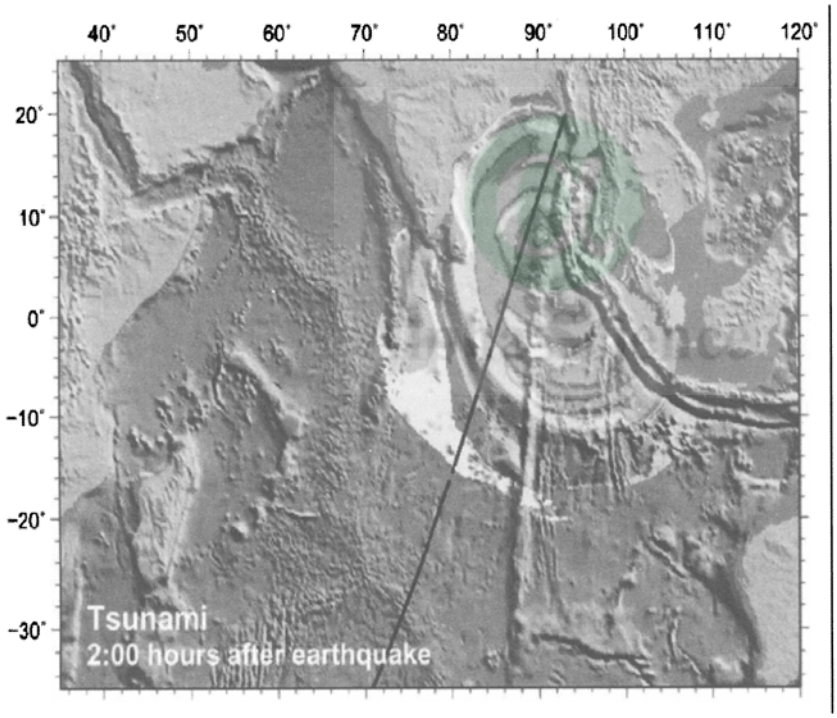

MOST Model results

General comments

The MOST simulation is quite accurate also at distances very far from the epicenter. Particularly good is the time of arrival in Tanzania, predicted with 15 minutes delay, after 9h travel time.

Project sift

Emergency managers and other officials are urgent need of operational tools that will provide short term inundation forecasting for tsunamis as guidance for rapid, critical decisions is which lives and properly are at stake. Recent advances in tsunami measurement and numerical modeling technology can be exploited, combined, and integrated is create an optimal tsunami forecasting system. Even a prefect SIFT capability requires a finite period of time to acquire seismic and tsunami data and execute a forecast algorithm. In emergency management terms, SIFT will be more effective in the case of a distant tsunami than the case of a local tsunami . this can be started in simple mathematical terms as follows:

$$t_F = t_c - (t_M + T/4)$$

When t_F is the time available to acquire adequate tsunami data and provide a forcast before the tsunami strikes, t_M is the tsunami travel time to a measurement station , t_c artrival time at a coastal community and T is the (effective) periods of the first tsunami wave.

$$t_F = (t_c - t_M) - T/4 = t_{CM} - t/4$$

Where t_{CM} is the time difference between arrival of the first wave at the coastal community and the measurement station. Thus, the greater the inequality $t_{CM} > T/4$, the more effective we can expect the forecast to be.

Disaster Mitigation Plan

It may be understood that tsunami hazards, cannot be prevented with our present technological advances but loss of life and property can be reduced appreciably by resorting to preparation and execution of a well thought out Disaster Mitigation Plan. It is to be realised that the degree of loss due to a hazard leading is disaster is very much dependent on the nature of the hazard and the time and place of occurrence.

Two types of Disaster Mitigation plan can be envisaged short term and long term. The plan should concern the regions or places prone to the disaster that did strike the place on earlier occasions and further occurrences are anticipated. The short term plan includes monitoring of hazard related parameters, predicting the time and place of the likely occurrence of the disaster, issuing warning to the people likely to be affected, mobilizing men, materials and other essential facilities arrangement of evaluation and relief. The long term plan which is essentially the community preparedness plan includes risk evaluation of respective disaster prone areas by preparing risk macro and micro-zoning maps, land use mapping utilising information as contained in GIS (geographic Information system) prepared from all available surface and satellite based records. Besides these non – structural measures, proper structural measures like designing buildings and other structures resistant to the hazards and their proper implementation, preparation of proper building codes and its strict of enforcement are some of the tasks that should form a part of the long term plan.

The other as puts disaster mitigation are the Emergency Action Plan (EAP) to be executed by government and non-government orgaanisations during the time and after a disaster strikes a particular region. The EAP should include responsibility of all concerned government machineries in establishing control rooms maintaining communication links for reaching the warning to the people likely to be affected, activating administrative people for arranging evacuation, mobilizing first – air and relief etc.

The important aspect of long term measures is public education ad awareness.

1. Risk assessment is a required step for the adoption of adequate successful disaster reduction policies and measures.
2. Preventive measures are most effective when they involve participation at all levels, from the local community through the national government to the regional and international level.
3. Disaster prevention and preparedness are of primary importance in reducing the need for disaster relief.

References

Murthy T.S (1984) : Storm surges-meteorological ocean tides.Bull212, Fish.Res.Board.Canada.Ottawa.897 pp.

Shuto, N. (1991) : Numerical simulation of tsunamis in Tsunami Hazard.Benard E(ed).Kluwer Academic Publishers.Dordrecht.The Netherlands 171-191

Titov.V.V. and Synolakis(1995) Modelling of breaking and nonbreaking long wave evolution and run up using VTCS-2. J Waterways.Ports.Coastland Ocean Engineering 121(6),308-316

Disaster Management
Editors: N.C. Mahanti et al.

Cyclonic Storm Movement Over Bay of Bangal and its Disaster Preparedness

K.K. Chakrabarty and G.C. Basu

India Meteorological Department, Regional Meteorological Centre, Alipore, Kolkata-700 027, India

Introduction

Cyclonic storms in Bay of Bengal are most hazardous in nature where colossal loss of lives and properties are involved. In cyclonic storm, 80 % of damages including loss of lives are caused by storm-surge. The mechanism involving to the genesis and intensification of such cyclonic disturbances, the changes that occurred in the vertical structure of the atmosphere during the formation and movement of those disturbances are required to be studied in detail. The air-sea interaction during formation and movement of a cyclonic storm is very important throughout its life period. During the course of its movement slowly in the sea, it intensifies and gets energy gradually due to transfer of momentum. The variations in upper wind profile during approaching of a cyclonic storm give good indication for its movement. Climatology of the cyclonic storm study in the Bay of Bengal is very much helpful in prediction of its paths.

So many authors have studied cyclonic storms and its genesis through different methods of diagnostic analysis. To understand the movement and approaching of the cyclonic storm variation of windfield, divergence and pressure fields alongwith satellite imageries and Radar echoes are required to study critically. Srivastava K.B.(2002) has studied the super cyclone October 1999 over Orissa through monitoring its movement and assessment of the intensity of the cyclone by Radar tracking. Basu G.C.(2002) has examined the vertical structures of super cyclone and very severe cyclonic storm in October 1999 over Bay of Bengal associated with divergence at Upper levels and the temperature-entropy (T- Φ) solenoidal field patterns in respect of each cyclonic storm disturbances. To know the nature and behavior of the cyclonic storm, the very genesis and life-cycle of each of the storm is essential.

Genesis of cyclonic storm

Some factors are favourable for cyclogenesis during the formative stage of cyclonic storm

(i) Sea surface temperature (SST) warm and greater than 26 deg Celsius.
(ii) Lower level convergence and upper level divergence
(iii) Positive vorticity at lower level
(iv) Large convective instability through process of CISK(conditionally Instability of second kind)
(v) Sufficient moisture (Large relative humidity) upto mid-troposphere
(vi) Existence of Coriolis parameter which requires for wind turning
(vii) Weak vertical wind shear

Life-cycle of cyclonic storm

Generally most of the cyclonic storms over Indian ocean have life-span for 4 to 5 days. Sometimes, its stay-period over sea are more than one week long with movement in its path following recurves or loops. During the course of its life-cycle, the cyclonic storms come into existence through four stages. These are

(i) Formative stage
(ii) Pre-mature stage
(iii) Mature stage
(iv) Decaying stage

During formative stage, the cloud-masses are unorganised with wind circulation circular or elliptical and the centre of the storm is ill-defined. In this stage, it is unpredictable to say about formation of cyclonic storm. In pre-mature stage, convergence at lower level is noticed and cloud bands are organized, while in mature stage, the cloud-bands in cyclonic storm are more organized with well-defined centre and sometimes with 'Eye' of the cyclone is clearly seen through satellite imagery. The structure of a mature cyclonic storm is given by a schematic diagram in fig 1. and heavy to very heavy rainfall with gale wind speed are experienced during passage of the cyclonic storm. In decaying stage, the cyclonic storm starts losing its intensity and it occur generally at the time of landfall near coast and decay consequently after crossing coast.

History and climatology of the cyclonic storm

By long period (1891-1990) study of cyclonic storm, it is seen that 82% of the cyclonic storms are formed in Bay of Bengal, out of total cyclonic storms over Indian Ocean (Arabian Sea and Bay of Bengal). The decadal analysis and by the monthly distribution of the cyclonic storms during the said period (1891-1990) show the highest frequency of the cyclonic storm in November month and is given by the monthly cyclone distribution table 1. Mondal G. S. (1991) has shown the highest numbers 98 of cyclonic storms crossing Orissa coast amongst all coastal states of India during 1891-2000.

Cyclonic storm movement and track prediction

Prediction of development and movement of cyclonic storm is very important for disaster mitigation and management.

Development and movement of cyclonic storm over ocean is monitored by satellite and radar. The intensity of cyclone over sea is estimated by satellite imageries and the wind speed associated with the system. The intensity of cyclonic storm at various stages are categorized with different 'T' numbers for satellite cloud configurations. These configurations are continuously changing by feeder band clouds and the associated wind speed. In the matured stage of the cyclonic storm, the centre is well–defined with an 'eye' clearly visible and its path of movement are tracked through successive satellite imageries. During tracking of the Orissa super cyclonic storm (fig.2) when it was crossing coast near Paradeep, a clear 'eye' was visible with an estimated wind speed of 260 kmph having organized eye-wall cloud band (fig 3).

Numerical Model

So many numerical models have been developed for cyclone prediction track. Cyclonic storm and it movement by numerical method of 5-generation Meso-scale model (MM5) is used for prediction. A global model of T-80 with nested-grid of high resolution domain (30 Km) is also used for forecasting of the storm. A numerical method by Quasi-Lagrangian model with 1° × 1° (latitude /longitude) resolution is also applied for prediction of cyclonic track. Prasad, K. and others (1997) have suggested Numerical Weather Prediction (NWP) model for operational use in cyclonic track forecasts for limited area.

Storm Surge

At the time of land falls of the cyclonic storm near coasts, storm-surges, gale-wind and torrential rains are experienced which causes great destruction and damages. Most of the damage of 80% in cyclonic storm is due to storm-surge. This storm-surge has three disastrous components. The prediction model of probable maximum storm-surge on the coast have been developed by Das, P.K. (1974) and Ghosh S.K. (1977) on the basis of two-dimensional SPLASH model of Jelesnianski, C.P. (1965). Recent model of storm-surge prediction has been studied by Dube, S.K.(1997) on the bais of empirical method. Nomograms for peak storm-surges are prepared on different parameters like pressure drop, radius of curvature of maximum winds, vector motion of cyclone and offshore bathymetry of the coast near the landfall point of the cyclone. In October 1999 super cyclone crossed coast near Paradeep, Orissa during noon of 29th, inundated coastal area due to storm surge of 5.5 m with loss of human lives about 10000. The probable maximum storm-surge (in mtr) in Indian Coasts (Bay of Bengal & Andaman sea) is given by fig 4.

Vulnerability

Vulnerability assessment (V) in the coastal area due to cyclonic storm is defined as the product of three parameters and is given by

$$V = F \times T \times P$$

Where, 'F' is the frequency of cyclones per year in the coastal area ; 'T' is the coastal topography (i.e height above sea level) and bathymetry; 'P' is population per sq. km. area.

By the study, it reveals that very high-risk area is West Bengal-Bangladesh coasts due to dense population and moderate-risk area is Orissa coast.

Damages associated with cyclonic storm and its preparedness for mitigation

Destruction and damages are caused during the time of landfall of the cyclone near coast with the following reasons

(i) intensity of the cyclonic storm approaching coast
(ii) angle of approach of the cyclonic storm during landfall of cyclone near coast
(iii) radius of curvature of maximum wind associated with the cyclone
(iv) tangential wind vector with associated gale wind
(v) nature of cloud bands associated with the cyclone causing heavy rainfall
(vi) high tidal waves associated with storm-surge at the time of landfall of cyclone

Precautionary measure to mitigate cyclone disaster through preparedness programmes

(i) quick dissemination of cyclone warning massages to the coastal area affected by cyclone
(ii) evacuation of people from the affected area as early as possible to a safer place
(iii) adequate medical facilities and sufficient foods may be kept ready for the affected people
(iv) alternative arrangement may be made for restoration of good communication system in the cyclone affected area
(v) all local bodies / authority may be alerted to meet the situation through awareness programme

Conclusion and remarks

Different methods and models have been developed to predict the movement and intensity of the cyclonic storm still extensive study is required to analyse critically from its formative stage through satellite imageries, radar echoes, synoptic weather charts, as each cyclonic storm has its individual characteristic. The hazardous phenomena of the cyclonic storm cannot be prevented, but it is possible to reduce loss / damages by increasing lead time, accuracy of landfall prediction, timely forecasting its movement, intensity and dissemination of cyclone warning messages.

Some precautionary measures in the possible affected area by cyclonic storm (cyclone prone area) may be taken to reduce damage and loss of lives by preparing adequate number of cyclone shelters in coastal region so that people along with their valuable belongings can be shifted there as soon as cyclone warning messages are received specially when advised for evacuation. Appropriate steps may be taken for mitigation of cyclone disaster through awareness/preparedness programmes.

Acknowledgement

Authors would like to express their thanks to the Director General of Meteorology, India Meteorological Department for pursuing

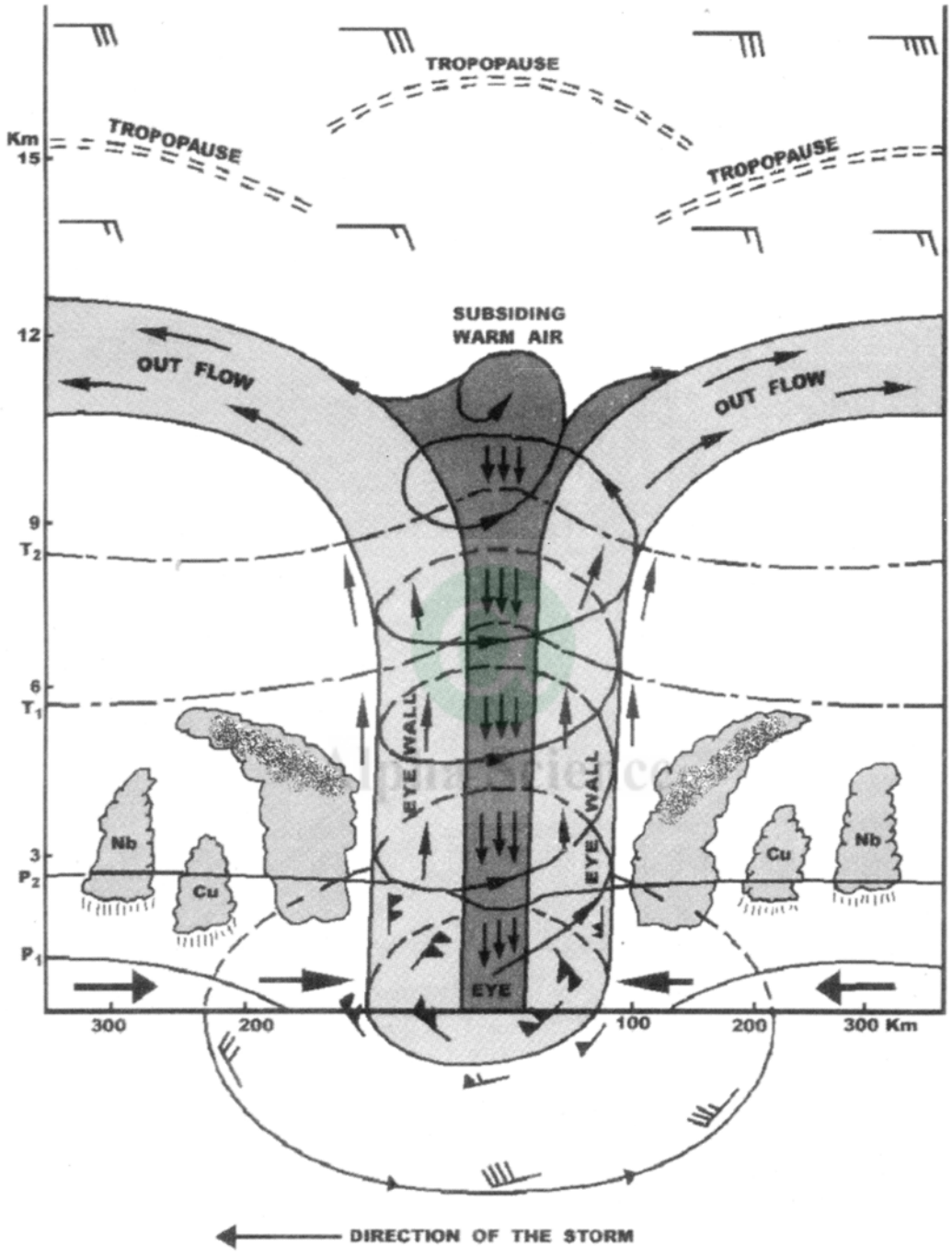

Fig.1 : Schematic diagram of a matured cyclonic storm

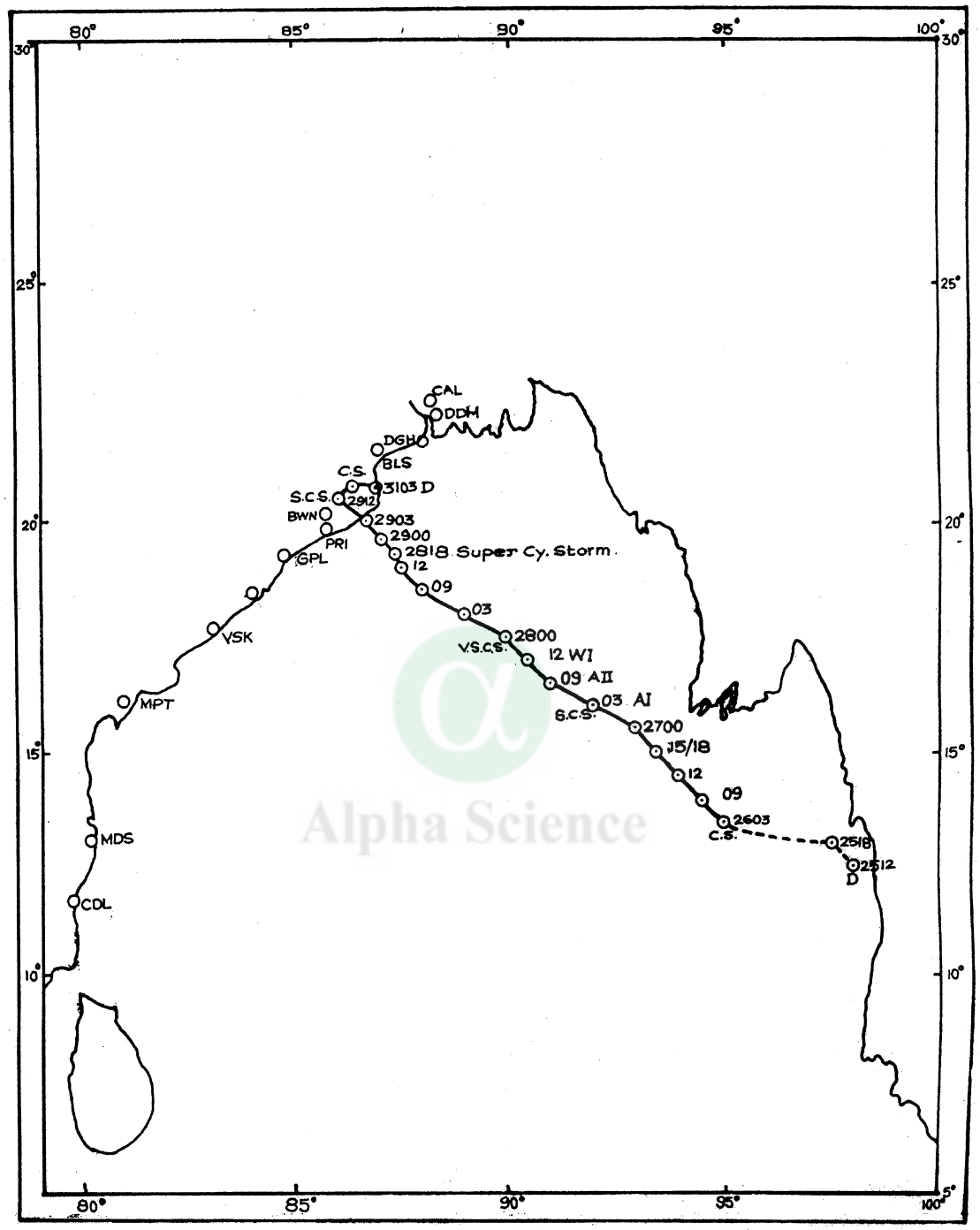

Fig.2 : Track of Orissa Super Cyclone October 25 – 31, 1999

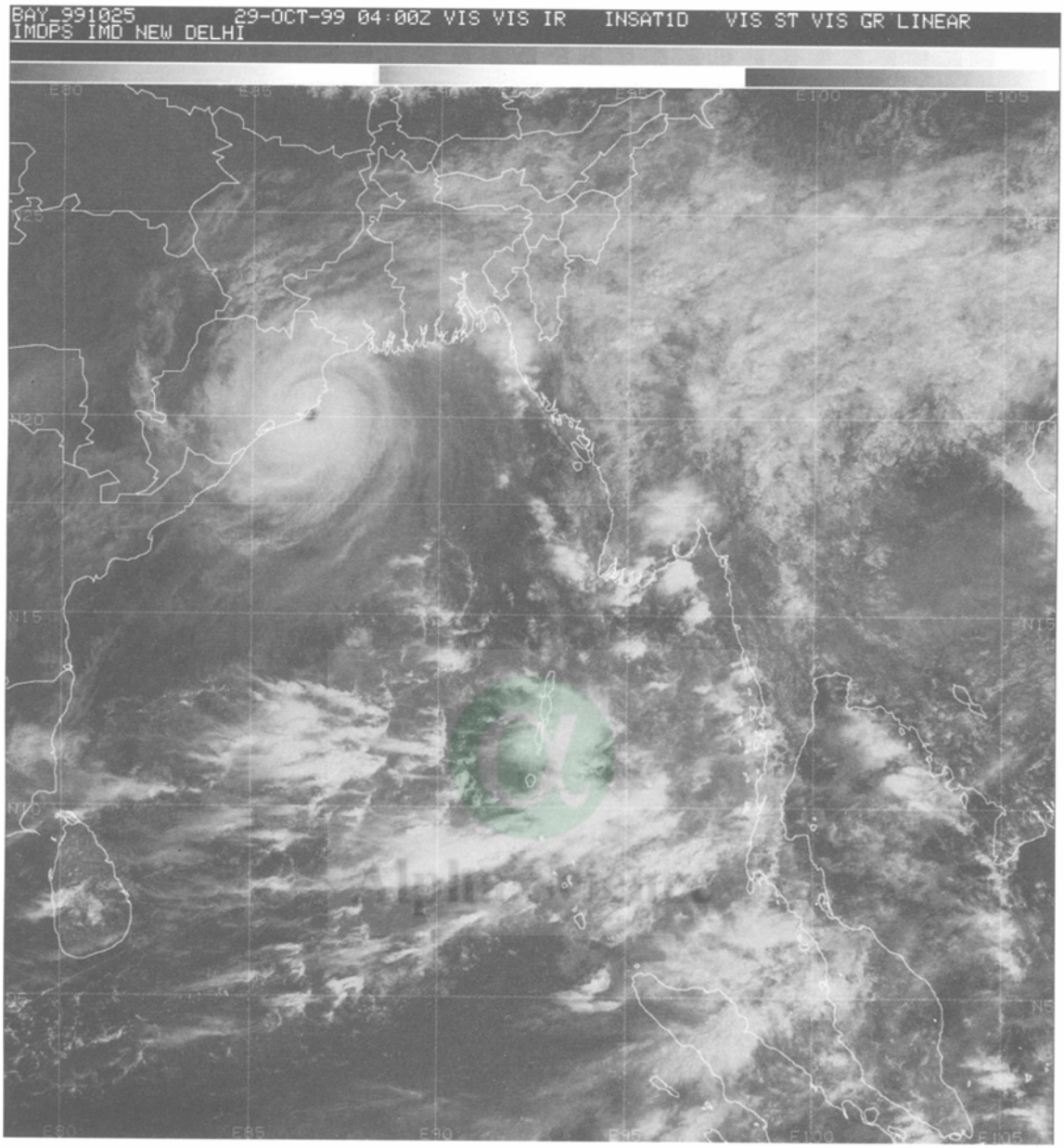

Fig.3 : Satellite imagery of the 'eye' of Orissa Super Cyclone at landfall

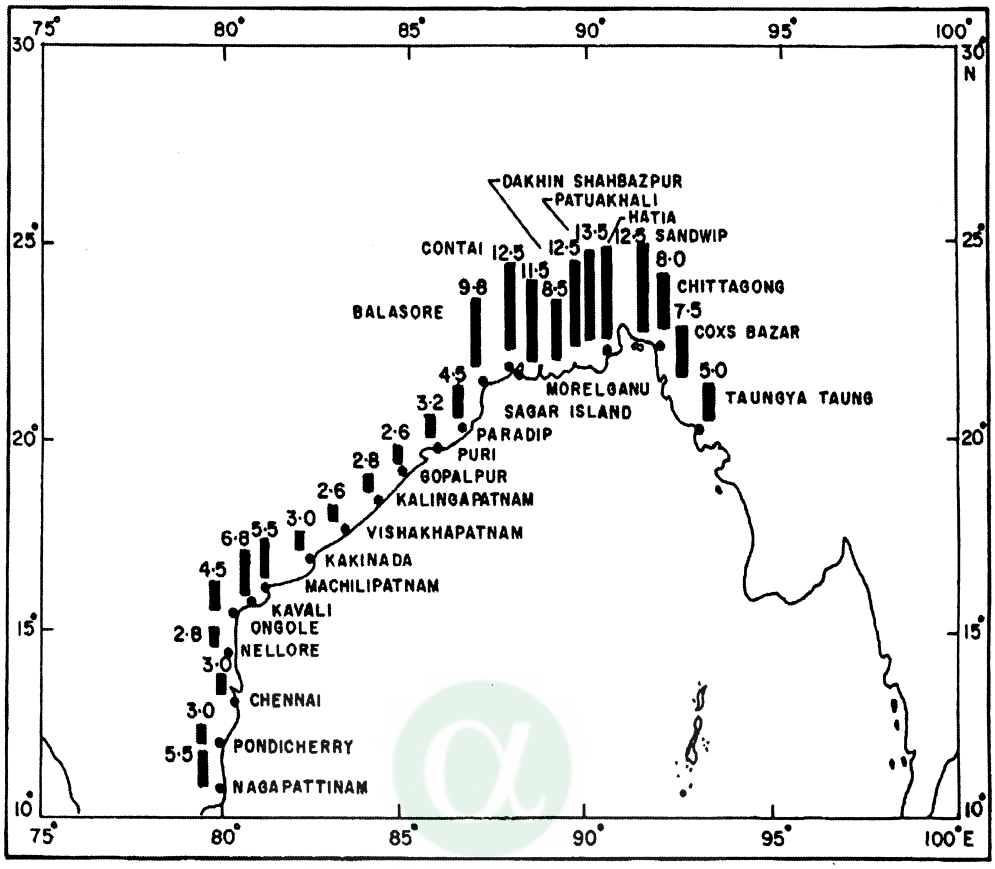

Fig.4 : Maximum probable storm surge at Bay of Bengal coast

References

Basu, G.C.(2002), 'Diagnostic study of vertical structure of a few cyclonic storm disturbances in Bay of Bengal',National symposium and Workshop on Forecasting and Mitigation of Meteorological Disasters: Tropical cyclones, Floods and Droughts, TROPMET-2002, IMS, 12

Das, P.K.(1972), 'Prediction model for storm surges in the Bay of Bengal' Nature, 239, 211-213.

Dubey, S.K. and others(1997), 'Storm surge in the Bay of Bengal and Arabian Sea : The problem and its prediction', Mausam, 48, 283-304.

Ghosh, S.K.(1977), 'Prediction of storm surges on the east coast of India', Ind. Jour. Met. Hydrol. Geophys, 28, 2, 157-168.

IMD (2002), 'Damage potential of Tropical cyclones', ADGM(R), Pune

Kalsi S.R. and others(2004),'A review of different storm surge models and estimated storm surge height in respect of Orissa Super cyclonic storm of 29 October, 1999, IMD, New Delhi

Mondal, G.S.(1991), 'Tropical cyclone and their forecasting and warning systems in North Indian Ocean' , W M O, TD No. 430, Tep. No. 28, WMO, Geneva

Prasad, K. and others (1997), 'Tropical cyclone track prediction by a high resolution limited area model using synthetic observations', Mausam,48, 3, 351-366

Srivastava, K.B. (2002) ' A radar study of Super cyclonic of October, 1999', National Symposium and Workshop on forecasting and mitigation of Meteorological Disasters: Tropical cyclones, Flood. and Droughts, TROPMET-2002, IMS, 34.

Table 1 : Month-wise distribution of cyclonic storm during 1891 – 1990 over Indian Seas (Bay of Bengal and Arabian Sea)

Month	Jan	Feb	Mar	Apr	May	Jun	Jul	Aug	Sep	Oct	Nov	Dec
Total	7	1	4	27	70	57	45	33	47	99	114	47

Disaster Management
Editors: N.C. Mahanti et al.

Satellite Inputs for Better Disaster Management of Tropical Cyclones

P.N. Mahajan

Indian Institute of Tropical Meteorology, Pune-411 008, India

Abstract

Major part of Indian land mass is prone to several natural disasters, with the east and west coast being affected by severe cyclones. In recent years, the focus of disaster management community is increasingly moving on to more effective utilization of emerging technologies such as satellite remote sensing enabling for mitigating potential impacts. In this study, an integrated approach of multiple satellites such as INSAT, METEOSAT, TRMM and IRS-P4 has been made for receiving some signatures of development/dissipation of cyclonic storms over the Indian region. All eight cases of tropical cyclones observed during 1999-2001 over the Arabian Sea and the Bay of Bengal are studied in detail. In this study, characteristic features of very severe cyclonic storm that formed over the Bay of Bengal and hit the Orissa coast during 13-18 October 1999 are highlighted in detail. Here, especially geophysical parameters obtained from our Oceansat-1 satellite are considered to evaluate possible major impacts. It is revealed that an integrated approach of multiple satellites certainly minimizes the response time for public warning and relief operations during the occurrence of such disastrous events. It is obvious that signatures received from satellite inputs will definitely formulate better and effective strategy for disaster management to overcome the public grievances.

Keywords. Multiple satellites, Tropical cyclones, Disaster management

Introduction

Tropical cyclones are most violent natural disasters affecting many countries around the globe causing tremendous loss of lives and property. India is worst affected by tropical cyclones in virtue of its geographical location surrounded by the Arabian Sea, the Bay of Bengal and the south Indian Ocean. Space-based techniques have revolutionized the studies of very severe weather systems such as tropical cyclones over the different parts of the globe. The detail study of tropical cyclone with only conventional data is rather difficult, as very limited data are generally available due to highly destructive nature of cyclonic storm. Satellite remote sensing is the only possible mean to study such weather systems in detail. Frequent visible and infrared pictures help for monitoring the intensity and landfall points resulting in saving of human life and property. However, more accurate quantitative estimation of geophysical parameters such as surface winds, sea surface temperatures, integrated water vapour and cloud liquid water content are made available by passive microwave sensors onboard various non-geostationary satellites like Special Sensor Microwave/Imager (SSM/I) onboard DMSP, Multi-channel Scanning Microwave Radiometer (MSMR) onboard IRS-P4 (Oceansat-1) and TRMM Microwave Imager (TMI) onboard the TRMM (Tropical Rainfall Measuring Mission) satellite.

IRS-P4 satellite provides measurements of brightness temperatures at 6.6, 10.65, 18 and 21 GHz frequencies in both horizontal and vertical polarization. The utility of 10.65 GHz channels in both polarizations overcomes the contamination problem in the ocean surface brightness temperature caused by light precipitation and water vapour in propagation path (Connor and Chang 2000). The presence of 10 GHz channel in MSMR relaxes the rain flagging definitions generally used to determine precipitation interference criteria for the wind retrieval. This allows more accurate wind speed retrievals over the wide range of precipitation conditions. Moreover, 10 GHz channel also offers a better rain retrivals as it can penetrate through the entire column of the cloud (Mugnai et al. 1993).

The operational geophysical parameters available from MSMR measurements are Sea Surface Winds (SSW), Sea Surface Temperature (SST), Integrated Water Vapour (IWV) and Cloud Liquid Water (CLW) content over the global oceans (Gohil et al. 2000). MSMR derived geophysical parameters except cloud liquid water content are well compared with similar products from other satellites (Varma et al. 2002a). The

operational MSMR parameters are very often flagged off in very severe weather conditions like tropical cyclones. To overcome this problem and to take the advantage of 10 GHz channels mentioned above, Varma et al. (2002b) developed new algorithms by regression using concurrent values of geophysical parameters, like SSW, SST, IWV and CLW from TMI and brightness temperature values from MSMR. Their algorithm was found to work reasonably well for all parameters, and particularly, worked extremely well as compared to operational algorithm for CLW (Varma et al 2002b, 2003).

Data

IRS-P4 MSMR data is obtained from the National Remote Sensing Agency, Hyderabad. It is well known that before supplying of this data to any organization it is first scrutinized and validated taking co-operation from different agencies and research institutes such as Space Applications Centre (SAC), Ahmedabad; India Meteorological Department (IMD), New Delhi; Indian Institute of Science (IISc), Bangalore; National Centre for Medium Range Weather Forecasting (NCMRWF), New Delhi; CSIR Centre for Mathematical Modelling and Computer Simulation (C-MACS), Bangalore; National Institute of Oceanography (NIO), Goa; National Institute of Ocean Technology (NIOT), Chennai; National Centre of Antarctic and Ocean Research (NCAOR), Goa; National Physical and Oceanographic Laboratory (NPOL), Kochi etc. Different institutes and organizations for their studies use these data sets.

The data products are validated with in situ observations from moored buoys and ships. The comparison of all geophysical parameters agreed well with in situ and analysed fields except CLW, because for the validation of CLW synchronized aircraft observations are required which could not be done due to technical problems. MSMR grid data for sea surface temperature, sea surface wind speed, integrated water vapour and cloud liquid water content was utilized for monitoring the variability of geophysical parameters for the complete life cycle of tropical cyclone formed during 13-18 October 1999.

Synoptic situation and Methodology

Very severe tropical cyclone was formed over the Bay of Bengal during 13-18 October 1999. Figure 1 shows track of tropical cyclone obtained from India Meteorological Department. The positions of the systems at 0300 and 1200 UTC are marked in the diagram. This tropical cyclone is studied with respect to IRS-P4 derived geophysical parameters and INSAT observed cloud imageries. Figure 2 depicts INSAT visible imageries at 06 UTC for the complete life cycle of tropical cyclone during 13-18 October 1999. Initially, a low was formed over SE Bay of Bengal on 13 October 1999. It became well marked low (WML) on 14 October 1999 and then intensified into depression (13.5° N / 92.5 E°) on 15 October. It further intensified suddenly into cyclonic storm and severe cyclonic storm (16.0° N / 88.5° E) on 16 October. Keeping same northwest track of the system, it later strengthened into very severe cyclonic storm (18.6° N / 86.0° E) on 17 October. It was in the same form of very severe cyclonic storm, while hitting the coast of Orissa

IRS-P4 derived data for ascending and descending passes are combined for each day during the life period of tropical cyclone and met-ocean parameters are plotted on the maps using the GrADs software of the Centre for Ocean-Land-Atmosphere (COLA), USA. The domain of the study is 60° E to 100° E and Equator to 30°N. IRS-P4 derived data for ascending and descending passes are combined for each day during the life period of tropical cyclone and met-ocean parameters are plotted on the maps using the GrADs software of the Centre for Ocean-Land-Atmosphere (COLA), USA. The geophysical parameters viz. SST, SSW, IWV and CLW are presented on the maps for the period 13-18 October 1999 i.e. three days before the formation of tropical cyclone and one day after its landfall (Figs. 3-6). Some pockets in the figures are data void because, the MSMR data are available over the oceanic region 200 km away from the coast and the sea surface parameters were not retrieved under precipitation condition (Gohil et al., 2000). Similarly, the data suspected to be erroneous are not considered in the analysis. The day-to-day variation of the geophysical parameters is described below.

Results and Discussion

IRS-P4 derived geophysical parameters viz SST, SSW, IWV and CLW are analysed and produced in figures 3-6. Their variations from initial stage of development till attaining the stage of very severe cyclonic storm are highlighted in Table 1.

Sea surface temperature

IRS-P4 derived SST values are shown in Fig.3. Here, variations in sea surface temperatures during each stage of tropical cyclone i.e. genesis, development, mature stage and hitting the Orissa coast of India are highlighted. On 13th and 14th October, the oceanic region in the southeast Bay of Bengal, where low and well marked low were formed was associated with sea surface temperature of the order of 28°-29° C. From 15th October till it's hitting the coast of Orissa, the track of the system was in northwest direction. On 15th October when depression was formed, the SSTs were of the order of 29° C and further during the development of cyclone and very severe cyclone the SSTs range was of the order of 29°-30° C. These SSTs decreased further to 26°-27° C on 18th October when the cyclonic storm dissipated to depression.

Sea surface winds

The SSW values are depicted in Fig.4. During the process of development of low and well marked low on 13th and 14th October, sea surface wind speed was of the order of 8-10 mps. On 15th October, SSWs to the south of low-pressure area were strengthened to 12-14 mps, favoring to the formation of depression. On 16th and 17th October when depression was intensified into cyclonic storm and very severe cyclonic storm SSWs were increased from 18 to 22 mps. It was noticed that there was slight decrease in wind speed while hitting the coast of India and it was of the order of 18-20 mps. Arial coverage and variations in wind speed with respect to the positions of the different stages of tropical cyclone can be seen in Fig.4.

Integrated water vapour

Like sea surface winds and sea surface temperatures, the IWV data are available near the core location of the system. (Fig.5). Integrated water vapour of the order of 6-7 gm/cm^2 was continuously persisting during all the stages of development of low into very severe tropical cyclone. However, while hitting the Orissa coast the values of IWV slightly decreased and they were of the order of 5-6 gm/cm^2.

Cloud liquid water content

Figure 6 shows CLW distribution over the Bay of Bengal during the complete life period of tropical cyclone i.e. during 13-18 October 1999. The magnitude of CLW may not be that accurate as described earlier. Apart from the accuracy of the numerical values, it is observed that the CLW values increased systematically from 13 October onwards during each stage of enhancement of system. During the stages of low and well marked low, cloud liquid water content was varying between 5-to15 mg/cm^2. With the intensification of well marked low into depression the values of CLW increased in the range of 25-30 mg/cm^2 i.e. on 15 October. It further increased in the range of 30-35 mg/cm^2, when depression was intensified into cyclonic storm. During the development very severe cyclonic storm the CLW values reached to its maximum limit of the order of 40-45 mg/cm^2. But while entering in the land of Orissa coast these values suddenly decreased and come down to 5 mg/ cm^2.

Satellite inputs and mitigation of disastrous event

IRS-P4 derived SST shows values 28°-29° C over the southeast Bay of Bengal during 13 and 14 October 1999. Later, it was 29° C and more till low pressure system develops into very severe tropical cyclone. This persistence of high SST remained almost throughout the life period of tropical cyclone. Prevalence of high SST is one of the favourable conditions for the formation tropical cyclone over the Indian region. That criterion was fully satisfied over the Bay of Bengal during above period. Moreover, sea surface wind speed started increasing continuously during each stage of development of tropical cyclone. During the formation

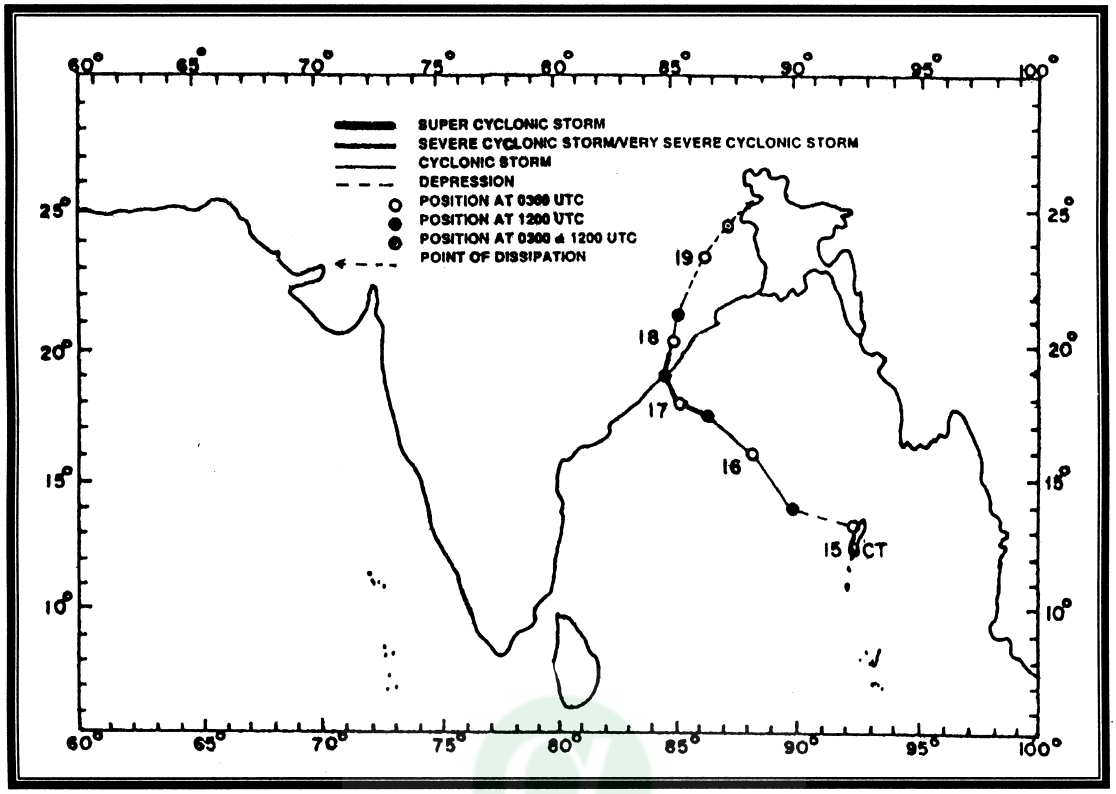

Fig. 1. Track of the cyclonic storm, October 1999

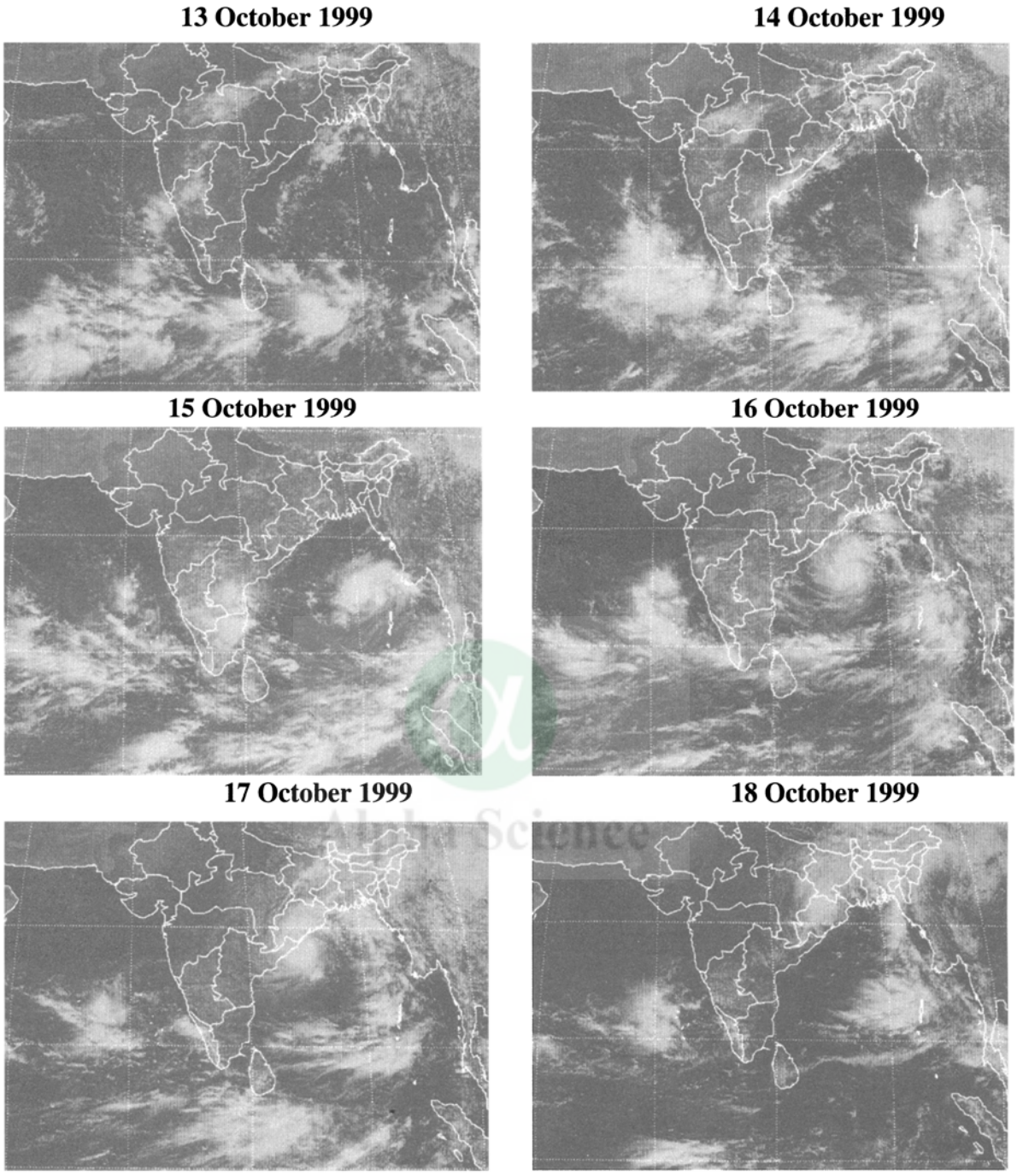

Fig. 2. INSAT visible imagery during 13-18 October 1999

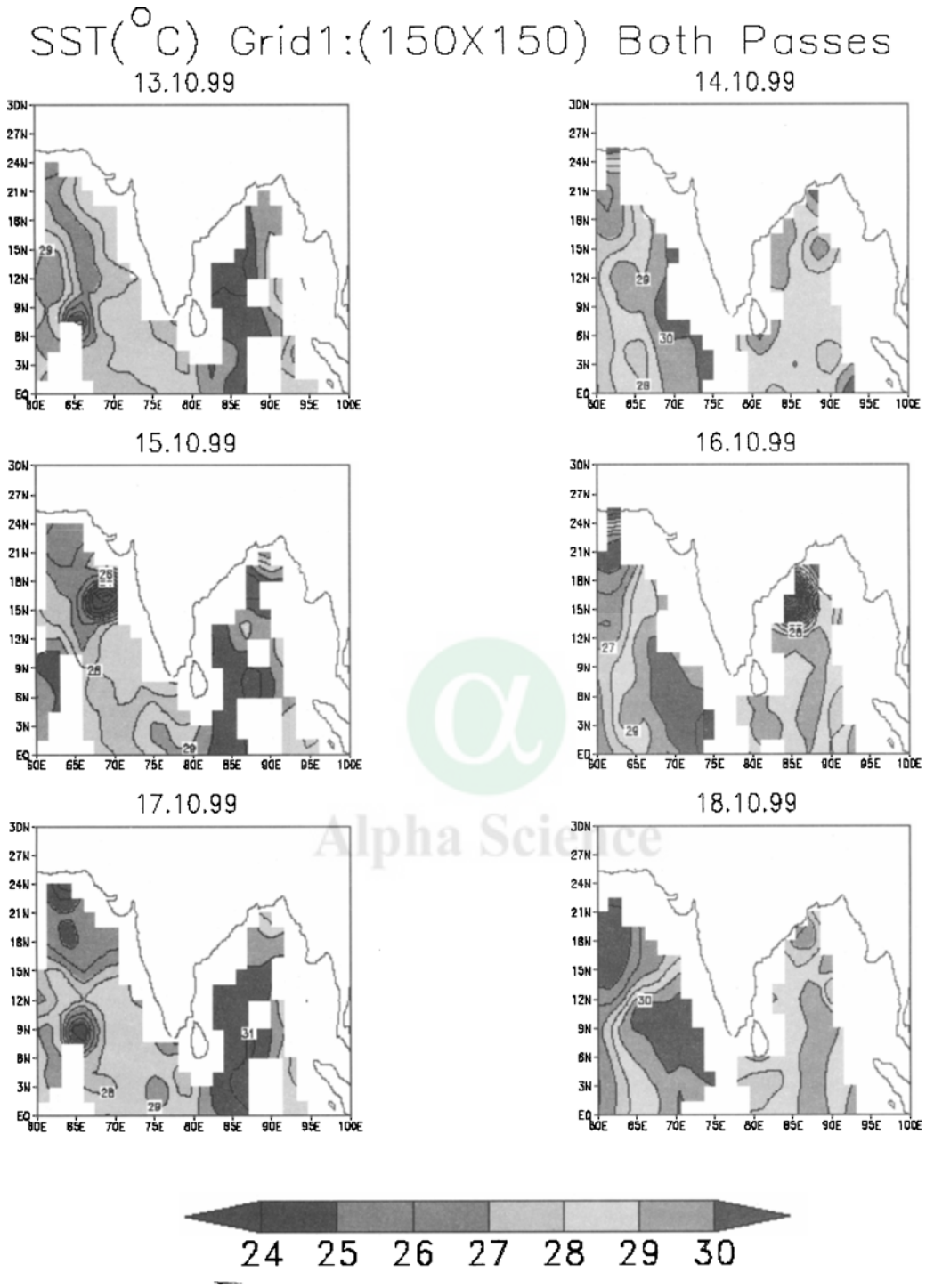

Fig. 3. IRS-P4 derived SST (°C) distribution during 13-18 October 1999

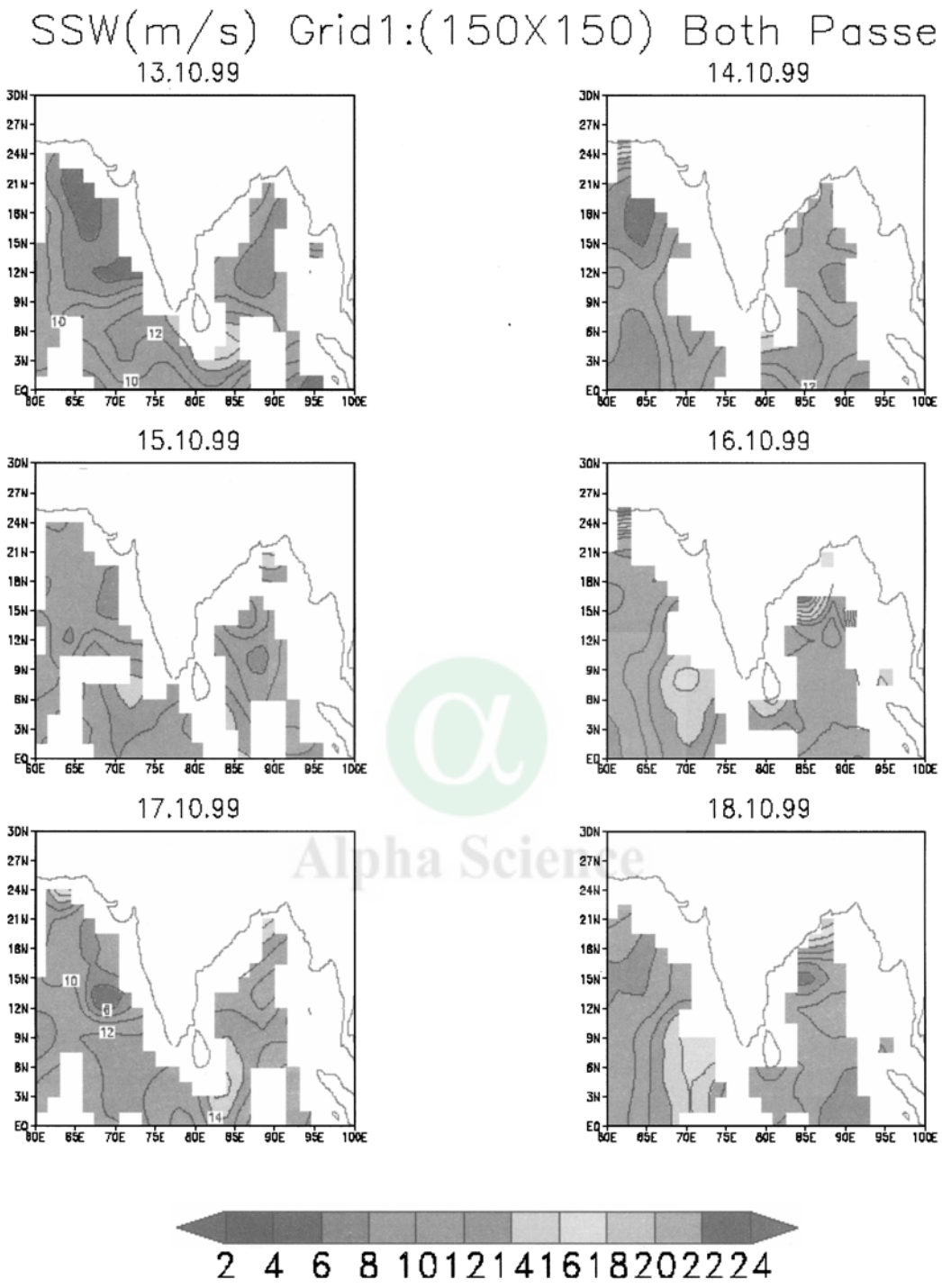

Fig. 4. IRS-P4 derived SSW (m/s) distribution during 13-18 October 1999

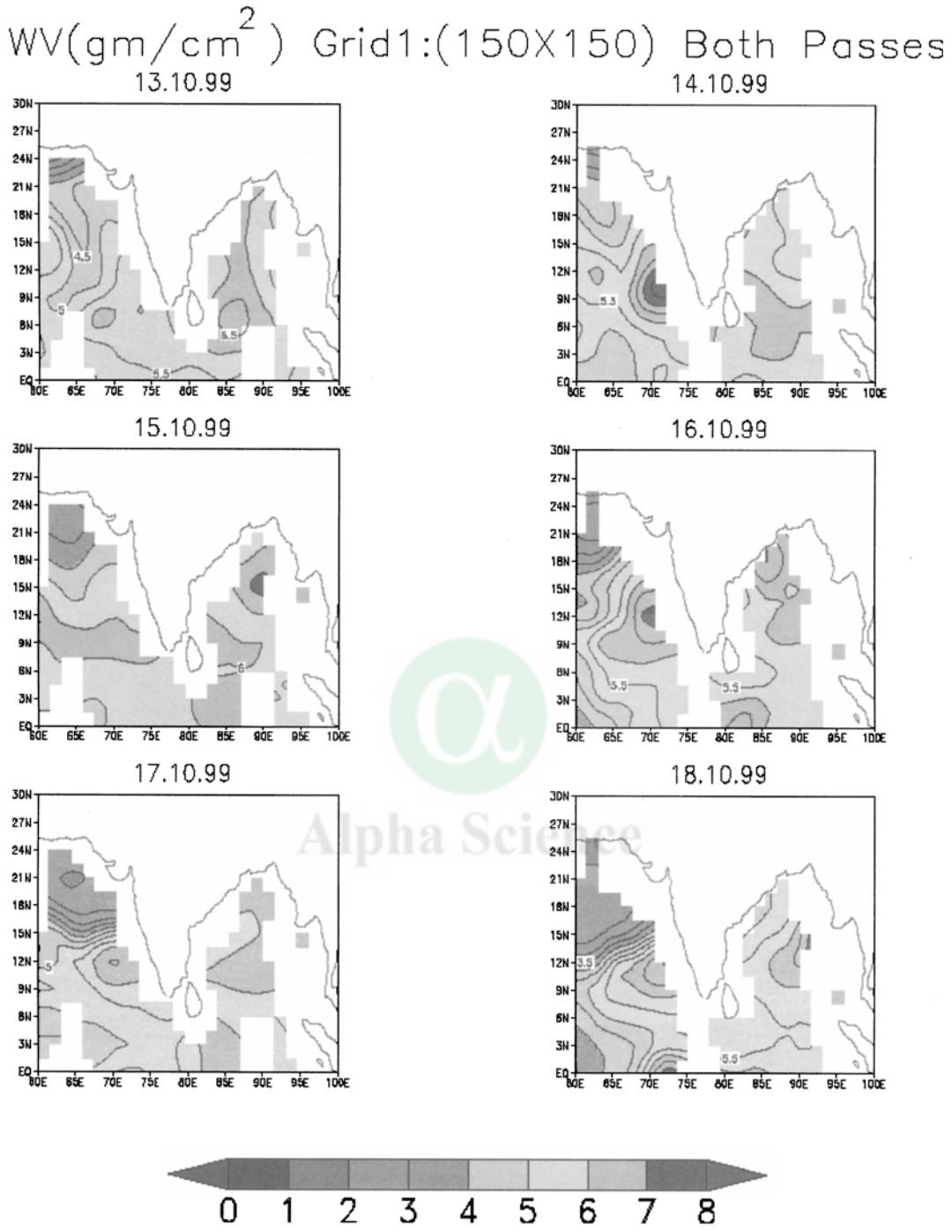

Fig. 5. IRS-P4 derived IWV (gm/cm^2) distribution during 13-18 October 1999

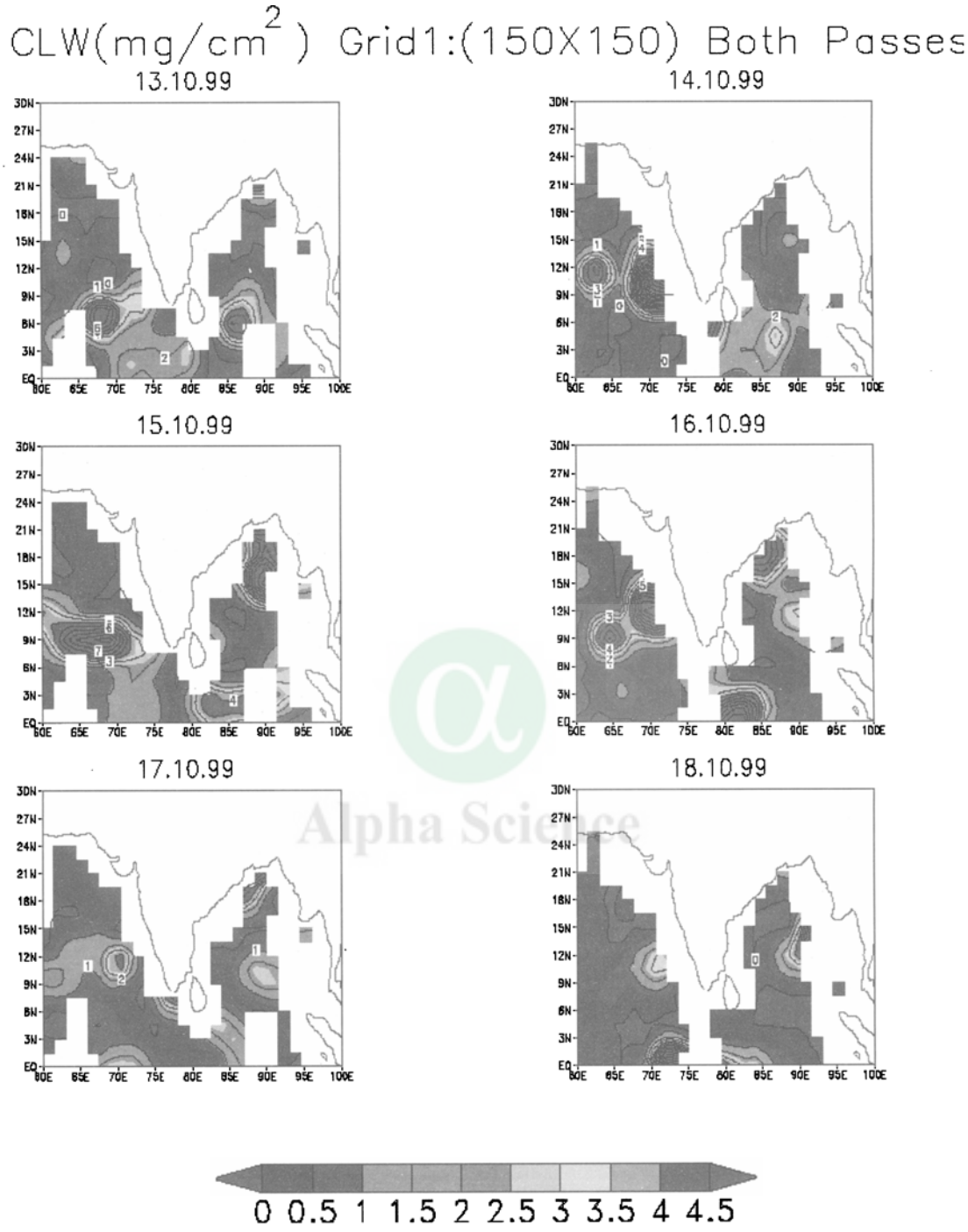

Fig. 6. IRS-P4 derived CLW (mg/cm^2) distribution during 13-18 October 1999

of low and well-marked low SSWs reached up to 10 mps. Later, during depression it intensified up to 12 mps. Further, during the formation of tropical cyclone it reached suddenly up **to 20 mps** and at the time of very severe tropical cyclone it achieved maximum value of 22 mps. Later, wind speed reduced due to frictional forcing of land while crossing the coast of Orissa. This precursor is very important because whenever any tropical cyclone is likely to hit the coast then one should have the idea about how much maximum surface wind speed likely to cross the coast. Accordingly, how much seawater is likely to enter in the land and with what intensity, this can be found out by computing wind stress at the time of landfall. Considering occurrence of low and high tide situations over the region of entrance of tropical cyclone, one can get signal of its major impact. This will certainly help to mitigate adverse effect of tropical cyclone, especially along the coast of India, where it is likely to hit.

In a similar manner, cloud liquid water content that was increasing in each stage of development of tropical cyclone will give idea about how much maximum rain is likely to occur in short duration of time, while hitting the coast. As already we have noticed that cloud liquid water content started increasing from 5 mg/cm² from the initial stage of development of tropical cyclone to 4.5 mg/cm² at the stage of very severe tropical cyclone. This will certainly give signatures about how much heavy rain is likely to pour down in different areas of tropical cyclone. Again, these signals will further mitigate devastation by warning associated people to take care from very heavy rainfall. Moreover, wind fields obtained from CMVs (Cloud Motion Vectors) and WVWVs (Water Vapour Wind Vectors) from our geostationary satellites like INSAT and METEOSAT will again alert the people from damaging their property in the area of tropical cyclone.

Conclusion

Remote sensing observations from Oceansat-1 satellite and CMVs & WVWVs from INSAT and METEOSAT satellites can be used along with conventional data for mitigating severe impact of tropical cyclones over the Indian region.

Acknowledgement

The author is grateful to Dr.G.B.Pant, Director, IITM and Shri P. Seetaramayya, Head, Forecasting Research Division for their encouragement during the period of the study.

Table 1

Date	13	14	15	16	17	18
Stage	Low	Low	D	CS/SCS	VSCS	CS
Location Lat (°N)/Long (°E)	-	-	13.5/92.5	16.0/88.5	18.6/86.0	20.5/85.0
SSW (m/s)	6-8	8-10	10-12	12-22	12-14	12-18
SST (°C)	29-30	26-29	29-30	25-29	29-30	26-28
IWV (gm/cm^2)	5.5-6	5-5.5	6.5-7.5	5.5-6	5.5	4-5
CLW (mg/cm^2)	5-45	5-15	15-40	20-45	15-45	5-15

References

Connor, L. N., and Chang, P.S., 2000, Ocean surface wind retrievals using TRMM Microwave imager. IEEE, *Transaction on Geosciences and Remote Sensing,* 38, 2010-2016.

Gohil, B. S., Mathur, A. K., and Varma, A. K., 2000, Geophysical parameters retrieval over ocean from IRS-P4 MSMR. *Proceeding of Pacific Ocean Remote Sensing Conference,* 5-8 Dec, 2000 at NIO, Goa, India, 207-211.

Mugnai, A., Smith, E. A., and Tripoli, G. J., 1993, Foundation of statistical-physical precipitation retrieval from passive microwave measurements. Part II: Emission source and weighting functions properties of a time-dependent cloud-radiation model. *Journal of Applied Meteorology,* **32**, 17-39.

Varma, A. K., Gairola, R. M., Mathur, A. K., Gohil, B. S., and Agarwal, V. K., 2002a, Intercomparison of IRS-P4 MSMR derived geophysical products with DMSP-SSM/I and TRMM-TMI finished products. *Proceeding of Indian Academy of Sciences – Earth and Planetary Sciences,* **111**, 247-256.

Varma, A. K., Gairola, R. M., Pokhrel, S., Gohil, B. S., and Agarwal, V. K., 2002b, An empirical approach for retrieval of geophysical parameters from IRS-P4 MSMR, *Proceeding of ISPRS Commission VII International Symposium on Resource and Environmental Monitoring,* NRSA, Hyderabad, India, 3-6 December, edited by R. R. Navalgund, R. S. Nayak, R. Sudarshana, R. Nagaraja and S. Ravindran, 187-192.

Varma, A. K., Pokhrel, S., Gairola, R. M., and Agarwal, V. K., 2003, An empirical algorithm to estimate cloud liquid water from MSMR and its utilization in rain identification. *IEEE Transactions on Geosciences and Remote Sensing,* **41**, 1853-1858.

Disaster Management
Editors: N.C. Mahanti et al.

Natural Hazard Assessment Through Remote Sensing and GIS– a case study from Sikkim State, India

Akhouri Pramod Krishna, N. Kumar[1] and M.S. Nathawat

Department of Remote Sensing, Birla Institute of Technology (BIT), Mesra, Ranchi-835 215, India
[1]Department of Geology, St. Xavier's College, Ranchi-834 001, India

Abstract

This study has attempted to look into the significant geo-environmental implications of natural hazards in the mountain environment. Natural hazard is an event that puts something or someone in a position of risk as a natural phenomenon occurring in proximity and pose a threat to people, structures and economic assets caused by geological, hydrological, meteorological and biological conditions or processes in the natural environment. Singtam-Rangpo area falling in the state of Sikkim was investigated with typical terrain conditions of the Indian Himalayan Region (IHR). This took into account the assessment of host geo-environmental set-up of the study area with respect to pertinent natural hazards in the region.

This was facilitated through a combination of conventional methods as well as modern methods of geo-informatics such as Remote Sensing (RS) and Geographical Information System (GIS). Field and laboratory investigations were carried out on the envisaged geo-environmental characteristics of the area with respect to important natural hazards and their occurrences selecting relevant parameters. These include active landslides, flood-prone zones, toe erosion prone zones, lithology, drainage density, land use/cover, lineaments and slope information in terms of degree/ aspect/convexity.

Natural hazard maps were created using GIS by combining different maps with statistically assigned weight values and image processing. These maps bring out the areas and portions with different degrees of natural hazard susceptibilities based on the field level and RS data input to GIS. Such natural hazard potential areas in a predictive mode are perceived to be significant for disaster management purposes.

Introduction

Indian Himalayan Region (IHR) has one of the most rugged mountain topography in the world and forms a part of one of the youngest mountain range in the world geologically. Himalayas are geodynamically still active (Valdiya, 1992). Natural hazards in the mountain environments regionally are mostly considered in terms of geo-environmental and allied factors. IHR faces frequent problems of varied forms of natural hazards over its different areas, causing loss of lives and properties, which also badly affects the economy of the mountain states (Prasada Raju and Saibaba, 1999; Garg *et al*, 1996; Virdi *et al*, 1997). The impact of such hazards can be evaluated in terms of death, injury, economic loss and the environmental degradation such as change in landscape, river flow-path, bio-physical system etc. Such natural hazrds have been accelerated by anthropogenic activities mainly due to changes of land use pattern such as road building, overgrazing, commercial exploitation of forests as well as illicit felling of trees in the highland areas (Agrawal *et al*, 1997, Singh and Pandey, 1996).

Sikkim Himalaya falls in the eastern portion of IHR and is totally covered by hills of 300 m to 8598 m amsl with highly undulating topography. Mount Khangchendzonga (8598 m amsl) is the 3rd highest peak of the World falling in Sikkim. This State is bound in the south by Great Rangit river, Chumbi valley in the east, Nepal in the west and Tibet (China) in the north covering an area of 7096 sq. km (Raina and Srivastava, 1981). Figure 1 shows the location map of Sikkim State. This Himalayan State in India faces problems of significant natural hazards such as landslides, flash-floods, river toe-erosion as well as other forms of erosion from time to time due to a geologically fragile host terrain coupled with heavy rainfall and other natural and anthropogenic factors (Bhandari, 1987; Krishna, 1997). On a regional scale, Sikkim Himalayan region is characterized by high denudation rates reaching upto 500-1000 ton/sq. km/year calculated on the basis of suspended load (Starkel and Basu, 2000). In high relief mountain areas with steep energy gradients,

many geomorphic processes such as landslides, debris flows, snow/ice avalanches, flash floods/torrents and glacial lake outburst floods are significant natural hazards. The nature, spatial and temporal distributions of such processes are strongly controlled by climatic factors involving temperature and precipitation thresholds. These in turn depend on the geology and physiography.

Natural hazard is an event that puts something or someone in a position of risk as a natural phenomenon occurring in proximity and pose a threat to people, structures and economic assets caused by geological, hydrological, meteorological and biological conditions or processes in the natural environment. Landslides and avalanches are natural hazards specific to mountain areas. As per OFDA/CRED international database (http/www.cred.be), about 213 disastrous events of landslide/avalanches between 1900-2001were recorded from 27 countries in Asia. The frequency of this event was highest in India followed by China, Indonesia, Philippines, Japan, Nepal, Pakistan, Turkey, Afghanistan, Papua New Guinea, Hong Kong, North Korea and Tajikistan. Similarly, countries with more than 500 people killed from landslides and avalanches are India, China, Indonesia, Philippines, Nepal, Japan, Afghanistan and Turkey.

Increasing population pressure and anthropogenic activities along slopes are leading to agricultural expansion and deforestations rendering many places vulnerable to such hazards. Various forms of mass wasting, erosion and allied hazards along roads are common in this State. Road is one of the important infrastructures and main life line in mountain regions and such hazards affecting roads in turn disrupt regular traffic interrupting essential and economic/commercial activities from time to time. This is further compounded with huge costs involved in maintenance/repairing of this infrastructure.
In natural hazard assessment, the geo-informatics tools like RS and GIS based techniques are widely used (Van Westen *et al*, 2000; Van Westen and Terlien, 1996; Krishna, 2000; Dai and Lee, 2002; Krishna, 1997; Kundu and Krishna, 2002). This hazard analysis has been done using these techniques along NH31A alignments between Singtam and Rangpo. The approach has been the evaluation of terrain conditions under which such hazards have occurred in the past and using those specific terrain conditions to statistically predict the natural hazard susceptibility zones.

Study area and terrain characteristics

Sikkim State has four districts which are North, East, South and West. Among these, East district is most populated with a total population of 244790, decadal growth rate of 37.17% and population density of 257 persons per sq. km (Anonymous, 2001). As per the biogeography of the Himalaya, the Sikkim Himalayan region falls in the boreal zone encompassing Eastern Himalaya as biotic province which includes alpine, temperate and sub-tropical zones as its distinct biomes. This part of the Eastern Himalaya has a high rainfall intensity with humid climate due to full thrust of monsoon from the Bay of Bengal. Much of the monsoon clouds are trapped by the south-easterly bend of the Himalaya.

This study has been conducted along Singtam-Rangpo areas close to selected stretch of National Highway 31A from the valley to ridge top sections through slopes. This is an important road stretch on this Highway falling between latitudes $27^0$11'N to $27^0$15'N and longitudes $88^0$29'E to $88^0$33'E. Lithology in general shows the presence of phyllite and quartzite rocks of Reyang formation and Lingtse granite gneiss. The topography of the study area is highly undulating with hills of 300 m to 1000 m amsl surrounding the road stretch. Gangtok is the capital of Sikkim, which is located 25 km north of Singtam. Rangpo and Singtam are two important localities along this road. Rangpo is located at the state boundary. Tista River, Rani Khola and Rangpo Chu are important rivers forming the main drainage pattern of the area along with other rivers/streams (called 'Khola', 'Chu' locally).

The study area is distributed within subtropical ecozones in an elevation range of 300-1200 m amsl. The average annual rainfall of subtropical ecozones is within the range of $\geq$1000 mm to $\leq$3200 mm. This area almost entirely falls in the Lesser Himalayan portion. In the Himalaya, the area falling between the main central thrust and main boundary fault is termed as Lesser Himalaya, which is a rugged and highly dissected mountain region.

Methodology

Hazard zonation is an important aspect of assessment of natural hazards which refers to the division of land into homogeneous areas and the ranking of these areas according to their degree of actual or potential hazard caused. In recent times, with the help of Remote Sensing (RS) and Geographical Information System (GIS) as valuable tools, deciphering the topography, lithology and tectonics of any area is facilitated in a large number of investigations through out the world. This leads to updated knowledge of the eco-systems prevailing in those areas. The geology of an area constitutes the main component of abiotic factors, i.e. land, water and mineral resources on which biotic factors thrive as such constituting the ecology of an area. It is relevant to use RS and GIS techniques so that a proper and comprehensive picture emerges. For assessment of natural hazard, remote sensing, GIS, field and laboratory investigations using suitable tools were carried out and integrated.

Spatial data integration

The synoptic coverage of RS provides an effective tool in identification and characterizations of natural hazards (Garg *et al*, 1996). The RS data products such as Indian Remote Sensing Satellites (IRS) 1C/1D LISSIII bands 2, 3, 4 and FCC images have been used to extract terrain information and affected ground surface. Natural hazard occurrence depends on complex interactions among a large number of partially interrelated factors. Analysis of hazards requires evaluation of the relationship between various terrain factors and occurrences. A GIS allows the storage and analysis of information concerning different terrain factors as distinct layers and thus provide an excellent tool for hazard susceptibility zonation. It combines all the factor maps into a map of homogeneous units, which is then overlaid with the hazard map to produce a hazard density for each unique combination of input parameters.

The interpretation of hazards from remote sensing (RS) data requires knowledge of the distinctive features associated and of the image characteristics associated with such features. Spatial data of the study area were extracted from the satellite images of IRS 1C/1D LISS III band 2, 3 and 4 of the year 1997 (spatial resolution of 23.5m; 1:50,000 scale), topographic maps and other collateral data sources. LISS III bands 2, 3 and 4 were subjected to image processing techniques, which include scene registration, geo-referencing, enhancement, re-sampling as well as FCC generation. The image processing operations were carried out using ERDAS Imagine 8.5 and ILWIS 2.1 softwares.

Geo-environmental parameters integration

Suitable parameters such as active landslides, flood-prone zones, toe erosion prone zones, lithology, drainage density, land use/cover, lineaments and slope information in terms of degree/aspect/convexity were interpreted and analyzed. Satellite images in conjunction with collateral ground level as well as base map level information were used for extracting different thematic details. Interpreted features of the study area were finalized by detailed ground-truthing as well as topographic map supports on 1:50,000 scale for relevant details with respect to the actual on ground position.

This led to infer all the parameters contributing to natural hazards in the area. These include slope, drainage density, lithology, lineaments, land use, river toe erosion-prone zone, river flood-prone zone, landslide mapping, road alignments, settlements and rainfall.

GIS integration

In bivariate statistical method, the role of individual or combination of parameters in regard to hazards is statistically evaluated. Based on the above premises, hazard assessment has been done by considering the parameters discussed above. This analysis method is suitable for medium scale (1:25,000 to 1:50,000 scale) surveys. In this method, a weight-value for a parameter class, such as a certain lithological unit or a certain slope class, is defined as the natural logarithm (ln) of the hazard density in the class divided by the hazard density in the entire map. This is depicted by the following formula (Van Westen, 1997):

ln Wi = ln (Densclas/Densmap) =
ln [{(Npix(Si)/Npix(Ni)}/{∑Npix(Si)/∑Npix(Ni)}]
where,
Wi = the weight given to a certain parameter class (e.g. a rock type or a slope class)
Densclas = hazard density within the parameter class
Densmap = hazard density within the entire map
Npix(Si) = number of pixels, which contain hazards, in a certain parameter class
Npix(Ni) = total number of pixels in a certain parameter class

This type of statistical analysis of hazards leads to evaluation of the terrain conditions under which hazards have occurred in the past and by using this specific terrain condition, prediction of future hazard areas. The ILWIS 2.1 (The Integrated Land and Water Information System) GIS software was used for the data organization and analysis. Point, segment, polygon and raster map of all the parameters like active landslides, flood-prone zones, toe erosion prone zones, lithology, drainage density, land use/cover, lineaments and slope information in terms of degree/aspect/convexity were prepared considering the domain classes. Following digitization (points, segments, polygons) and rasterisation, values of all the parameters were divided into classes. Based on the information generated for each hazard site, a domain table was created in a GIS. In the activity map, the information related to each hazard and non-hazard areas were stored. Then map crossing operations were performed using this map and each of the parameter class maps. Map crossing in a cross table led to the calculation of density of hazards per parameter class by information on pixels generated.

Tables were created for all the parameter maps and relevant pixel information was generated. Standardized values of these densities were obtained by relating them to the overall density in the entire map. In this study the hazard density per class was divided by the hazard density in the entire map. Tables of each parameter classes were created and jointed with activity tables of respective parameter classes. Some classes were found to have a density of zero, which was adjusted for possible weight values by suitable calculation after Van Westen (1997). Thus, final weight of each map was calculated.

Finally, Natural Hazard Susceptibility Zonation (NHSZ) map was created by combining weights through addition of all the weight maps. This was followed by the calculation of histograms of the final maps for deciding the boundary values of hazard categories. Subsequently, image processing operations were performed with suitable slicing techniques to create the NHSZ map (figure 2). The hazard categories in the NHSZ map generated are very low, low, moderate, high and very high hazards for the area covered along the road stretch as well as valley to ridge top sections. Figure 3 shows the orientation of major road stretch as well as settlements of the area with respect to NHSZ spatial distribution in the map. Towards quantitative understanding of the distribution of hazard susceptibility zones, GIS based analysis has given rise to the spatial percentages of various classes as contained in the map (figure 4)

Results and Discussion

This study takes into consideration the importance of host geo-environmental characteristics itself rather than accounting for the occasional triggering events (such as prolonged heavy rainfall, seismicity, cloud burst etc.) of hazards. These include active landslides, flood-prone zones, toe erosion prone zones, lithology, drainage density, land use/cover, lineaments and slope information in terms of degree/aspect/convexity and rainfall condition in terms of elevation zones. An assumption has gone into the study that entire area is exposed to uniform triggering conditions both natural as well as anthropogenic. RS data helped in getting the comprehensive synoptic real time details of the area in a faster and efficient way.
In a nutshell, activities performed include RS data interpretation, ground truth and other field based details collection, data automation and digitization (points, segments, polygons, rasterization, creation of domain items for hazard characteristics, table creation and linking to each map), creation of activity map which shows active hazard and no hazard areas, crossing the parameter maps with the activity map, calculation of hazard densities using already prepared crossed maps, counting the number of pixels falling in the study area and deducting the pixels outside the study area, final weight-value calculations by generating natural logarithm of the density in the class divided by the density in the map, table creation and joining the

parameters, production of weight maps for each parameter class, combining weight by addition of all the weight maps, calculating histogram of the final map for deciding the boundary values hazard categories and finally, image processing and slicing techniques to create the NHSZ map (figure 2).

Since an expert system based approach has been adopted in the study by incorporating the detailed knowledge of known hazards along the road alignments in the region to statistically predict the susceptibility of contiguous portions, this study is perceived to be very effective at the local scale. The zones denoting 'very low' indicates generally stable areas which are very less prone to hazard occurrences; whereas, the 'low' hazard susceptibility indicates less hazard prone areas. The zones of 'high' and 'very high' categories have high potential for hazard occurrence and these zones need much careful approach for future developmental works in such areas.

Major hazard zones were included towards input of host geo-environmental conditions, therefore, natural hazard susceptibility zones reflected in the study point to the predicted areas for likely major occurrences. Rainfall data were used indirectly as the study area falls in the subtropical eco-zone, which has uniform rainfall within this elevation zone for the entire area. Thus, there has been uniform weightage of rainfall. Since this area lies in the subtropical ecozones at relatively lower altitudes, the possible anthropogenic reasons contributing in the occurrence of significant hazards are easy accessibility and greater farming land use such as crop land, paddy field, grazing lands as well as settlements in this zone in addition to the road itself. Therefore, rate of soil erosion is high and forests are not so intact. The maximum road length as well as settlements fall within this zone. Thus, the susceptibility of the area to possible natural hazards could be brought out with spatial details on a geo-referenced scheme in a GIS (figures 3 & 4)).

NHSZ map prepared shows the areas and portions with different degrees of hazard susceptibility along the roads. In this process, an output scale of medium range (1:25,000 to 1:50,000) could be achieved. This map refers to the zonation of the area into various predicted susceptibility classes purely statistically evaluated depending on the conditions of the known hazard zones. Thus, such GIS based information on hazard susceptibility has the potential of ready inferences regarding vulnerability and risks of important infrastructures in the area. Thus, it can provide valuable clues for either to undertake prevention or mitigation measures more rationally.

Conclusions

This study of natural hazard assessment along selected areas close to road stretch of an important highway namely NH 31A in Sikkim has used modern geo-informatics tools such as RS and GIS coupled with extensive ground level field-works. The premises of the study have been the prediction of natural hazard susceptibility by using information on host geo-environmental characteristics of known active hazards of major and significant dimensions in the area. An assumption has gone into the study that entire area is exposed to uniform triggering events both natural as well as anthropogenic. Therefore, the role of host geo-environmental factors is integrated to the fullest possible extent.

GIS made it possible to use remotely sensed data in conjunction with conventional field data for a better understanding of the phenomena of natural hazards in terms of characterization and hazard susceptibility zonation. The hazard susceptibility categories interpreted both spatially and quantitatively shall be important for any further development of infrastructures like roads and settlements in the area. Required planning level precautions and mitigation efforts can be suitably supplemented to minimize the incidences of natural hazards and environmental degradation with this NHSZ map produced on a medium scale for the area.

A GIS based information support shall have the capability to provide not only hazard susceptibilities as a whole, rather investigation and analysis of individual parameters contributing to the same can also be inferred by drawing comparisons from NHSZ map and each parameter map. Vulnerability and risk aspects of natural hazards to work out the disaster management implications can essentially follow. This can help in designing and implementing any infrastructure development project and making decision for techno-economically feasible land use utilization in such areas with due consideration to avoid future hazards on the specific locations.

Figure 1. Location map of study area in Sikkim state, India

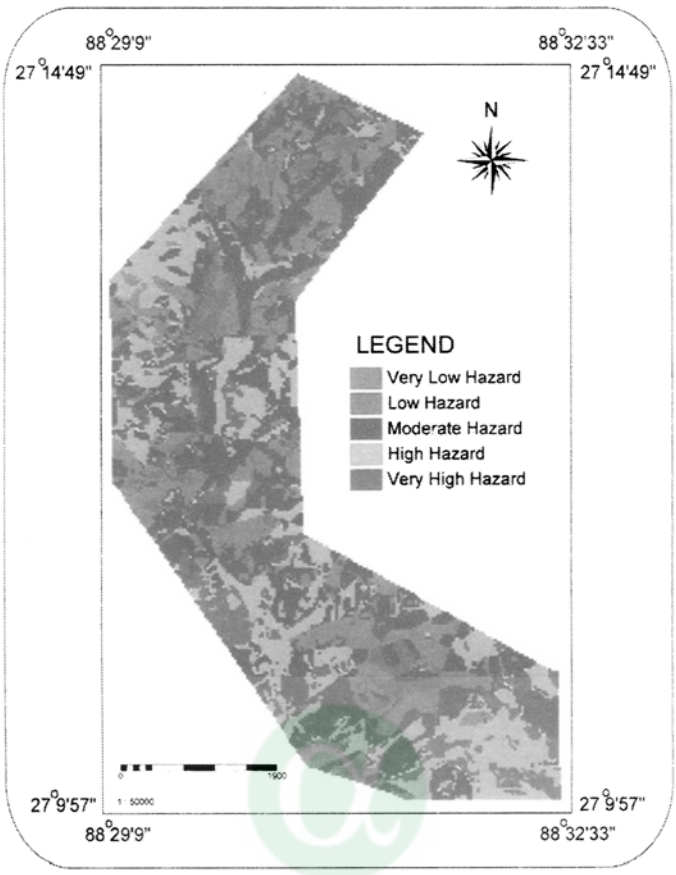

Figure 2. Statistically generated Natural Hazard Susceptibility Zonation (NHSZ) map through GIS, Singtam-Rangpo area, Sikkim

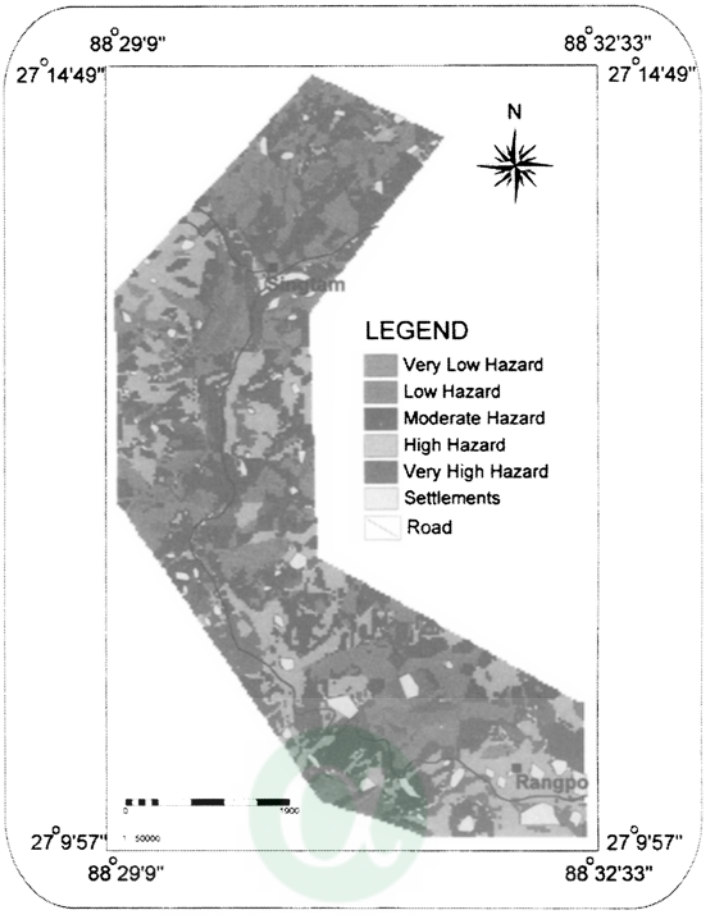

Figure 3. Orientation of road and settlements by GIS overlaying on the NHSZ map of the study area

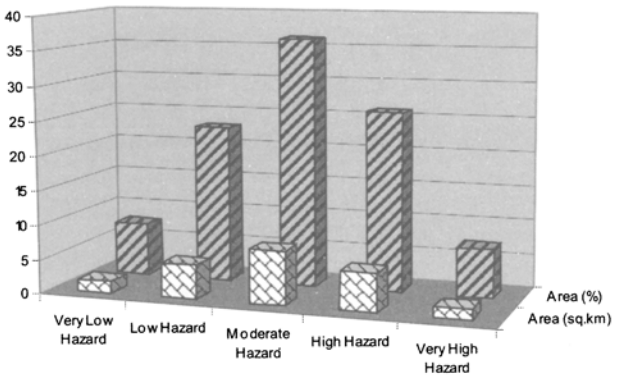

	Very Low Hazard	Low Hazard	Moderate Hazard	High Hazard	Very High Hazard
Area (sq.km)	1.64	4.91	7.76	5.57	1.52
Area (%)	7.66	22.94	36.26	26.03	7.1

Figure 4. GIS quantified spatial distribution of the hazard classes of the Singtam-Rangpo area, East Sikkim

An effective disaster management is very much dependant upon availability, dissemination and proper use of such information. A better disaster management approach can be facilitated through available information on natural hazards for suitable prevention/mitigation measures of specific locations. Thus, appropriate attention and initiatives can be supported in line with the modern concept of disaster management towards 'culture of safety' through prevention, preparedness and mitigation.

Acknowledgements

The authors are grateful to Birla Institute of Technology (B.I.T.), Mesra, Ranchi for giving an opportunity to present this paper in the seminar addressing a vital issue of disaster management. They are also grateful to the Institute for providing Institutional facilities for working on this manuscript. A part of the work was done earlier at G.B. Pant Institute of Himalayan Environment and Development, Sikkim Unit, former affiliation of the first author with the support of a project from ISRO, Department of Space, Govt. of India and the same is thankfully acknowledged. Dr. S. Kundu and Mr. A.K. Sharma associated with the above project are thanked for their helps and support.

REFERENCES

Agrawal D K, Krishna A P, Joshi V, Kumar K, Palni L M S (eds.) 1997. *Perspectives of Mountain Risk Engineering in the Himalayan Region.* Gyanodaya Prakashan, Nainital, P. 241.

Anonymous. 2001. *Provisional population totals*, Series 12. Directorate of Census Operations, Sikkim.

Bhandari R K. 1987. Slope instability in the fragile Himalaya and strategy for development. Ninth IGS Annual Lecture, *Indian Geotechnical Journal* 275-322.

Dai F, Lee C F. 2002. Landslides on natural terrain: physical characteristics and susceptibility mapping in Hong Kong. *Mountain Research and Development* 22(1):40-47.

Garg J K, Narayana A, Arya A S, Murthy T V R, Narain A, Joshi V, Saxena K G. 1996. *Landslide hazard zonation around Tehri Dam using Remote Sensing and GIS techniques.* In: Proceeding of International conference on Disaster and mitigation, Anna University, Chennai, India 1:19-22.

Krishna A P. 2000. Landslide management in the Himalayas. *Geo Asia-Pacific*, June-July issue 30-32.

Krishna A P. 1997. *Geological remote sensing applications for landslide hazard assessment in parts of Sikkim Himalaya, India.* In: Proceedings of Twelfth International Conference on Applied Geologic Remote Sensing, 17-19 November 1997, Denver, USA, II:173-178.

Kundu S, Krishna A P. 2002. *Landslide hazard assessment along the selected highways in Sikkim Himalaya– a remote sensing and GIS based approach.* In: Nagarajan R (ed.) Landslide disaster: assessment and monitoring. Anmol Publications, New Delhi, 104-112.

PrasadaRaju P V S P, Saibaba J. 1999. *Landslide hazard zonation mapping using remote sensing and geographic information system techniques- a case study of Pithoragarh area, U.P.* In: Proceeding of International Geosciences and Remote Sensing Symposium (IGARSS), Hamburg, Germany, (CD-ROM).

Raina V K, Srivastava B S. 1981. Tectonic evolution of the Sikkim Himalaya. In: Sinha A K (ed.) Contemporary Geoscientific Researches in Himalaya, Bishen Singh Mahendrapal Singh, Dehradun, India 1:109-115.

Singh R B, Pandey B W. 1996. *Landslide hazard in Indian Himalaya and Canadian Rockies- A comparative analysis.* In: Chacon J, Irigaray C, Fernandez T (eds.) Landslides: Proceedings of the Eighth International Conference and Field Trip on Landslides, Granada, Spain, 27-28 September 1996. Balkema AA (Publ.), Rotterdam 63-69.

Starkel L, Basu S R. 2000. *Rains, landslides and floods in the Darjeeling Himalaya.* Indian National Science Academy, New Delhi, India.

Valdiya K S. 1992. *Environmental problems in Himalaya: geological aspects.* In: Himalayan Environment and Development - Problems and Perspectives. Gyanodaya Prakashan (Publisher), Nainital, India.

Van Westen C J, Soeters R, Sijmons K. 2000. Digital geomorphological landslide hazard mapping of the Alpago area, Italy. *International Journal of Earth Observation and Geoinformation* 2(1):1-10.

Van Westen C J. 1997. *Statistical landslide hazard analysis.* In: ILWIS 2.1 Application Guide. ILWIS Department, ITC, Enschede, The Netherlands.

Van Westen C J, Terlien M T J. 1996. Deterministic landslide hazard analysis in GIS- A case study from Manizales (Colombia). *Earth Surface Processes and Landforms* 21:853-868.

Virdi N S, Sah M P, Bartarya S K. 1997. *Mass wasting, its manifestations, causes and control: some case histories from Himachal Himalaya.* In: Agrawal D K, Krishna A P, Joshi V, Kumar K, Palni L M S (eds.), Perspectives of Mountain Risk Engineering in the Himalayan Region. Gyanodaya Prakashan, Nainital, 111-130.

Disaster Management
Editors: N.C. Mahanti et al.

Recent Asian Tsunami Hazard and Disaster Management Programs Over India

Bhanu Kumar, O.S.R.U

Department of Meteorology and Oceanography, Professor Rokkam Ramanadham Laboratories
Andhra University, Visakhapatnam, India

Abstract

An attempt is made in this article to narrate a brief history and some important characteristic features of 26th December, 2004 Indian Ocean tsunami, as revealed by tide gauge and post- survey of tsunami data. The tide gauge datasets of the Survey of India were analysed for the period of tsunami to mark its impact at different places of coast of India and the Jason-1 altimetry data supported the life history and characteristics of above tsunami. Secondly post-tsunami field survey results and data obtained by the Department of Meteorology & Oceanography, Andhra University over six districts of Andhra Pradesh at fifteen coastal stations relating to time of occurrence of tsunami , its maximum height, its time of maximum height occurrence, inundation and number of occurrences of waves to the coast are examined and presented in a table. Regional impact of tsunami at above fifteen places is commented. Finally, the necessity and working of a tsunami warning system in the Indian Ocean and the importance of mitigation programs are also suggested at the end. India should think initiation of Natural Disaster Warning Centre, which is multiple use rather than tsunami warning centre alone.

Introduction

India is having a vast coast line of about 6,500 km with a very dense population and it is often affected by natural hazards like surges due to tropical storms, monsoon depressions and tsunamis etc. In the past, tsunamis were often referred to as tidal waves. The term "tidal wave" is a misnomer. Tides are the result of gravitational influences of the celestial bodies, but tsunamis are not caused by the tides and are unrelated to the tides. Similarly tropical storms which form over warm seas are going to generate storm surges which inundate coastal regions like tsunamis. But they are different from tsunamis. Tsunami is a Japanese word meaning "Harbor wave"; it has been adopted for general use in 1963 at an International Scientific Conference. There are, of course, many causes to trigger a tsunami, but the most prevalent one is an earthquake. In addition, landslides, volcanic eruptions, explosions, and even the impact of cosmic bodies, such as meteorites, can generate tsunamis. Coming to the historical evidence, there were so far five tsunami incidents recorded due to different earthquakes in the Indian Ocean and chronologically they were on 31st December, 1881, August 1883, 26th June, 1941, 27th November, 1945 and recent 26th December, 2004 which is the fourth largest in the world earthquake from the records of the U.S. Geological Survey. Next, it is customary to compare an earthquake intensity scales with equivalent energy in weight of TNT. Recent earthquake of magnitude 8-9 on the Richter scale is equivalent to 47, 50,000,000 tons of TNT energy and this resulted in total damage and waves seen on the ground surface of entire coast of India. Next, a tsunami on the other hand has nothing to do with atmospheric disturbances.

On Sunday 26th December, 2004, the tsunami, which caused destruction in a complex ways, was triggered by an earthquake of magnitude 9.0 on the Richter scale at 3.4^0N, 95.7^0E off the coast of Sumatra in the Indonesian Archipelago at 7:58 am local time which is known as "Ring of Fire" at a depth of about 29 km. The main reason for the above earthquake is that in the Indian Ocean the Indo-Australian plate was sub ducted approximately 1200km beneath the Eurasian plate at its east margin and therefore tsunamis generated by vertical displacement of water column owing to earthquakes. Tsunamis were propagated towards the southwest shore of Java and Sumatra rather than into the Indian Ocean. The sea floor overlying the thrust fault would have been uplifted by several meters as a result of the earthquake. Generally, the size of tsunami is directly related to the shape of the rupture zone, the rate of displacement and sense of motion of the ocean floor in the epicenter area and the depth of water. Hence earthquake alone cannot generate tsunamis all the time. For example on 29th March, 2005 an earthquake of 8.7 on the Richter scale was struck near the epicenter of the previous one in the Indian Ocean, but it could not generate any tsunami (Tandon

and Srivatsava 1974). The main factors of destruction from tsunami are inundation, wave impact on structures and erosion. Next, there were "foreshocks" and "aftershocks" observed with the main event. Unfortunately, foreshocks were not observed, while aftershocks were clustered around Andaman-Nicobar Islands.

General characteristics of tsunamis in the Oceans

Tsunamis have been recorded to occur in all the major oceans of the world and mainly it is a physical oceanography phenomenon. Oceanographers often refer it as "seismic sea wave" (Pacheco et al 1992) as they are the result of sudden rise or fall of a section of the earths crust under or near the bottom of the ocean. A seismic disturbance can displace the water column, creating a rise or fall in the level of ocean above. This rise or fall of sea level is the initial formation of a tsunami wave. The maximum onshore vertical height of tsunami above sea level is called "run-up height" upto 30 meters and run-up is also referred to as the amplitude or height of the tsunami. Tsunamis demonstrate the terrifying strength of moving water even more graphically than floods and dam bursts.

Though the tsunamis are rare among other natural hazards, they are disastrous which can be generated in all the world oceans, inland sea and in any large body of water. The characteristics of tsunami in the world oceans appear to have its own cycle of frequency and pattern in generating tsunami that range in size from small to large and highly destructive events. Most tsunamis frequently occur in the Pacific Ocean and its marginal seas and are least expected surrounding the Indian subcontinent. It is a series of waves of extremely long wavelength and long period in a body of water produced by an earthquake/volcanic eruptions/land slides and an earthquake with a Richter magnitude exceeding 7.5 can produce a destructive tsunami. The size of tsunami is directly related to magnitude of earthquake, depth, fault characteristics and coincident slumping of sediments etc. In the open oceans, the tsunamis are harmless because of their small wave height, but they are represented by shallow water equation on reaching the coast. When the tsunami waves approaches the coast, they feel bottom and speed diminishes which results in increasing the wave height in order to conserve the total energy. Typical speeds of tsunami in the open ocean are of the order of 600-800 km per hour and the period of tsunami waves may range from 5 to 90 minutes with a wavelength of 500 km. The tsunami energy flux, which is dependent on both its wave speed and wave height remains nearly constant. When it finally reaches the coast, a tsunami may appear as a series of breaking waves. The tsunami's energy and height diminished rapidly away from the source area and is hardly recorded by tide gauge stations in the coastal regions.

The characteristics of tsunami in the Indian Ocean is entirely different from that of the Pacific and the Atlantic oceans. Both the Pacific and the Atlantic oceans are open towards north-south poles, while Indian Ocean is restricted towards its north pole side. This results is to struck very destructive tsunamis in the Indian Ocean, besides the socio economic situation. Uniqueness of the Indian Ocean makes it vulnerable to a very destructive tsunami than in the Pacific and Atlantic Oceans. Maximum tsunami travel time in Indian Ocean is 2-5 hrs compared to 20-23 hrs in the Pacific and hence tsunami takes less dispersion and energy dissipation. Ideally we want more frequency dispersion and less amplitude dispersion, which is true for the Pacific and Atlantic oceans but not for the Indian Ocean.

Results and discussion

Analysis of tide gauges data to study tsunami characteristics

There are about 22 tide gauges (fig.1) around the coast of India and the tide gauge data is maintained by the Survey of India. Tsunamis cause abnormal fluctuations in sea level along the coasts (Dasgupta et al 2000). The tide gauges installed on the coast of India to measure the rhythmic rise and fall of sea levels due to astronomical tides are also capable of recording such abnormal fluctuations in sea levels. The analysis of tide gauge records along the Indian coast and elsewhere showed that the recent event of tsunami that occurred on 26th December, 2004 was well recorded by the tide gauges in the Indian ocean and from the records it is noted that first wave of tsunami first hit at Cuddalore at 8:00am (IST), Chennai 8:40 am and Paradhip, Visakhapatnam and Machilipatnam at 9:00 am of east coast of India, while it reached Tuiticorin at 9:57 am, Cochin at 11:10 am and Marumgoa at 12.25 pm (IST). Incidentally, such records are the only

means to scientifically document the arrival timings and relative amplitudes of tsunami at various locations (Murty 1984). It is possible that such events occurred in the past escaped our attention because of their low impacts on human life and property. The recent observations at a tide gauge located at Manzanillo, Mexico, a location very far from the epicenter of 26th December, 2004 tsunami, showed the signature of Indian ocean tsunami. At present, it is not known how many such events occurred in the past in Pacific or Atlantic have left their trace in the tide gauges along the Indian coast. Identifying such events in instrumental data and developing the ability to simulate them will allow us to generate reliable statistics. In the case of tsunamis, confidence in a model is critical because it will then allow us to prepare a scenario database that can be used when tsunami is triggered. Similarly, in the case of storm surges, identifying past surges and simulating them accurately will lead to better, more reliable models and statistics. An analysis of tide gauge data in the ports of Visakhpatnam and Kochi are presented in fig.2 which, shows the time of occurrence of tsunami. Tsunami is not a single wave but a series of waves. First wave is generally the smooth one in which the sea gently rises. This is followed by a violent sucking sound as the sea retreats, leaving rocks, reefs and sunken ships exposed and anchored ships on dry ground. It is interesting to note that in the Indian Ocean, second/third tsunami wave is very dangerous out of probable 5 waves. On comparison with other dangerous tsunami waves, it is noted that above phenomenon is completely different from that of Pacific and Atlantic oceans.

Field report on the impact of Tsunami over coastal Andhra Pradesh:

26th December, 2004 tsunami caused major destruction over 6 districts namely Nellore, Prakasam, Guntur, Krishna and East & West Godavari in Andhra Pradesh (fig.3) where the death toll reached upto 800 and many people rendered homeless. The survey mainly intended to study the physical accepts of post tsunami event and collected data on several physical oceanographic parameters like wave height, time of occurrence, time of maximum wave height occurred, number of occurrences and inundation. Also studied the physical setup of beaches where tsunami effect is more. Beach profiles survey has been carried out for 15 stations and drawn to analyze the tsunami effect. It is found that the intensity of tsunami along the coast is solely depending on both wave propagation and near shore morphology. It is interesting to note that above tsunami event has brought on sediment transport and coast line configuration. The data were presented in a tabular form. Tsunami occurred as a sudden event, with no antecedent features were found. Tsunami event occurred between 8 am to 11 am along Andhra coast. The maximum height of wave observed between 12 to 15 feet. The time of occurrence of maximum wave height varied from 8:30 am to 12 noon. Maximum inundation observed upto 1.5 kilometers at Manginipudi, Krishna district where large number of deaths were occurred while less inundation occurred at South Pallipalem, Ongole. Manginapudi beach, where people gathered to have a holy bath suffered a large number of deaths, because of the wide width of the beach. Observations made it clear that total number of waves struck the coast were 4. The summary of observations made was tsunami effect is less where thick vegetation present where as less elevated, flat areas was badly effected. The wave trimmers were observed through out the day. Some locations were encountered a recede in the coastline up to 50 meters (South Pallipalem, Ongole) and it took a half a day to normalize the coast line. Because of the tsunami waves huge number of dunes were eroded and in some areas dunes were flattened. Along the entire Andhra coast, the second and the third waves were said to be killer waves because of their speed and elevation. At Pallipalem near Gangapatnam,, the situation is some what different from other villages, where the village is surrounded by two inlets (creeks). The tsunami wave entered from both inlets and water piled up to cause severe damage to village. Fig. 3, map showing the districts visited.

Establishment of tsunami warning system in the Indian Ocean

Since science cannot predict when earthquakes will appear, science also cannot determine exactly when a tsunami will be generated. Our knowledge of tsunami generation is incomplete because the generation phenomenon has been neither observed nor measured directly. But with the assistance of previous records of tsunami and numerical models, science can give an idea as to where they are most likely to be generated. Past tsunami height measurements and computer modeling help to forecast future tsunami impact and flooding limitations at specific coastal area. As a part of the U.S. National Tsunami Hazard Mitigation Program (NTHMP), deep-ocean tsunameters have been developed for the early detection, measurement, and real-time reporting of tsunamis in the open Pacific Ocean. Tsunameters were developed by the Project

DART (Deep-ocean Assessment and Reporting of Tsunamis) at NOAA's Pacific Marine Environmental Laboratory (PMEL). The DART system consists of sea floor Bottom Pressure Recording (BPR) system capable of detecting tsunamis and a moored surface buoy for real time communications. An acoustic link is used to transmit the data from the BPR on the sea floor to the surface buoy. The data are then relayed via a satellite link to ground stations, which demodulate the signals for immediate dissemination to the NOAA's tsunamis warning centers and PMEL. Now India is concentrating in this direction along with neighboring countries. Similar to Pacific Ocean warning systems, DART stations should be situated in the regions with a history of generating destructive tsunamis to ensure early detection of tsunami and to acquire data critical to real time forecast in the Indian Ocean. But one should be careful of false alarms of warning system.

Having experienced devastation by 26th December, 2004 tsunami, India is very keen to develop indigenous methods for documenting disasters, disaster recording instruments and type of spade work that Indian scientists should undergo. India is planning to develop a tsunami warning system namely Deep Ocean Assessment and Reporting System (DOARS) to locate tidal formation from undersea disturbances. The DOARS will be placed at a depth of 6 km under the Indian Ocean and will have the capacity to detect even the slightest change in the movement of water. About 10-12 data buoys are already in the Indian Ocean and we will add 15-20 more in the present programme. This will cover the Arabian Sea and all fault lines from Sumatra to Myanmar, apart from benefitting Kutch. We also plan to share this network with Indonesia, Myanmar and Thailand. The DOARS system can detect even a 1cm-change in the height of the water. It will then send this information in the form of digital waves to the satellite concerned, which will send it to stations on land. This way, we can get real time intelligence on the height and pressure of water within minutes. We have the basic expertise for developing software which can predict if an earthquake will happen anywhere on the fault line, how much energy will be released, and how much damage it can cause. Details of the dissemination system have not been decided yet. The Government of India plans to establish above warning system by spending Rs.125crore.

Remote sensing techniques to study tsunamis in the Indian Ocean

Judicious use of remote sensing and satellite altimetry could help us in identifying the behavior of tsunami, if it is in the track of a satellite. Satellite radar altimetry was started in 1970s with a view to assess tsunami as one of the important phenomena and first time it detected mid-ocean tsunami waves in 1993 (Okal et al 1999). The NOAA researchers proposed that the best of satellite data to improve tsunami hazard forecasts would be a reconnaissance mapping of the ocean floor from spaces. Right now satellite observations of tsunamis are unique and of tremendous value for testing and improving tsunami computer models and developing future tsunami early warning system and this technique is not a first line of defense in tsunami hazard monitoring and warnings, but it gives scientists a window to tsunami activity in the deep and in remote parts of an ocean basin, to far away from coastal tide gauges and other instruments they could detect it. The information of sea surface height from the satellite has many other applications and can be used to aid navigation, offshore operation, tropical cyclones forecasting and fisheries etc...

Jason-1 altimetry (NASA) from a height of 150 Km was over the Bay two hours after earthquake time and detected most important features of Indian tsunami on 26th December, 2004 and proved that altimeters in orbit can measure sea surface height variations with sufficient resolution (Jim Gower 2005). But there is a very low probability of capturing observations in any given location within two hours of an event. Satellite altimetry, perhaps from an expanded constellation of instruments, may well have a role in a global warning system. At present as the analyses of altimetry data relating to tsunami takes 5-6 hrs minimum, remote sensing techniques may not be helpful for the warning of tsunami wave in the Indian Ocean and hence its usage is limited at present.

Mitigation programs over tsunami affected areas

As we were not prepared for the recent tsunami, it caused a total death toll of about 1.7 lakhs and many more formers and fishermen rendered homeless. Of the total death toll, one third is children below 17 years. To alleviate the distress of farming and fishing families etc. the following mitigation programs must be performed by immediate measure, medium and long term basis. In the immediate measure water shelter, sanitation health and revival of livelihood and psychological rehabilitation are at top priority. In the medium

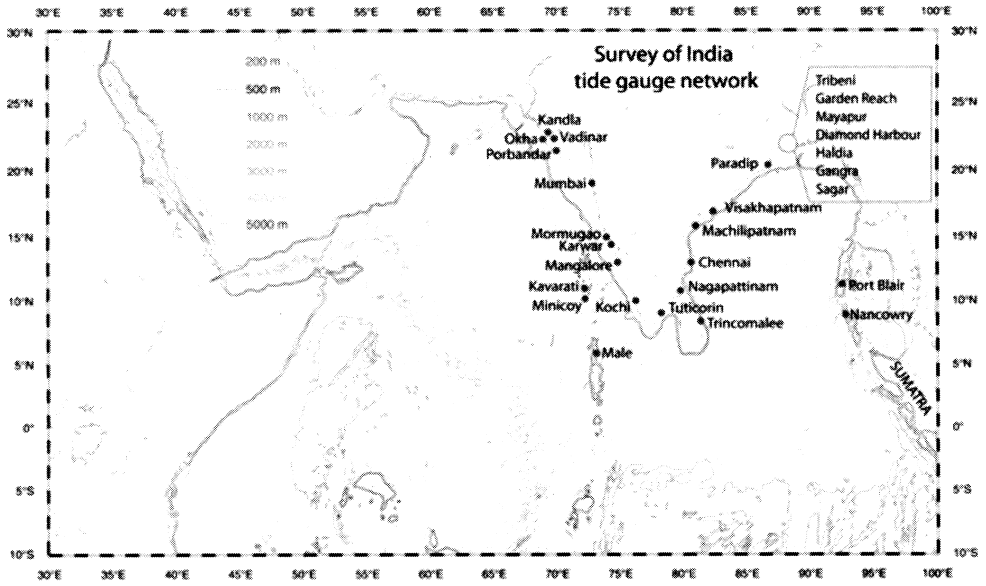

Figure1: India tide gauge data network

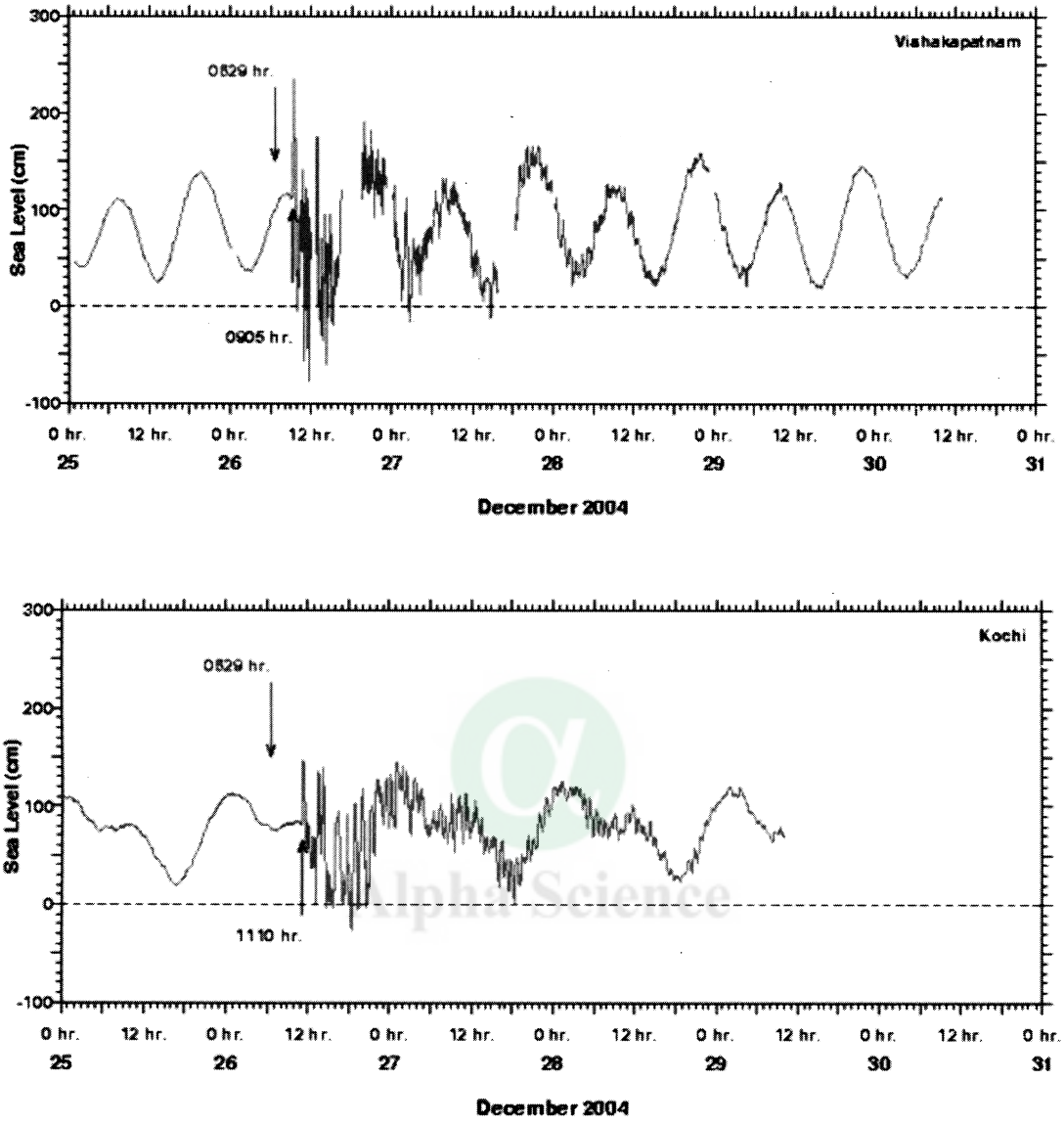

Figure2: Analysis of tide gauge data for Visakhapatnam and Kochi

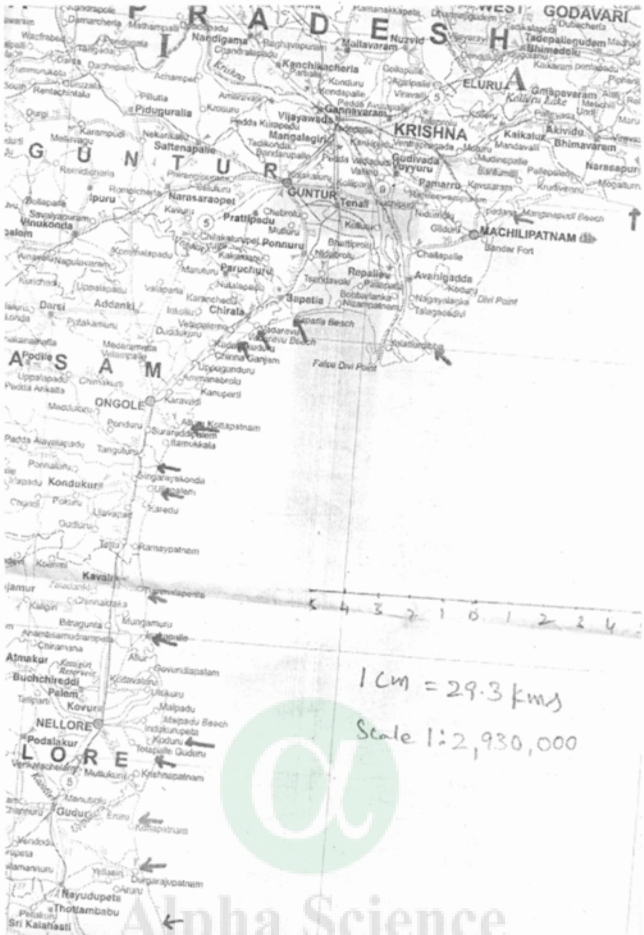

Figure3: Map for the survey conducted along Andhra Pradesh coast

S.No	Station	Time of occurrence	Maximum Height	Time of Maximum height occurred	**Inundation**	Number of occurrences	Remarks
	Nellore						
1	Tupili palem	9 to 10 30 Am	10 to 15 feet	10 30	300m	8	
2	Vadapalem	9 to 11 00 Am	15 feet	11	100m	6	Thick vegetation reduced the effect
3	White Kuppam	9 to 11 00 Am	15 feet	10	800m	3	Flat beach, No vegetation
4	Mypadu East Pattapu Palem	8 to 11 00 Am	15 feet	8 30	200m	3	
5	Mypadu West Pattapu Palem	8 to 11 00 Am	15 feet	8 30	300m	3	
6	Gangapatnam Pallipalem	9 to 11 00 Am	15 feet	8 30	1KM	3	Village is surrounded by two creaks (Max. Damage)
7	Allur Iskapalli Pattapupalem	8 to 10 00 Am	15 feet	9	100m	7	
8	Pakala Pallipalem	9 to 1 Pm	12 feet	10	1KM	5	Water entered from low areas
9	Chellammagari Pattapupalem	9 to 1 Pm	15 feet	12	1KM	5	
	Ongole						
10	Ullapalem Devalavartha Pallipalem	9 to 11 Am	12 feet	10	1KM	5	
11	Ongole Kothapatnam S. Pallipalem	9 to 10 30 Am	15 feet	9	Elevated Road Obstructed The Inundation	3	Sea receaded up to 50 m
12	Vetapalem Potti subbarayudipalem	9 30 to 11 Am	15 feet	9 30	800m	3	Thick vegetation
	Guntur						
13	Bapatla Surya lanka	9 to 12 Am	8 feet	12	150m	4	Beach Slope is more
	Krishna						
14	Manginapudi	9 to 11 Am	10 feet	11	1.5KM	4	Flat beach
	East Godavari						
15	Uppada Kakinada, East Godavari Dt	830 to 12 Am	10 feet	10	70m	4	

Table: Impact of tsunami, 26th December, 2004 at different stations over six districts of Andhra Pradesh.

and long term mitigation programs top priority should be given to coastal Bio-shield moment along the coastal areas, involving the raising of mangrove forests, plantations of casuaria, salicornia, laucaena, artiplex, palms, bamboo and other tree species and halophytes which can grow near the sea. Bio-shield moment will confirm multiple benefits to local communities as well as to country as a whole. The serious loss of life and property caused by tsunami highlights the vision and wisdom of former Prime Minister late Smt. Indira Gandhi when nearly 24 years ago who took proper steps to ensure that no permanent construction is permitted within 500 meters of high tide. Next, Urban Development Authorities, Municipalities and villages near sea shore should strictly observe Coastal Regulation Zone rules. This will definitely help to reduce the loss of lives and property due to tsunamis and tidal waves caused by tropical cyclones. The Indian Institute of Disaster Mitigation should play an active role through district collectors to avoid death toll by giving expert knowledge of Disaster Management.

Summary and Conclusions

By and large Indian community first time heard after independence the impact of Indian Ocean tsunami, 26th December, 2004 which is the fourth biggest earthquake in the world records of the U.S. Geological Survey. In fact we are not prepared for it. Where as we prepared tropical cyclones and its related surges.

Indian Ocean tsunami is more dangerous than the tsunamis that are produced in the Pacific and Atlantic Oceans because of the topography of Indian Ocean.

Both tsunami warning center and Bio-shield along the coast will help to reduce the loss of life and property.

The India government should come forward to launch a Natural Disaster Warning Centre which will take care of the hazards caused by tropical cyclones, monsoon depressions and tsunamis. Tsunami warning centre alone may not be helpful as it is a rare event and one should take care of false alarms produced by the DOARS. Experts suggested, Visakhapatnam as the main forecasting centre of tsunami covering the Indian Ocean.

Acknowledgements

Author is very thankful to Prof.T.S.Murty, University of Ottawa, Carleton, Canada for his valuable suggestions in the studies of tsunamis in the Indian Ocean.

References

Dasgupta, S., Pande, P., Ganguly, D., Iqbal, Z, Sanyal, K, Venkatraman, N.V., Dasgupta, S., Sural, B., Harendranath, L., Mazumdar, K., Sanyal, S., Roy, K., Das, L.K., Misra, P.S., Gupta, H., "Seismotectonic Atlas of India and its Environs", Geological Survey of India, 2000.

Murty, T.S., "Storm surges - meteorological ocean tides", Bulletin of the Fisheries Research Board of Canada, Ottawa, 1984.

Okal, E.A., Piatannesi, A., and Heinrich, P., "Tsunami detection by satellite altimetry", Journal of Geophysical Research, 104, 599-615, 1999

Pacheco, Javier F., and Sykes, Lynn R., "Seismic moment catalog of large shallow earthquakes, 1900 to 1989", Bulletin of the Seismological Society of America, v. 82, no. 3, p. 1306 - 1349, 1992.

Tandon, A.N., and Srivastava, H.N., "Earthquake occurrence in India: Earthquake Engineering", Sarita Prakashan, Jai Krishna Vol., 1-48, Meerut, 1974.

Disaster Management
Editors: N.C. Mahanti et al.

Air-Sea Interaction Study During Convective Processes Over Bay of Bengal

Sumana Paul, Meenakshi Chatterjee and Goutam Kumar Sen

School of Oceanographic Studies, Jadavpur University, Kolkata 700 032, India

INTRODUCTION

This study is aimed at understanding the Air-Sea Interaction processes during convective activity over the Bay of Bengal. Specifically, we intend to look for direct linkages between fluxes at the air-sea interface and other oceanic variables to understand the role of the thermodynamics processes. The impact of monsoon disturbances on ocean-atmosphere interface transfer processes has been investigated.
The tendencies of the different meteorological parameters have been calculated and the variation of the pressure tendency is used to identify occurrences of the low pressure systems over the Bay.

A detailed study on the different level temperature (upto 20mt. level) has done to study the variation of the temperature with depth in the different synoptic situation. It has seen from this study that the temperature gradient become smaller during the time of depression but salinity rate is different during the deep depression phase. During the depression phase we get the peaks in all the three levels of temperature. The temperature profiles upto 20 meter depth have been analyzed .

To get some idea about the interrelationships, daily correlations between 1)Flux and salinity, 2) Flux and the air temperature tendency (dTa/dt) and 3) the SST tendency (dSST/dt) and Q (= SHF+LHF) were computed for this period. We next attempted to pursue statistical analyses to understand the role of other variables on Total Heat Flux generation.

DATA SOURCE :

In this investigation, atmospheric as well as oceanic data obtained during the BOBMEX Stationary Period-I (26th July to 6th August , 1999) has been used.

During the Stationary Period-I intense low pressure systems formed viz.,

(a) A Deep Depression (27th-28th July),
(b) A Well Marked Low (2nd-4th August)

These systems initially developed as low pressure area with surface central positions around (1) 21^{0}N,89^{0}E on 25th July, (2) 20^{0}N,88^{0}E on 1st August. On the day they reached peak intensity their corresponding centers were located around (1) 23^{0}N,86.5^{0}E and (2) 21^{0}N,88.5^{0}E . During stationary period I, all the meteorological parameters near Sagar Kanya were mainly influenced by the formation and movement of the two well marked systems. The sky remained overcast with occasional spells of rainfall from 30th July to 1st August and 3rd to 5th August respectively.

The surface parameters we are using are Latent Heat Flux (LHF) , Sensible Heat Flux (SHF), Momentum Flux (MF), Sea Surface Temperature (SST), Air Temperature (AT), Salinity, Wind Speed (WS), Pressure etc. The oceanic data we are using are different level temperature. The data are taken in the 3 hour interval of time.

During these low pressure systems pressure tendency changes vary abruptly and pressure tendency rate shows the high negative value. These are shown in the figure 1 below.

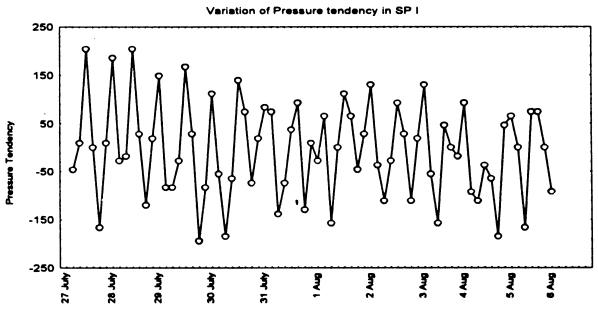

Figure 1

RESULTS AND DISCUSSIONS :

HEAT FLUX :

The time series plot of the total heat flux is shown in figure 2. A very rapid changes in the heat flux is observed all through out the SP I. On 27th July the increasing trend in the heat flux has found. After then from 28th to 30th July the heat flux became in decreasing trend. 31st July to 2nd August decreasing trend continued but in a slower rate of decrease than previous days. But on 3rd August the heat flux again increased with a high rate. 4th August onwards it was in decreasing trend.

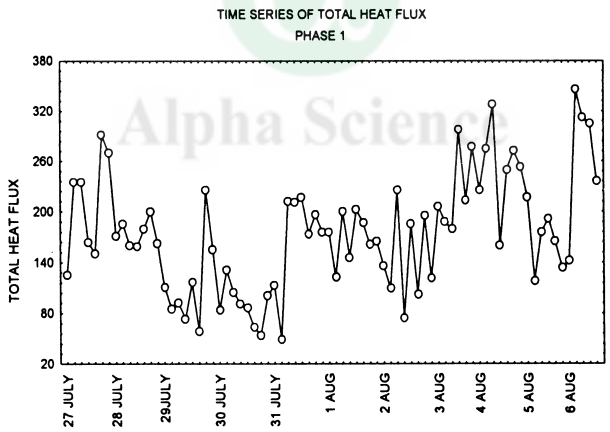

Figure 2

From the synoptic features of that time we found that on 27th July there was a deep depression and on 3rd August there was a well marked low over the Bay of Bengal.

WIND

From the time series plot (Figure 3) of the wind speed it is observed that wind speed was very high in the end of the first phase. From 27th to 29th July the wind speed was moderately high. But from 30th July to 1st August the wind speed showed the lower values. On 2nd August it was in increasing trend and on the 4th and 5th August wind speed became very high .

During 30th July to 1st August there were no low pressure system. From 2nd August to 4th August there was a well marked low. So high wind speed value occurred when there were low pressure systems over the Bay of Bengal. All throughout, the higher values of heat flux corresponds to the high wind speed.

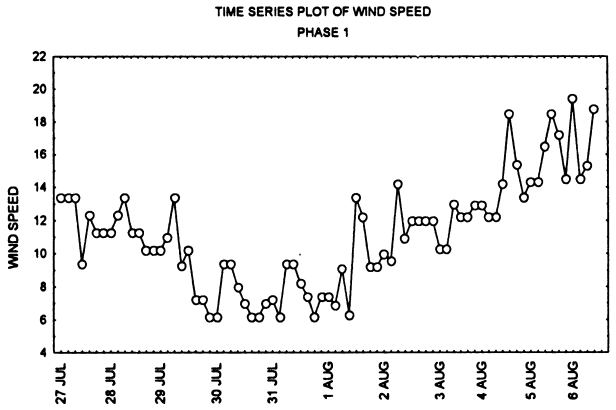

Figure 3

SST

The SST did show (in Figure 4) not much more variation all through out the stationary period 1. Initially from 27th July to 1st August there was not very high variations in the SST changes. From 1st to 2nd August the SST decreased very rapidly with a very high value. The increasing trend observed again from 2nd August to 3rd August and again on 4th and 5th August the variation in SST became very small.

Two low pressure systems were found the Bay of Bengal during SP I were 27th to 29th July a Deep Depression and 2nd to 4th August a Well Marked Low. So high value of SST is associated with the low pressure system.

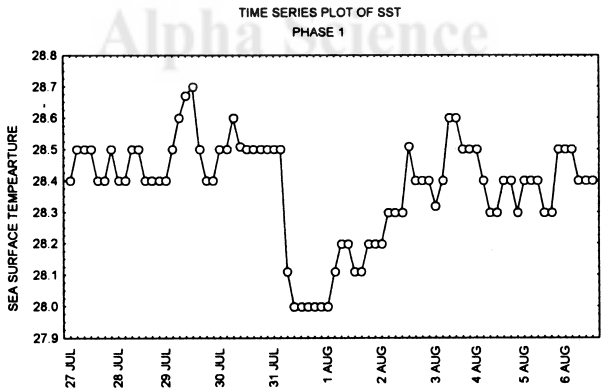

Figure 4

AIR TEMPERATURE

The variation of Air Temperature is very abrupt in compare to SST changes is shown in the figure 5. Initially the AT was high.31st July to 1st August: Air Temperature becomes low in compare to the other days of the experiment and during this time there was no low pressure system over the Bay of Bengal. 2nd August to 5th August : Air Temperature becomes again high enough.

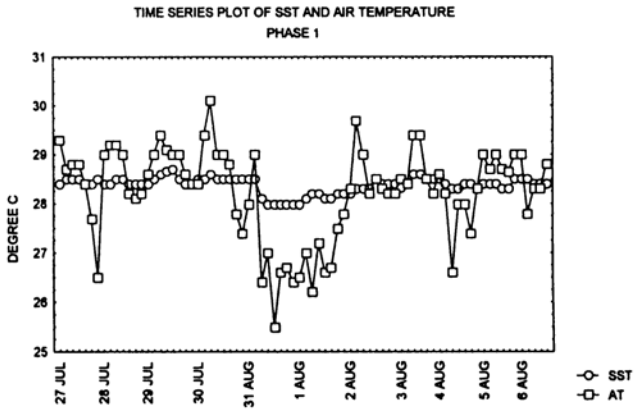

Figure 5

TEMPERATURE PROFILES OF THE OCEAN :

The ocean temperature profiles have plotted in the figure 6. From these profiles, drawn for the 5mt., 10 mt. and 20 mt. of depth, it is obvious that during the time of depression the temperature difference at level 5mt., 10mt., 20mt. become more close to each other.

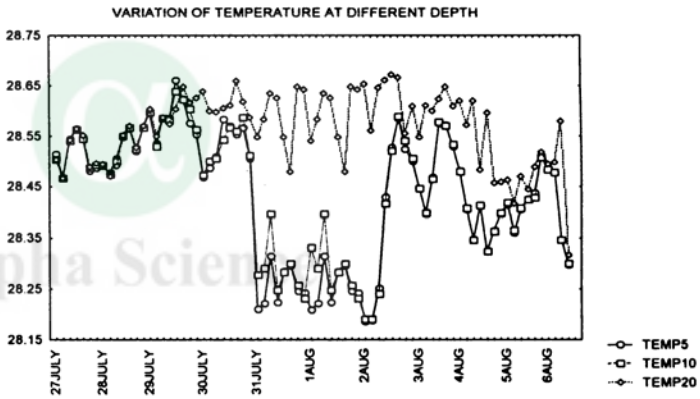

Figure 6

We next attempted to pursue statistical analyses for making a diagnostic model to understand the role of other variables on Total Heat Flux generation. Variation of model predicted flux patterns and the observed patterns are shown in the figure 7 and figure 8 below.

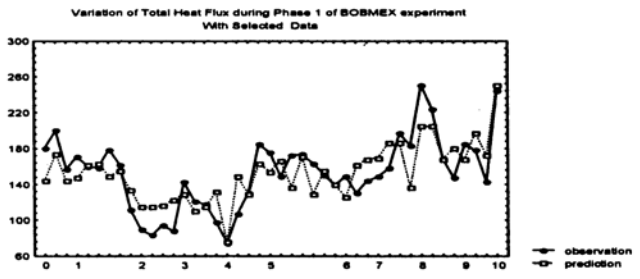

Figure 7

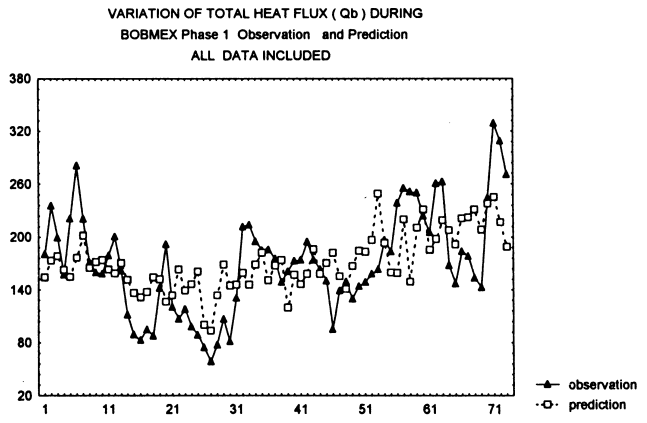

Figure 8

Statistical model was prepared to forecast temperature at 5 meter depth in response to changes in total heat flux, SST, Air Temperature, Wind Speed and Pressure. Several profiles (Statistical models) emerged for different time span. The forecast for the 5 mt. level ocean temperature has shown in the figure 9.

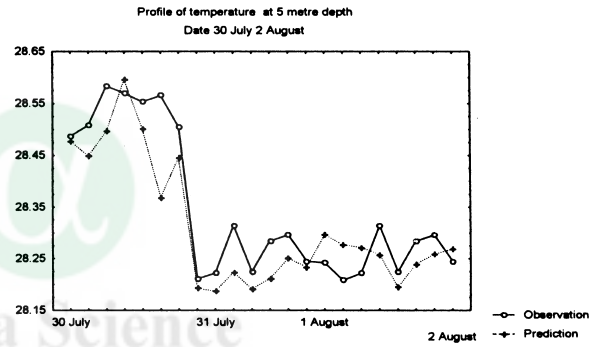

Figure 9

Forecast of temperature at 10 meter level is shown in figure 10.

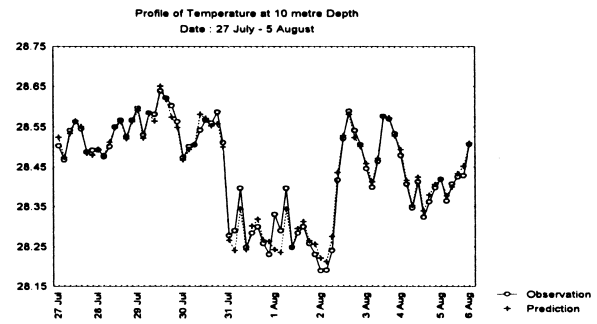

Figure 10

CONCLUSIONS:

Analysis of surface marine meteorological parameters taken onboard ORV Sagar Kanya during Stationary Period I (SP I) and the synoptic weather conditions observed over the Indian region during BOBMEX-99 is discussed here. The surface pressure gradient is observed to be strong in SP I over the Bay region. At air sea interface the high value of heat flux is seen to be associated with the higher values of wind speed. The prolonged rainfall event on 30th July showed considerable decrease in sea surface temperature is due to incursion of fresh water to the sea surface. The high value of SST was associated with low pressure systems. So during the SP I the SST was one of the important reason for the occurrence of the convective systems over the Bay of Bengal.

During the convective processes over the Bay of Bengal the exchange process between air sea interface was continuously changes from sea to air and vice versa. But when there was no low pressure system, the SST was always greater than the air temperature. So the exchange in the air sea interface was always from the sea to air.

From the temperature profiles at different depth it seems that during the time of convective processes the temperature gradient with depth became smaller. There was a prolonged rainfall from 30th July to 1st August. So due to the mixing of fresh water from to the sea, the upper layer (5Mt. and 10 mt.) temperature was reduced. But upto 20mt. depth, there was no mixing, so no abrupt change in the sea temperature. And so the temperature gradient became smaller at that time.

These ocean-atmosphere interaction processes need further study.

ACKNOLEDGEMENT :

Authors wish to acknowledge Department of Science and Technology for financial support in the form of research grant under which this work has been carried out.

References :

Bhat G.S., Gadgil S., Hareesh Kumar P. V. , Kalsi S.R., Madhusoodanan P., Murty V.S.N., Prasada Rao C.V.K., Ramesh Babu V., Rao L.V.G., Rao R.R., Ravichandran M., Reddy K.G., Sanjeeva Rao P., Sengupta D., Sikka D.R., Swain J. and Vinayachandran P.N. (2001) : *BOBMEX: The Bay of Bengal Monsoon Experiment,* Bulletin of the American Meteorological Society, **82, 10** 2217-2243.

Bhide U.V., Nagar S.G., Mahajan P.N. and Sikka D.R. (1986) : *Fluxes of Sensible and Latent Heat at the Air-Sea Interface over the Equatorial Arabian Sea During MONEX-79,*Current Science, **55,** 699-701.

Gadgil S., Joseph P.V. and Joshi N.V. (1984) : *Ocean-Atmosphere coupling over monsoon regions,* Nature , **312,** 141-143.

Ghanekar S.P., Mujumdar V.R., Seetaramayya P. and Bhide U.V. (2001) : *Variations of surface fluxes and meteorological parameters during the field phase experiment BOBMEX-1999in relation to the prevailing monsoon conditions,* Proceedings of TROPMET 2000, National Symposium on Tropical Meteorology, Cochin University of Science and Technology, Kochi, February 2001, 390-395.

Ghanekar S.P., Mujumdar V.R., Seetaramayya P. and Bhide U.V. (2003) : *Ocean-Atmosphere interaction and weather conditions in association with the two contrasting phases of monsoon during BOBMEX-1999*, Proc. Indian Acad. Sci. (Earth Planet Science), **112,** 283-293.

Sam N.V., Mohanty U.C. and Satyanarayana A.N.V. (2000) : *Conserved variable analysis of the marine boundary layer and air-sea exchange processes using BOBMEX-pilot data sets*, Proc. Indian Acad. Sci. (Earth Planet Science), **109,2** 305-314.

Disaster Management
Editors: N.C. Mahanti et al.

Study on Coastal Vulnerability of Digha-Shankarpur Region

Sayanti Sen, Meenakshi Chatterjee and Goutam Kumar Sen

School of Oceanographic Studies, Jadavpur University, Kolkata 700 032, India

ABSTRACT

Coastal tract, an interface or transition zone between two distinct environmental domains of the land and the sea, is inhabited by three Quarters of the world population, Coastal eco-system is subjected to Dynamic physical features like erosion, accretion, storm and cyclone, sea level changes etc. This zone is a priority site for ports, ancillary industries, urban growth centers, aquaculture, mariculture, tourism, agriculture and waste disposal. Degradation of coastal and marine ecosystem, declining water quality and population, over exploitation of coastal resources are some of the major concern areas of the Coastal Zone Management.

Digha, Sankarpur, Dadanpatra area from sea font to landward is represented by beach face, coastal dunes, sandfilled interdunal depression, older dunes and older tidal flats. The coastal dune in this area is threatened by landward migration of high tide line and therefore the township has been protected by sea wall near Digha. This has resulted in acceleration of erosion on the beach and the unprotected eastern side from Old Digha to Digha Mohana (entire zone of Sankarpur is severely threatened by coastal dune retreat). However the western part of the unprotected coastal stretch (from Old Digha to mouth of Subarnarekha river) and part of Dadanpatrabar are under accretion. Coastal erosion and increasing tidal activity, wave interaction, excess rise of water level during depression are responsible of this increasing erosion.

In this study attempts have been made to look into the zones vulnerable to dynamic physical force like coastal erosion, coastal inundation and sea level changes which causes extensive damage of coastal properties.

To carry out this study tide data have been collected for last one year. This data have been analyzed to demarcate the changes in tide level at different season. Position of Tide level or water level along the coastal stretch have been marked using GPS and this data have been analyzed extensively to compute the variation of water level from extreme low water line (during lowest tide) to extreme high water line (highest tide). This spatio temporal variation of tide line have been shown using GIS model in a map for different season.

It has been felt from Government sector that appropriate coastal zone management plan by taking into consideration the results of such study need to be prepared so as to determine development strategies from the point of view of sustainable development. This aspect will also be discussed here.

INTRODUCTION

1.1 Importance of coastal areas:

Coastal tracts, the interface or transition zone between two distinct environmental domains of the land and the sea, which is inhabited by 75% of the world's population. These coastal eco-systems are subjected to dynamic physical processes like erosion, accretion, and impacts from cyclones and associated storm surges, earthquakes and sea level changes etc. Studies by the International Geographical Union's Commission on the Coastal Environment have shown that more than two third of the world's sandy coastline have retreated during the past few decades, and only less than 10% have prograded (Bird, 1996). This situation is expected to deteriorate if sea level rises at predicted rates. (IPCC, 1996). With the majority of the world's population located in the coastal zone and the main population growth for the coming decades predicted to be in coastal areas, the need to estimate potential coastal erosion and associated property damage caused by sea-level rise is acute. The development of coast-effective method to asses risk, which allows coastal managers

and planners to rapidly determine high-risk areas in the coastal zone, is important to manage the coastal zone effectively over the next five to ten decades. (Hennecke.2000)

STUDY AREA

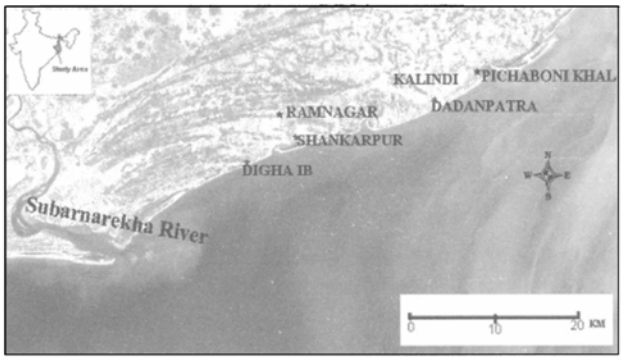

Figure 1

The coastal stretches of Medinipur a district in West Bengal are well connected with the district headquarters at Medinipur and state capital Kolkata. A network of metalled road exists in the area that makes accessibility easy. The study area within Digha and Sankarpur located between 21°36'50"N and 21°39'00" N Latitudes and 87°29'40"E and 87°37'00" E Longitudes extends along the coastline starting from Sankarpur up to the mouth of Subernarekha River across the Orissa border.

The physical features of the area of Digha, Sankarpur moving landwards from the sea front consists of beach faces, coastal dunes, sandfilled interdunal depressions, older dunes and older tidal flats. The coastal dune in this area is threatened by landward migration of the high tide line and therefore the township has been protected by a sea wall near Digha. In Sankarpur this inward migration of flood tide line other aggravates the situation during storms Season (pre-monsoon and post –monsoon phase). As a result of which continues breaking of lines take place and beach slope tends to be flatten as more dune erosion occurs. This has resulted in an acceleration of the erosion of the beach. In fact, the entire beach of Sankarpur is severely threatened by coastal dune retreat. However, the western part of the unprotected coastal stretch, from Old Digha to the mouth of River Subarnarekha, and part of Dadanpatra bar are under accretion. Coastal erosion and increasing tidal activity, wave interaction, excess rise of water level during depression are responsible for this increasing erosion.

DESCRIPTION OF COASTAL STRETCH

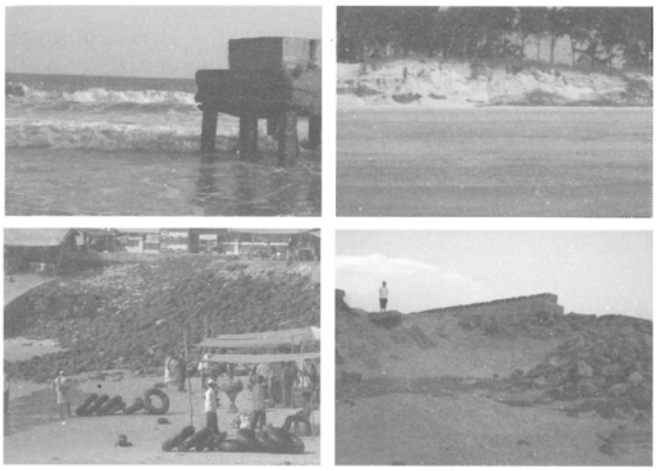

Figure 2

The coastal stretch of the study area extends from the mouth of Subarnarekha River to the entire zone of Sankarpur and Dadanpatrabar coast, up to Pichaboni Canal. The coastal Plain is characterized by an almost flat terrain at places separated from the sea by a chain of sand dunes. This plain is formed mainly by the interaction of marine coastal, fluvio-deltaic, fluvio-tidal and fluvial processes. Regional picture shows a very gentle slope from north to south towards sea. The present area comprises marine coastal landforms, which on the whole reveals a rolling topography exemplified by the dune ridges with intervening flats. The general slope of marine coastal landforms varies in different terrain units. The beach in New Digha shows a very gentle slope towards the sea. The township is situated on old dune complexes and on the intertidal flats. A narrow strip of Casurina has been planted by the Forest Department Govt. of West Bengal along the coastal belt for the protection of the beach from erosion as seen in the above picture. It is very astonishing to observe that these trees are now severely depleted by the human activities over the years.

The Sankarpur beach, to the east of Digha is larger than Digha and several undulations are noticed in places. This basin is wide and flat with hard sand, bordered by well-vegetated beachfront and dunes. At places along the Sankarpur coast, several places have been broken down by the waves during the high tide, which has caused large loss of property and life. One of the prominent features of the beach at Sankarpur the sandy pits all over the coastline, which are usually formed due to the flood tidal activity.

DATA COLLECTION METHODS

The main emphasis of this paper is to describe a method that allows a quick and cost effective estimate of physical impacts of rise in sea level on open-coast and deeply embedded shorelines (K.R Thompson 1997). This method allows the study of the zones vulnerable to dynamic physical forces like coastal erosion, coastal inundation and sea level changes that cause extensive damage of coastal properties. Sea level change means the changes in the water envelope due to the varying tidal features, wave activity etc. The data comprises of the positional information of water level on the coast as tide level varies with time. This data has been analyzed to identify the seasonal changes in tidal levels. Tide or water level along the coastal stretch has been recorded using a GPS and this data have been analyzed extensively to compute the variation of water level from extreme low water line (during ebb tide) to extreme high water line (flood tide). A beach profile along the coastal stretch of Digha and Sankarpur has been created using a Theodolite and graduated staff. A GIS based model has been developed

a. To simulate the water envelope at different times and locations.

b. The rate at which water increases/decreases seasonally.

c. The rate at which water increases/decreases during high and low tides.

METHODOLOGY

The waterfront along the coastal stretch has been recorded using number of GPS at different locations and times of the year along the land water interface (coastline which varies with tide level). This data has been analyzed extensively to compute the variation of water level from extreme low water line (during ebb tide) to extreme high water line (flood tide) as it happens during the day. A beach profile along the coastal stretch of Digha and Sankarpur has been measured at different locations using a Theodolite and graduated staff. Firstly the Theodolite was taken to a location then the stand was leveled with the help of the bubble attached to the stand. The A, B, C, D vernier in the Theodolite was adjusted to start with. Then the graduated staff was placed at different points on a line normal to the coast from the Theodolite, which was placed at one end point of this line away from the coast. Here we take measurement of vertical angle corresponding to the lowest point of the staff with the horizontal line of sight. The Slope of the beach has been calculated by taking the horizontal water line as well as the vertical line across the coast. The vertical slope is taken by the help of Theodolite that gives the height from the ground and also the slope. Horizontal water line has been taken with the help of two GPS to mark the positional value at same position along the opposite direction from the vertical line. This whole process of taking the horizontal positions varies from time and distance along the either sides of the vertical line. Using this information we can know the gradient of the coastal

stretch. The data collected was processed using GIS techniques and the Mapbasic routines enabled getting visual representation of the data gathered during field data surveys. The rates of water level increase/decrease were computed with numerical computation program using C++. Using GIS techniques, it was demonstrated as to what are the estimated levels of water based on basic data gathered on rate of change in water level.

RESULTS AND DISCUSSION

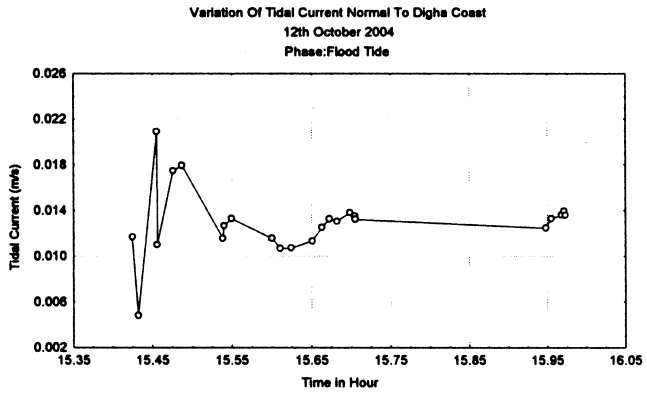

Figure 3

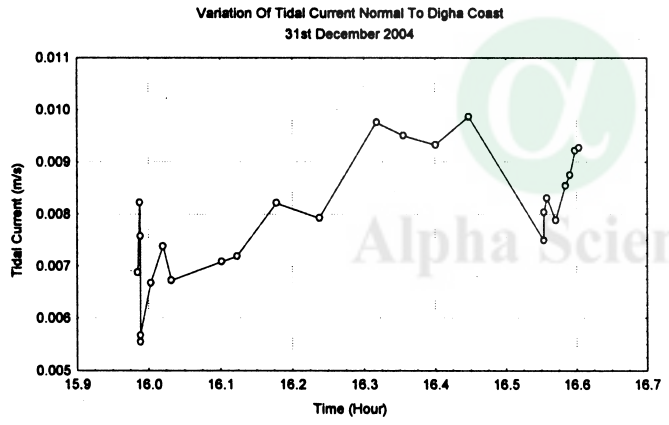

Figure 4

RESULTS AND DISCUSSION (contd)

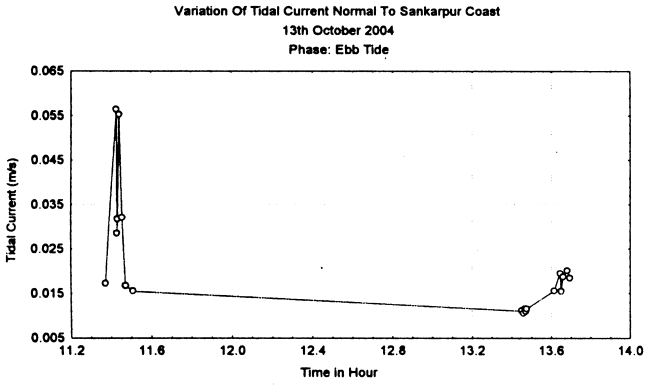

Figure 5

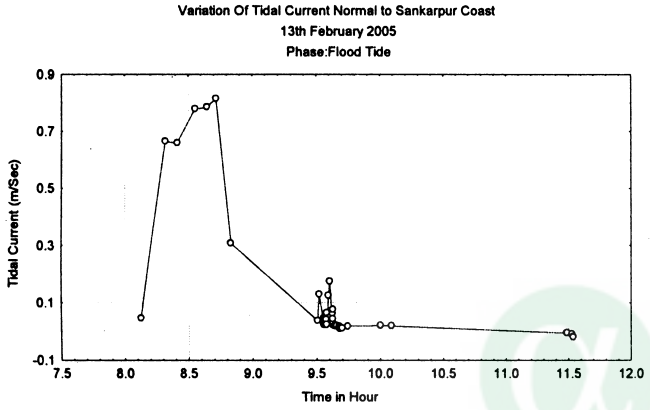

Figure 6

The above graph shows the variation of tidal current along Digha and Sankarpur Coast. This graph has been extracted from the data taken. In this graph X-axis represents the time in hour where as the Y-axis represents the rate of change of tidal current in meter per seconds. In Figures 3 and 4, the graphs are of two different months of the same year but are of the same phase of the tidal line. These two graphs show the tidal rate change for 1 hour. From the two figures, it is apparent that rate of change of tidal current is more at Sankarpur than that at Digha. During the month of October, initially the rate of tidal current remained high but with passage of time the rate lowered and gradually reduced to a steady state value. In December, the tidal current had low absolute values but there has been a continuous wide change of tidal current during the period.

Variation of tidal rate during post monsoon period i.e. the month of October in Sankarpur shows a wide range of tidal rate from 0.005 to 0.065m/s. In the pre-monsoon phase i.e. during February the tidal rate range extends from -0.1 to 0.9 m/s. These two phases have been taken into account during the two tidal extremes (high tide) and (low tide). Although being a phase of low tide during post monsoon, Sankarpur has seen a wide change in tidal current as depicted particularly on figures 5 and 6.During the pre-monsoon phase, Sankarpur faces huge variations in tidal rate during the first few hours of the high tide. Later during the day, the rate decreases.

VARIATION OF WATER LEVEL AT DIGHA AND SANKARPUR COAST

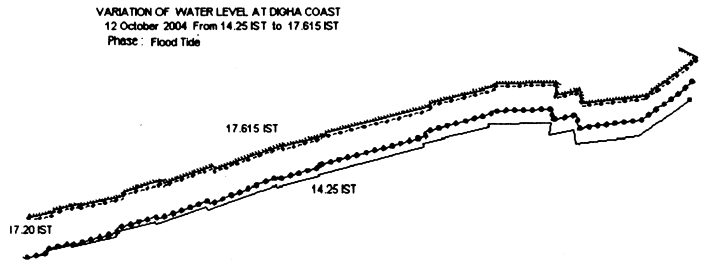

Figure 7

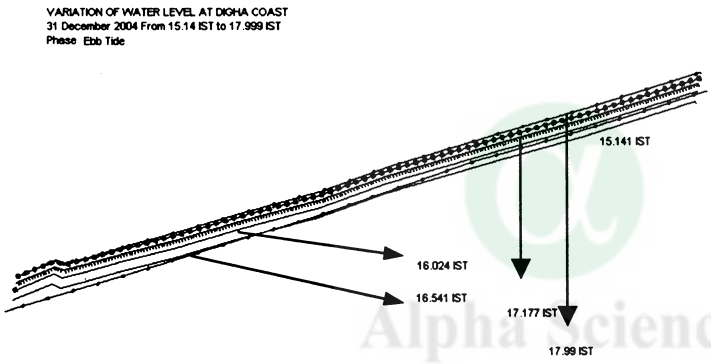

Figure 8

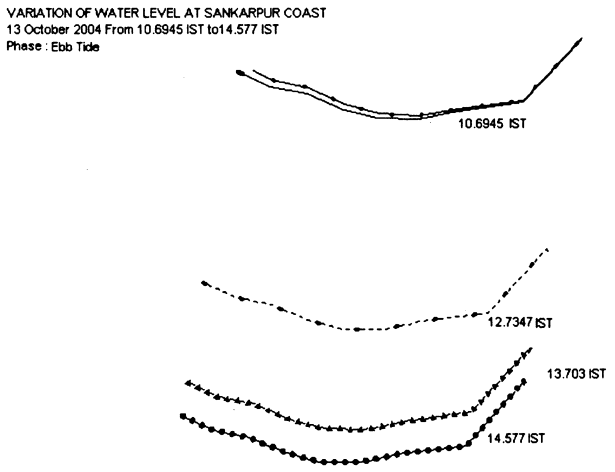

Figure 9

Figure 10

During post-monsoon at Bay of Bengal, the possibility of generation of storm becomes very prominent as a result of which tidal activity and wave activity becomes more vigorous during these phases.Wave amplitude also increases after being coupled with tidal waves. During this phase the tidal range becomes very high.Here we have shown in Fig 7 and 8 variation of tidal current at Digha coast on October 12, 2004 and December 31, 2004. From the above diagrams, the feature of tidal range variation during immediate post-monsoon month and winter month is easily discernable. Tidal range is very high in post monsoon month and comparatively low in winter months(February). Fig 9 and 10 shows variation of water level at Sankarpur coast on October 13, 2004 and February 13, 2005. In immediate post-monsoon months, the variation is very high over a time span of 4 hours. It may be noted that the time difference between flood tide and immediate ebb tide is 6 hours. In the month of February, this difference in tidal activity over a time period of 3 hours is quite low. If we compare the vigorness of tidal activity in two locations in the immediate post monsoon months, we find that at Sankarpur tidal mark activity and its impact are more severe than that observed at Digha. For this reason Sankarpur region has become a zone of intense tidal activity. It may be noted that asymmetry in flood and ebb flow patterns can cause effective tidal flusing and rapid growth of bivalves leading to severe coastal erosion. It may be concluded that tide measurements at two different coasts needs to be carried out to understand this feature with elaborate details.

SALIENT FINDINGS

- Tidal as well as wave activity is more severe in post monsoon months.
- Tidal and wave activity is less severe in winter months.
- Tidal activity at Digha is less severe that at Sankarpur.
- Information obtained through this subsequent analysis when processed through GIS model can easily contruct GIS map with respect to risk zones at different stretches of coast.

CONCLUSION

Coastal Management issue related to disaster management needs study on variation of tide pattern with time as well as space. In this investigation a method has been adopted to take account of physical impacts for nearshore circulation due to variation of tides. From this study distinctive features of variation of tide pattern with season as well as at different coastal cells have become prominent. From these features it is possible to make assessment about the degree of risk due to aggravated coastal erosion. During post-monsoon storm season the variation of tidal range is significantly high in Shankarpur region than that at Digha. Our comparative study also shows that in winter season variation of tidal range is more than that in Digha. The variation of the tidal cycle along the coastal track of Digha and Sankarpur region shows that the asymmetry in flood and ebb tide causes high rate of coastal erosion, which has resulted in destruction of sand dunes along the coast. This is due to the fact that through continued processes of erosion in Sankarpur there is significant lowering of beach slope in this region as a result of which more tidal water finds inroad towards the landward side and during post monsoon storm season more surface waves can easily get access to destroy the sand dunes. From these studies we can easily mark the risk zones along the Digha Sankarpur stretch of West Bengal coast. \

ACKNOWLEDGEMENT

Authors wish to acknowledge Indian Space Research Organization for financial Support in the form of research grant under which this work was carried out.

REFERENCES

Bird EFC.1996.Coastal erosion and sea level rise. In: Milliman JD, Haq BU, editor. Sea-level rise and coastal subsidence. Kluwer Academic Publishers.Dordrecht;p 84-104.

Bruun P.1983. Review of conditions for uses of the Bruun Rule of erosion. Coastal Engineering, 7; 77-89.

Bruun P.1988.The Bruun Rule of erosion by sea-level rise: a discussion on large-scale two-and three-dimensional; usage. Journal of Coastal Research, 4(4): 627-648.

Hennecke G Werner, Greve a Catharina, Cowell J Peter, Thom G Bruce .2000.GIS-dased modeling of sea-level rise impacts for coastal management in southern Australia.

K.R Thompson, D.E Kelley, D.Sturley, B.Topliss and R.Leal.1997.Nearshore circulation and synthetic aperture radar: an exploratory study.

Disaster Management
Editors: N.C. Mahanti et al.

Use of Satellite Observations for Tropical Cyclone Monitoring and Prediction for Disaster Management

P.K. Pal, C.M. Kishtawal, Randhir Singh and P.C. Joshi

Atmospheric Sciences Division, Meteorology and Oceanography Group Space Applications Centre
Ahmedabad-380 015, India

Introduction

Satellite observations of tropical cyclones can be divided into two categories viz. "diagnostic" and "prognostic" applications. For a diagnostic application, satellite data are used to determine a specific property of a tropical cyclone such as the position, intensity, etc. The Dvorak classification technique is an example of a diagnostic algorithm for storm intensity. For a prognostic application, satellite data are assimilated to more accurately determine the initial condition for a statistical or numerical TC prediction model. Satellite-derived winds are a good example here. We propose that current and planned satellite-derived data will be useful toward both of these types of tropical cyclone applications.

Satellite Observations for Tropical Cyclones

The specific types of satellite observations with applications to tropical cyclones can be divided into six basic categories: 1) Visible/Infrared Imagers, 2) Infrared Sounders, 3) Microwave Imagers, 4) Microwave Sounders, 5) Scatterometers, and 6) Radar Altimeters. The first two types of measurements are available from geostationary and polar-orbiting satellites. The last four are currently only available from polar orbiting satellites (and this will be true for the foreseeable future). Listed below are some of the satellites/instruments that will provide these measurements. In the following sections we present a discussion on how these systems can be used for tropical cyclone analysis and forecasting. Although the TC applications are listed separately for each group of measurements, the full value of the satellite observing system will be realized only when the best aspects of all of systems are combined (The list below includes only those satellites that are relevant to Indian Ocean cyclones)

1) Visible/Infrared Imagers

Geostationary:

INSAT (India)
Meteosat Second Generation/Advanced Imager
KALPANA (India)

Polar:
NOAA AVHRR (current-2010)
DMSP/OLS (current-2015)
Terra, Aqua/MODIS (current-2007)
METOP/AVHRR (2005-?)
NPP/VIIRS (2005-2011)
NPOESS/VIIRS (2009-?)

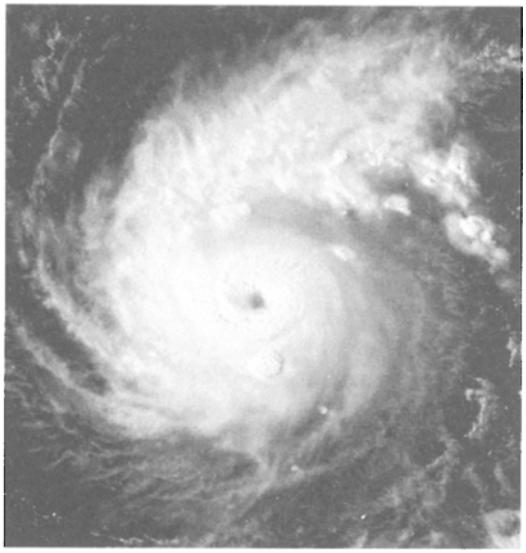

Fig-1 : Cyclone seen by IR-Sensor.

The imagers on the geostationary (GEO) and polar-orbiting (low earth-orbiting (LEO)) satellites provide the data for the position and intensity diagnostic algorithms that complement the aircraft data. In many tropical cyclone basins, position and intensity estimates from satellite imagery are the primary sources of these

parameters. The visible and IR Dvorak methods have been used for about two decades, and research is currently underway to refine objective versions of these algorithms. As additional imager channels with higher resolution become available, new research will be required to improve the position and intensity estimation methods, and develop new methods that are not necessarily constrained the current Dvorak rules.

Satellite IR imagery is used for tropical cyclone precipitation estimation, which is of particular importance in landfall situations. The geostationary instruments have the advantage of high time resolution, while the polar-orbiting instruments tend to have higher spatial resolution. For the analysis of Atlantic and Pacific cyclones, the GOES hydro-estimator technique developed by NESDIS makes use of the IR window channel, and a newer multi-spectral method uses all five of the current GOES imager channels, and similar techniques may be useful with the help of INSAT-3D data. The advanced imagers of the future will have many new channels. In the near-term, research in improved rainfall estimation methods could also be performed using new imager channels on polar satellites (MODIS, NPP, etc). These data will provide new opportunities for improving IR-based tropical cyclone rainfall estimates. The bigger payoff may likely be the increased number of passive microwave sensors and their combination with IR sensors.

The primary energy source for tropical cyclones is oceanic heat content. Changes in the upper-oceanic thermal structure can affect the intensity trends of tropical cyclones. Satellite-based Sea Surface Temperature (SST) analyses make extensive use of the AVHRR imager channels, and more recently TMI channels. These analyses have the potential for improvement by taking advantage of new channels which are becoming available to better correct for aerosols (for example, from moisture or African dust). Combined SST analyses making the best use of IR (GEO + LEO) and passive microwave measurements will likely lead to improved all-weather products.

Information derived from the IR imager channels (current and future) has the potential to improve tropical cyclone numerical model forecasts by assimilation of the radiances. Cloudy radiances can be assimilated directly into the model and together with other variables can be used to improve the model precipitation fields. Clear-sky radiances can be assimilated in the tropical cyclone periphery to better establish the environmental conditions. Initial conditions for the model forecasts can also be improved by directly assimilating the satellite precipitation estimates through a procedure called physical initialization, which adjusts the model moisture/precipitation fields to agree with the observations.

2) Infrared Sounders

Geostationary:
INSAT-3D -- 19 Channel Sounder (2008-)

***Polar*:**
NOAA 15-17/HIRS (current-2010)
AQUA/AIRS -- hyperspectral (2002-2006)
METOP/HIRS (2003-?)
NPP/CRIS (2005-2011)
NPOESS/CRIS (2009-?)

The primary tropical cyclone application of the IR sounder data is through assimilating the radiance information into numerical models. This will lead to large improvements in the vertical resolution of the derived temperature and moisture profiles in clear areas and above cloud top level. These measurements would improve the representation of the initial temperature and moisture fields in the storm environment. Moreover, diagnostic intensity algorithms could be developed from this data. To better describe the tropical cyclone environment, the high-resolution sounders will have immediate application via improved height assignments for cloud and water vapor motion winds. Research is needed on developing a method for tracking moisture or temperature structures derived from clear-sky sounding fields, where the altitude of the features is already resolved by the retrieval.

3) MicrowaveImagers

***Polar-only*:**
DMSP/SSMI (current)
TRMM/TMI (current)
AQUA/AMSR (2002-2006)
ADEOS-II AMSR (2002-?)
WindSat (2002-2005/7)
DMSP/SSMIS (2003-2012?)
Advanced AMSR (GCOM B1) (2007-?)
NPOESS CMIS (2008-202?)
GPM (2008-?)

The primary advantage of microwave observations is that they can provide information below cloud tops. Tropical cyclone applications of microwave imager data include qualitative methods for determining storm position, structure (eyewall, rainbands below the cirrus shield, etc), and for quantitative surface wind speed (outside raining areas), rain rate estimation, total precipitable water, and cloud liquid water. These data have the advantage over IR data for rainfall estimation because the measurements are more physically related to the precipitation. Fruitful areas for tropical cyclone research are to combine the high temporal and spatial resolution precipitation estimates from IR imagery on the geostationary satellites with the more physically based, but lower temporal and spatial resolution of the microwave precipitation algorithms .

The quantitative use of the microwave imager data for diagnosing tropical cyclone intensity has not been fully exploited. In particular, there is TRMM in recent years, and also a goldmine of SSMI data dating back to 1987. The "radar-like" signal presented by the SSMI microwave imagery differs from the IR in that only active (precipitating) clouds are delineated. This eliminates much of the tropical cyclone storm canopy cloud that can often hide important structure from the IR techniques. Storm organization and contracting eyewall cycles can be much more easily recognized in these data, which can lead to improved intensity diagnoses. Research in this area is highly recommended, especially if fused with existing/proven IR-based objective methods (Bankert and Tag, 2002).

4) Microwave Sounders

***Polar only*:**
NOAA-15-17/AMSU (current-2010)
HSB – Aqua (2002-?)
DMSP/SSMIS (2003-?)
METOP/AMSU/MHS (2005-?)
NPP/ATMS (2005-2011)
NPOESS/ATMS (2009-?)

Similar to the microwave imager data, the microwave sounder data can provide valuable information below cloud-top level. Tropospheric thermal measurements can be obtained in non-raining cloudy regions (although at reduced vertical resolution). One of the largest reduction in errors in global forecast models occurred when NWP centers began to assimilate the radiances from the AMSU instrument. In tropical cyclone applications, the microwave sounder data have proven to be useful for diagnosing storm intensity and size. Current algorithms are limited by the footprint size (50 km near nadir) of the AMSU instrument. However, these algorithms are showing great promise as an alternative to the IR-based methods. Further research (near term) is needed to refine these techniques, and develop integrated algorithms that exploit the microwave sounder with the imager (i.e., SSMIS) and IR. These algorithms can be further advanced as the microwave sounding technology improves (i.e., with the introduction of ATMS).

5) Scatterometers

***Polar-only*:**
QuikSCAT (current-2003)
ADEOS II SeaWinds
METOP/ASCAT
SeaWinds (AlphaSCAT)
NPOESS/ASCAT
OCEANSAT-2

The primary application of the scatterometer is for ocean surface wind vectors. These data are already proving to be very useful for determining the outer wind structure of tropical cyclones, identifying closed circulations of developing systems and providing lower limits for maximum sustained winds. Efforts are also underway to assimilate these data into numerical models (ECMWF and NCEP currently assimilate operationally and FNMOC will by 2003). The current QuikSCAT system is limited by the fairly large footprint size and attenuation in heavy rain areas, and can only reliably estimate surface winds up to 40 kt. These limitations should become less of a problem as the scatterometers continue to improved by moving away from Ku-band that is so susceptible to rain. The alternative is to have collocated passive microwave to allow rain correction. Further research on the development of specific tropical cyclone surface wind algorithms is encouraged.

6) Radar Altimeters

***Polar-only*:**
ERS-2 (current)
Topex-Poseiden (current)
Jason-1 (2002-?)
Envisat (2002-06)
Icesat (2002-05)
Cryosat (2004-07)
ISS Abyss (2006-12)
Wittex (2006-10)
Geosat Follow-On (current)
Jason-2 (2007-11)

Many studies have shown that ocean sub-surface thermal structure plays an important role in tropical cyclone intensification. In areas such as the western Caribbean and near warm-core rings in the Gulf of Mexico, the warm water extends to much larger depths than in other areas, so there is much more heat energy available to the tropical cyclone. The sub-surface ocean structure can be inferred from satellite altimetry data. Research to better use this information in statistical forecast algorithms and in coupled ocean-atmosphere models has the potential to improve tropical cyclone intensity forecasts.

The altimeter observations would be more useful with improved temporal and areal sampling. However, this is difficult due to the necessity for repeat tracks required for many applications. Proposed scanning or multi-beam altimeters potentially can dramatically increase spatial sampling and fill in data voids. International cooperation is required and is moving forward. Fortunately, time scales for many oceanic phenomena are much slower than their tropospheric counterparts, so that even limited temporal observations still provide useful information.

The future appears bright for our space-based observing system. Advanced, multispectral (visible, IR, and passive microwave) imagers, sounders (infrared and microwave) and scatterometers are planned for launch in the near future. Hyperspectral measurements from newly developed interferometers are expected to be flown experimentally by 2006. The information content will vastly exceed that of the current measuring devices. Instead of a few dozen viewing channels, these instruments will have more than a thousand channels over a wide spectral range. The satellite data downloads are expected to exceed several terabytes

per day. Fortunately, communications and computing capacity are increasing at a rate that hopefully can accommodate this data explosion. Emerging new technologies (including the use of rapidly-developing visualization tools) will be employed. It is important that the evolving space-based observational system keep one step ahead of the demands being placed by the user community and advances in numerical weather prediction. While it will become an enormous task and challenge to assimilate this wealth of data into meaningful parameters, the outlook is bright for unlocking the still-unresolved mysteries toward improving our understanding and prediction of tropical cyclones.

Future Scope : Optimum utilization of distributed satellite observations for Tropical Cyclone monitoring

Interest in dividing the functions of a single large satellite among several smaller and simpler units working in tandem is gaining more momentum for an increasing number of space applications. Satellite clusters that include several smaller satellites that collaboratively work together on a satellite mission, thus forming a "virtual" satellite, are commonly referred to as *Distributed Satellite Systems (DSS)*. Multiple, distributed agent-based satellite systems are envisioned because they are capable of higher performance, lower cost, better fault tolerance, reconfigurability and upgradability. For tropical cyclone monitoring, a system of satellites, each capable of delivering a specific kind of observation (e.g. distributed observations by Imager, Sounder, Altimeter, and Scatterometer from four different small satellites, as discussed in the previous sections) and arranged in a *optimum formation* can be an ideal strategy. There are two general cases of formation flight: leader-follower, and same ground track. The most basic configuration in which spacecraft can fly in formation is that of leader and follower shown in Fig. 2(a). In this configuration, the orbital elements of each spacecraft are intical except for the true anomaly, meaning that the spacecraft follow the same orbital path at different times. This formation is an ideal stepping-stone to more difficult formations such as same ground track. The another formation flight configuration (same ground track) named "ideal" by NASA Goddard , illustrated in Fig. 2(b), is one in which two or more satellites have identical ground tracks. The leader-follower configuration described above does not produce identical ground tracks in any non-equatorial orbit due to the rotation of the Earth under the inertial orbital frame. It is possible under Keplerian conditions to define two circular orbits that create identical ground tracks at different times.

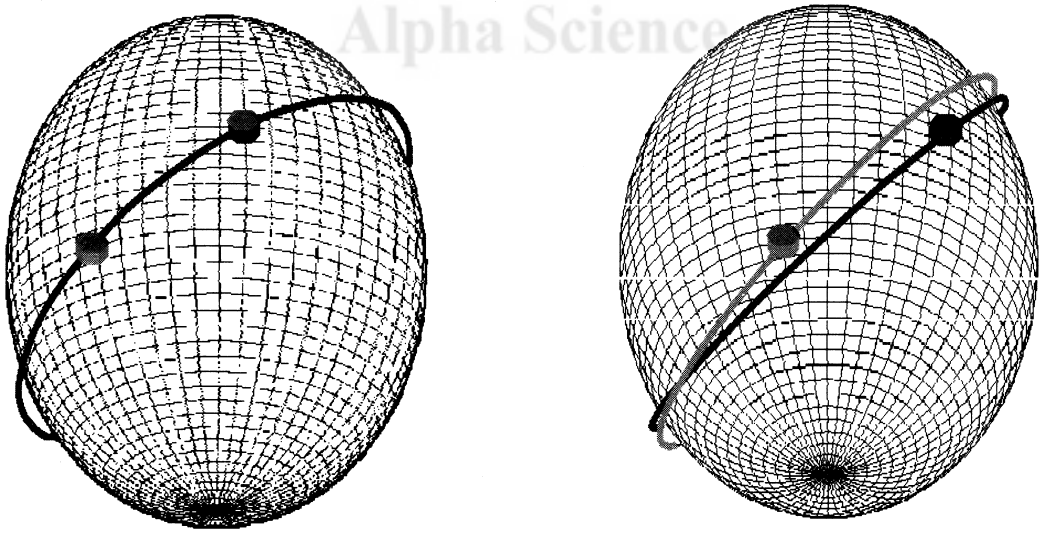

Fig. 2: (a) Leader-Follower and (b) Identical ground track formation

While the Identical ground track formation is preferred for a number of advance remote sensing applications like interferrometry, sensor performance calibration, and studies of atmospheric processes like convection using a number of sensors, a simpler *leader-follower formation* would be more suitable for cyclone monitoring where the emphasis lies on obtaining more frequent observations of a moving system. Leader-follower formation provides higher probability of tracking the position and intensity of a moving cyclone. If we consider the case of 4 small satellites in low-earth orbit (~ 400 km altitude), the time separation between the passes of two successive satellites will be about 25 minutes, making it easier to track all the satellites with a single ground station. Moreover, the sensor components can be distributed among these satellites to optimize the quantum of information that these satellites may provide. For example the satellites in the formation flying may have the following sensors (1) Microwave Imager (2) Microwave Sounder (3) Microwave Imager (4) Scatterometer. All of these sensors have the capability of detecting accurate location of the cyclone center, while the observations of precipitation and convection patterns from microwave sounders and imagers can be utilized for the analysis and forecasting of tropical cyclone intensity.

References

Bankert R.L., and P.M. Tag, An automated method to estimate tropical cyclone intensity using SSM/I imagery, *Jour. Appl. Meteor., 41*, 461-472, 2002.

Dvorak, V.F., Tropical cyclone intensity analysis and forecasting from satellite imagery, *Mon. Wea. Rev., 103*, 909-918, 1975.

Dvorak, V.F., *NOAA Tech Rep., NESDIS,11*, 47 pp., 1984.

Disaster Management
Editors: N.C. Mahanti et al.

Coupling of Evapotrnspiration Rate, Hydrological Cycle and Land Surface Processes Over Sabarmati River Catchment Area

Manoj Kumar, Vyas Pandey and A.M. Shekh

Department of Agricultural Meteorology, B.A. College of Agriculture
Anand Agricultural University, Anand-388 110, India

Past few years an upsurge in studies on the land component of the hydrological cycle over various temporal scales. It is now well recognized that the hydrological processes at the land-atmosphere interface play a crucial role in maintaining long-term climate and the temporal variability of weather and climate. The lands that do not have the capability to withstand agriculture are being put under agriculture, to meet the additional demand, causing severe hydrological imbalance. These increased culturable area demands, additional water to meet the irrigation requirements. To meet these demands, reliance on groundwater has been rapidly increasing, especially in the arid and semi-arid regions like India, where the current groundwater potential (43.2 Mha-m year $^{-1}$) needs to be judiciously utilized.

Imprudent exploitation of groundwater resources may often result in undesirable and irreversible consequences and thus demands better and simplified means of recharge predictions at micro level. Researchers (Harpaj, 1971; Athavale, 1988; Johnson, 1987; Sharma, 1987; and Rai et al., 1997) have come out with numerous methods/procedures for estimating GW recharge. These includes the use of base flow hydrographs, hydrologic budgeting/water balancing, empirical models, GW level fluctuation method, two dimensional and three dimensional GW hydrological models.

Most of the previous researches have dealt GW budgeting at a bigger scale i.e., basin/regional scales (Beven and Kikby, 1979) with using precipitation, stream flow (which integrates precipitation over an entire drainage basin), and other meteorological variables for many areas of the earth (Schulman, 1995; Stockton and Jacoby, 1989; Cook and Jacoby, 1983; Cleaveland and Stachle, 1989; D'Arrigo and Jacoby, 1991) have worked for reconstruction over central Asia and studies over stream flow of river basins.

In arid/semi-arid region, where LASPEX was conducted over Sabarmati river basin of Western India, different researchers to assess the water resource potential have done many studies. Pandey and Patel (1988) and Pandey and Gupta (1991) have worked out the water balance technique of selected stations of Gujarat. Pandey et al (2000) have worked out to asses the water resource potentials of Gujarat state using more than 150 stations spread over all parts of Gujarat state.

Studies have also been carried out to parameterization of land-atmosphere interface processes linked with hydrological processes (Famiglietti and Wood, 1994a). In his study, different component processes of the hydrological cycle was first determined over high resolution spatial and temporal scales and later aggregated to desired scales by cumulative totaling and then efficient algorithm of hydrological components estimation and their spatial aggregation through a statistical dynamic approach. Other scientists also linked hydrological approach with soil-vegetation atmosphere transfer schemes. Recently it has became easier to validate the GCM-calculated surface energy fluxes and other parameters due to a new dataset of the worldwise measured experiments (Garratt, 1994; Wild et al., 1995; Garratt and Prata, 1996).

In view of the importance of the knowledge of the agrometeorological parameters and assessment over any regions, Pandey et al. (2001) used water balance technique to asses the agroclimatic features of the LASPEX region with a synoptic view on physiology, edaphic, vegetation and climate. In their study, only five stations of LASPEX were chosen for the study but it has felt to have a comprehensive and composite picture of energy and water balance of the basins where LASPEX was conducted to prepare a document through specified research programs. Hence, the present work is undertaken.

Based on LASPEX data, surface layer parameters were found out for the entire experimental year. These surface layer parameters are stability deciding factors (Richardson number and stability factor), friction

velocity, roughness length, aerodynamic resistance, exchange coefficient for the momentum, stress, Monin Obhukhov length, and drag coefficients. Using these parameters, study on surface fluxes have been done. In the present study, attempt has also been made to find out the inter-relationship between different surface layer parameters using statistical model by correlation and then regression equations have been developed which were subsequently used to validate this model using the derived parameters and observed one.

MATERIAL AND METHODS

Experimental set-up

The experiment was conducted to study land surface processes (LASPEX) over Sabarmati river basin of Gujarat, which lies in the semi arid part of the western India with its central nodal point at Anand (lat 22 °35' N, long 72 °55' E, alt 45m). This area provided contrasting meteorological conditions from one season to another as well as intra-seasonal variability of weather parameters on the various scales, which was homogeneous with respect to vegetation and landscape.

A specially fabricated data logger with 32 channels was utilized in this experiment. The data logger DL 1032 was a self-contained battery operated data collection system for meteorological parameters. The unit worked on a lead acid maintenance free battery (11V-6.5 AH). A solar panel with charge controller was provided to charge the battery during daytime for uninterrupted power supply for successful operation of the system. Various sensors were used to measure wind speed, wind direction, air temperature, relative humidity, long wave radiation, short wave radiation, net radiation, soil temperature, atmospheric pressure and rainfall at desired time interval. The data logger acquired data from these sensors and stored the data in memory module at desired intervals of time.

Data thus stored on memory module were then transferred to the computer at Anand at 7 to 15 days time period.

WATER SUPPLY SYSTEM OVER GUJARAT REGION

According to Gujarat Water Supply and Sewerage Board (GWSSB), the villages of Gujarat State, out of total 19017 are broadly classified for purposes of planning of drinking water supply schemes, i. 1043 villages are difficult and scarcity villages; ii. 3230 are under especially backward areas; iii. 11092 village having unsafe water supply; iv. 3219 villages having inadequate water sources to be stepped up in per capita water supply; and v. 433 villages are deserted villages.

Hydrological cycle over Semi arid region of India

The western India comprises with different river basin, amongst them Sabarmati river basin is part of the mainland of Gujarat and west region of Rajasthan, India extending from Runn of Kutch and Aravali Hills in the north to river Damanganga in the South (Fig.1). It has total catchment area of 21674 sq km. The mainland is almost flat plain between altitudes 0 to 75 m AMSL made up to alluvial soil except for some sandy soils in the north. In terms of the standard climatic types arid, semi arid and dry sub humid climates are spread over this region. The regions in extreme north of the grid are under arid climate, the south under dry sub humid while central part comes under semi arid climate region with average rainfall of the basin 787.5 mm by the southwest monsoon.

HYDROLOGICAL SYSTEM OF THE SABARMATI RIVER BASIN

Data on hydrological system of Sabarmati river basin, which consists of both surface and groundwater resources, was obtained from the Government of Gujarat. Sabarmati river basin has a total drainage area of 21,674 km² of which 4124 km² (19.03%) is in Rajasthan. The maximum length of the basin is 300km and maximum width is 105 km. Basin's surface water resources are mostly concentrated in rivers and their tributaries. Sabarmati trunk, which is 371 km long, is the main source of surface water in the Basin. The

river has six tributaries namely, Sei, Wakl, Harnav, Hathmati, Watrak, and Bhogavo. Each of these rivers has its tributaries. The rivers Sei and Wakal flow in the Rajasthan part of the Basin and also originate from the Aravalli hills and flows South West parallel to the Sabarmati river up to their confluence with the river in Gujarat.

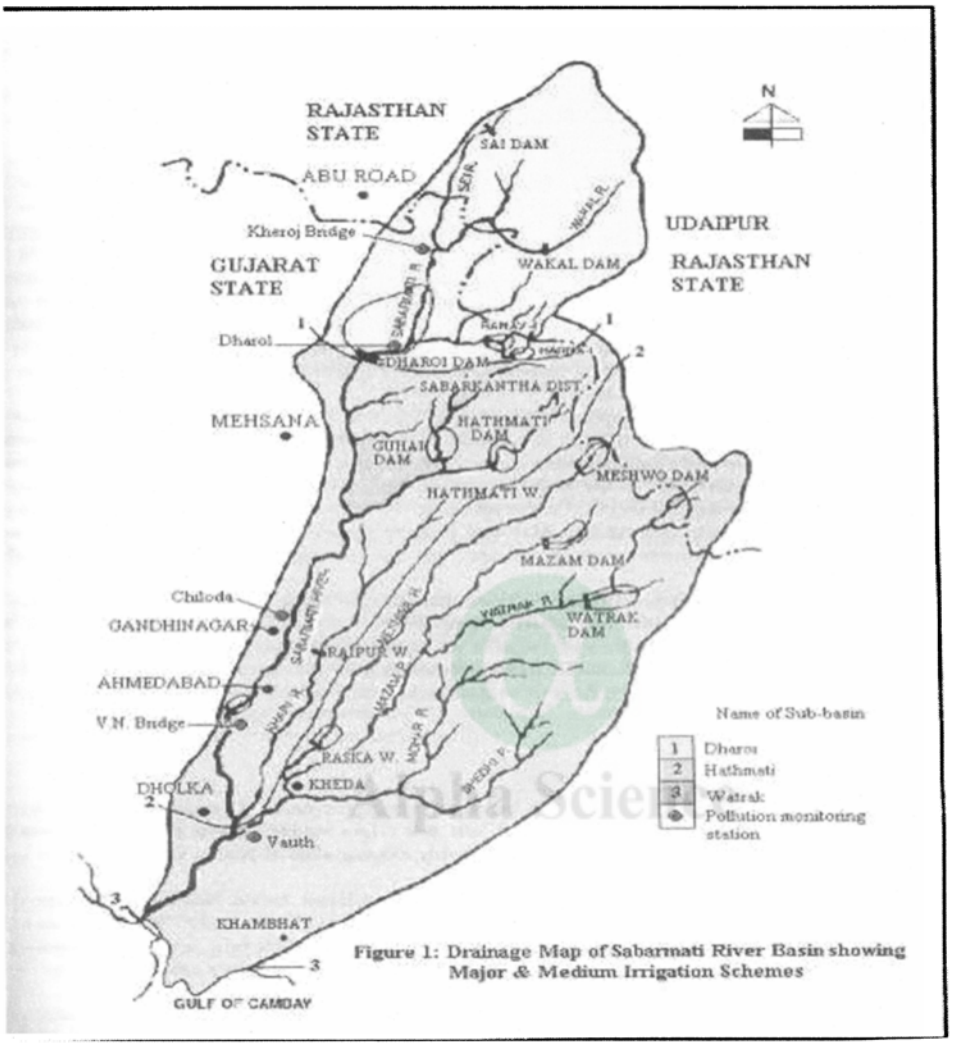

Figure 1: Drainage Map of Sabarmati River Basin showing Major & Medium Irrigation Schemes

Hathmati river has two tributaries, namely, Guhai and Indrasi. Watrak has four tributaries, namely, Khari, Meshwo, Mazam and Shedhi. According to the data obtained from the Govt. of Gujarat, out of three sub-basins, the maximum runoff observed in Dharoi sub-basin corresponds to the year 1973. the maximum estimated runoff of Hathmati and Watrak sub-basin corresponds to the year 1976. The maximum runoff of all the sub-basins was in 1987, when both Gujarat and Rajasthan faced one of the worst droughts of the century. The total dependable yield of the basin is 1987.67 MCM.

Table: Characteristics of the Sub-basins in Sabarmati Basin

Name of the Sub-basin	Catchment area (km^2)	Maximum Runoff	Minimum Runoff	Dependable Yield (Runoff) (MCM)
Dharoi	5540	3677.38	58.80	415.18
Hathmati	5656	1812.24	51.20	272.18
Watrak	10478	5151.09	67.30	1098.31
Total	**21674**			**1787.67**

Basin's Rainfall

Annual rainfall is the only source of water in the basin. This rainfall causes runoff and groundwater recharge. The basin has high to moderate rainfalls. The average of mean annual rainfall for the basin was estimated as 750mm. High rainfall occurs in the North Eastern hills that are part of the Aravalli mountain ranges. Magnitude of rainfall is low in the plains in the South-Western parts. The total quantum of rainwater falling over the basin area is estimated to be 16,000MCM. Out of 150 rainguage stations, data are available for 40 stations for significant number of years. In Watrak sub-basin, the mean annual rainfall varied from a minimum of 638mm in Vadgam to a maximum of 918mm in Modasa. In the case of Hathmati sub-basin, the maximum mean annual rainfall is 920mm in Dehgam and the minimum mean annual rainfall values are 780mm and 601 mm in Khedbrahmha and Hada respectively. Thus, the maximum spatial variation s in Hathmati river basin. The CV % varied from 40-61% in the case of Watrak, 41-63% in Hathmati and 42-55% in Dharoi. In the case of Hathmati sub-basin, only one out of the 15 stations had mean annual rainfall exceeding 750mm, while in the case of Watrak, only 12 out of 118 recorded stations recorded mean annual rainfall exceeding 750mm. In the case of Dharoi, two out of the five stations recorded more than 750mm of mean annual rainfall. The mean annual rainfall for Watrak, Dharoi and Hathmati sub-basins are 794mm, 729mm, and 692mm respectively.

Basin's Runoff

- The mean annual runoff : 3881.06 MCM
- 56.5 % comes from Watrak sub-basins
- Highest CV % : Dharoi sub- basin (76.7 %)
- Minimum CV %: Watrak sub-basin (63.3%)
- The slope of upper catchment areas of Dharoi sub-basin are very steep due to the Aravali mountain ranges in Rajasthan from which the Sei and Wakal rivers originates.
- The slopes in Hathmati towards the SW parts of the catchment.

Basin's Groundwater Resources

- ✓ The main source of groundwater : Natural recharge from rainfall.
- ✓ The basin area of Kheda district falling under Mahi irrigation command, has shallow groundwater table, alluvial soils and perennial irrigation from Mahi canal where Paddy is a major crop.

Table: Basin's groundwater resources

Name of Sub-basin	Gross GW Recharge		Utilizable GW Recharge	
	1991	1997	1991	1997
Dharoi	188.48	224.65	160.21	179.82
Hathmati	1330.67	1437.42	1132.03	1149.6
Watrak	763.20	896.20	648.59	716.96
TOTAL	**2282.0**	**2552.0**	**1940.0**	**2046.38**

- Source: GOG 1992 and 1999

Water balance components over basin

Thornthwaite and Mather (1955) technique has been used to assess the agroclimatic features of stations lying within Sabarmati river basin catchment area for normal year as well as for year 1997. In addition to

these stations, the remaining stations study has also been done. The actual evapotranspiration (AET) showed less variation than that in rainfall and it is equal to potential evapotranspiration remaining during June to September in the southern grid. In the district of Banaskantha, Sabarkantha, Patan and Mahesana (North east of river basin) the AET equal to PET only in July (In table 2 only annual value has been shown). This region experiences water deficit having no water surplus during the year. On normal basis it varied between 601 mm at Derol to 745 mm at Khandha whereas during 1997 (values shown in parentheses) it was between 544 mm at Derol to 883 mm at Arnej. AET during 1997 was less than the normal at most of the stations. This was due to less atmospheric demand and heavy rainfall received in one or two spells. These heavy spells of rain during 1997 resulted in surplus water (WS) between 159 mm at Arnej to 696 mm at Anand against the normal of 0 to 360 mm. It may be noted that Arnej and Sanand which do not expect excess water on normal basis, experienced surplus water of 159 and 436mm respectively. The water deficit is the highest (1935 mm) at Arnej followed by Sanand (1662 mm), Anand (1236 mm) and Khandha (1041 mm) under normal condition. During year 1997, the water deficit was considerably less than the normal. It varied between 955 mm to 1501 mm at different stations. Hence, water deficiency is observed over north-east grid region of the river basin (Patan, Banaskantha, Arnej and Sanand) with no surplus water over these region.

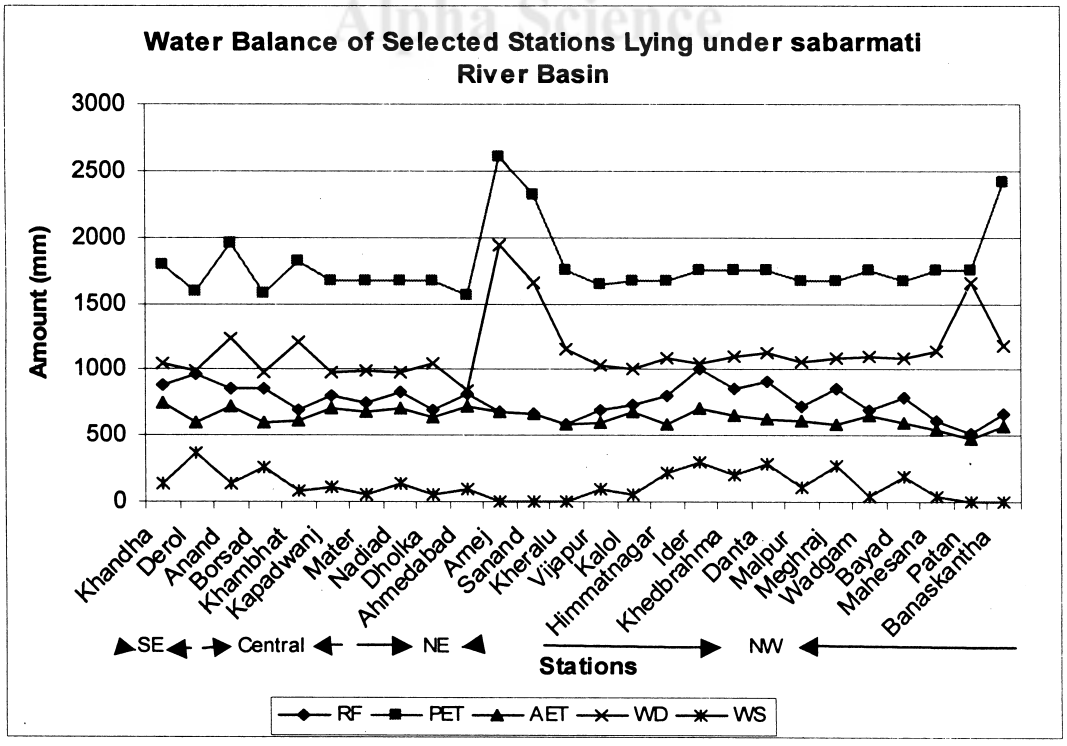

Land surface processes over Sabarmati river basin

The LASPEX-97 data were also scrutinized and corrected for the entire year (i.e. from January'97 to December'97). All the surface layer parameters were computed for the year and presented here on monthly basis. The parameters used were pressure, wind speed air temperature at different levels (1, 2, 4 & 8 m heights), soil temperature (at surface, 5,10,20,40 & 100cm depths), incoming and outgoing short-wave & long-wave radiation. These data are available on the minute wise for the Intensive Observational Period (IOP from 13 to 17th of every month) and on 10 minute average intervals for each month. The data were averaged on hourly, daily and then monthly basis. The monthly data for the respective stations (Anand, Sanand, Arnej, Khandha, and Derol) were then again normalized for the entire region, which comprises 200km x 200km area. The parameters exhibit for the entire region for a grid point area. In addition to these slow response tower data, fast response data were also obtained using Sonic and Metek anemometer. Based on these data, surface layer parameters were found out for the entire experimental year. These surface layer parameters are stability deciding factors (Richardson number and stability factor), friction velocity, roughness length, aerodynamic resistance, exchange coefficient for the momentum, stress, Monin Obhukhov length, and drag coefficients. Using these parameters, study on surface fluxes will be done. Figures show the self-explanation for these parameters. Month wise study of these parameters are explained hereunder:

Pressure : Winter season (November-February) experienced high pressure level during all the periphery of the LASPEX (1012.1mb) with lowest in the month of June when it was minimum annual pressure 989 mb.

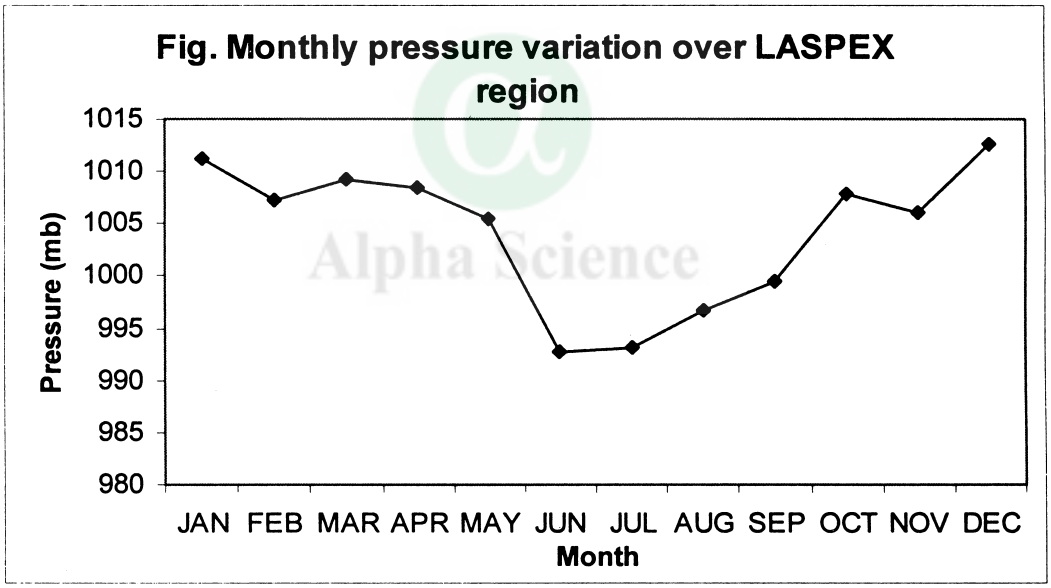

Wind speed and direction : Wind speed fluctuates from slow (0.8m/s) to moderate wind speed 3.0 m/s over the region with strong wind during monsoon season (~2.6 m/s). Higher wind was observed at 8 metre height in comparison to 1 meter height.

Fig. Monthly variation in wind speed over LASPEX region

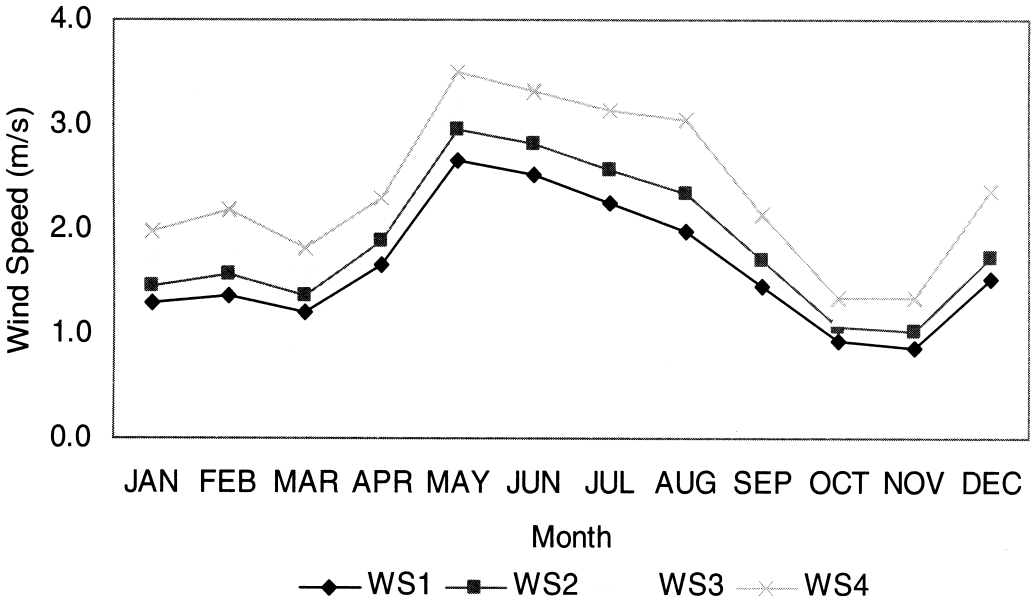

Air temperature : Air temperature varied from annual lowest during winter (23.1°C) to annual highest during May (36.5°C) over the region. During summer it was high and suddenly dropped as the monsoon started.

Monthly air temeprature at different height over LASPEX region

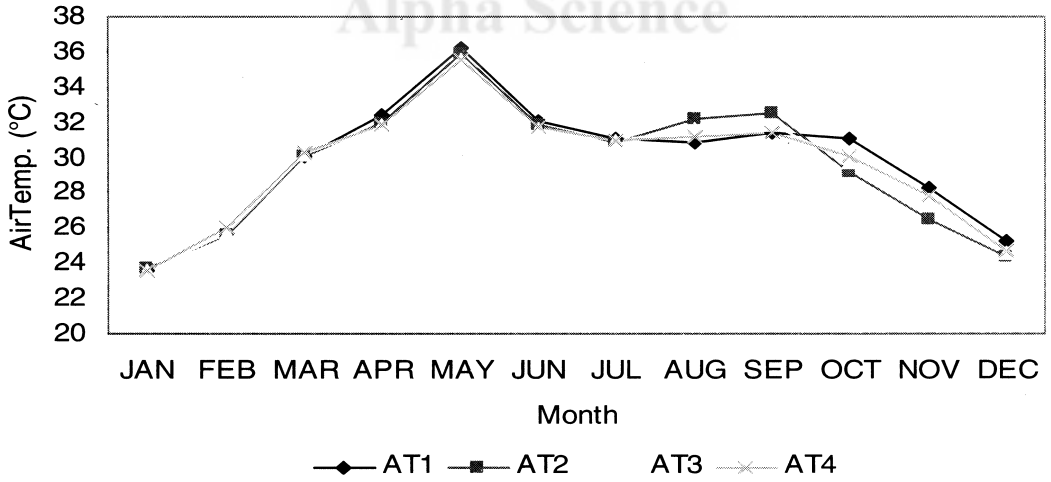

Soil temperature: The profiles of soil temperatures in the LASPEX field over its natural condition using the soil temperature were measured at the surface and at depths of 5 and 10cm are presented in the Table. Soil temperature is important surface layer parameter, which is highly dependent upon surface characteristics and moisture content within the surface. The decrease in soil temperature in crop field depends upon the soil covered by the plant, its density and height. The monthly mean soil temperature varied considerably within depths. Highest surface temperature during the experimental period was observed at surface summer (May) over the region and it was almost 4-5°C higher to the depth of 5cm

(42.5°C). It is also observed that maximum variation from the surface and within surface soil temperature was observed during the month of May (extreme summer month and was ~4.5-6.0°C) from. At lower depths the soil temperature did not vary much more and was at around 25.0°C. Due to rain during monsoon soil become moist and fully saturated and did not show much more variation between the surface and within surface, but it was more at few stations due to water logging during the monsoon season and its effect prolonged even after withdrawal of monsoon.

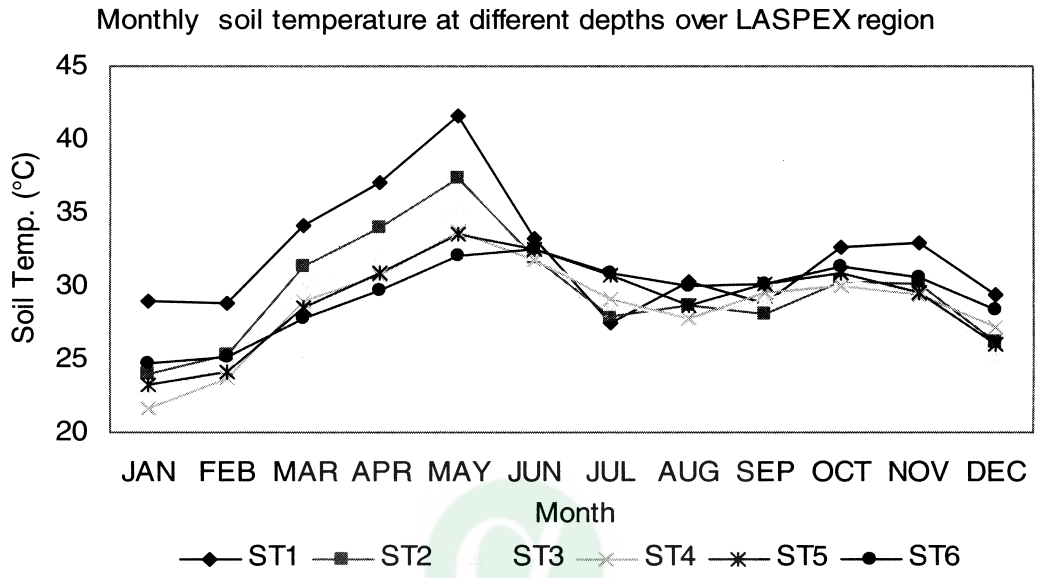

Net radiation component, albedo and sensible heat flux: Radiant energy plays an important role not only in plant growth and development processes through photosynthesis and thermal effects but also in determining the microclimate near the ground depending upon the radiative properties of the surface. Both the bare soil and vegetation-covered soil receive at a given instant the same radiation per unit area. Both types of surface also give off the same amount of radiation by day and night, provided their surface temperatures are equal. Only the difference in albedo can bring about the difference in radiation balance. The net radiation, which is the balance of net short wave radiation and net long-wave radiation, is the fundamental source of energy responsible for most of the physical processes taking place in the environment. Thus the diurnal and spatial variation of various components of the radiant energy incident on a surface is necessary to understand the complex processes involved in biosphere and atmosphere. The incoming short wave radiation (SW1), also known as insolation at the ground has great importance. It has strong diurnal variation in absence of fog and cloud and has a peak value at around noon hours.

The radiation components varied place to place on seasonal and diurnal basis. It has been seen that the incoming short wave radiation depleted in the presence of aerosols/pollutants present in the atmosphere. The reflectivity depends upon the surface characteristics and weather condition. Similarly net radiation also depends upon the incoming solar radiation and surface characteristics. The reflectivity for the region observed to be varied from 0.19 to maximum about 0.29. The sensible heat flux was lower in the monsoon season due to wet soil surface and maximum evaporative heat.

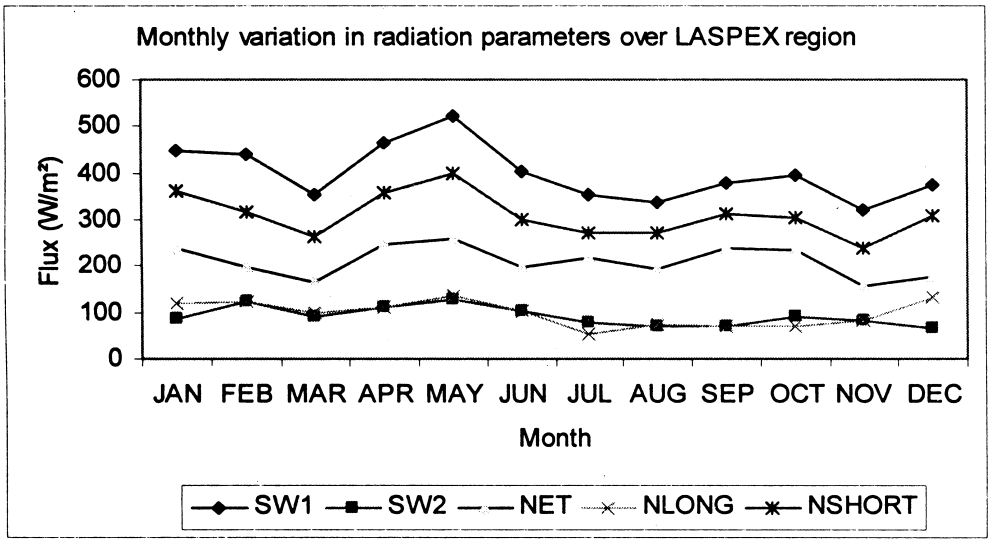

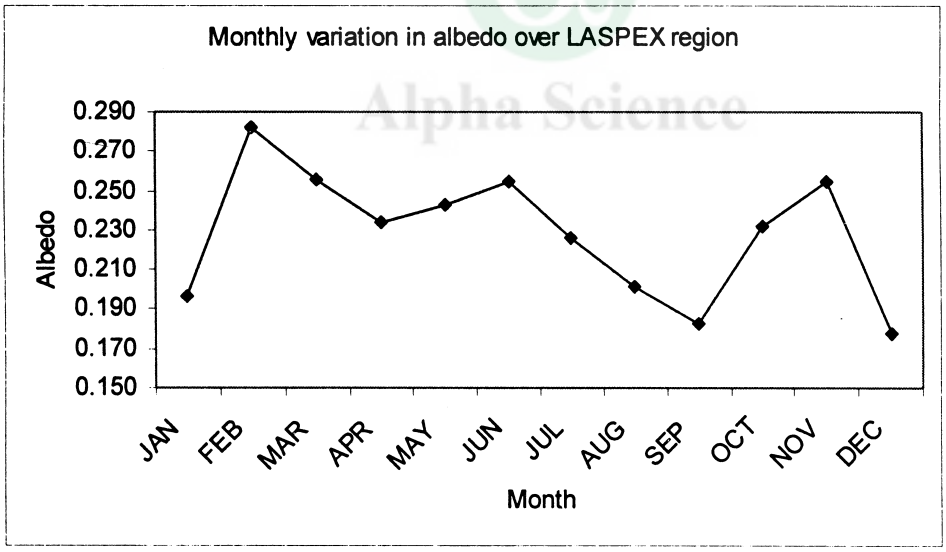

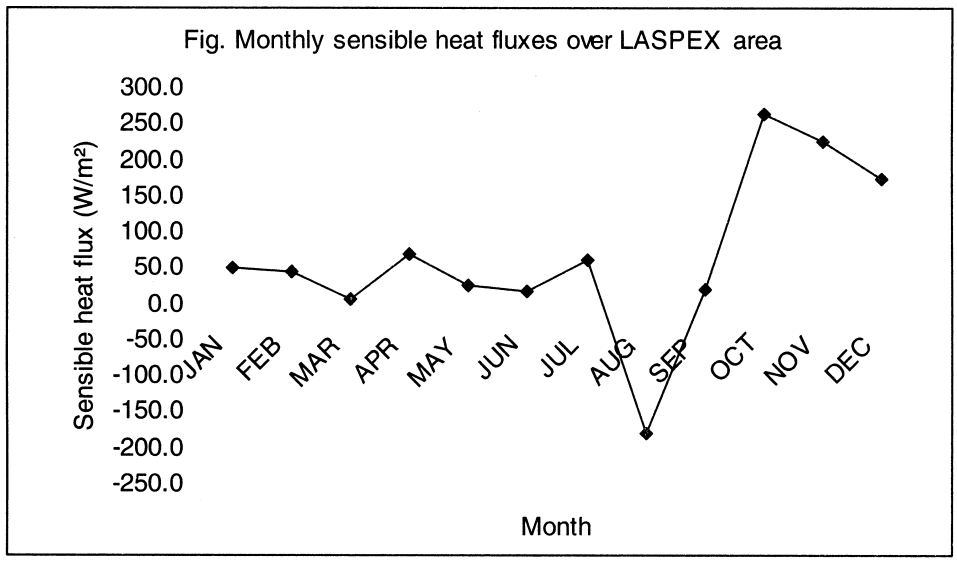

CONCLUSIONS

The information generated by this work on different mass exchange processes with radiative properties and detailed behavior of energy balance components over semi to arid region of western India lying under the river catchment area may be very useful for a full understanding of the ways in which plant communities respond to the environmental stresses encountered so that the appropriate methods for weather forecasting can be developed. The results obtained so far may be used as reference value for the further study. During LASPEX-97 it was felt that crop phenology based observations including hydrological aspect under different atmospheric conditions, statistical analysis should be undertaken. This may also helpful in better understanding of these parameters over varying surfaces particularly over bare soils and different crop fields. The information given in the present work may be utilized to modify the microclimate near the surface to get maximum benefit in not only in crop yield but also weather modification because these surface layer parameters directly or indirectly related to wind variation, radiation and temperatures. These parameters have directly influence the surface weather condition and ultimately influence the global weather condition.

REFERENCES

Athavale, R.N., and Rangarajan, R. 1988. Natural recharge measurement in the hard rock region of semi arid India using tritium injection: A review. In: Estimation of natural groundwater recharge (Ed. I. Simmers) : pp 175-194. Publisher, D. Reidal Co. Dordrecht, Bostan.

Baven, K.J., and Kirkby, M.J. 1979. Aphysically based, variable contributing area model of basin hydrology, Hydrol. Sci.Bull., 24, 43-69.

Bolle, H.J., and Streckenbach, B. 1995. The Echival Field Experiment in a Desertification. Threatened Area (EFEDA), Final Report. Berlin, August, 1993.

Dyre, A.J. 1974. A review of flux profile relationships. *Boundary Layer Meteorol.*, 7, 363-372.

Famiglietti, J.S. and Wood, E.F. 1994a. Multiscale modeling of spatially variable water and energy balance processes, Water Resour.Res., 30, 3061-3078.

Gaur, M.I., and Singh, Punjab. 1995. Application of watershed concepts in developing degraded wastelands of Bundelkhand region. In: Agro forestry systems for degraded lands. Vol.-2 (Eds. Punjab Singh, P.S. Pathak and M.N. Roy), pp:Pub. Oxford & IBH Co. Pvt.Ltd., New Delhi, India.

Harpaj, Y. 1971. Artificial groundwater recharge by means of wells in Israel. J.Hydraul.Div., ASCE, hy 12, pp1947-1964.

Jaegar, L., Hutchison, B.A., and Hicks, B.B. 1985. Estimations of surface roughness and displacement heights above a growing pine forest from wind profile measurements over a period of ten years. *The forest atmosphere-interaction.* 71-90.

Johnson, P.O. 1987. Estimation of groundwater recharge in sandy soil with two different methods using groundwater level fluctuations. J. Hydrology, Vo.-90, pp: 183-198.

Oke, T.R. 1987. Boundary Layer Climates, 2nd ed., Mathuen & Co. Ltd., 372 pp. Halsted Press, John Willey & Sons. New York.

Pandey, V. and A.T. Patel. 1987. Agroclimatic appraisal of Khedbrahmha, GAU Res.J., Vol-13(1), pp: 21-27.

Pandey, V., and B.R.D. Gupta. 1991. An agroclimatic study of some district of Gujarat, Geog. Review of India., Vol.-53 (4), pp-1-7.

Pandey, V., manoj kumar, and A.M. Shekh. 2000. Water resource potentials of Gujarat state. In Proc. On National seminar on GWR, pp: 109-114.

Pandey, V., Manoj Kumar, and A.M. Shekh. 2001. Agroclimatic features of LASPEX sites. J.of Agrometeorol. Vol.3 (1 & 2) pp: 39-55.

Rai, S.N., D.V. Ramanna, andA. Manglik. 1997. Modelling of water table fluctuations in a finite aquifer system in response to transient recharge. In: Proceed. International symposium on emerging trends in Hydrology, Vol-1, Dept. of Hydrology, University of Roorkee, pp: 243-250.

Shrma, M.L. 1987. Measurement and prediction of natural groundwater recharge – an overview.J.Hydrology (NZ), Vol-25, pp: 49-56.

Singh, Bharat. 1997. Water resources of development in India-A perspective. In: In: Proceed. International symposium on emerging trends in Hydrology, Vol-1, Dept. of Hydrology, University of Roorkee, pp: 1-17.

Thom, A.S. 1975. Momentum, mass and heat exchange of plant communities. In "Vegetation and the Atmosphere", Vol. 1. Principles (J.L. Moneteith, ed.), pp. 57-109. Academic Press, New York.

Thornthwaite, C.W., and Mather, J.R. 1955. The water balance. *Climatology*, **8**, 1-104.

Disaster Management
Editors: N.C. Mahanti et al.

Land Surface Processes Over Sabarmati River Basin (Laspex-97)

A.M. Shekh, P. Sanjeeva Rao[1], Manoj Kumar and Vyas Pandey

B.A. College of Agriculture, Anand Agricultural University, Anand-388 110, India
[1]Scientist F, ESS Division, Department of Science & Technology, New Delhi-110 016, India

Abstract

The multi-institutional, multi-disciplinary research project Land surface processes experiment (LASPEX-97) was conducted over Sabarmati river basin to understand the land surface processes coupled with hydrology and vegetation during the year 1997-98. A complete surface and sub-surface atmospheric-hydrological data base against which parameterized models for land surface processes i.e., energy exchange, radiative, sensible and latent heat fluxes has been tested for improvement and further development. The results shows that the values of z_o were higher under near neutral condition and varied from 0.03 to 0.6 cm during the study period. Under neutral condition the drag is significantly high at low winds and decreased linearly with increasing of wind speed. Under unstable conditions (- 4.0 < Ri < - 1.0), C_d are not consistent and varied up to 0.003,0.008,0.03 and 0.01 during May, July, September and December respectively. Data obtained during the period was also verified by the AVHRR and LISS. Study on variation of momentum flux has also been discussed in the paper.

Key word LASPEX, stability parameters, land surface parameters

The multi-institutional, multi-disciplinary research project Land surface processes experiment (LASPEX-97) was conducted over Sabarmati river basin to understand the land surface processes coupled with hydrology and vegetation during the year 1997-98. A complete surface and sub-surface atmospheric-hydrological data base against which parameterized models for land surface processes i.e., energy exchange, radiative, sensible and latent heat fluxes has been tested for improvement and further development. The results shows that the values of z_o were higher under near neutral condition and varied from 0.03 to 0.6 cm during the study period. Under neutral condition the drag is significantly high at low winds and decreased linearly with increasing of wind speed. Under unstable conditions (- 4.0 < Ri < - 1.0), C_d are not consistent and varied up to 0.003,0.008,0.03 and 0.01 during May, July, September and December respectively. Data obtained during the period was also verified by the AVHRR and LISS. Study on variation of momentum flux has also been discussed in the paper.

Land surface processes (LSP) are those associated with the exchange of mass, momentum and energy between the land surface and the atmosphere. These processes have significant impact on climate variability at different time scales (Rao, 2001). It is thus necessary to understand physical processes of individual components and the feedback between different components close to the land-air interface more specifically the microclimate processes close to the earth's surface, since the boundary layers significantly influences the evolution of the atmospheric circulation on the medium and long-range time scales. Till recently land-surface-atmosphere interactions were parameterized in GCMs by using simple schemes, which treated the processes of radiative transfer (albedo), momentum transfer (roughness length), and the surface hydrology (sensible and latent heat transfer) as independent and separable entities. These three are closely related to each other through characteristics of vegetation, soil, and land use at a given location which act as a trigger to the physical processes related to climate and its variation. Besides, transfer of water from soil to atmosphere is partly controlled through vegetation, land use, and available water. Therefore it was felt that it was necessary to carry out special field experiments in areas representative of different types of land surfaces aimed to provide a data base such as surface and subsurface hydrology, soil, land surface and atmospheric parameters which are needed for testing and incorporate into the general circulation models.

In order to study of these parameters in detail, the Department of Science and Technology (DST), Government of India, constituted an expert committee under the chairmanship of Dr. R.N. Keshavmurthy,

Director, IITM (Indian Institute of Tropical Meteorology, Pune) in January 1993 for formulation of a proposal for land surface process (LSP) experiment. The committee brought out a draft proposal giving all technical details and financial estimates and the project proposal was approved during March 1994 with the following objectives:

- To collect a complete surface and sub-surface atmospheric-hydrological data base against which parameterized models for land surface processes i.e., energy exchange, radiative, sensible and latent heat fluxes can be tested for improvement and further development.

- To foster the development of observing techniques, data management and assimilation systems.

- The generated data shall be used in addressing the problem of determining evaporation flux and parameterizing land-surface processes at the scale of GCM-grid square, i.e., approximately 100x100km.

- To provide in-situ measurements as ground truths for the data to be obtained through ERS-I, for evaluating soil moisture over the region.

Instrumentation and Data collection

For conducting the main experiment from January 1997 to February 1998, 10m towers were installed at all the stations along with one 30m tower at the central station, Anand. Different sensors to measure temperature, humidity, wind speed and direction have been installed at 1,2,4 and 8m height. Incoming and outgoing short wave and long wave radiation and net radiation sensors were instrumented at approximately 2m heights along with pressure and rainfall measuring systems. Soil temperature sensors were measured at the surface and the depths of 5,10,20,40 and 100cm. At Anand, all the three components of the wind were measured by the Sonic and Metek anemometer. At each station soil moisture by the Capacitance and Neutron probe at different depths and the rate of evaporation by evaporimeter were measured. Soil moisture measurement was also taken by gravimetric method (Shekh *et al.*, 2001). Other than the tower instrumentation, at Anand, for the analysis of the thermodynamic diagram for convective instability and thunderstorm forecasting, inversion and lapse rate, mixing depths, etc., five RS/RW launches per day (at 0530, 0830, 1130, 1430 and 1730 IST) during each Intensive Observational Period (IOP) were conducted by India Meteorological Department. For the study of diurnal variation of lower troposphere winds, and influence of troposphere on low level winds, IMD also conducted Pilot Balloon Observation five times daily at each peripheral station. A Doppler SODAR was operated for a limited period at central station Anand for the study of the all the three wind components at various heights starting from 45m above the surface to 1000m. Lyman-Alpha Hygrometer was also procured and observations were taken during February 1998.

Data acquisition system

A specially fabricated data logger DL 1032 with 32 channels was utilized in this experiment. Data are stored on a 2MB memory module and when it is full the data are transferred to the PC at the central station Anand and subsequently to IITM, Pune, for editing and processing. The data are available minute wise for the IOP, but for the rest of days as on 10-minute averages. At each of the tower stations a group of trained personnel from IITM and GAU Anand were engaged in acquiring the data according to the plan.

Site description of LASPEX

The region, wherein the LASPEX-97 was conducted, is part of the mainland of Gujarat State, India extending from Runn of Kutch and Aravali Hills in the North to river Damanganga in the south. The mainland is almost flat plain between altitudes 0 to 75m above mean sea level (AMSL) made up of alluvial soil except for same sandy soils in the north. The LASPEX region lies between latitudes 22°02' to 23°04'N and Longitudes 75°15' to 73°45'E with elevation ranging from 28 to 85m above mean sea level. Although

all stations fall under semi-arid climatic region, the western part of LASPEX (Arnej and Sanand) is more prone to experience arid environment as the rainfall less and evaporation rates are high. On the other hand the southeastern parts of the grid receive higher rainfall and have less evaporation rates resulting in semi-arid environment (Pandey *et al.*, 2001). During experimental year (1997) all the stations recorded 40-70% higher rainfall than normal. This resulted in lower water deficit and higher amount of surplus water.

During the experimental period bare soil/grass cover in summer, sunhemp (a green manure crop) and groundnut crops provided the surface cover in the different seasons at central station, Anand. Short and tall grass situations, differing vegetation cover in the representative months, which influence the atmospheric processes or flux rates were available during the course of the experiment near and in the surroundings of the tower sites. These conditions were considered ideal and unique for the LASPEX.

Radiation and energy budget study

Assessment of surface radiation components at LASPEX sites

The incoming and reflected short wave radiation alongwith the net radiation observed at 0900, 1100, 1300, 1500 and 1700 hrs IST in four months (May, July, September and December) for each station. Average of daytime hourly values of radiation components are presented in Table 1.

On an average Anand received short wave radiation of 687 W/m² during summer while during monsoon and withdrawal phase of monsoon season it received 461-462 W/m² of radiation (Table 1). The lowest radiation (438 W/m²) was received during winter season. Average daytime reflected short-wave radiation was observed to be 153 W/m^2 during summer, which was 22% of the incoming short wave radiation. The presence of sunhemp crop over field reduced the average reflected short wave radiation during active phase (July) and was 98 W/m^2, which was 21% of the incoming short wave radiation. During withdrawal phase of monsoon (September), due to rains the reflectivity decreased to 18% even though no crop was present while during winter season (December) it further decreased to 16%. The average net radiations were 409 W/m² followed by 328, 363 and 273 W/m² during summer, monsoon, withdrawal and winter season respectively.

At Arnej daytime mean value of incoming short-wave radiation was observed to be 707, 467, 450 and 437 W/m² during summer, monsoon, withdrawal and winter seasons respectively (Table1). The reflectivity (albedo) decreased during monsoon season and was 20% and 13% during active phase of monsoon and withdrawal phase of monsoon respectively against that of 26% during summer. The lowest reflectivity (13%) was due to the water logging during the September month due to black saline sodic soil. Thus this soil acted as a sink and absorbed most of the incoming short wave radiation. The result is well supported by Mayer (1981) who reported 22% reflectivity for mixed grass, Idso *et al.* (1975) and Cipra *et al.* (1971) who showed higher reflectance for dry than for wet soils. It is interesting to note that although the incoming short wave radiation during July was about 65% of that of May, but the net radiation was 71% of the short wave radiation in comparison to 53% during summer. This might be due to the overcast condition with stratus cloud which absorbs much of outgoing long wave radiation and re-emit to the ground which results the damping of diurnal surface radiation budget.

The daytime short wave radiation at Sanand was highest during summer (694 W/m^2) followed by 482, 437 and 418 W/m^2 during active monsoon, post monsoon and winter season respectively. Daytime average reflected short wave radiation was highest during summer (165 W/m^2) and minimum in withdrawal phase of monsoon (99 W/m^2). The soil of Sanand is sandy loam with short to high grass covering may have affected the reflectivity. During all the season the reflectivity was almost same and was 24%, 23%, 23% and 27% during summer, active monsoon, withdrawal phase of monsoon and winter phases, respectively in spite of the rain occurred during the monsoon periods. Daytime average net radiation was observed to be 380 W/m^2 in summer, 216 W/m^2 in active monsoon season, 328 W/m^2 during withdrawal phase of monsoon and 202 W/m^2 in winter seasons respectively.

At Derol the daytime mean incoming short wave was observed to be 677, 422, 362 and 423 W/m^2 respectively for these periods. Daytime mean reflected short wave radiation at Derol was observed to be 199,

118, 97 and 127 W/m^2, respectively. The reflectivity (albedo) at Derol was always high and was 29%, 28%, 27% and 30%, respectively for summer, active monsoon, withdrawal phase of monsoon and winter seasons, respectively. The present result is in consonance with those previous results suggested by Sellers (1965) who proposed 30% albedo over the sandy soil.

At Khandha the daytime mean value of incoming short wave radiation was highest during summer and was 568 W/m^2 followed by 357, 317 and 331 W/m^2 in monsoon, post monsoon and winter season respectively. The average reflected short wave radiation was observed to be 246, 184, 122 and 170 W/m^2 respectively during these periods. Reflectivity also depends upon the soil characteristics and vegetation cover. Since Khandha's soil is black cotton soil with medium dense grass cover, reflectivity lowered down. Approximately 13.2% of the incoming solar radiation was reflected back as reflectivity (albedo) during summer followed by 19%, 11% and 10% during rest of the season. The average net radiation was highest during summer and was observed to be 389 W/m^2 followed by 260, 263 and 229 W/m^2 during active and withdrawal phases of monsoon and winter seasons, respectively.

Table 1: Seasonal average values of radiation balance components at LASPEX sites

Components	Summer (May)	Monsoon (Jul)	Post Monsoon (Sep)	Winter (Dec)
Anand				
SW1	686	461	462	438
SW2	153(23)	98(21)	81(18)	71(16)
Net	409(60)	328(71)	363(79)	272(62)
Arnej				
SW1	707	467	450	437
SW2	186(26)	92(20)	59(13)	--
Net	378(53)	385(71)	280(62)	261(59)
Sanand				
SW1	694	482	437	418
SW2	165(24)	119(23)	99(23)	113(27)
Net	380(55)	216(65)	328(75)	202(48)
Derol				
SW1	677	422	362	423
SW2	199(29)	118(28)	97(27)	127(30)
Net	441(65)	291(69)	264(73)	262(62)
Khandha				
SW1	568	357	317	331
SW2	75(13)	68(19)	34(11)	32(10)
Net	389(68)	260(73)	263(83)	229(69)

Parentheses shows the percentage in terms of incoming short wave radiation

Radiation balance components over crop surface and bare soil surface

The incoming short wave radiation received by the bare soil and crop surfaces at any moment of time are same at any place but the reflected short wave radiation and outgoing long wave radiation may influenced greatly resulting in large variation in net radiation. The variation in net radiation within crop canopy depends on height, density and structure of the plant cover. In the present section, comparative studies have been carried out between the radiation components at two tower sites (10m and 30m) at Anand where different crops were grown during different seasons (May, July, September and December). In all four seasons, both sites differed in crop/vegetation types. Hence, in each season the variation in radiation components are

discussed. The diurnal variations of different components of radiation budget incoming and outgoing short wave, net long wave and net radiation over different surface and in different seasons are depicted in Fig 1(a-d).

During May at one site it was short grasses and at the second site it was bare soil surface. The variation in radiation over these two surfaces is depicted in Fig. 1 (a). Due to presence of grass, not much more variation in reflected short wave radiation was observed but the net long wave radiation was greatly increased over grasses resulting in higher net radiation over grasses than bare soil.

During July when one surface was covered with sunhemp, green manure crop and other covered with groundnut crop, reflected short wave radiation also did not vary much over two crop surfaces, but showed comparatively lower value over these surface might be due to heavy rainfall during this period which lead to lower reflection from wet surface. The diurnal variation of net long wave radiation showed large fluctuations over groundnut crop, which may be uneven coverage of the surface by crop under wet condition whereas the sunhemp, which was very dense crop with uniform canopy, showed less fluctuation. This resulted in net gain in radiation i.e. net radiation was higher over sunhemp than groundnut. The significant differences in net radiation over two crops were observed during nighttime.

During September (Fig. 1 c) one site was kept bare as the sunhemp crop was embedded in soil for green mannuring and at other site groundnut crop was at pod development stage (height 30-32 cm). During nighttime there were no differences reflected short wave and Net long wave radiation were observed over both the surfaces. Over groundnut crop once again large fluctuations in net long wave radiation during daytime was observed in comparison to bare soil, which resulted in higher net radiation (Fig. 1 c).

During December the site, which was kept fallow during September, was covered with wheat crop under irrigated condition whereas the other site was having bare soil due to harvesting of groundnut crop. Since the crop was only 15 days old, there were not many differences in different radiation components. Net receipt of radiation was generally lost during nighttime resulting reduction in net radiation over both the surfaces. The reflected short wave radiation was higher over wheat crop resulted slightly higher net radiation over wheat crop.

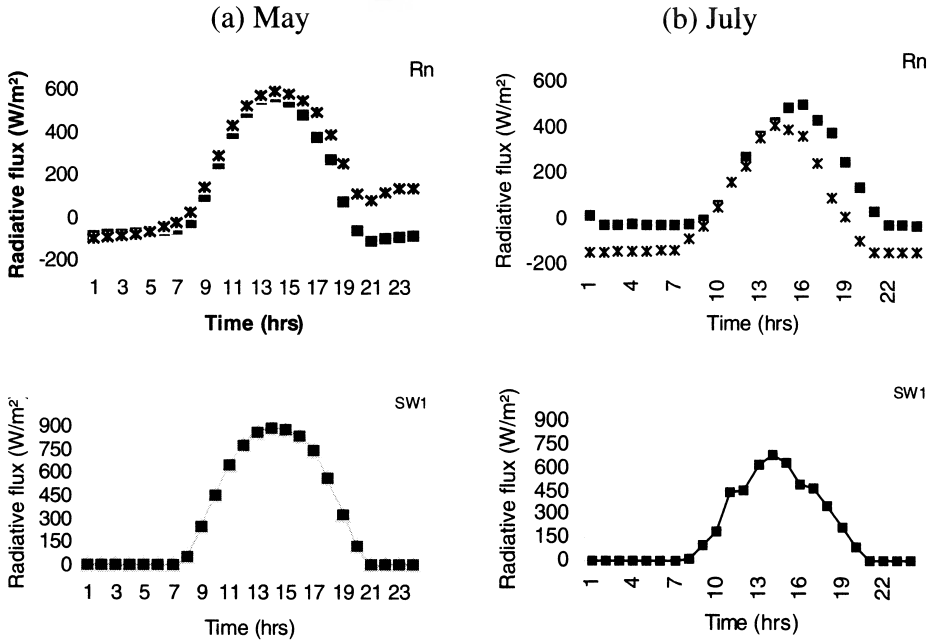

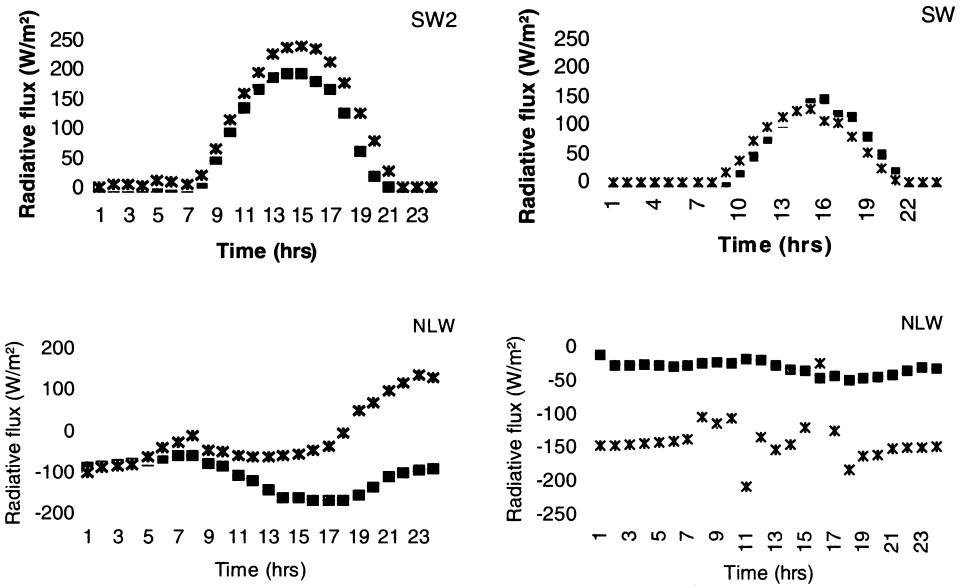

Fig.1 (a-b): Diurnal variation of radiation budget under crop (■) and bare (Ж) surface

Energy budget over different crop canopies

Partitioning of radiation energy between plant and soils with vegetation allows hydrologists to understand more about the energy balance and water use in the vegetation especially for different seasons. It is well understand that net radiation is partitioned into different forms such as sensible heat flux (H), latent heat flux (L), and soil heat flux (G). These components vary with soil condition and vegetation cover. The ongoing discussion deals with some of the above aspects of evaluation of energy balance over crop surface and bare soil surface. Energy balance has been depicted over crop and bare soil conditions (Fig. 2).

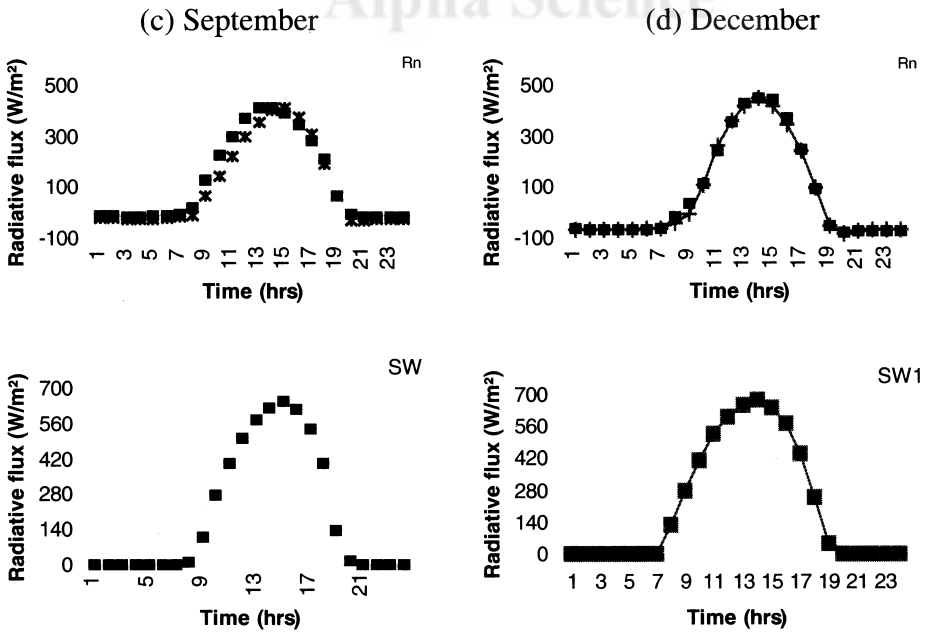

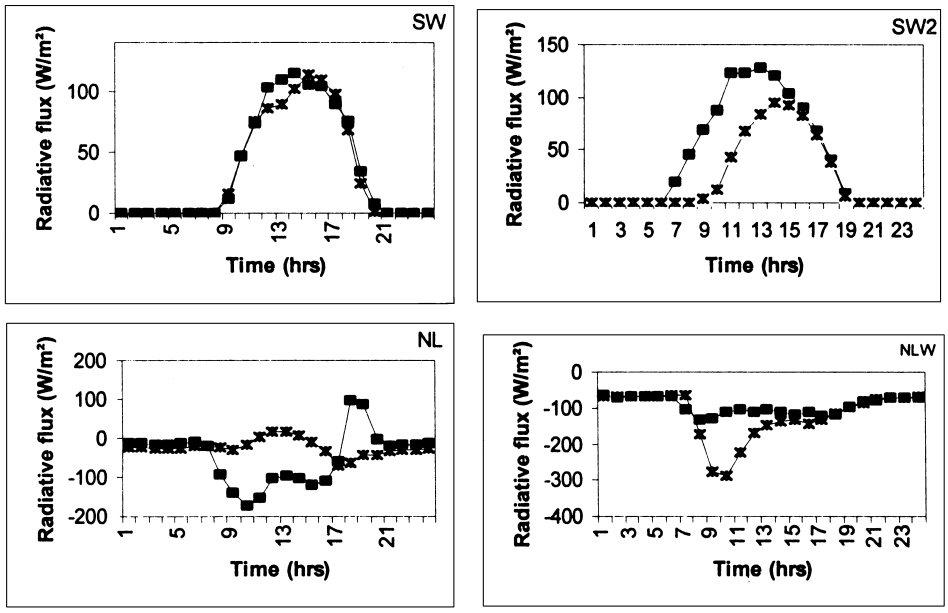

Fig.1 (c-d): **Diurnal variation of radiation budget under crop (■) and bare (Ж) surface**

During May and September bare soil conditions were prevailing at the site while during July and December it was covered with crops like sunhemp, groundnut and wheat, respectively. During May short grass was grown near the tower. During this period, the sensible heat flux (H) was positive during daytime with strong diurnal variation and at around 13 hrs it was more (190 W/m²). At night when the temperature gradient is positive, the sensible heat directed from atmosphere to the surface. The nighttime sensible heat was –20 W/m^2. The latent heat flux should be less during summer, but chilli and bajra crop was grown around the tower site and irrigation was done during observational period in these plots. Due to this reason it is possible that latent heat flux might have increased. The ground heat flux also observed to be more during May (50 - 100 W/m^2).

During active monsoon season (July), the green manure crop sunhemp was grown near the tower; the maximum sensible heat was observed between 13 to 15 hrs of the day with a value 120 W/m^2. This was due to wetness of the soil. During this period, the nighttime H was observed to be -10 W/m^2. Similar result was observed during September, when the surface was bare but wet due to rains.

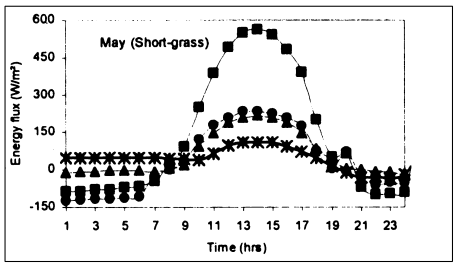

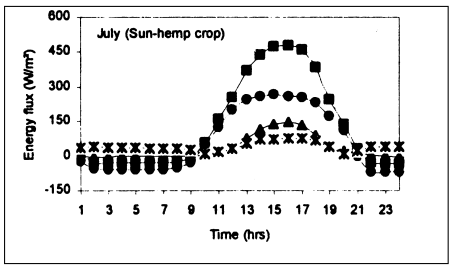

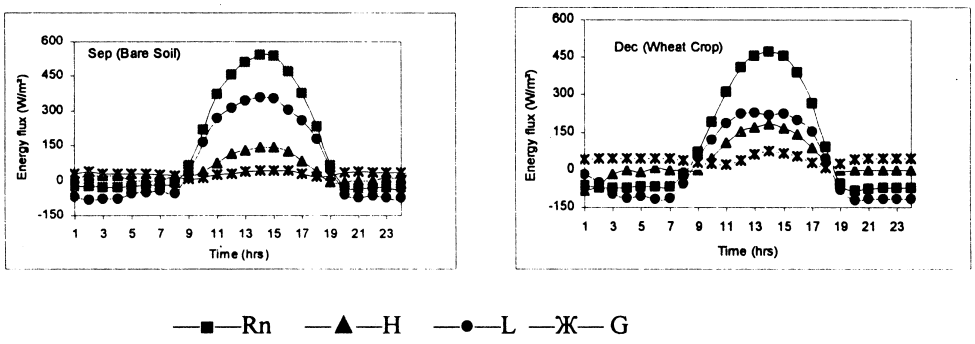

Fig.2 : Diurnal variation of energy components over different crop surfaces

During winter (December) the field was covered with wheat crop with 10-11cm heights during the observational period. The sensible heat was observed to be more than that of the monsoon phase with daytime maximum of 170 W/m^2 and nighttime minimum –20 W/m^2, respectively. Latent heat flux as well as soil heat flux was observed to be more during December.

Wind, surface processes and soil temperature

Relations between wind speed, frictional velocity, roughness length, drag coefficient, wind direction for Anand location under different stability and crop cover conditions were also studied.

Surface roughness

Roughness length (z_o) decreased with increasing wind speed during all the months. In the lower wind speed range, the inferred roughness length from forced log fit could be very large and inconsistent with the roughness elements at the surface. The reason for this criterion was that the winds couldn't be measured accurately when they were low (<0.5 m/s), due to the inertia of the cup. The roughness length was observed to varied between 0.01-0.25cm during summer (May) when the site was not totally obstacle free due to presence of bajra crop in the southwest of the tower but near the tower only short grass was present for the wind directions 150° - 210° and between 230° - 270°. During this period, in the prevailing wind direction, the fetch was not totally open due to the presence of different field crops near the tower as mentioned above, resulting in non-consistent values of z_o. During active phase of monsoon (July) the field was covered with sunhemp, green manure crop with height 10-15cm, leading to higher value of the roughness with values between 0.01-0.5cm. During active monsoon period (i.e. during the month of July) the wind direction were confined between 230° to 290° while during withdrawal phase of monsoon (i.e. during the month of September) the direction varied between 130° to 310°. The result obtained was well supported with Sauer *et al.* (1996) who found the ratio between z_o and canopy height to be 0.058. During September when the sunhemp crop was embedded for the green manuring z_o varied between 0.05-0.8cm. Few data points were available when the z_o value reached upto 1.0 cm. During this period the field was totally saturated due to heavy rains and it became porous acting as relatively higher rougher surface than during July when the surface was smooth due to weathering and compaction. Even the field was covered with short crop. The other reason was flow of wind being not fully obstacle free due to the presence of relatively taller crop surrounding the tower during September. Field was covered with wheat crop during December with heights increased from 5 cm from beginning to 15 cm by the end of the month and the z_o ranged between 0.01-0.4cm. The average values of roughness lengths for different months were thus found to 0.015 cm, 0.2, 0.56 and 0.19 for the months of May, July, September and December respectively.

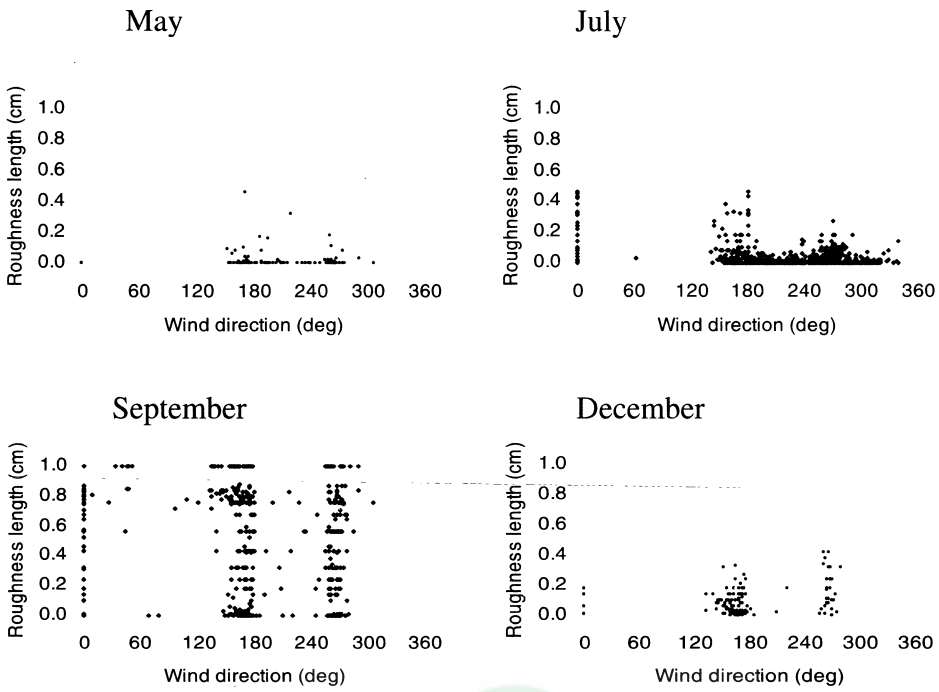

Fig. 3: Surface roughness lengths under near neutral condition at Anand

Surface drag coefficient

Figure 4.(a-d) depicts the dependence of drag coefficient on wind speed under near neutral, unstable and stable conditions for the month of May, July, September and December representing summer, active and withdrawal phase of monsoon and winter seasons, respectively. Under near neutral conditions (Fig. 4.) the drag was significantly high at low winds and thereafter decreased linearly with increasing of wind speed. It is seen that the data were consistent with an approximate inverse dependence of C_d on u at low winds. The numbers of data points were more than 9500 during the periods of investigation, so it was sufficient to draw a firm conclusion that drag coefficient varies inversely with the wind speed may be nearly linear. During MONTBLEX, over Jodhpur, which is nearer to LASPEX site, Kusuma *et al.* (1997) and Mohanty *et al.* (1997) reported that drag coefficient was strongly wind dependent and varied nearly linearly with wind speed.

Under neutral condition, drag coefficient found to vary from 0.001 to 0.006 during summer (May) with an average value 0.002; 0.001 to 0.007 during active phase (July) with average value 0.0037; 0.001 to 0.009 during withdrawal phase (September) of monsoon with average value 0.004 and again decreased to 0.004 during winter season (December). During the month of September under any stability condition the drag coefficient was higher and ranged from 0 to 0.009 where as during the month of July, it was relatively low and ranged form 0 to 0.007. During September the surface was wet due to rain, which increased the drag coefficient. A similar study has been reported by Grant and Nickling (1998) who showed that the porous element had a higher drag coefficient; suggesting that loose, fresh residue soil presented a comparatively rough surface than that was smoothed by weathering and compaction. A similar study has been reported by Patil *et al.* (2001) for the neutral condition and C_d varied between 0.0035 to 0.008 during IOP (Intensive Observational Period) for the month of July and September respectively for the same station Anand.

Figure 5 depict the relationship between drag coefficient and roughness length in all the wind sectors. Drag coefficient increased nearly linear with surface roughness but increased significantly in September.

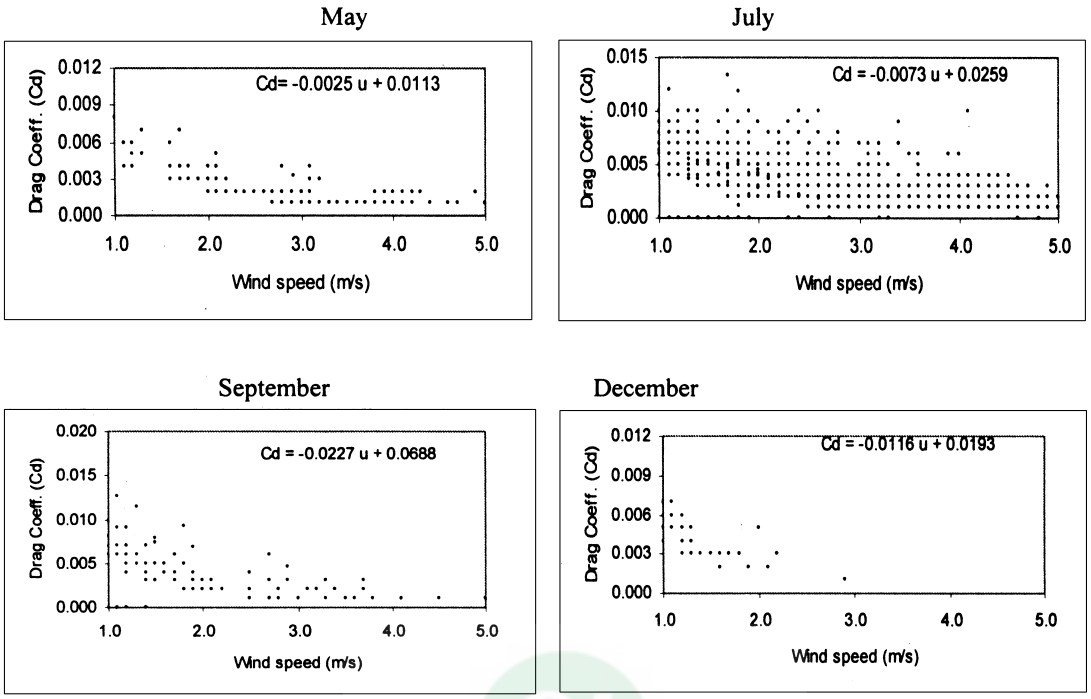

Fig. 4: Dependence of drag coefficient over wind speed under near neutral condition at Anand

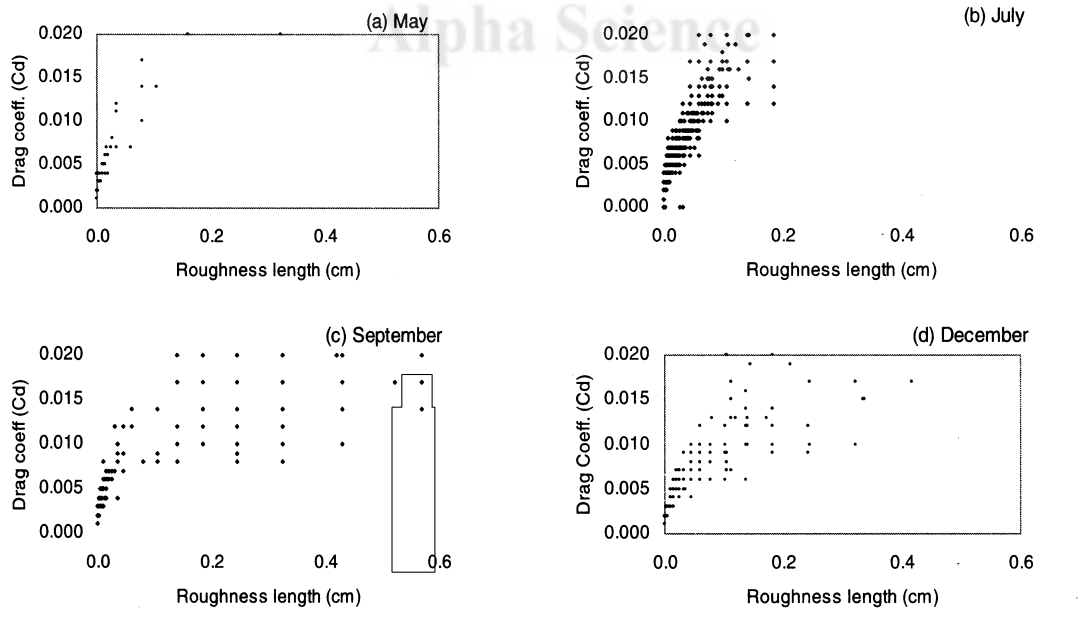

Fig. 5: Dependence of drag coefficient over surface roughness

Heat flux by fast response and slow response data

LASPEX-97 fast response Metek sonic anemometer data was also used to calculate surface layer parameters directly and results were compared with those calculated by profile methods. Results showed that the friction velocity and momentum flux observed by profile method were underestimated during most of the time that of eddy correlation techniques used in fast response data. Sensible heat flux by profile flux obtained from the profile method was underestimated (by 15-20%) during summer (May) but overestimated during rest of the months, compared to directly measured eddy correlation method. The nighttime minimum sensible heat during May was –20W/m² with a maximum during daytime (175W/m²). But the average value (24-hours average during IOP) was observed to be lower during monsoon season (50-70 W/m²). Large variation was observed between two methods in winter season during daytime, unlike the momentum flux.

The sensible heat flux derived by both methods was more or less same during nighttime in all the seasons. However, during daytime differences were comparable. Two methods performed well during summer when daytime differences were very less while during winter (December) the differences were more. Between these two methods the sensible heat fluxes computed by profile method were higher. This might be due to small variation either in the wind gradient or temperature gradient, which might cause large variation in sensible heat flux computed by profile method. The other reason for this discrepancy might be the result of frequency band limitations with the eddy correlation technique, which lead to an underestimation of the turbulent fluxes typically of the order of 5-10% (Moore, 1986).

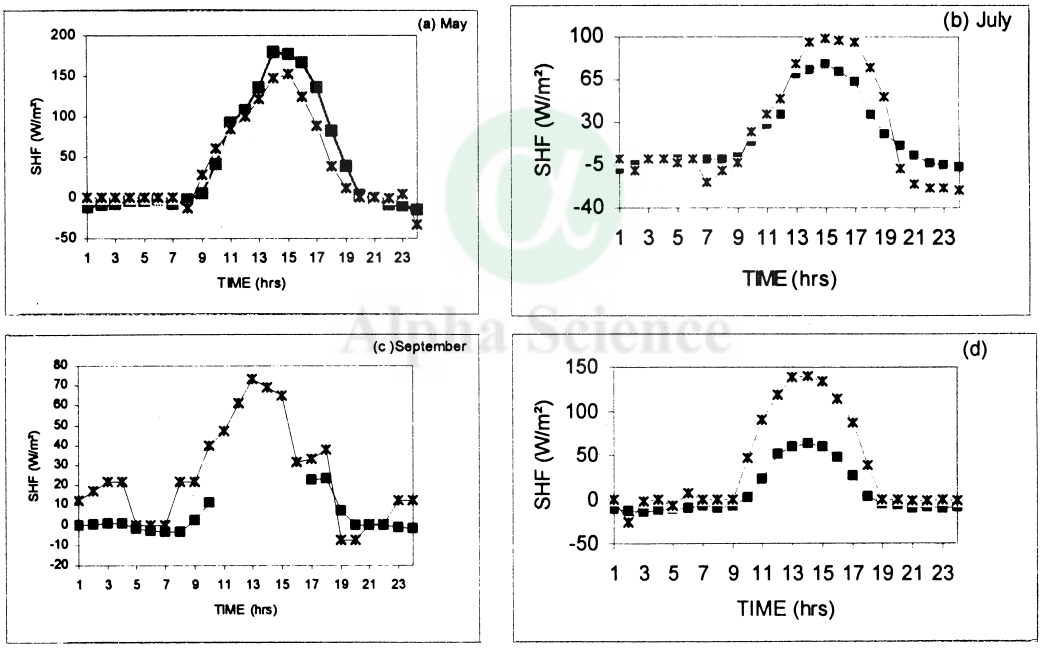

(—Ж—Aerodynamic method —■—Eddy correlation method)

Fig.6 : Variation in sensible heat flux computed by eddy correlation (SHF-E) and Profile (SHF-P) method

STUDY OF LAND SURFACE PROCESSES OVER WHEAT CROP FIELD

In order to understand the role of land surface processes over vegetative field, study have been done for Anand region using LASPEX-97 data with the following objectives:

i. To understand land surface processes over vegetative surface
ii. To study the radiation balance of wheat crop
iii. To study the diurnal and seasonal variation of energy balance components in relation to growth of wheat crop
iv. To study the variation of turbulent fluxes in the surface layer.

Salient features of results obtained:

i. Soil temperature in bare and wheat crop field: At surface, 37-45% higher surface temperature was found in the bare field at time of beginning and at the end in comparison to wheat field during its growth period and this difference reduced with depths. During vegetative stage surface temperature recorded 24.6 to 26.0 °C during experimental year over wheat field whereas in bare field surface it found 31.4 to 33.4°C.

ii. Higher wind speed during booting phase was detrimental for wheat. Higher wind may cause lodging of crop resulting in poor yield.

iii. During dough formation stage of wheat crop, friction velocity and momentum flux attained maximum value (0.221 m/s and 0.27 N/m²) whereas during milking stage roughness length and drag coefficients were found maximum (1.24cm and 0.0116) due to maximum LAI. Roughness length was found to be 0.91 cm during entire growth period whereas drag coefficient 0.0094.

Table 1: Phase-wise surface layer parameters over wheat crop field

Surface layer parameters near earth-atmosphere continuum												
	Friction velocity(m/s)			Roughness length (cm)			Drag coefficient			Momentum flux (W/m²)		
Phase	99-00	00-01	Pooled	99-00	00-01	Pooled	99-00	00-01	Pooled	99-00	00-01	Pooled
1	0.131	0.063	0.097	0.95	0.14	0.55	0.0059	0.0092	0.0076	0.217	0.047	0.13
2	0.161	0.093	0.127	1.20	0.52	0.86	0.0046	0.0099	0.0072	0.392	0.031	0.21
3	0.192	0.140	0.166	1.20	0.74	0.97	0.0056	0.0125	0.0090	0.484	0.075	0.28
4	0.170	0.120	0.145	1.29	0.85	1.07	0.0061	0.0157	0.0109	0.461	0.052	0.26
5	0.235	0.193	0.214	1.37	1.10	1.24	0.0073	0.0159	0.0116	0.417	0.057	0.24
6	0.224	0.218	0.221	1.05	0.98	1.01	0.0081	0.0150	0.0115	0.347	0.189	0.27
7	0.188	0.140	0.164	0.75	0.53	0.64	0.0066	0.0090	0.0078	0.086	0.140	0.11
Avg.	0.186	0.138	0.162	1.11	0.70	0.90	0.0063	0.0125	0.0094	0.343	0.084	0.21

Phases: *1- Sowing to crown root initiation(25 days); 2- Tillering (15 days); 3 – Booting (15 days); 4 – Flowering (15 days); 5 – Milking (15 days); 6- Soft dough formation (15 days) and 7- Physiological maturity stage (up to harvest)*

iv. Aerodynamic resistance at beginning and later stage of wheat crop was found more while was found lower () during middle stage of crop growth.

v. Due to comparable difference between soil surface temperature and air temperature, sensible heat flux computed by profile method was overestimated to aerodynamic resistance method.

vi. Daily mean incident solar radiation during the crop season received by the wheat field was 393 W/m² with standard deviation of 45.5, reflected back to the atmosphere 75.8 W/m² i.e. 19.5% reflected back to the atmosphere as albedo, while 63% consumed as net radiation. In comparison to the 21% long wave emissivity during year 1997-98 from wheat crop, 17.5% emitted during 1999-01 might be due to increase in surface temperature during these years.

vii. Daily mean albedo varied from 0.154 during middle phase of crop (maximum LAI) of crop growth to maximum 0.207 at beginning and at the end of crop growth with average albedo 0.195. The prediction equation for daily albedo was found to

Albedo = $0.0023n^2-0.21n+0.2292$; $R^2 = 0.98$; where n = no. of phase

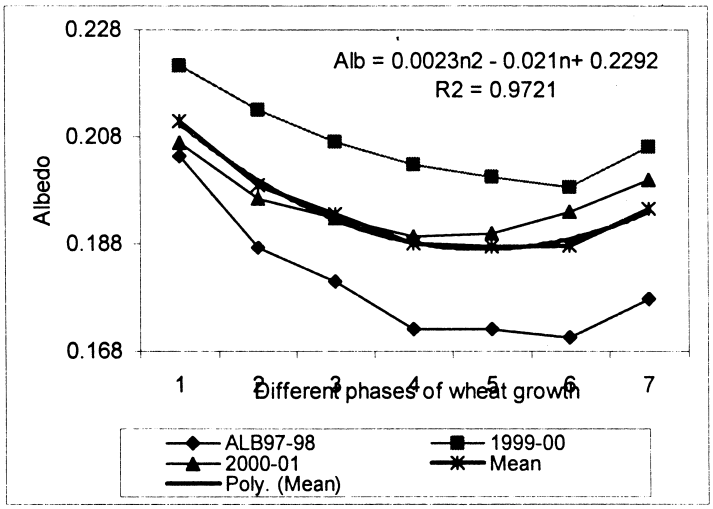

Fig. 7: Phasewise variation over wheat crop field during its physiological stages

viii. Approximately 15% reduction in surface albedo was found after irrigation at earlier stage and this difference reduced in middle phase of crop growth.

ix. During dry/stressed conditions, surface albedo found to 0.230 and 0.221 during year 1999-00 and 2000-01 respectively whereas after irrigation it was 0.196 and 0.169.

x. The correlation between air and surface temperature were found to be 0.984 and 0.925 over wheat crop field whereas 0.975 and 0.976 over bare field during years 1999-00 and 2000-01 respectively.

xi. Significant correlations were found between surface and at 5cm depths (0.991 and 0.987) over wheat field and 0.974 and 0.997 over bare surface during the experimental years.

xii. The negative significant correlations between surface temperature and net long wave radiation (-0.9449), net long wave and net short wave radiation (-0.9384) and between incoming and outgoing short wave (-0.954).

xiii. The prediction equation using one dependent variable also find out and expressed below:

Sr.No	1999-00	2000-01	Surface
1	ST_o=1.096 AT+3.99 R^2 = 0.951	ST_o = 1.1898 AT+1.0114 R^2 = 0.961	Bare
2	ST_o = 0.7844 AT+4.116 R^2 = 0.923	ST_o = 0.7806 AT+5.3987 R^2 = 0.856	Wheat
3	ST_5 = 1.0164 ST_o +4.129 R^2 = 0.982	ST_5= .9531 ST_o +0.4155 R^2 = 0.948	Bare
4	ST_5 = 0.8489 ST_o +1.797 R^2 = 0.984	ST_5 = 1.0039 ST_o-1.5419 R^2 = 0.976	Wheat
5	ST_o = -0.0838 NLW+16.045 R^2 = 0.839	Not found	Wheat
6	RSW=0.205 ISW-2.4128 R^2 = 0.838	RSW=0.213 ISW-8.4563 R^2 = 0.911	Wheat
7	NLW = -8.8192 ST_o+127.8 R^2 = 0.837	Not significant	Wheat
8	NLW=-0.314 NSW+45.474 R^2 = 0.881	Not significant	Wheat

xiv. In addition to this, the value of NPP of various types of natural vegetation in the semi-arid region of Western India obtained through the Chikugo model proposed by Uchijima and Seino, 1993 using the climatic data. The validity of this model is tested by comparing NPP-data for individual stations of Sabarmati river basin region. Results shows that linear relationship between annual net radiation and net primary productivity as influenced by the dryness of climate. Results also indicate that NPP-values in each RDI zone are approximately proportional to annual net radiation and that the proportionality constant (alpha) between NPP

and Rn decreases considerably as the climate become drier. This suggests that the efficiency of plant photosynthesis decreases rapidly as climate becomes more dry, agreeing well with results obtained in crop experiments. Net primary productivity for Gujarat region is observed to be ranged between 22-26 t dry matter/ha.yr and the total net productivity for 100x100km area is in order of 10^6 t dry matter per year.

CONCLUDING REMARKS AND APPLICATION POTENTIAL

The project has yielded useful results. Implementation of the LASPEX has provided a long felt opportunity for the participating scientists in the country to gain first hand experience in planning and conducting land surface processes experiment with inter-institutional collaboration, maintenance and working of equipment, data acquisition, quality check procedures, processing and analysis. On the basis of available data sets, a comprehensive and composite study of energy and water balance of the basin where LASPEX -97 was undertaken may be used as a document for the specified research programs. A better understanding of the boundary layer heights of the LASPEX region may be helpful in medium range weather forecast using these valuable data This may also helpful in better understanding of these parameters over varying surfaces particularly over bare soils and different crop fields. The information given in the present study may be utilized to modify the microclimate near the surface to get maximum crop yield.

Acknowledgements

The authors are thankful to the Department of Science and Technology, Govt. of India for funding the LASPEX-97 to conduct the field experiment and also to the Gujarat Agricultural University, Anand for providing all the infrastructure for smooth functioning of the project

Reference

Cipra, JE, Baumgardner, MF, Stoner, ER, and MacDonal, RB. 1971. Measuring radiance characteristics of soil with a field spectroradiometer. *Soil Sci. Soc.Am.Proc.* **35**:1014-1017.

Grant, PF and Nickling, WG. 1998. Direct field measurement of wind drag on vegetation for application to windbreak design and modeling. *Land degredation and Development*, **9(1)**: 57-66.

Rao, Kusuma G. 1997. Roughness length and drag coefficient at two MONTBLEX-90 tower stations. *Proc.Ind.Acad.Sci.*, Bangalore, 245-259.

Mohanty, UC, and Parihar, PS, Venugopal, T, and Parshuram A. 1997. Estimation of drag coefficient over the western desert sector of the Indian summer monsoon. *Proc.Ind.Acad.Sci.,* Bangalore, 261-275.

Moore, CJ.1986. Frequency response correlations for eddy correlation system. *Bound.Layer Meteorol.*, 37: 17-24.

Idso, SB, Jackson, RD, Reginato, RJ, Kimball, BA, and Nakayama, FS. 1975. The dependence of bare soil albedo on soil water content. *J.Appl. Meteorol.*, 14: 109-113.

Patil, MN, Murthy, BS, and Parasnis, SS. 2001. Characteristics of momentum and sensible heat flux during the monsoon conditions over LASPEX-97 regions., *J.Agrometeoro.*, 3(1-2): 107-117.

Rao, P Sanjeeva. 2001. Large field experiments and modeling land surface processes: A review. *J.Agrometeorol.*, **3(1-2)**:1-21.

Shekh, AM, Vernekar, KG, and Keshamurthy, RN. 2001. The beginnings of LASPEX-97. *J.Agrometeorol.*, **3(1-2):** 31-38.

Sellers, PJ, Mintz, Y, Sud, YC, and Dalehar, A. 1986. A simple biosphere model (Sib) for use within general circulation model. *J.Atmos.Sci.*, **43:** 505-553.

Sauer, JJ, Hatfield, JL, Prueger, JA. 1996. Aerodynamic characteristics of standing corn stubble. *Agron.J.*, **88(5):** 733-739.

Disaster Management
Editors: N.C. Mahanti et al.

Hydrological Variations in Lahul-Spiti, Himachal Pradesh, India During the Past 800 Years as Inferred from Tree Rings

Ram R. Yadav, Jayendra Singh, Bhasha Dubey and Krishna G. Mishra

Birbal Sahni Institute of Palaeobotany, 53 University Road, Lucknow, India

Abstract

Himalayan cedar ring width chronologies spanning AD 1222-2003 and 1217-2003 were prepared from two moisture stressed sites in Chandra-Bhaga river basin, Lahul and Spiti district, Himachal Pradesh. The chronologies were calibrated with the precipitation records available for Keylong. Strong relationship between ring width chronologies and precipitation of previous year's September to July of the current growth year enabled to reconstruct the precipitation for the common chronology period 1222-2003. The reconstructed precipitation showed strong year-to-year and inter decadal variability. Such reconstructions using tree-ring data network are useful to understand precipitation variability in the semi arid to arid regions vulnerable to climatic extremes.

Introduction

Hydrological regime over the catchment area of major rivers originating in the Himalayan region is crucial for the well being of local and downstream inhabitants as these rivers are the important feeders of irrigation, hydroelectric and potable water supply projects. Precipitation, besides the glacier melt, contributes major share of the total river flow. Barely century long precipitation records do not provide sufficient data length to understand the recurrence behaviour of extreme events. In such cases high-resolution proxy records could be used to supplement the precipitation records back to several centuries and even millennia. Tree-rings provide high-resolution record of environmental variables, as these could be precisely dated to calendar years (Fritts, 1976). Tree-ring parameters such as widths, density and isotopic composition could be calibrated with the instrumental weather records to develop long-term weather informations. Record of millennium long chronologies of Himalayan cedar from the western Himalayan region (Singh *et al.*, 2004) shows the potential of developing long-term climatic reconstructions. Such long-term records provide valuable database to understand natural climate variability and also the validation of climate prediction models.

Chandra-Bhaga river basin lies on the northern ridge of Pir Panjal range in the Lahul and Spiti district of Himachal Pradesh. It falls in the monsoon arid transition zone and is considered to be a potential indicator of the northern limits of the intensity of monsoon. The area is influenced by monsoon in summer and westerlies in winter. Long-term weather records from such marginal areas are of high importance to humanity. We present here the precipitation reconstruction from previous years September to concurrent July for Keylong using tree-ring chronologies of Himalayan cedar (*Cedrus deodara* (Roxb.) G. Don) from two moisture stressed sites in Chandra-Bhaga river basin in Lahul and Spiti district, Himachal Pradesh.

Data and Methods:

Tree ring data

Materials for the present study in the form of increment cores from Himalayan cedar trees growing in open forests at moisture stressed two sites on right and left bank of Chandra-Bhaga river (Fig. 1) were collected in May-June 2004. Healthy, undisturbed trees growing distantly at both the sites were sampled using increment borers. Usually two increment cores from opposite sides at breast of the stem perpendicular to the slope direction were taken. The openness of the stands maximizes the climate variance in tree ring sequences as the effect of inter tree competitions among the trees are greatly reduced. Tree rings were dated employing usual dendrochronological techniques (Stokes and Smiley, 1968; Fritts, 1976). The ring widths of dated samples were measured with 0.01 mm accuracy using linear encoder coupled with personal computer. The dating of ring width sequences were verified using computer assisted COFECHA program (Holmes, 1983), which identifies tree-ring width series segments that may have dating or measurement

errors. Such samples showing dating irregularities were rechecked and errors corrected. Negative exponential or straight-line curve fits was used to remove the biological age trend in measurement series and retain climate related common variance (Cook and Kairiukstis, 1990) using computer programme ARSTAN (Cook, 1985). The ring-width indices were derived by dividing the measured value by curve value in each year. After removing the autocorrelations using an autoregressive model selected on the basis of the minimum Akaike criterion, these indices were combined across all series in each year using biweight robust estimation of the mean to discount the influence of outliers. Standard, residual consisting of high-frequency variations and an arstan chronology composed of the residual incorporated with the pooled autoregression was prepared. The chronology statistics are given in tables 1 and 2. The two chronologies displaying close year-to-year similarity (Fig. 2) showed highly significant correlation ($r=0.82$, $p<0.0001$, AD 1222-2003) indicating the influence of common forcing factor i.e., climate.

Precipitation data

For calibration of tree-ring data weather records from stations close to the sampling sites are required. In present case the precipitation records of Keylong meteorological station (Fig. 1) falling nearest to the sampling sites were used. Though the data length ranges from 1904-1999, there were large data gaps. The weather data of Koksar (1951-1969 with missing records for 1961-1965) and Srinagar (1893-2003) were used to estimate the missing data in Keylong records. The monthly precipitation values for Keylong as indicated by standard deviation show high variability (Fig. 3).

Relationship between tree ring and precipitation data

Crosscorrelation analyses between prewhitened tree-ring chronologies and monthly precipitation of Keylong from previous growth years September to concurrent September were computed to understand the relationship between tree growth and precipitation. Both the chronologies showed direct relationship with precipitation in most of the months except August (Figures 4, 5). This indicates that the trees at both the sites are growing under moisture stress. Precipitation of previous years September to concurrent July showing stronger correlation was used for calibration and reconstruction.

Calibration, verification and reconstruction

The two site chronologies with strong year-to-year variation follow each other very closely (Fig. 2). This indicates the influence of common forcing factor, i.e., climate affecting growth of trees at two sites. To overcome the effect of multicollinearity in the predictor tree-ring chronologies we transformed them into principal components. The first principal component showing 91% common variance in the chronologies correlated significantly with previous years September to concurrent July precipitation and was used for reconstruction using simple regression analysis. Cross-calibration was used to test the fidelity of relationship between tree-ring and precipitation data. For this the precipitation data were split into two equal halves, i.e., 1904-51 and 1952-1999. The regression equation accounted for 26% and 38% of the variance in instrumental precipitation data (R^2 adjusted for loss of degrees of freedom) in two sub-period calibrations, which produced significant verification statistics such as crosscorrelation, product means test, sign test and reduction of error (RE) in respective sub-periods (Table 1) (Fritts, 1976). After cross-verifying the calibration models of both the sub-periods tree-ring and precipitation data were calibrated for the whole period (1904-1999) that captured 37% of the variance in instrumental data. The whole period calibration model was used to estimate the precipitation for the early periods covered by tree-ring data. The use of entire calibration interval enhances the ability of the regression model to reconstruct low frequency variability in the precipitation. The decadal-interdecadal scale variations in precipitation very closely follow the trend in tree ring variations (Fig. 6) indicating the ability of our reconstruction model in capturing low frequency variations.

Results and Discussion

The precipitation reconstruction (AD 1222-2003) showed strong year-to-year variability superimposed over the decadal and interdecadal fluctuations (Fig. 7). Extreme dry and wet 20 and 50-year periods of the series

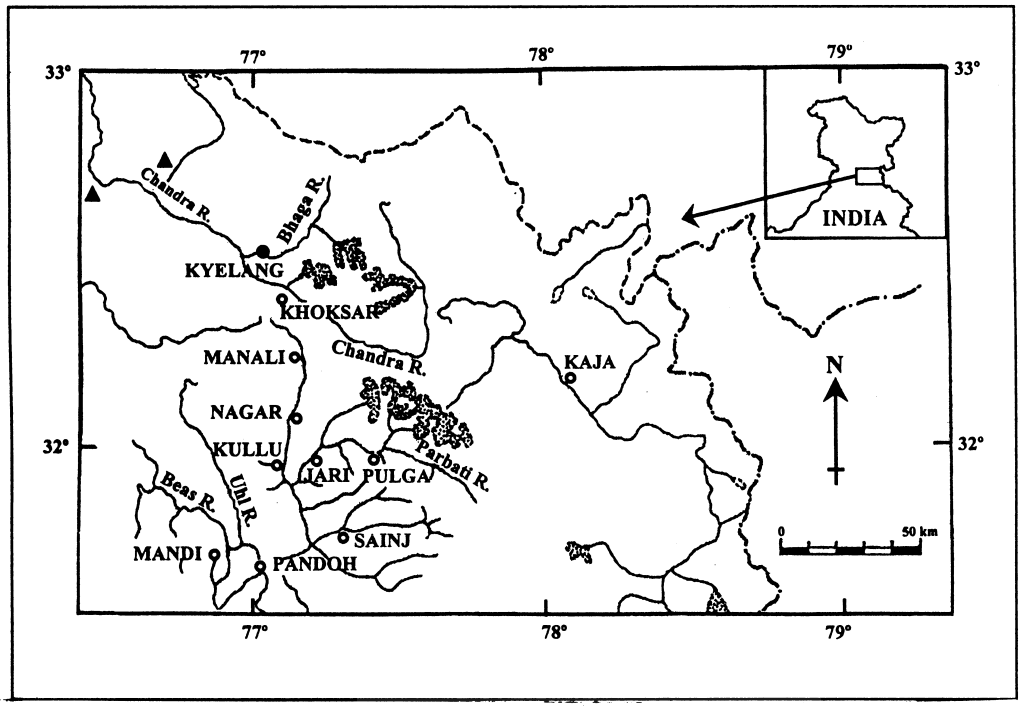

Fig. 1. Map showing the sampling sites (filled triangles) and meteorological station (filled circle)

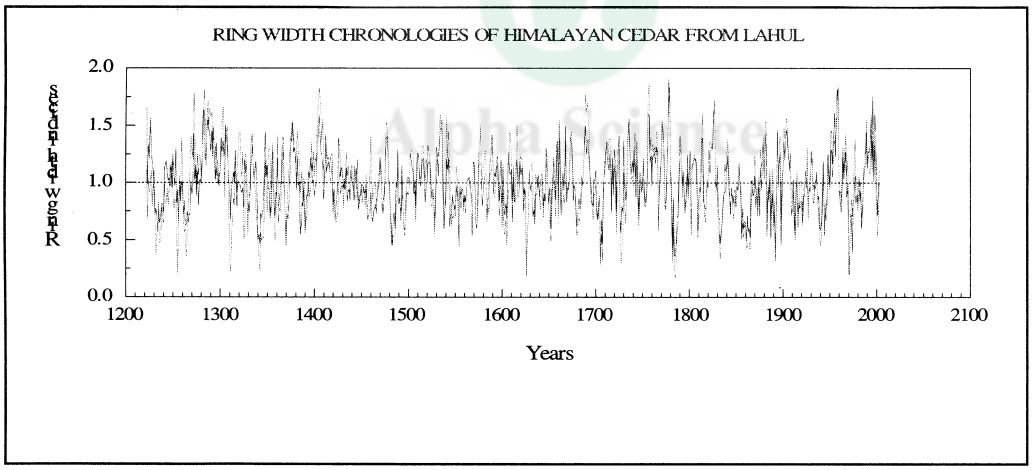

Fig. 2. Ring width chronologies of Himalayan cedar from two sites overlaid to show similarity in year-to-year departures

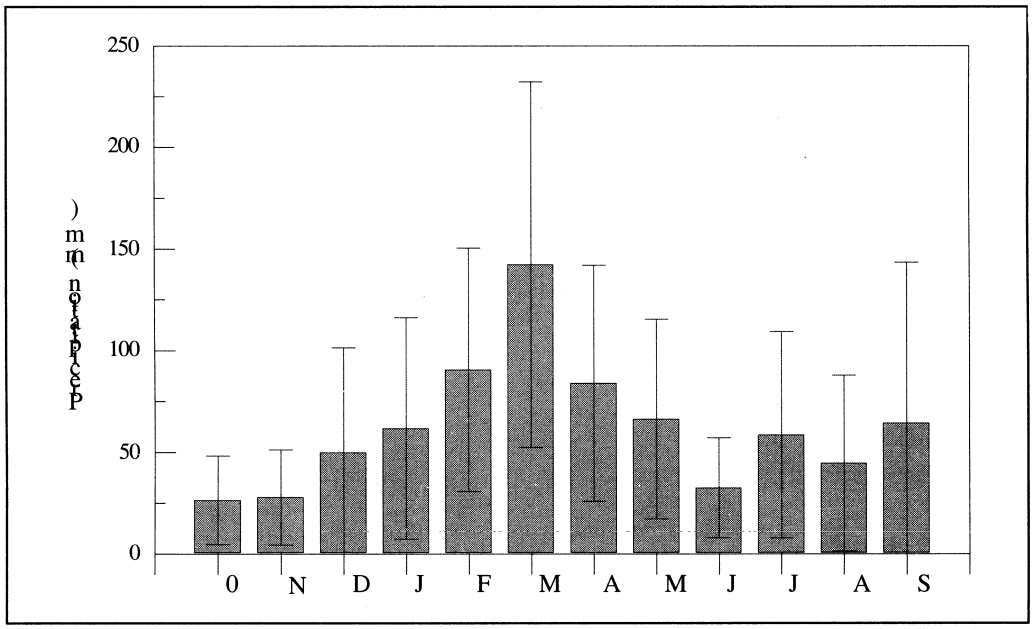

Fig. 3. Monthly precipitation profile of Keylong

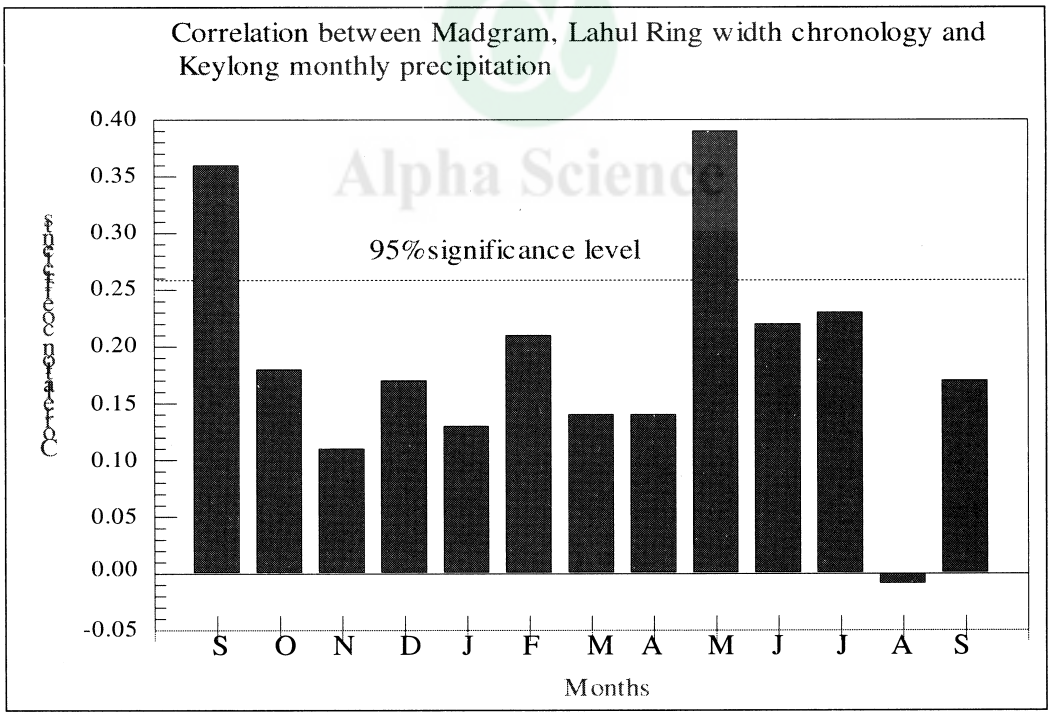

Fig. 4. Correlation between ring width chronology of Himalayan cedar from Madgram (Lahul and Spiti) and Keylong monthly precipitation. Dashed horizontal line represents the 95% significance level.

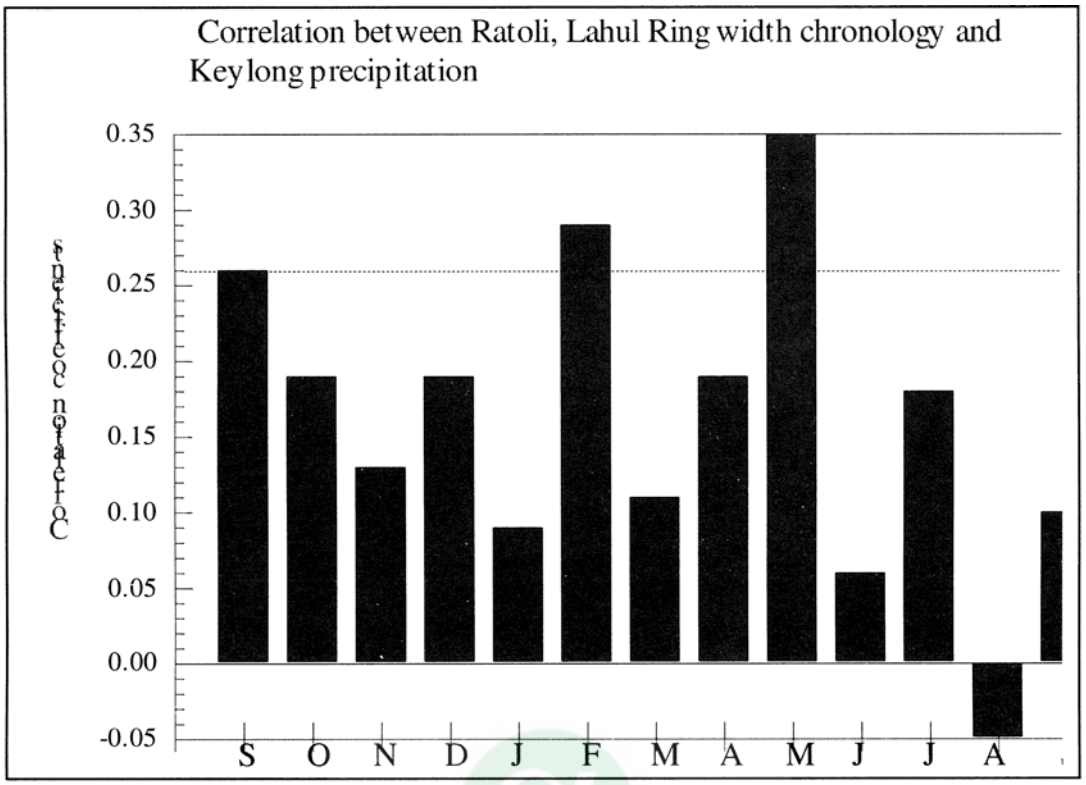

Fig. 5. Correlation between ring width chronology of Himalayan cedar from Ratoli (Lahul and Spiti) and Keylong monthly precipitation. Dashed horizontal line represents the 95% significance level.

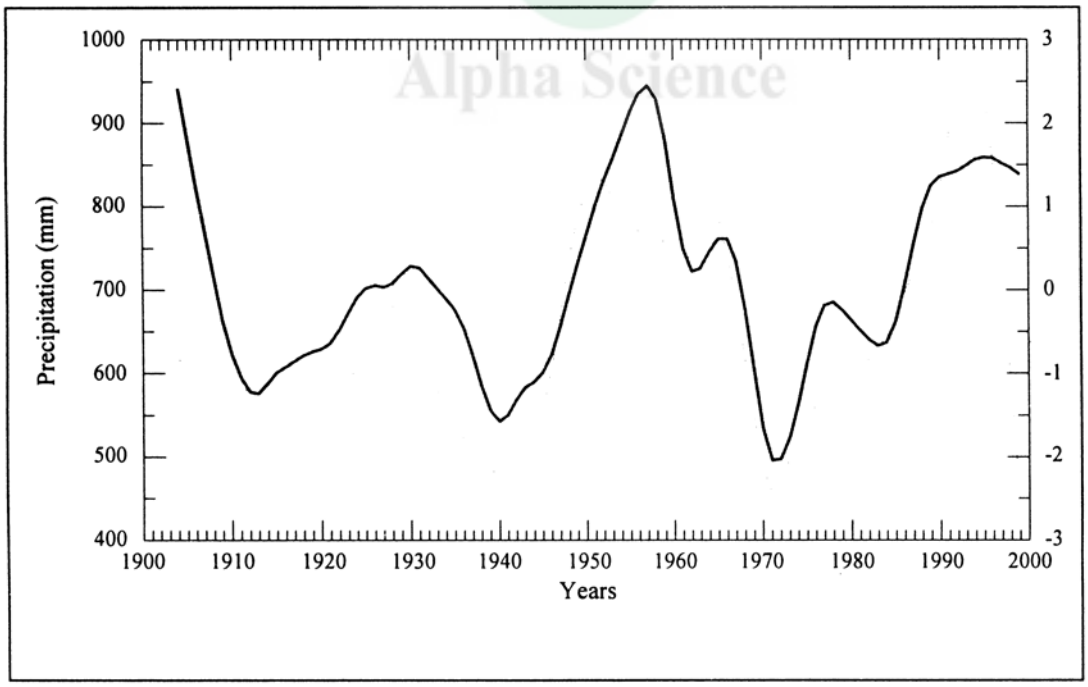

Fig. 6. Filtered version of precipitation and tree-ring chronology scores plotted together to show fluctuations at 10 years and above. Dotted line represents the precipitation and complete line tree-ring chronology scores.

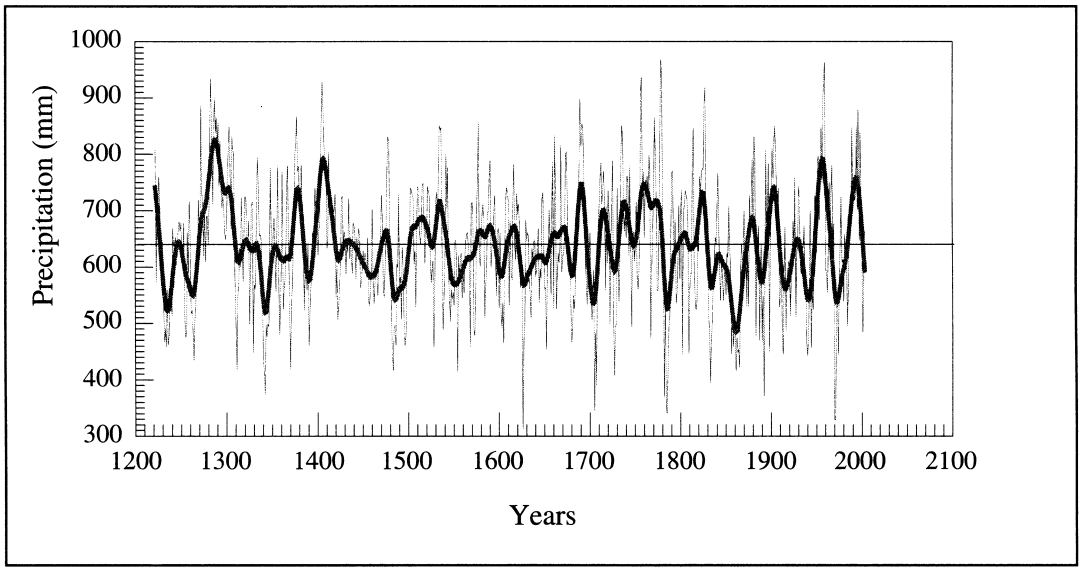

Fig. 7. Precipitation reconstruction (AD 1222-2003). Thick line demonstrates the fluctuations on timescales of 10 years and above.

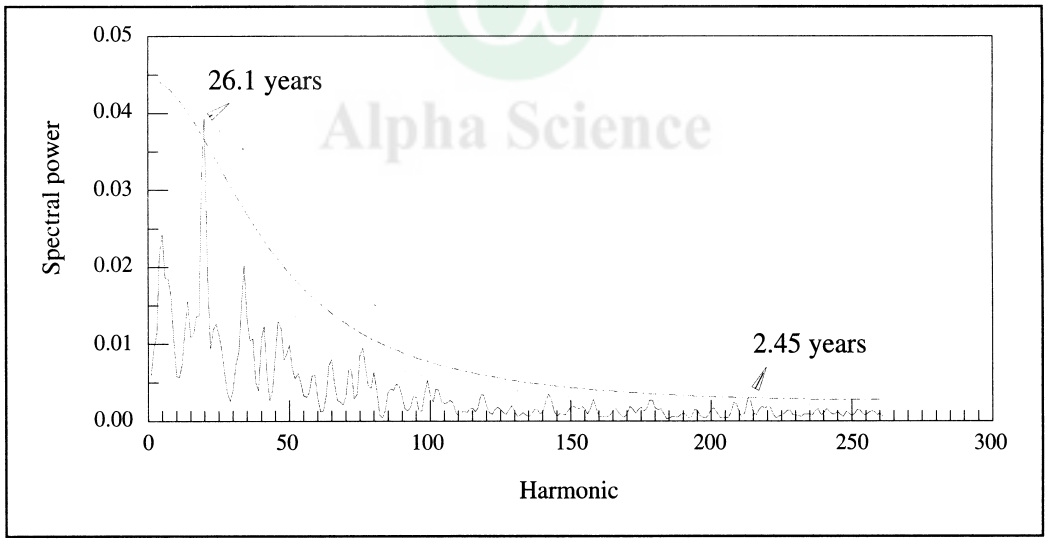

Fig. 8. Power spectrum of the reconstructed precipitation series (AD 1222-2003). The lower limit is 95% and upper 99% confidence level.

Table 1. Statistics of standard ring width chronology of *Cedrus deodara* from Madgram, Lahul and Spit district, Himachal Pradesh

Chronology span	AD 1222-2003 (782 years)
Trees/radii	21/41
Mean sensitivity	.21
Standard deviation	.27
Autocorrelation	
order 1	.54
order 2	.08
Common interval statistics	AD 1665-2003 (339 years)
Trees/radii	19/36
Mean correlations:	
Among all radii	.46
Between trees (Y variance)	.46
Within trees	.51
Signal-to-noise ratio	16.33
Variance in first eigenvector	48.69%

Table 2. Statistics of standard ring width chronology of *Cedrus deodara* from Ratoli, Lahul and Spit district, Himachal Pradesh

Chronology span	AD 1217-2003 (787 years)
Trees/radii	15/18
Mean sensitivity	.22
Standard deviation	.31
Autocorrelation	
order 1	.65
order 2	-.02
Common interval statistics	AD 1623-1984 (362 years)
Trees/radii	13/14
Mean correlations:	
Among all radii	.51
Between trees (Y variance)	.51
Within trees	.72
Signal-to-noise ratio	13.54
Variance in first eigenvector	55.06%

Hughes, M. K. (1992). Dendroclimatic evidence from the western Himalaya, in *Climate Since AD 1500*, edited by R. S. Bradley, and P. D. Jones, pp. 415-431, Routledge, London.

Singh, J., R. R. Yadav, B. Dubey, and R. Chaturvedi (2004). Millennium-long ring-width chronology of Himalayan cedar from Garhwal Himalaya and its potential in climate change studies, *Curr. Sci.*, **86**, 590-593.

Singh, J. and R. R. Yadav (2005). Spring precipitation variations over the western Himalaya, India, since AD 1731 as deduced from tree rings. *J. Geophys. Res.*, **110**, d01110, doi:10.1029/2004JD004855.

Stokes, M. A., and T. L. Smiley (1968). *An Introduction to Tree-Ring Dating*, The University of Chicago Press, Chicago, London.

Table 3 Summary of calibration and verification statistics

Calibration		Verification				
Period	R^2 adjusted	Period	r	T value	Sign test	RE
1904-1951	26%	1952-1999	0.63***	4.07*	$39^{+}/9^{-}$*	0.48
1952-1999	38%	1904-1951	0.53***	4.34*	$35^{+}/13^{-}$*	0.42
1904-1999	37%					

R^2 adjusted- variance accounted for by the calibration model adjusted for degrees of freedom, r – Pearson correlation coefficient, T value- sign test- RE- reduction of error statistic; * -p= (0.05), *** -p=0.0001

Table 5. Driest and wettest 20- and 50-year mean periods in the reconstructed precipitation series

20-year mean

Driest		Wettest	
Period	Precipitation (mm)	Period	Precipitation (mm)
1847-1866	534.0	1282-1301	781.2
1480-1499	548.1	1400-1419	741.9
1780-1799	571.9	1948-1967	737.8
1339-1358	572.8	1754-1773	733.1
1968-1987	574.2	1980-1999	698.2
1249-1268	574.7	1811-1830	691.6
1544-1563	576.2	1365-1384	687.5

50-year mean

Driest		Wettest	
Period	Precipitation (mm)	Period	Precipitation (mm)
1828-1877	575.1	1272-1321	722.1
1448-1497	593.2	1730-1779	706.6
1222-1271	600.2	1372-1421	691.1
1324-1373	602.7	1950-1999	679.7
1597-1646	612.5	1498-1547	665.6

are indicated in (Table 2). Though wet and dry periods occurred in the whole span of reconstruction, the driest episode occurred during the mid part of the 19th century followed by the later part of the 15thth century. Late 15th to early 17th century consisting major part of the Little Ice Age (LIA) were relatively dry. Distinct wet periods occurred during the late 13th, early 14th and 18th centuries. The precipitation relatively increased during the recent decades of the 20th century. Low precipitation during 15th to 17th and 19th century observed in our reconstruction coincide with low monsoon activity in South Asia as inferred from *Globigerina bulloides* abundance in the Arabian Sea (Anderson *et al.*, 2002). The precipitation variability in such marginal cold arid regions has serious implications for the human population. The reduced precipitation during the 19th century noted in our study coincides with the failure of summer monsoon in the Indian region, which has been responsible for major famine of 1877 in India (Burroughs, 1997).

The two other tree-ring based reconstructions available for the Valley of Kashmir (Hughes, 1992; Borgaonkar *et al.*, 1994) could not be compared with the present reconstruction due to different seasons precipitation as well as their very short length. The tree-ring based premonsoon precipitation reconstruction for the western Himalayan region using network of 15 tree-ring width chronologies (Singh and Yadav, 2005) does not show resemblance with the present reconstruction at least on decadal-to-interdecadal scale which could be due to length of different seasons as well geographic region.

Power spectral analysis of the reconstructed precipitation series revealed significant spectral power at around 2 and 26 years cycles (Fig. 8). Such high frequencies are also recorded in premonsoon precipitation reconstructed from the western Himalaya (Singh *et al.* under preparation) indicating the realness if the variations in precipitation.

Conclusion

The present study is the first attempt in reconstructing the hydrological conditions spanning over around 800 years for a precipitation deficient cold desert region of Lahul and Spiti in the trans Himalayan region. The use of only two site ring width chronologies in the predictor model accounted for 37% of the variance in the instrumental precipitation data. Such reconstructed data provide valuable base line to understand the natural variability in precipitation in long-term perspective. However, for sound applicability of precipitation estimates more robust reconstructions are needed to be developed using network of tree-ring data from moisture stressed sites.

References

Anderson, D.M., Overpeck, J.T. and A.K. Gupta, (2002). Increase in the Asian southwest monsoon during the past four centuries. *Science*, **297**, 596-599.

Borgaonkar, H. P., G. B. Pant, and K. Rupa Kumar (1994). Dendroclimatic reconstruction of summer precipitation at Srinagar, Kashmir, India since the late-eighteenth century. *Holocene*, **4**, 299-306.

Burroughs, W.J. (1997). Does the weather really matter? The Social Implications of Climatic Change. (Cambridge University Press, Cambridge)

Cook, E. R. (1985). *A Time Series Approach to Tree-Ring Standardisation*, Unpublished Ph.D. dissertation, University of Arizona, Tucson, Arizona, USA.

Cook, E. R., and L. A. Kairiukstis (Eds.) (1990). *Methods of Dendrochronology: Applications in Environmental Sciences*, 394 pp., Kluwer Academic, Dordrecht.

Fritts, H. C. (1976). *Tree Rings and Climate*, Academic Press, London.

Holmes, R. L. (1983). A computer-assisted quality control program, *Tree-Ring Bull.*, **43**, 69-78.

Disaster Management
Editors: N.C. Mahanti et al.

Post-Disaster Communications in Underground Coal Mines for Trapped Miners

L.K. Bandyopadhyay[1], Sudhir Kumar[1], P.K. Mishra[1]
A. Narayan[2] and M.K. Sinha[3]

[1]Scientists, [2]Project Fellow, [3]Research Intern, Central Mining Research Institute, Dhanbad-826 001, India

Abstract

Underground mines are typically extensive labyrinths that employ many people working over an area of a few square kilometers. In underground mines sometimes due to fissured strata, the roof or sidewalls of a gallery collapse and miners get trapped inside sealed area. Many miners get trapped beneath the big chunk of fallen roof. A communication link between the trapped miner and rescue team is essential to find out the actual location of trapped miner for rescue operation. Studies and experiments conducted reveal that very high frequency (VHF) and ultra high frequency (UHF) have comparatively less penetrating power than low radio frequency (RF). As there is restriction of power (2 Watts maximum) for underground mines to satisfy the intrinsically safe criteria, a compromise has been made and it was found that low RF is suitable for communication through hard structure. This paper describes about the experiments carried out in underground coal mines with RF transceivers. Clear and loud signal was heard on the receiving end of rescue team when transmitting end was placed on either side of a large thickness of coal block of about 30 metres. The paper concludes with the details of the experiments carried out in different underground coal mines.

Keywords: Post-Disaster, Trapped Miners, MF communication, Short-range Locator, Rescue Team, Mine disaster

Introduction:

Mine disasters are still inevitable especially in underground coal mines. They have a major impact on underground mining from both an economic and psychological perspective apart from the loss of lives of miners and subsequent impact on their families. The use of blasting mechanism to extract coal may sometimes lead to serious environmental health hazards like release of undesirable toxic gases. Fires, cave-ins, floods and roof fall are other unwanted outcomes. As a result of this, the miners working inside the mine get entrapped and there is no way to get out of the calamity. They are also not equipped with sufficient resources and manpower to get out of the post-disaster situation.

The post-disaster communication system must possess the ability of exchanging information among miners and rescue team through the earth or coal or rock. In addition the communication gadget provided to worker must be economical, lightweight and low-powered for practical use. Various communication systems – some of them used in advanced countries-are discussed in this paper.

This proposed system has been discussed in the paper with its functional role, practical use, merits and any possible modification. Theoretical and experimental work indicated that medium frequency (MF) signals due to their low attenuation properties propagate through natural media (water, rock, coal strata, etc.) and down the passageways of the underground mine.

Limitations of other existing systems for post-disaster communication:

The Bureau of Mines, Pittsburgh has developed through-the-earth seismic and electromagnetic (EM) location systems [1, 2] that enhance escape and rescue to a large degree. The seismic-based system is presently operational and the EM-based system is still in the research and development stage. Nevertheless, even if fully implemented, there will never be any assurance that all miners have truly been located. Injury or other factors may make it impossible to utilize the features of either the seismic or EM systems. The keystone of any rescue effort is, and will remain, the rescue team. Equipping every miner with a transmitter (EM system) is economically not viable; also deploying an antenna might be impossible if the miner were

injured or confined. Furthermore since highly specialized location equipment would be required, it is possible that 24 to 48 hours would be needed to move the system to the site of a disaster and deploy it.

Features of the proposed locator:

Because of the limitations of old systems, it is concluded that a light-weight, inexpensive, short-rangelocation system [1] for use in underground is needed. Short range locator has the capability to operate over the range of at least 30 metres in air and through 3 or more metres of rock. This range would be adequate in most post-mine disaster scenarios. The short-range system consists of a low-power radio transmitter carried by each miner capable of being detected by a receiver available with the rescue team. The prototype transceivers are powered by 3.6 V Lithium batteries. Following a disaster, the transmitter would serve as a radio beacon to help rescue personnel and locate trapped miners with an acceptable degree of accuracy under or behind roof falls or debris, or in other inaccessible areas. It is believed that such a system would enhance the chance of post-disaster survival to locate trapped and possibly injured personnel. Rapid location of victims has the added advantage of reducing the time. Thus, the locator could be a significant factor in enhancing the safety of the rescue team even in cases where the victims failed to survive the initial accident. The locator, which was modified recently and laboratory experiment is under process doesn't need an additional power source; it is powered by the miner's cap lamp battery itself.

Trapped Miner Communication technique

In underground mines, sometimes due to fissured strata, the roof or side wall of a gallery collapse and miners get trapped inside sealed area. Many miners get trapped beneath the big chunk of fallen roof. A communication link between the trapped miner [2, 3, 4] and rescue team is essential to find out the actual location of trapped miner for rescue operation. Studies revealed that attenuation of low frequency is comparatively lower through coal block. The low frequency tone signal modulated over RF signal 457 kHz can be transmitted through large thickness of coal block.

Development and Field Trials

Instrumentation Division of Central Mining Research Institute, Dhanbad is actively engaged in development of various wireless communication systems for different locations in underground mines. One of the instruments is short range location system also called trapped miner locator. Which is still in developmental phase. Therefore, prototype proposed trapped miner locator was built with optimum frequency selection of 457 KHz with a transmitting power output of 50 mW. CMRI, Dhanbad has done several laboratory and field trials in this regard for evaluating its performance. The results were encouraging. The low frequency tone signal modulated over MF signal of 457 KHz can be transmitted through large thickness of coal block. The detailed results and studies have been presented in the paper after trials in various mines.

Results and discussions

Bagdiggi Mine, BCCL:

The field trials were performed in the 9^{th} pit of Bagdiggi Colliery (depth of around 200 m from ground to surface) with trapped miner locators.

The trapped miner locator had a range of about 30 m in a straight gallery and was able to penetrate a 3-4 m thick wall.

The experiment was also performed with modified (with same Lithium batteries) trapped miner locator in 12^{th} pit as shown in Fig. 1. The transmitting and receiving ends of the system were available with persons 1 and 2 standing in the 8^{th} seam and 7^{th} seam, respectively. The parting between both the seams is about 12-15 m. The signal was heard but that was not clear and loud.

Nandira Mine, Talcher Area, MCL:

Bandyopadhyay L. K., Kumar S., Mishra P. K., Narayan A. and Sinha M. K, Studies on Wireless Communication systems for Underground Coal Mines, Global Coal-2005, Int. Seminar on Coal Science and Technology: Emerging Global Dimensions, April 12-13, 2005, New Delhi

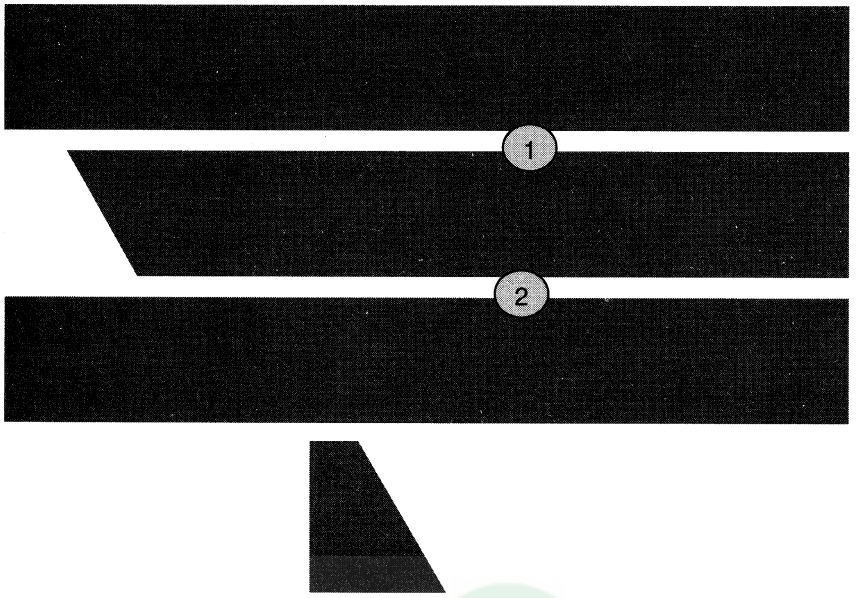

Figure 1: Schematic diagram of 7^{th} and 8^{th} seams of Bagdiggi mine

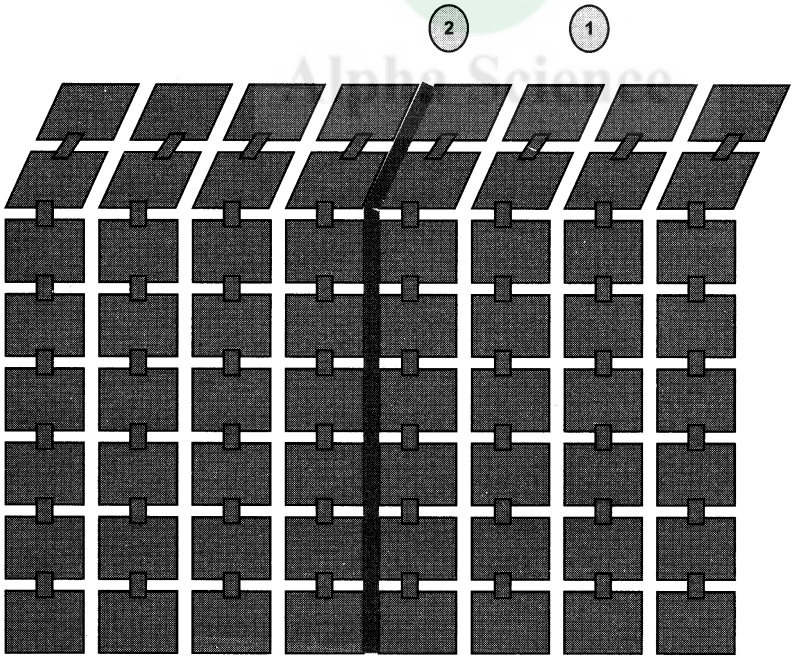

Figure 2: Schematic diagram of a underground mine gallery of Chinakuri mine

Nandira mine is an inclined mine. The field trials were conducted with the same system used in Bagdiggi Mine.

The locators were tried to search the person beneath rubbles or coal dump. One transceiver was engraved in a coal dump of about 1.5 m deep in transmitting mode. Transceiver in receiving mode clearly indicated the location of engraved transceiver.

Chinakuri Mine, ECL:

Chinakuri mine of Eastern Coal Field is the deepest coal mine in India. The depth from surface to underground is 612 m. The field trial was conducted with modified (with same lithium batteries) trapped miner locator.

The modified trapped miner locator penetrated a 40 m thick wall (between points 1 and 2 as shown in Fig. 2) in underground. The transmitting and receiving ends were put to either side of the side walls (thickness 40 m) keeping in view that the signal did not leak from the bend of the gallery.

Conclusion:

The proposed trapped miner locator is technically, economically and operationally feasible, and it would enhance the chances of survival of trapped miners after a mine disaster. The experiments at laboratory and mines have authenticated the utility of such a system. Tests indicated that 457 KHz (MF) is a usable frequency for the short range locator. The power output of 50 mW is well below the prescribed limit of 2 W for use in underground. The locator can be made intrinsically safe and ill pose no hazard to blasting material. The cost of such a unit would be low, and the unit would require no action on the part of the distressed miner.

It is to be noted that discrete technique was implemented and work can further be done by repackaging the unit into a much smaller integrated circuit. This will make it even lighter and possible modifications could also be done to strengthen the signal strength for increasing the system's range through any media.

The proposed post-disaster communication system could also be integrated with a communication system (featured with voice communication) using the same MF range for its normal operational functioning. It will thus be possible to establish a voice communication link between trapped miner and rescue team. This technology could then further be extended for communication among different mine levels through hard and concrete strata.

Acknowledgement

Authors are thankful to Director, Central Mining research Institute, Dhanbad for giving permission to present the paper. Authors are also grateful to mine management of Bagdiggi Colliery of BCCL, Nandira Mine of MCL and Chinakuri Mine of ECL for providing necessary help during the field studies. Sincere thanks are also due to the DoE, MCIT, Govt. of India, India for sponsoring this development project.

References

A Short-Range Locator System for Detecting Trapped Miners, RI 8844, Bureau of Mines Report of Investigations, 1984.

Underground Mine Communications, Control and Monitoring, IC 8955, Bureau of Mines Information Circular, 1984.

Kumar A., Chaulya S., Kumar S. and Bandyopadhyay L. K., Trapped miners detection, location and communication. Minetech Vol. 24 No. 6 pp. 1 – 13, Nov.- Dec. 2003.

Disaster Management
Editors: N.C. Mahanti et al.

Waiting for Inevitable Natural Disaster in Lesser Himalayas, Garhwal–A Geoinformatics Based Geoenvironmental Perspective on Feasibility of Tehri Dam

Arvind Chandra Pandey

Department of Remote Sensing, Birla Institute of Technology, Mesra, India

Abstract

The Himalaya is the youngest and the highest mountain chains of the world. It measures for about 2400 km in length and 370 km in width. The area under investigation lies in the Lesser Himalayas in Tehri and Uttarkashi districts of Uttaranchal. It is located between 78°15' – 78°45' E longitudes and 30°15' – 30°50' N latitudes and measures for about 2700 sq. km. The 260.5 meter high earth and rock fill Tehri dam located in this area is under final phase of construction near the confluence of Bhagirathi and Bhilangna rivers at Tehri town. The dam site lies in a seismically and tectonically active zone of the Lesser Garhwal Himalayas, which have experienced Uttarkashi earthquake in 1991 and Chamoli earthquake in 1999. Land degradation due to land sliding constitutes a major geoenvironmental hazard in the Tehri dam and its environs. The geoenvironmental perspective on feasibility of Tehri dam was studied for 2700 sq km area considering various geoenvironmental factors viz. geology, geomorphology, land use, slope, drainage, lineaments and landslides. These features were mapped on 1:50,000 scale using remote sensing data and collated data followed by field checks. In Himalayan terrain the regional coverage of the terrain acquired by remote sensing satellite helps in evaluating the spatial control of various landforms vis-à-vis their genetic control. Quantitative analysis of key factors, exerting prime control on land sliding in the peripheral region (579 sq. km) of Tehri dam, has been performed using Geographic Information System (GIS). The fragility of the geo-environment in the region has been discussed with due focus on land degradation, siltation and seismic activity.

Introduction

The Himalaya is the youngest and the highest mountain chains of the world. It measures for about 2400 km in length and 370 km in width. The study area lies in the Tehri and Uttarkashi districts of Uttaranchal. It is located between 78°15' – 78°45' E longitudes and 30°15' – 30°50' N latitudes (Fig 1.1) and measures for about 2700 sq. km in the Survey of India topographic sheets 53 J/5, J/6, J/7, J/10, J/11, J/9. Tehri and Uttarkashi are the two major towns of the area. The area is characterized by steep hills and narrow valleys associated with erosional and depositional landforms. The general landscape of the area ranges from 700 m to 4000 m above the mean sea level. The mean minimum and mean maximum temperature records near Tehri is 9.97 C and 17.23 C and the mean annual precipitation is 1008 mm.

The earth and rock fill Tehri dam is in final phase of its construction on the Bhagirathi river at 0.5 km downstream of Tehri town in Tehri district of Uttaranchal state (Fig. 1 & 2). The Tehri dam with a proposed height of 260.5 meters will be the fifth highest dam in the world. It will impound 3.22 million cubic meters of water. The reservoir will extend upto 45 kms in the Bhagirathi valley and 25 kms in the Bhilangna valley with a water-spread area of 42.5 sq.kms. Tehri dam reservoir will submerge Tehri town and 23 villages in its vicinity along with partial submergence of 72 other villages. Around 70,000 persons will be displaced because of the dam (Bhumbla et al., 1990).

The selection of present dam site has been topic of debate not only because of its majestic estimated height of 260.5 meter or its total catchment area of about 7511 sq km but also because of its location in a geo-dynamically fragile Himalayan domain where the earthquakes and land sliding are usually manifest. The area is seismically active and has witnessed a major earthquake of intensity 6.6 on Richter scale at Uttarkashi in 1991.

In the present work the geoinenronmental perspective on feasibility of Tehri dam was studied for 2700 square kilometers area considering various geoenvironmental factors viz. geology, geomorphology, land use, slope, drainage, lineaments and landslides. The affect of various terrain factors with respect to land degradation, siltation and seismic activity in the region was also discussed.

Remote sensing techniques were applied for better demarcation of lithounits, structures and geomorphic landforms whereas Geographic Information System (GIS) techniques were used for spatial data analysis. Based on visual interpretation of IRS-1C geocoded, False Colour Composite (FCC) satellite images various thematic maps viz. geology, geomorphology, landuse-landcover, lineament and landslide have been prepared on 1:50,000 scale. The maps prepared by using remote sensing techniques were updated during the field investigation. Surveys of India (SOI) topographical sheets were used for the preparation of slope and drainage maps. The various thematic maps prepared were digitized and analyzed under ARC-INFO GIS environment for spatial analysis in Tehri dam reservoir and environs.

Remote Sensing and GIS Techniques in Terrain Mapping

Remote Sensing is an important and effective aiding tool in geological- geomorphological studies and landuse mapping. Remotely sensed images provide a wealth of information of large areas of the earth's surface and permit evaluation of regional geological structures, broad lithological discrimination, spatial distribution of landforms and associated landuse patterns. The regional coverage acquired by satellite images provided pictorial representation of geological units with imprints of drainage, geomorphic landforms, landuse and erosional characteristics. Dynamic changes on land pertaining to landuse-landcover, erosion and landslide etc. can be monitored using sequential images. Inaccessible terrain covered by dense forests and steep slopes can be surveyed fairly. Geographical Information System (GIS) provides a scientific framework for storage, analysis and retrieval of spatial (thematic) and non-spatial (attribute) data.

Landuse- Landcover

Satellite images of IRS-1C of Tehri-Uttarkashi area (Fig. 3) were visually interpreted for demarcating Various types of landuse-land cover present in the area (Fig. 4). The towns of New Tehri, Tehri and Uttarkashi are the major urban settlements in the area. The villages are mainly located in the agricultural lands on the lower and middle slopes of the Bhagirathi and Bhilangna valleys. Intensive agriculture is practiced on river terraces along the Bhagirathi and Bhilangna rivers and their major tributaries. The forest occupies a major portion of the area. The mixed monsoon forest in the southwestern part of the region is dominated by tree species of Pinus roxburghii and Banj. The dense forests of Banj are replaced at higher altitude (>2555 m) by fir forests. In the northern part around Uttarkashi open to dense Pine forests and forests of Kahrsu occur on lower altitude whereas the dense Banj and Burans forests are present on higher altitudes. The extension of agricultural lands into the forest areas, cutting of forests for fuel wood and indiscriminate felling of trees, resulted in degradation of the forests in this region. The degraded forests are present mainly in the peripheral zones of the open and dense forests. The occurrence of degraded forests around agricultural lands and lower valley slopes indicates their development from degradation of dense and open forests due to human interference. A number of forest blanks were identified within a dense forest in Dharam Ganga and Balganaga valleys. This probably indicates a selective clearing of trees within dense forest. The Scrub lands are found associated with agricultural and forest lands with dominance of shrub species like, *Lantana cam mare, Rubus elipticus, barberis asiatica* etc. The excessive biotic pressures, like grazing, retarded vegetation growth in these areas. Barren lands are generally noticed at a number of places along the steep and precipitous slopes. The development of barren lands over agricultural lands (river terraces) is also noticed at Tehri. These terraces are being utilised as sites of construction material for use in the Tehri dam. The major rivers and their tributaries constitute the main water bodies whereas Maneri dam reservoir is an artificial water body of the region.

Geology of the area

The geological investigations were carried out on a regional scale to prepare a regional geological map of the area (Fig. 5). The contributions made by other geoscientists were also utilized. Since a large portion of the area is forest covered and the rocks are exposed only along the major roads, satellite images were utilised together with fieldwork to reconstruct the geology.

The investigated area consists of Simla Group (Simla slate), Krol Group (Blaini slate, Infrakrol slate, Krol limestone and Tal quartzite), Jaunsar Group (Chandpur phyllites and Pratapnagar quartzite and Kotga-Banali Calc Zone) and Central Crystalline Group (Budhakedar and Jutogh schist & gneiss) of rocks (Fig. 2). These rocks are confined to nappes delineated by well-defined thrusts. Each of the nappes is characterized by a distinct lithology and metamorphism.

A number of thrusts of regional extent viz., Garhwal thrust, North Almora thrust, Pratapnagar thrust, Budhakedar thrust (MCT-III) and Jutogh thrust (MCT-II) traverse the area. These thrust show NW-SE trend with a northeasterly dips varying 25°- 45°, except for the North Almora thrust, which dips in south. In the Bhagirathi valley, a number of transverse and oblique faults were delineated using satellite images. Major N-S trending transverse faults like Ganwan fault, Rano Fault and Shyalam fault were delineated within the Pratapnagar quartzites north of Uttarkashi. A major E-W trending fault is located at Uttarkashi, along which the Bhagirathi river flows in an E-W direction for about 7 km. The Bhilangna and Balganga rivers flow along the major tear faults. Such tear faults trending NW-SE and NE-SW are present at Chhatera and Raunsal respectively. The lineament distribution in the study area indicates four prominent trends. These are N55°E-S55°W, N50°W-S50°E, N90°E-S90°W and N5°E-S5°W.

Geomorphology

Based on satellite image interpretation and field investigations, a number of geomorphic landforms viz., hills and river valleys, ridge lines, summits, flood plains, sand bars, alluvial fans, fluvial terraces, gully erosion, landslides etc. were identified (Fig. 6). These landforms are categorized with reference to their genesis under (1) landforms of structural origin, (2) landforms of fluvio-glacial origin (3) landforms of fluvial origin and (4) forms of mass wasting. River terraces and river profiles of the Bhagirathi river and its major tributaries are analyzed with reference to morphotectonics. The slope analysis was done to understand the development of slopes in various lithological units of the area.

In the area under investigation the landslide constitutes a major landform of mass wasting in addition to subsidence, creep, rill and gully erosion. On the satellite images landslides are categorised as active and old landslides which commonly occur along the Bhagirathi and Bhilangna rivers, thrust zones, faults and the metal roads. The terrain possesses a variety of slopes, ranging from very gentle sloping river terraces to precipitous scarps. The development of slopes largely depends on the rock composition, its structure and the geomorphic processes operating in the region. Soft rocks like slates, phyllites and limestones are susceptible to weathering and are prone to development of variety of slopes. Hard rocks like granite gneisses and quartzites are resistant to erosion and develop steep slopes. In addition to this presence of faults, joint planes, folds etc., also affect the development of slopes.

The Bhagirathi Basin exhibits multicyclic evolution of its landscape. Development of five levels of fluvial terraces in the Bhagirathi valley suggests at least five episodes of regional uplift of valley in the recent geological past. Incised meanders developed at Seansu, Dharasu and Tehri in the zone of North Almora thrust points to rejuvenation and neotectonic activity in the valley.

Spatial analysis around Tehri dam

Spatial analysis in the Tehri dam environs was carried out in an area of about 579 sq. km. The GIS techniques were used for spatial analysis of thematic maps pertaining to lithology, landuse-landcover, slope, elevation and landslides in the environs of Tehri dam. The area statistics of lithounits show that majority of area of Tehri dam and its environs is occupied by Chandpur phyllites (57%). The landuse-landcover around Tehri dam reservoir constitute 47.9% of agricultural land, 7.1% dense forest, 21.2% of open forest and degraded forest (14.1%). Moderately steep slopes (25°-35°) are observed in 57% of the total area surrounding the Tehri dam.

The spatial distribution of landslides over various terrain parameters was calculated to understand the main factors of landsliding. Active (92) and old (69) landslides demarcated in the area occupy 1.6 sq. km and 8.2 sq. km respectively. It is noticed that about 46 active and 8 old landslides will be submerged in the reservoir. Majority of active landslides are located along the drainage channels and roads indicating that the

Fig. 1 (TL) Satellite Image of Tehri dam and its environs
Fig. 2 (TR) Field photograph of Tehri dam
Fig. 3 (BL) Satellite Image of Tehri-Uttarkashi area
Fig. 4 (BR) Landuse-landcover map of the study area

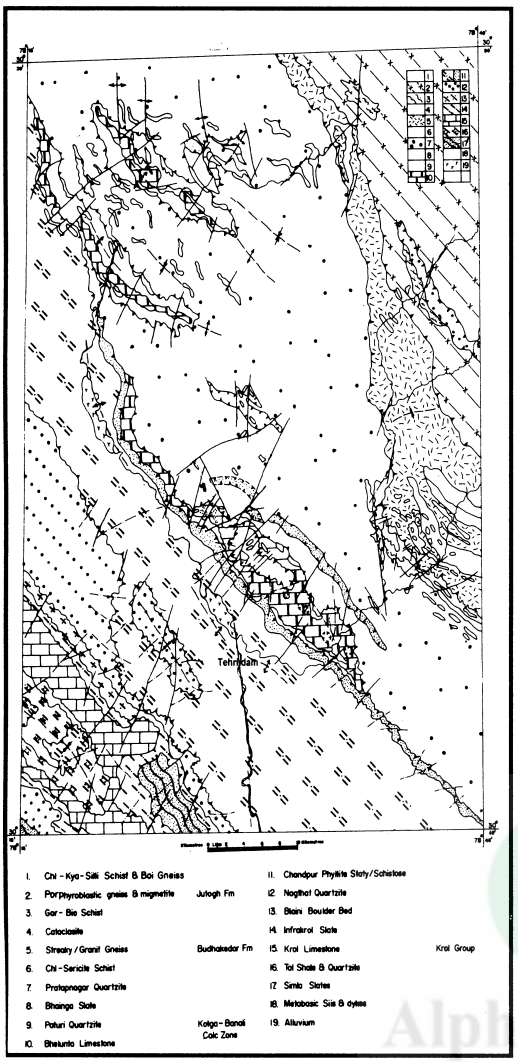

Fig. 5 Geological map of the area

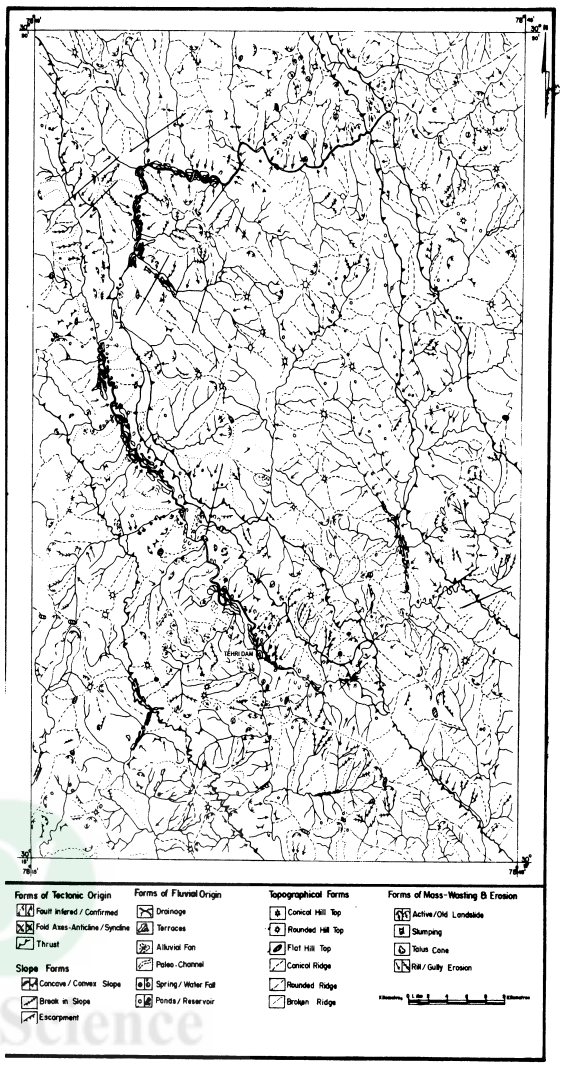

Fig. 6 Geomorphological map of the

dynamic processes of fluvial action and anthropogenic activities related to road and infra-structure development are mainly responsible for landslides in the region. There are 79 landslides on the northern aspect (including 29 old slides). On comparing the landslide occurrence over various landuse categories it is noticed that landslides are maximum in number over agricultural lands (35 active and 40 old landslides). There are 30 active and 11 old slides over the scrubland, 18 active and 9 old slides over degraded forests and 9 of each category over open forests. Landslide occurrence over different slope classes revealed that majority of active (78) and old slides (65) are occurring over 15°- 45° slopes, out of which 38 active and 40 old slides are located between 25°-35°. About 79% of the active landslide areas lie under elevation of 1200m. Majority of old slides are confined between 800-1400m (53%).

Results and Discussion

Land degradation due to landslide leading to subsequent siltation in the reservoir and seismicity of the region are two important factors, which needs due attention and discussion pertaining to feasibility of Tehri dam on geoinenronmental perspectives.

On seismic grounds it is to remark that the Tehri dam site is located in a seismically and tectonically active zone of the Central Himalayas, which have experienced Uttarkashi earthquake (M-6.6, in MCT zone) in 1991 and Chamoli earthquake (M-6.5) in 1999. Earthquake shocks of magnitude 5-6 have been recoded for the Garhwal region in 1809, 1816, 1966, 1967, 1968, 1976, 1979, 1986, 1991, and 1999. Frequent seismic

activity of intensity 3 or less was also recorded near the dam site (Agarwal et al. 1982). In Garhwal Himalayas seismic events with mag. (mb) 4.0 and above are noticed in regions north of Main Central thrust (MCT) and between MCT and the North Almora thrust (Verma et al., 1995). In the investigated area, the North Almora thrust (NAT) is located in the close proximity of Tehri dam (nearly four km.) in addition to the presence of MCT at a distance of about 15 km in Bhilangna valley. Further more, the NAT was affected by three phases of neotectonic activity in the past 11,000 years (Valdiya 1992). This is supported by the occurrence of 5 levels of river terraces near dam site in the vicinity of NAT. Such morphotectonic indicators in a seismically active zone indicate high probability of dam failure. Further filling up of the reservoir in a critically stressed region might induce large rock failures. If such dislocations occur near the dam it would eventually endanger the lives and property of people located at downstream of the Tehri dam in areas mainly Deoprayag, Rishikesh and Hardwar.

On aspect of land degradation in the catchments and subsequent siltation in the reservoir a regional perspective of Bhagirathi basins clearly depict very high rate of land degradation in subsequent years. The Bhagirathi basin with a catchment area of 7511 sq. kms consist of about 2328 sq.kms area under snow cover. The retreat of snout of the Bhagirathi glacier coupled with melting of minor associated glaciers in the region signify heavy mass movement of unconsolidated glacial debris down slope in to the valley to be transported downstream.

In the local perspective it is studied that the Paratapnagar quartzite formation is spread over a large region in the proximity of reservoir. Sediment laden river bringing quartz particles eroded from these quartzitic formation would corrode the steel structures like turbines, spillway & bucket affecting desired utilization of impounded water. Further the Chandpur phyllites, (which are highly sheared in the vicinity of the NAT) cover about 91.5% of the Tehri dam reservoir area. About 52.6% of the area are used for agriculture consist of loose soil which on submergence contribute to siltation. The major landslide zones are located in the upstream of dam site in Bhagirathi and Bhilangna valleys in the zone of MCT. Majority of these landslide zones are active triggering large number of slope failures during rainfall every year causing heavy silt accumulation in the riverbeds. The geoenvironmental analysis using remote sensing and GIS techniques show that 46.12% of the area around Tehri dam is occupied by moderately high to very high landslide hazards. (Pandey et al, 2002). A total of 92 active and 69 old landslides are identified in the vicinity of dam site. Majority of active landslides are located along the drainage channels and roads indicating that the dynamic processes of fluvial action and anthropogenic activities related to road and infrastructure development are mainly responsible for landslide in the region. Thus, the development of 25 km., 44 km. and 25 km. long roads, between Tehri town - New Tehri town, Tehri - Dharasu and Tehri - Ghansyali village, respectively, may further aggravate the problem of land degradation due to removal of material from road sections. These roads are now becoming vulnerable sites for landslide during rainy seasons causing heavy sediment load influx to river basin. The down slope movement of road material is perishing all natural vegetation on these slopes rendering them prone to rapid erosion. There are 46 active and 8 old landslides present in the reservoir area. Due to frequent changes in the reservoir water level the pore pressure can cause more landslides in the region. Submergence of active landslides and about 65 km. of road length will certainly induce new landslide and result heavy influx of sediments to the reservoir. Most of the reservoir area with moderately high to high slopes having active landslides occur in highly sheared Chandpur phyllites. This indicates heavy rate of siltation in the Tehri dam reservoir especially during submergence and heavy rains thus supporting the view of Valdiya (1992) i.e. the filling up of the reservoir can exert weight of about 3 billion tonnes in the area increasing the possibility of reservoir induced seismicity. The destabilization of Tehri town and the surrounding large river terraces after submergence would also contribute large sediment influx in the vicinity of dam. Further more the dynamic water level in the reservoir can promote localized collapse of the already denuded steep valley slopes causing reservoir to silt up rapidly thereby offsetting the anticipated benefits.

CONCLUSION

The Tehri dam is located in a seismically and tectonically active zone of the Central Himalayas, which have experienced Uttarkashi earthquake in 1991 and Chamoli earthquake in 1999. The filling up of the reservoir will exert weight of more than 3 billion tones signifying the possibility of reservoir-induced seismicity in highly sheared and schistose basement rocks of the reservoir. The stability of the dam will be in danger during a major earthquake because deep shear zones are associated with NAT, MCT in addition to shear

zones, which lie in the dam site. The major landslide zones are located in the upstream of dam site in Bhagirathi and Bhilangna valleys in the zone of MCT. Majority of these landslide zones are active triggering large number of slope failures during rainfall every year causing heavy silt accumulation in the riverbeds. There are 46 active and 8 old landslides present in the reservoir area. Due to frequent changes in the reservoir water level the pore pressure can cause more landslides in the region. Most of the reservoir area is covered by Chandpur phyllites are under moderately high-to-high slopes indicating heavy rate of siltation especially after filling up of the reservoir and during heavy rains. Construction of roads for a total length of 95 km has further destabilized the area. Submergence of 46 mapped active landslides and about 65 km. of road length will induce fresh landslides and result heavy influx of sediments to the reservoir. The 9.54% of the area that occur in high and very high landslide zones in the major river channels and on the thrust/ faults demands special geotechnical consideration. Retreat of glacier exposing unconsolidated glacial deposits may induce flash floods due to mass wasting and formation of natural dams in the upper catchment areas. Poor vegetative cover and prolonged denudation of steep slopes would result in rapid soil erosion and accumulation of silt deposits in the reservoir thereby reducing the life of the reservoir

Acknowledgements
Author is thankful to Dr. M.S. Nathawat, Prof. & Head, Department of Remote Sensing BIT, Mesra for critical review, fruitful discussions and permission to present this paper during the seminar.

REFERENCES

Agarwal R.C. and Agarwal P.N. (1982). Proc. 4th Intern. Geog. Eng. Geol., Oxford and IBH, New Delhi, 1982, vol. 8, pp.19-32.

Arya A.C., Joshi Varun, Murthy T.V.R., Narayana A., Saxena K.G., Garg J.K. and A. Naraina (1993). Geoenvironmental study of landslides using remotely sensed and ancillary data in Tehri Reservoir Rim; a case study. Proc. Nat. Symposium on Remote Sensing Applications for Resource Management with Special Emphasis on N.E. region, Guwahati, pp. 23-30.

Bhumbla D.R. et al. (1990). Environmental appraisal of the multipurpose Tehri dam project, Department of Environment, New Delhi (unpublished).

Garg, J.K., Narayan.A, Arya. A.S., Murthy. T.U.R, Narayain.A, Joshi.V and Saxena K.G., (1993). Landslide Hazard Zonation around Tehri Dam using remote Sensing and GIS Techniques (Personal Communication).

Khan, A.A.,Dubey, K.S., Saigal, M.N. and Awasthi, S.C., (1982). Jour. Geol. Soc. India, vol. 23, pp. 392-401.

Mazari, R.K. (1981). A preliminary report on the geomorphological observations of a part of Bhagirathi Catchment, Higher Garhwal Himalaya, based on photo interpretation without ground checks, Mimen pp.1-19.

Mehrotra, G.S. Dharmaraju, R. And Prakash,S. (1993). Landslide zonation and geo-environmental Appraisal of a part of Garhwal Himalaya, India. Proc. of Seventh Int. Conf. And field workshop on landslides, Czech and Slovak, pp. 103-110.

Pachauri A.K., Gupta P.V., Chander R. (1998). Landslide zoning in a part of the Garhwal Himalayas.Environmental Geology vol. 36 (3-4), Dec. 1998 pp. 325-334.

Pandey A.C., Chandra S. Dubey and Saklani, P.S. (2002). Geoenvironmental Factors of the Tehri Dam Reservoir Rim: Aspects on Terrain Evaluation. Published in Journal of Asian Earth Science, Vol. 20, No. 4A, April 2002.

Saklani, P.S., (1993). Geology of the lower Himalaya (garhwal). Intl. Books and Periodicals Supply Services New Delhi, p.-239.

Valdiya, K.S. (1992). Must we have high dam in the geodynamically active Himalayan domain ? Current Science, vol. 63, No.6, 25 Sept., pp. 289-296.

Verma R.K., Roonwal G.S., Kamble V.P., Dutta D, Kumar N., Gupta Y and Sood S (1995). Seimicity of Northwestern part of Himalayan arc, Delhi Hardwar Ridge and Garhwal –Kumaon Himalaya Region: a Synthesis of existing data. Uttarkashi Earthquake, Memoir 30, Geological Society of India, Bangalore, 1995.

Disaster Management
Editors: N.C. Mahanti et al.

A Study of Vorticity and Divergence Fileds in an Unusually Developed Tropical Cyclonic Storm Over the Bay of Bangal During 19-26 September 1997

G.R. Chinthalu, P. Seetaramayya and S.G. Nagar

Indian Institute of Tropical Meteorology Pashan Pune-411 008, India

Abstract

In the present study an attempt has been made to understand the distribution of vorticity and divergence fields in monsoon depression, which has unusually developed and transformed subsequently into a severe cyclonic storm during the period 19-26 September 1997 over the western Bay of Bengal with its centre at 15° N, 84°E on 23 September. For this purpose charts of daily vorticity and divergence fields at 850, 700 and 500 hPa level, are prepared using NCEP reanalysis wind data. INSAT ID satellite imageries are used to identify the areas of cloud cover with respect to the vorticity field at 850 hPa. These charts have revealed that there exists a closed concentric positive vorticity (ζ=2•10^{-5} s^{-1}) centered at 17°N, 83.5°E, very close to Visakhapatanam coast on 19 September, with two cells of negative vorticity over southern Bangla Desh coast (ζ = -1.5•10^{-5} s^{-1}) and off shri Lanka (ζ= -5•10^{-5} s^{-1}). This positive vorticity cell (ζ =2.5•10^{-5} s^{-1}) has moved subsequently southeastward and lay over western Bay of Bengal at 15°N, 84° E on 20 September. Having concentrated at the same point, it has increased to two fold (ζ= 4 •10^{-5} s^{-1}) on 21 September even more (ζ =5 •10^{-5} s^{-1}) on 22 September and subsequently developed into stronger vorticity (ζ= 6•10^{-5} s^{-1}) on 23 September. The India Meteorological Department (IMD), New Delhi, has declared the evolving system as a depression on 23 September 03 UTC.

A close examination of divergence field reveals that on 19 September, the area of convergence lies over area of positive vorticity. When the system developed into deep depression, this area shifts eastward of the centre of maximum vorticity. Similar circulation patterns are observed at 700 and 500 hPa.

Key words: vorticity, divergence, cyclonic storm, INSAT-ID, Bay of Bengal.

Introduction

In the earlier studies to understand the synoptic circulations over the Bay of Bengal limited data from coastal stations, ships and some radiosonde observations was available to the meteorologist. However, due to the availability of NCEP reanalysis wind data, it is now possible to study weather systems in greater details. Chhabra (1982) emphasized that the atmosphere is dominated by cyclones and anticyclones which are important features of large-scale atmospheric flow. The cyclones are characterized by positive vorticity with convergence in the lower and middle troposphere and negative vorticity with divergence in the upper troposphere. The relative intensity of lower level convergence and upper level divergence or lower level positive vorticity and upper level negative vorticity generally provides a measure for the intensity of cyclonic system. The synoptic forecaster, in the absence of any quantitative estimates of divergence or vorticity, looks for position of troughs and ridges, velocity gradients along the flow etc, to assess the vorticity and divergence in a rather subjective way. These observations provide vital information in the decision making process of the forecaster. Riehl (1948) suggested two criteria for the formation of a cyclonic storm i.e. a pre-existing low level disturbance and a region of upper level divergence or outflow above the surface disturbance. According to Koteswaram and George (1958) cyclonic development at sea level in the Bay of Bengal, occurs when and where an area of positive vorticity advection in the upper troposphere becomes superimposed upon a pre-existing trough at sea level. Koteswaram (1960) and George (1970) observed that given a pre-existing lower tropospheric feature causing convergence at sea levels along and near the Kerala coast, upper level divergence in the western portion of an advancing trough in the

easterlies or the left exit portion of an accelerating easterly wind maximum in the upper levels usually precedes and causes the onset of the monsoon over the Kerala coast.

The above observations, however, had the limitation of availability of the network of observation over land stations only and lack of upper air observations, over sea. Sarker (1988) have stated that depressions seldom acquire hurricane intensity presumably because of (i) presence of vertical wind shear and (ii) short travel over the ocean surface in the Bay of Bengal. Nevertheless, depressions have a high probability of intensification during September when the vertical wind shear slackens. Further, because of high potential in producing widespread heavy rainfall, the monsoon depressions have attracted the attention of Indian meteorologist for nearly a century ago. Despite a number of studies undertaken on monsoon depressions, the present state of knowledge is still inadequate. A clear understanding of the three dimensional structure of the depressions is yet to emerge due to lack of observational data and absence of the precise description of the disturbance while they are over the oceanic areas.

A monsoon depression has developed unusually and subsequently transformed into a cyclonic storm in the Bay of Bengal very close to the Andhra coast near Kakinada during 23-26 September 1997. In general it is observed that depressions, which formed in the Bay of Bengal, have a short travel of systems over the ocean (Sarker 1988). However, the system, which we have examined in the present study has traveled a long distance over Bay of Bengal parallel to the east coast of India The vorticity and divergence fields at 850, 700 and 500 hPa levels are examined to understand the areas of convergence and divergence.

Materials and methods

The NCEP reanalysis wind data for the period 19-26 September 1997 is extracted from the National Centre for Environmental Prediction web site. The daily 00UTC zonal (u) and meridional (v) components at 850, 700 and 500 hPa level have been utilized to estimate the vorticity (ζ) and divergence (D) fields with standard formulae as

$$D = \frac{\partial u}{\partial x} + \frac{\partial v}{\partial y} \quad \text{and} \quad \zeta = \frac{\partial v}{\partial x} - \frac{\partial u}{\partial y}$$

Finite difference method for a grid dimension of 2.5° x 2.5° is used for computation. Further INSAT ID satellite imagery and rainfall distribution along the Andhra coast are utilized to understand the flow patterns during the initial, developing and mature stages of cyclonic storm.

Prevailing synoptic weather conditions

Figure 1 shows the track of the monsoon depression along the east coast of India. The time and intensity of the depression are given by various symbols i.e. circle for 00 UTC, circle with a dot inside position at 03 UTC, bold circle position at 12 UTC and half bold circle position at 18 UTC. The symbols D, DD, CS, SCS show different stages of intensity of depression viz depression, deep depression, cyclonic storm and severe cyclonic storm respectively. The above system has initially been detected with the help of INSAT-I D imagery (figure 2a) and surface meteorological observations from coastal stations vide Table 1. The observations from CDR (cyclone detection radar) Visakhapatanam helped in fixing the position of the system. The CDR Khepuara has tracked the system from 18 UTC of 26 September when the system has come close to the coastal station. IMD has reiterated that this system is one of the rare depression which has come under the surveillance of all radars except CDR Karikal as it moved along the east coast of India. These observations have provided more realistic estimates of centre and intensity of the system. Table 2 gives the amount of rainfall for 24 and 25 September (when the system was intense) for some stations along the east coast of India the highest rainfall of 21 cm was observed at Bapitala on 24 September and of 40 cm at Kakinada on 25 September. The remaining stations have received rainfall between 12 and 21 cms. Figure 2(a-d) shows the INSAT I D imagery during evolutionary stages of the depression from 23-26 September 1997. Figure 2a clearly depicts an incipient development of the depression on the northern flank of maximum cloud zone (MCZ) with its centre close to south Andhra coast. The axis of the MCZ is running

eastwest along 13°N in southern Bay of Bengal. This MCZ has splitted into two prominent bands one close to Andhra coast and second lies over the Andaman sea separated by a cloud free zone in between them on 24 September 1997 (Fig 2b). The circular curvature of the cloud bands near the coast indicates that the system has developed into a tropical cyclone. Fig. 2c shows the cloud imagery on 25 September. It is clearly seen that thick convective clouds are concentrated over the Andhra coast resulting in heavy rainfall over some of the coastal stations, vide Table 2 (12 cm Ongole on 24 September; Bapattla 21 cm; Rajamundry 12 cm and Kakinada 40 cm on 25 September). The convective cloud mass over Andhra coast has dissipated on 26 September (Fig. 2d) while another cloud band which lay over Andaman sea has moved towards Orissa coast close to Head Bay region.

Results

Vorticity at 850,700 and 500 hPa

Figure 3(a-h) shows the vorticity fields at 850 hPa for the period 19-26 September 1997. Close examination of Fig. 3a reveals that there exists a well-organized closed concentric cyclonic ($\zeta > 0$) vorticity cell ($\zeta > 2.5*10^{-5}$) centered at 17°N, 83.5°E, very close to the Andhra coast near Vishakhapatanam. Two distinct cells of anticyclonic vorticity ($\zeta < 0$) are seen over southern Bangla Desh ($\zeta = -1.5*10^{-5}\ s^{-1}$) and off shri Lanka ($\zeta = 5*10^{-6}\ s^{-1}$). The cell of positive cyclonic vorticity cell has subsequently moved southeastward over western Bay of Bengal with centre at 15°N,84°E, on 20 September (Fig. 3b) the intensity has increased two fold ($\zeta = 4*10^{-5}\ s^{-1}$). It has further intensified on 21 September (Fig.3c) ($\zeta = 5*10^{-5}\ s^{-1}$) and on 22 September (Fig 3d) at the same location. within 24 hours from the previous day even more ($\zeta = 5*10^{-5}\ s^{-1}$). On 23 September (Fig. 3e) when the evolutionary system is in the stage of depression the areal extent of cyclonic vorticity has increased with a maxima of ($6*10^{-5}\ s^{-1}$) at the centre 16°N, 85° E. The system has further intensified in to cyclonic storm on 24 & 25 September with maximum vorticity^{y} ($\zeta = 6*10^{-5}\ s^{-1}$) and ($\zeta = 7*10^{-5}\ s^{-1}$) at its centre (Fig.3f,3g) From (Fig. 3f) it is seen the zone of maximum vorticity lay 16.5°N, 85°E, ($\zeta = 6*10^{-5}\ s^{-1}$) negative vorticity is noted near 15°N, 92°E, heavy rainfall was recorded at Kakinada about 40 cm in 24 hours vide Table-2, this shows the system has intensified rapidly and produced wide spread heavy rainfall along the Andhra coast. Further from (Fig. 3g) it is further seen that the zone of maximum positive vorticity lay 16°N,85°E ($\zeta = 7*10^{-5}\ s^{-1}$) and negative vorticity is located near Burma coast 16°N, 94°E, ($\zeta = -2*10^{-5}\ s^{-1}$). It is seen from (Fig. 3h) the zone of maximum vorticity has shifted northeastward with its centre at 19°N, 89°E ($\zeta = 7*10^{-5}\ s^{-1}$) the negative vorticity can be seen near 11°N, 93°E, ($\zeta = -4*10^{-5}\ s^{-1}$).

Figure 4(a-h) shows the vorticity fields at 700 hPa for the period 19-26 September 1997. It is seen from (Fig. 4a) the two zones of cyclonic vorticity one along the Andhra coast near 16.0°N, 82.5 ($\zeta = 1*10^{-5}\ s^{-1}$) and the other at 17°N, 92°E, ($\zeta = 2*10^{-5}\ s^{-1}$) are separated by a col region. The zone over Andhra coast has shifted eastward from Fig. 4b it is seen that the vorticity field has intensified and developed into well organized concentric cell with its centre, at 15°N,84°E, ($\zeta = 2*10^{-5}\ s^{-1}$). A remarkable intensification in the vorticity field almost two fold in the same location Fig. 4c with close concentric cells around 14°N, 85°E, ($\zeta = 4*10^{-5}\ s^{-1}$) is observed on 21 September. It has further intensified and moved northnortheastward with its centre near Machlipatanam 16°N, 84.2°E, ($\zeta = 5*10^{-5}\ s^{-1}$). It is seen that this cyclonic cell has moved close to the Andhra coast near Kakinada. On 23, 24 and 25 September (fig.4e, 4f, and 4g) with highest values of ($\zeta = 7*10^{-5}\ s^{-1}$) 16.5°N,86°E, this high value tend to decrease from the region of vorticity maxima. From figure 4f one can see the zone of maximum vorticity ($\zeta = 6*10^{-5}\ s^{-1}$) lay at, 16.5°N, 82.7°E, near the Andhra coast. Anticyclonic circulation with negative vorticity lay over south east Bay of Bangal hereafter (BOB) , 10°N, 92°E, , ($\zeta = -2*10^{-5}\ s^{-1}$). which has moved and lay over southeast Bay ($\zeta = -2*10^{-5}\ s^{-1}$), 10°N, 92°E. From (Fig. 4h) it is seen that the zone of positive vorticity has moved rapidly northnortheast ward with its centre at 19°N, 89°E, ($\zeta = 6*10^{-5}\ s^{-1}$). The anticyclonic cell lay over central BOB, extending up to southeast Bay, ($\zeta = -2*10^{-5}\ s^{-1}$).

Figure 5(a-h) shows the vorticity field at 500 hPa during 19-26 September 1997. Figure 5a shows the cell of maximum vorticity has centre at 15°N, 83°E, ($\zeta = 1.5*10^{-5}\ s^{-1}$), close to Andhra coast. It is seen from that the vorticity has increased two fold ($\zeta = 2.5*10^{-5}\ s^{-1}$) at 14°N, 83°E (Fig. 5b). From (Fig. 5c) it is seen that the vorticity has maintained the same rate of intensification ($\zeta = 4*10^{-5}\ s^{-1}$) and lay near 13°N, 83°E, on 21 September. On 22 September ($\zeta = 5*10^{-5}\ s^{-1}$) and lay at 12.5°N, 82.5°E. This vorticity field has concentrated in the same place (14°N,83°E) and further increased to ($\zeta = 6*10^{-5}\ s^{-1}$) on 23 September. (Fig.

5f & 5g) depicts the zone of positive vorticity ($\zeta = 6*10^{-5}\ s^{-1}$) has moved in a northnortheasterly direction centre at 16°N, 83°E, on 25 September. It continue to move in a northnortheasterly direction, and lay at 17°N, 84°E. On 25 September and has the same intensity. While moving northeastward on 26 September (Fig. 5h) with centre at 19°N, 88°E, its intensity reduces to ($\zeta = 4*10^{-5}\ s^{-1}$) . Anticyclonic vorticity is seen to developing over the region south of 8°N between 78°E and 98°E from 20 September. It has intensified and concentrated with its centre at 10°N, 92°E, ($\zeta = -\ 5*10^{-5}\ s^{-1}$) on 24 September, it further elongated southwest-northeast ward and weakened ($\zeta = -4*10^{-5}\ s^{-1}$) on 25 and 26 September (Fig. 5g & 5h).

Divergence at 850, 700 and 500 hPa

Figure 6(a-h) shows the divergence field at 850 hPa, from 19-26 September 1997. From (Fig. 6a) it is seen that the area of maximum convergence ($D = -8*10^{-6}\ s^{-1}$) lies over central BOB with its centre 15°N,87°E, on 19 September. It has further intensified ($D= -1*10^{-5}\ s^{-1}$) and has a NW-SE orientation on 20 September (Fig. 6b). Further from (Fig. 6c) it is seen that the area of convergence has moved in north northeasterly direction, located over the head bay region 20°N, 88°, ($D = -5*10^{-5}\ s^{-1}$). On 21 September (Fig.6d) depicts a closed cell of convergence extending from 15-20°N,82-84°E, ($D = -6*10^{-6}\ s^{-1}$). On 22 September further intensified along Andhra coast near 14°N, 80°E (Fig 6c) . Another cell of strong convergence ($D= -1.4*10^{-5}$) off Burma coast on 22 September (Fig.6d) has moved northward and is seen with its centre at 20°N, 93°E.. It has intensified ($D = -8*10^{-6}\ s^{-1}$) on 23 September lay along Andhra coast near 14°N, 80°E (Fig. 6e). Further it has intensified ($D = -4*10^{-6}\ s^{-1}$) on 24 September (Fig. 6f) lay near Ongale 14°N, 80°E on 24 September another cell of convergence is seen off shri lanka coast near (9.5°N,85°E). It seen from (Fig. 6g) two distinct cells of maximum divergence lay near Machlipatinam 16°N, 79°E, ($D = 4*10^{-6}\ s^{-1}$) in the central BOB with its centre at 11°N, 88°E, ($D = 4*10^{-6}\ s^{-1}$) separated by an area of convergence ($D = -4*10^{-6}\ s^{-1}$) over central BOB, which intensified ($D = -\ 8*10^{-6}\ s^{-1}$) further and moved northward (Fig. 6h).

Figure 7(a-h) shows the distribution of the divergence field at 700 hPa during 19-26 September 1997. The area of positive divergence ($D = 4*10^{-6}\ s^{-1}$) over BOB with centre at 10°N, 86°E, it is clearly seen on 19 September (Fig. 7a). The area of convergence is seen over Burma coast ($D= -5*10^{-6}\ s^{-1}$). The area of divergence has further intensified $D = -\ 1*10^{-5}\ s^{-1}$ with slight northward movement. The cell of convergence over east coast of India and (Burma coast) has moved northward (southward) and intensified to ($D = -\ 8*10^{-6}\ s^{-1}$) , ($D = -\ 1*10^{-5}\ s^{-1}$) with centre at 11°N, 80°E, (17°N,92°E) on 20 September (Fig. 7b).

From (Fig. 7c) it seen that the positive divergence field has moved northeastward and well organized into compact concentric isolines, along the east coast of India and central Bay of Bengal (BOB), ($D=6*10^{-5}\ s^{-1}$) and the cell of convergence over Burma coast has shifted southeastward on 21 September. It has splitted in to two cells on 22 September (Fig.7d) one over 20°N, 90°E, and the other more intense ($D = -1.2*10^{-5}$) over 11°N, 93°E. The areal extent and intensity of divergence has reduced to ($D=4*10^{-5}\ s^{-1}$). Another area of convergence is seen developing over east coast of India which has intensified ($D= -7*10^{-5}\ s^{-1}$) on 23 September (Fig.7e). The area of divergence has almost disappeared with a small patch observed between south of 80°N, between 84°E, and 94°E on 24 September (Fig.7f). The area of convergence along east coast of India is replaced by divergence field ($D= -1*10^{-5}\ s^{-1}$) 12°N, 84°E, which has moved westward on 25 September (Fig. 7g). At the same time the area of convergence over Orissa coast has shifted southward ($D= -6*10^{-5}s^{-1}$) at 15°N,93°E. It has further intensified into ($D= -2*10^{-6}\ s^{-1}$) at 15°N, 93°E on 26 September (Fig.7h), the divergent area has spread over BOB near Andhra coast .

Figure 8(a-h) shows the divergence field at 500 hPa during 19-26 September 1997. It is seen from (Fig.8a) that the east coast of India is under the influence of strong convergence at 13°N, 83°E ($D= -6*10^{-6}s^{-1}$) on 19 September. The intensity of convergence increases to ($D=1*10^{-5}\ s^{-1}$) at 10°N, 82°E on 20 September (Fig. 8b). A zone of divergence ($D= 5*10^{-6}s^{-1}$), 11°N, 90°E, which has shifted northward at 15°N, 92°E, on 21 September (Fig.8c). At the same time the area of convergence has shifted eastward over BOB.

Further from (Fig. 8d) it is noticed that on 22 September the field of convergence is well organized in to more compact concentric isolines along the east coast of India with maxima ($D= -1*10^{-5}\ s^{-1}$), centered 16°N,81°E, the area of divergence field tends to move in the north northeasterly direction. The most part of BOB is dominated by convergence ($D= -8*10^{-6}s^{-1}$) on 23 September with centre at 16°N, 82°E, (Fig.8e). It is interesting to note the sudden change in the area of convergence over BOB on 24 September

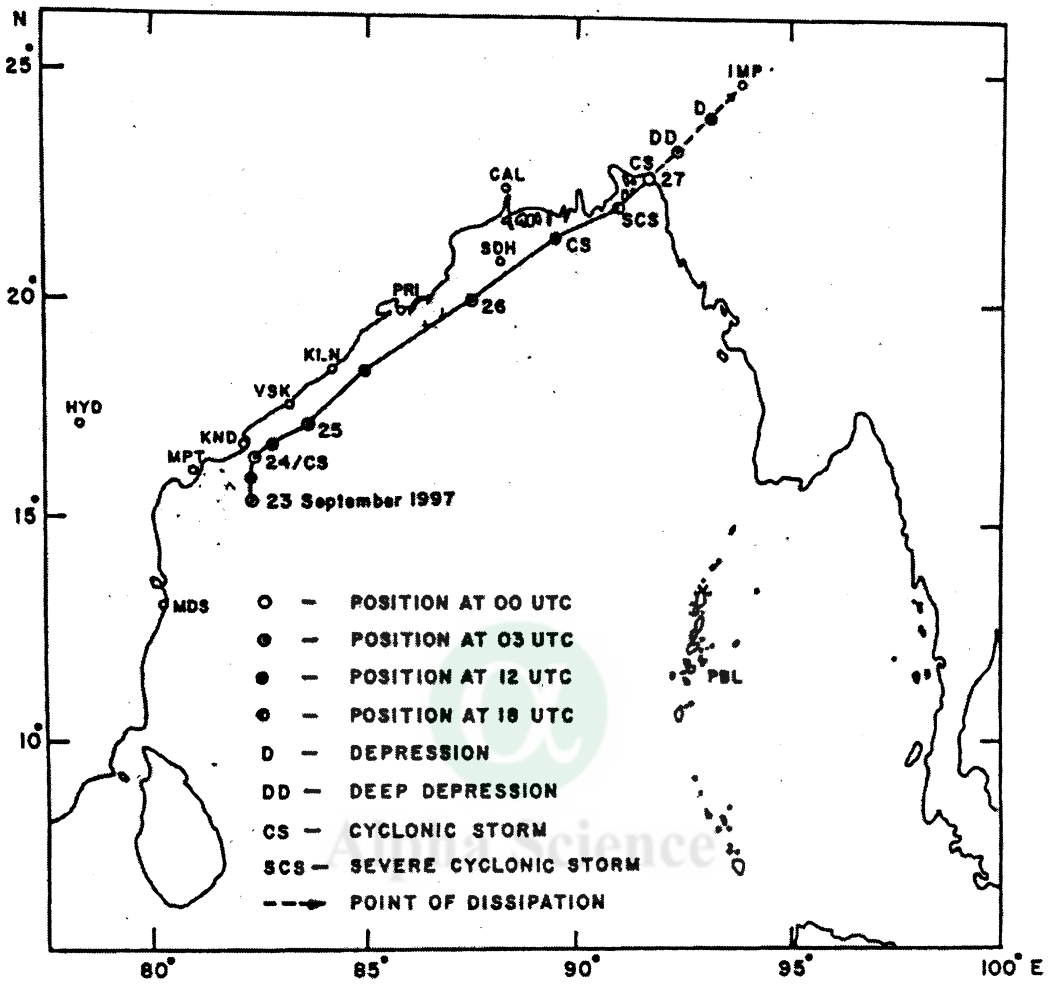

Figure 1: The track of the cyclonic storm during 23-27 September 1997.

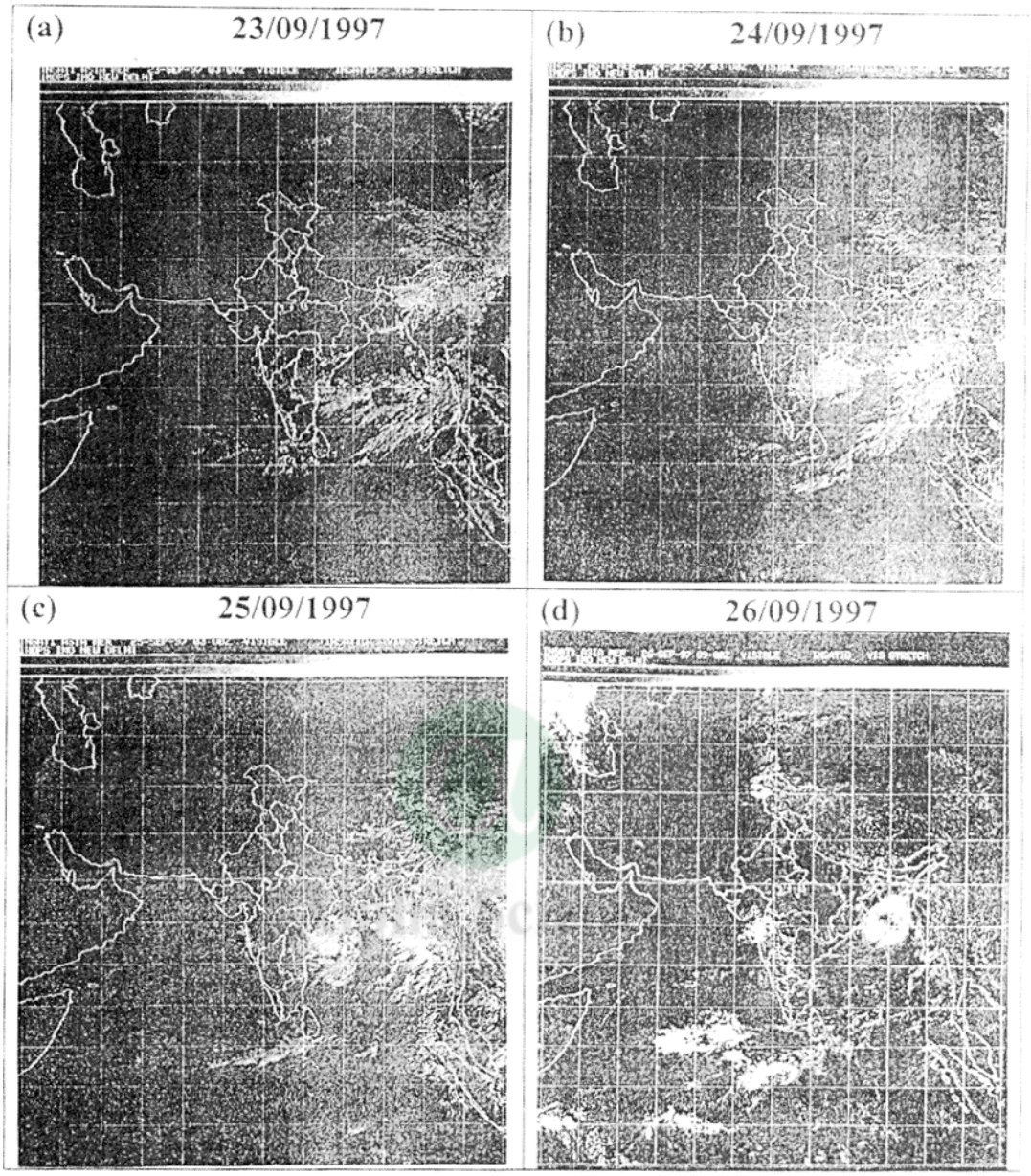

Figure 2: (a-d) INSAT 1 D imagery during active phase of the cyclonic storm (23-26 September 1997).

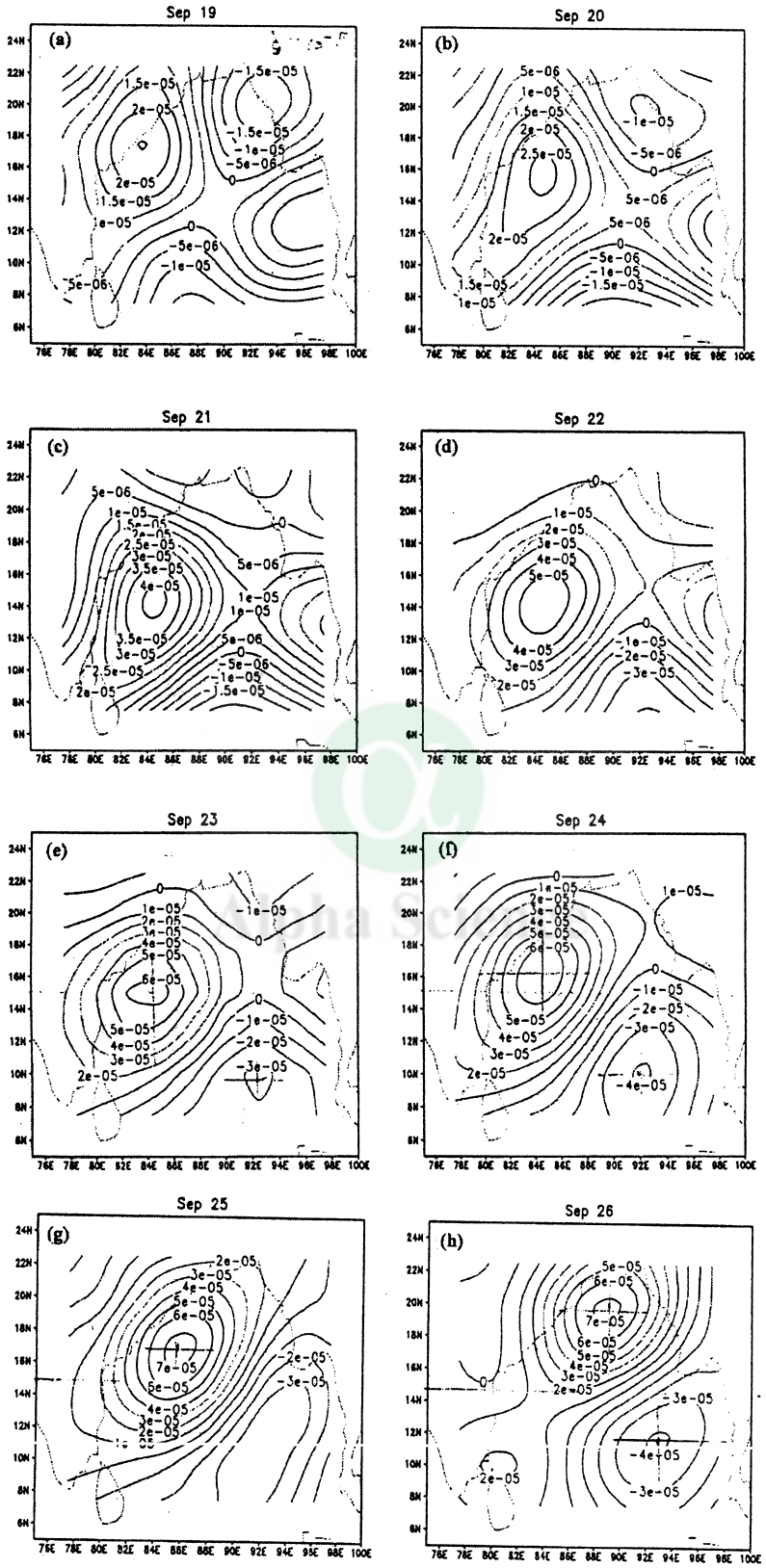

Figure 3: (a-h) Vorticity at 850 hPa.

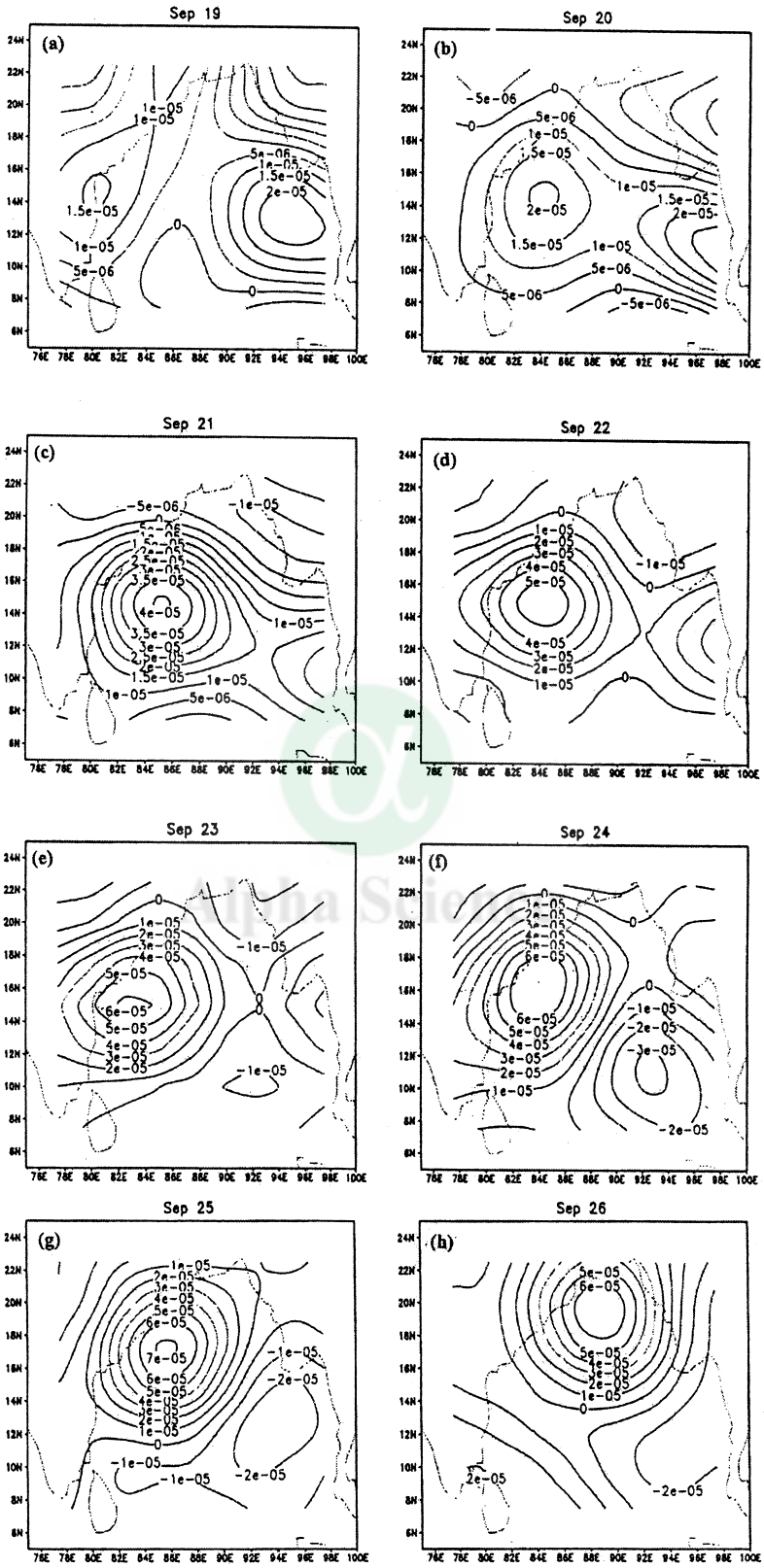

Figure 4: (a-h) same as figure 3 but for 700 hPa.

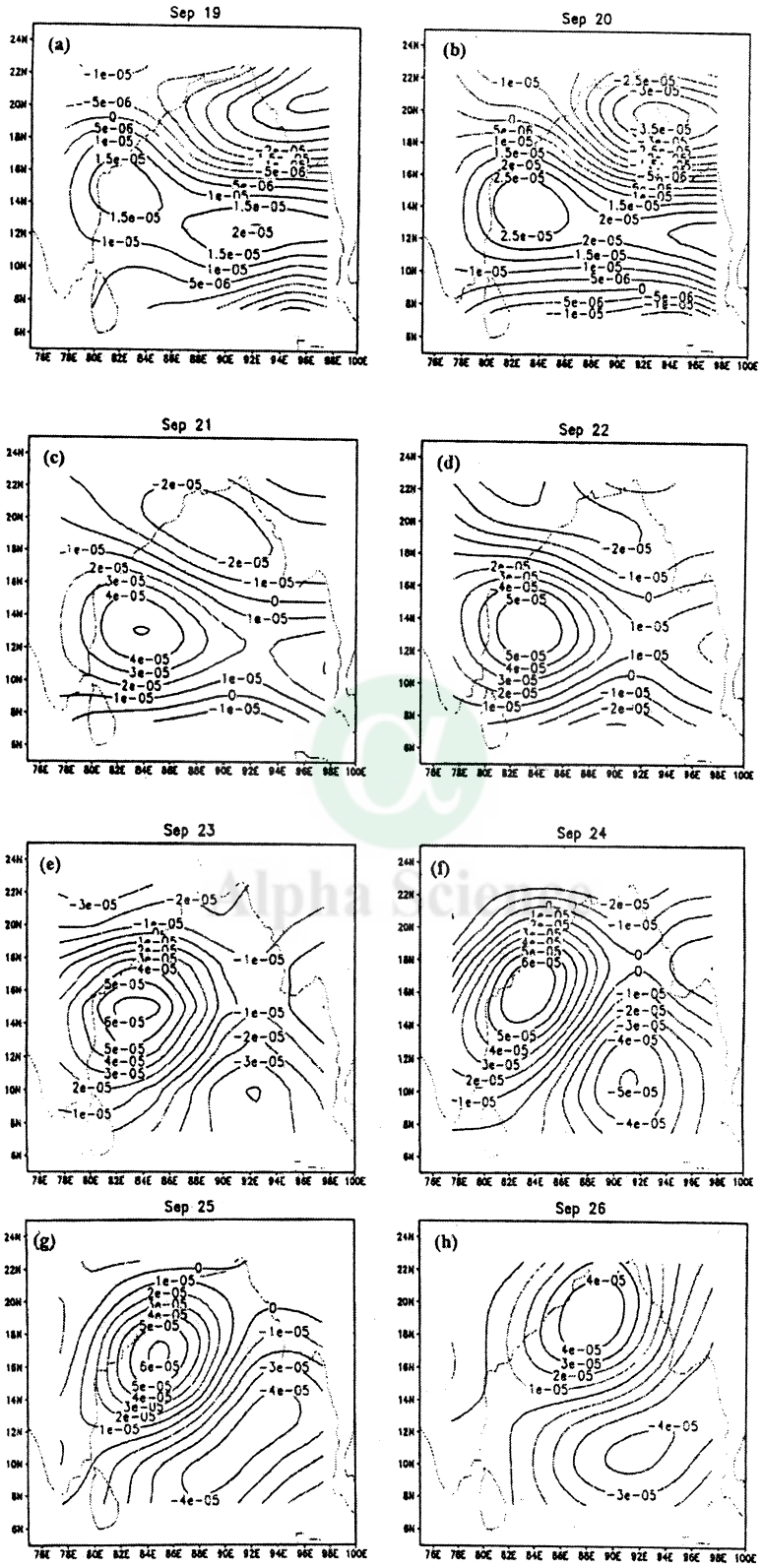

Figure 5: (a-h) same as figure 3 but for 500 hPa.

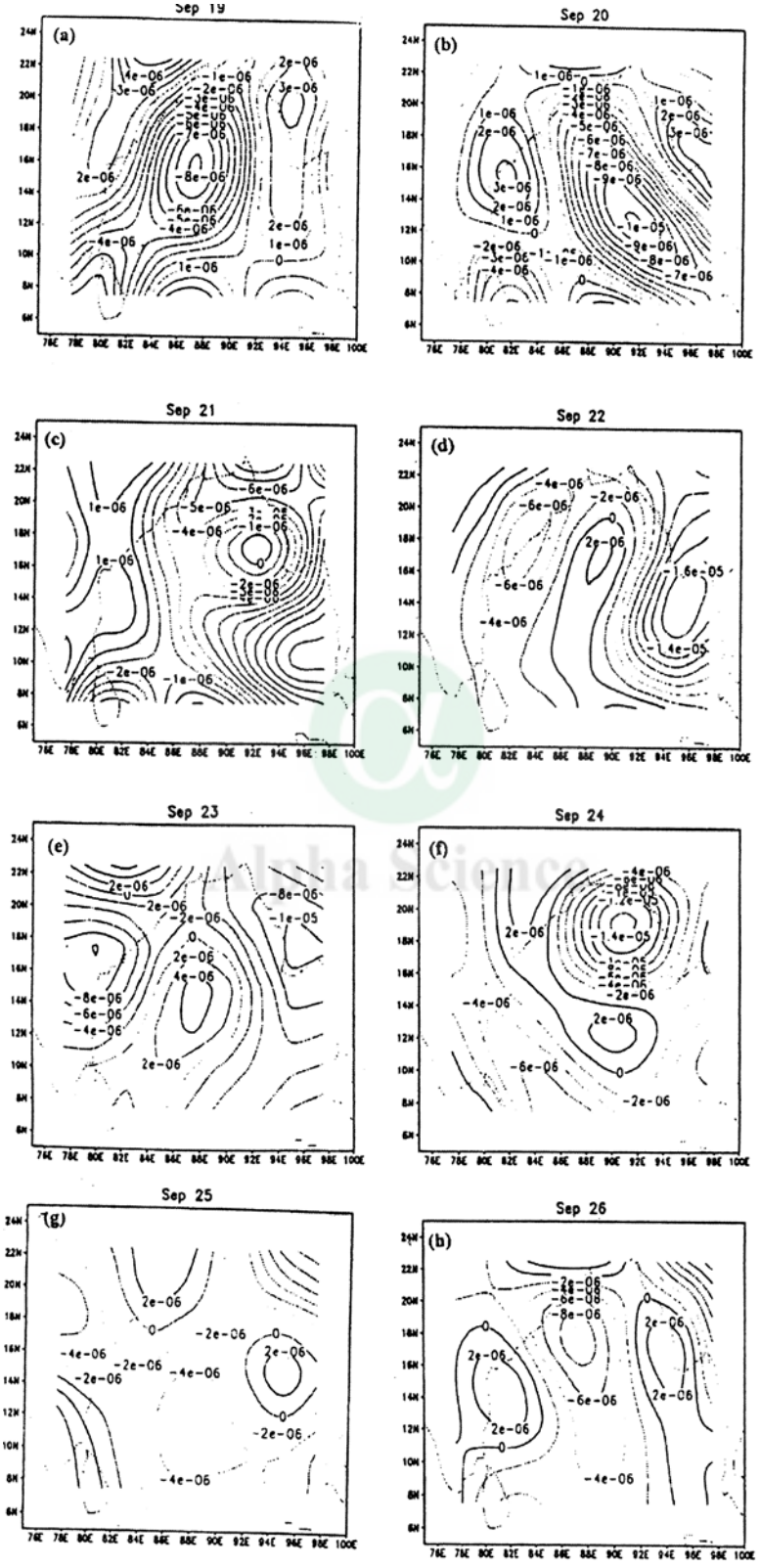

Figure 6: (a-h) Divergence at 850 hPa.

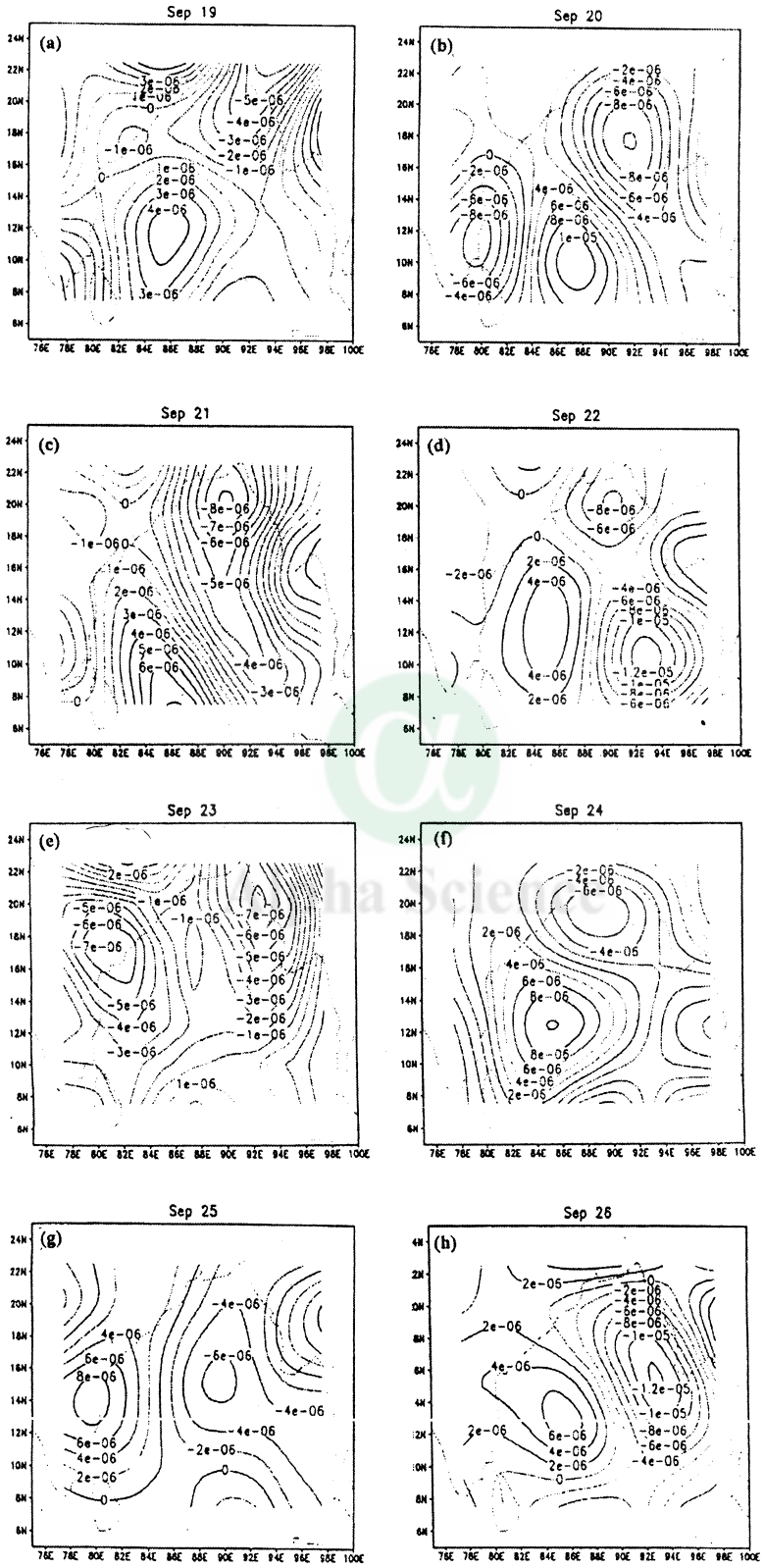

Figure 7: (a-h) same as figure 6 but for 700 hPa.

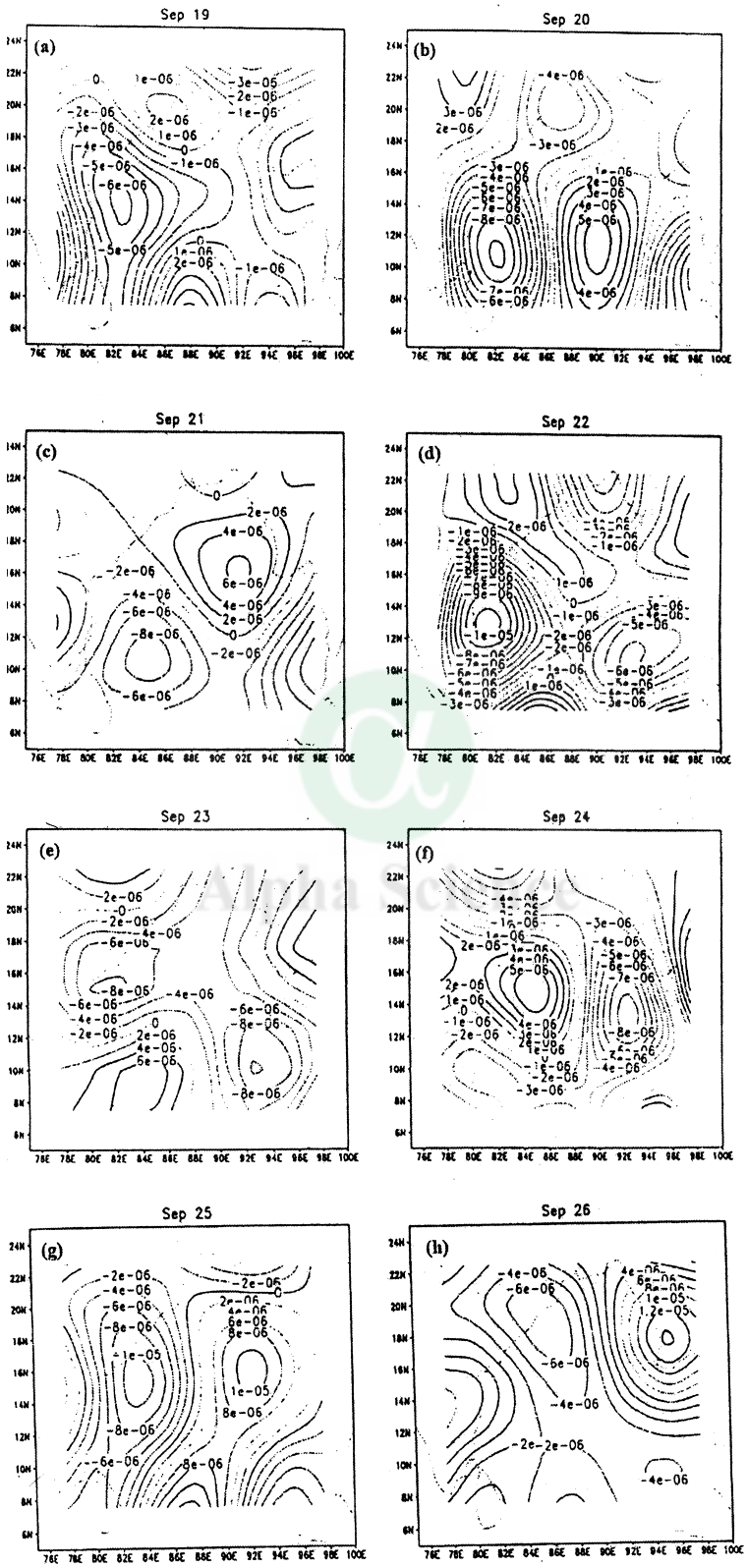

Figure 8: (a-h) same as figure 6 but for 500 hPa.

Table 1
Surface observations during 23-26 September 1997, along east coast of India
Pressure, temperature, wind and cloud amount

Date September 1997	Time UTC	Station	Pressure	Air Temp. (°C)	dd (Deg.)	ff (Knots)	Cloud amount (Oktas)
23	1200	MDR	1004.3	29.6	00	00	7
	1200	VSK	1003.6	30.0	210	14	6
	1200	MPT	1002.3	27.8	320	05	8
	1200	PRI	1005.4	30.4	290	04	5
	0300	SDH	1000.0	29.4	180	03	5
24	1200	MDR	1004.4	32.0	00	00	7
	1200	VSK	1003.1	27.2	100	03	6
	1200	MPT	1001.0	26.2	320	06	8
	1200	PRI	1005.4	31.0	110	05	6
	1200	SDH	1007.0	30.6	140	12	3
25	1200	MDR	1004.4	32.0	230	05	7
	1200	VSK	1003.1	25.0	190	16	5
	1200	MPT	1000.1	26.4	290	06	8
	1200	PRI	1003.5	29.6	105	03	7
	1200	SDH	1004.3	30.4	140	12	5
26	1200	MDR	1005.3	33.6	270	01	7
	1200	VSK	999.9	26.0	100	03	8
	1200	MPT	1002.6	29.4	00	00	8
	1200	PRI	1000.1	27.2	120	04	8
	0300	SDH	1001.1	25.6	110	27	8

MDR (Madras), VSK (Vishakhapatanam) MTP (Machilipatnam), PRI (Puri), SDH (Sand head)

Table 1 Daily rainfall along coastal Andhra Pradesh

Rainfall along coastal Andhra Pradesh during September 1997

Lat.°N, Lon.°E	Stations	Rainfall (cm)	Date
15 54 80 28	Bapatla	21	24
16 02 80 55	Avanigadda	20	24
1614 8039	Tenali	15	24
1634 8200	Amlapuram	14	24
1602 8051	Repali	13	24
1611 8108	Machilipatnam	13	24
1534 8003	Ongole	12	24
1602 7918	Yerraguntapam	12	24
1657 8214	Kakinada	40	25
1600 8100	Koderu	18	25
1721 8233	Tuni	17	25
1705 8208	Peddapuram	17	25
1750 8250	Chodavaram	16	25
1700 8146	Rajamundry	12	25

Table 2 Surface meteorological observations along east coast of India

Table 3
Track of Bay of Bengal cyclonic storm 23-26 September 1997 and computed daily (00 UTC) divergence and vorticity

Date Sep. / Time (UTC)	LAT °N	LON °E	INTEN -SITY	T.NO	Surf. P hPa	MAX WIN (Kt)	DIV*10^{-6} s^{-1}			VOR*10^{-6} s^{-1}		
							DIV 850	DIV 700	DIV 500	VOR 850	VOR 700	VOR 500
23 (03)	16.0	82.5	DD	2.0	998	30	-8	-7	-8	5	6	6
24 (03)	16.5	82.7	CS	2.5	998	35	-2	2	3	6	6	6
25 (03)	18.0	84.5	CS	2.5	994	35	-4	4	-8	7	7	5
26 (09)	20.5	88.5	CS	2.5	992	40	7	-2	-2	7	5	4

Table 3 daily 00UCT computed Vorticity and Divergence along the cyclone track at 850,700, 500 hPa

(Fig. 8f), this area is replaced by a stronger divergence (D= $5*10^{-6}s^{-1}$), now lies at 13°N, 92°E, the divergent area has further shifted north northeast ward with intensity (D= $1*10^{-5}s^{-1}$), at 15°N, 92°E on 25 September (Fig.8g) (D= $1.4*10^{-5}s^{-1}$), at 18°N, 93°E, on 26 September (Fig.8h). The intensity of convergence has reduced from (D= $1*10^{-5}s^{-1}$), on 25 September to (D= $-6*10^{-6}s^{-1}$), on 26 September.

Discussion of results

This study highlights the day to day variability of vorticity and divergence fields at 850, 700 and 500 hPa during the life period 19-26 September 1997 of a monsoon depression which subsequently intensified into a severe cyclonic storm in the Bay of Bengal. The track of the cyclonic storm (Fig. 1) shows the day to day movement of the system, the corresponding changes in the vorticity and divergence are seen in (Figures 3-8), which shows the broad circulation patterns that prevailed during the initial and mature stages voricity varied between (ζ = 4 to $7*10^{-6}$ s^{-1}) and divergence varied between (D=-2 to $-8*10^{-5}$ s^{-1}). The INSAT 1D satellite imagery (Fig. 2a-d) shows the corresponding changes in the cloudiness and cloud free zones, which is in close agreement with the computed vorticity and divergence fields. Warner (1984) using Summer Monex air-craft flight level dropsonde data, examined the central core structure of mature Bay of Bengal monsoon depression, has reported at 945 hPa convergence reaching ~ - $2*10^{-4}$ s^{-1} was found in areas of order 300 Km^2 to the south west of the depression centre and divergence and subsidence of roughly similar in magnitude. It is observed that our results are fairly comparable with those reported by Warner.

Further Table 1 shows the surface meteorological observations along the east coast of India, it is seen from this table Visakhapatanam recorded a drastic fall in Air temperature from 30.0 to 25.0 °C, a fall of 5°C within two days between 23-25 September , the maximum wind speed was 16 knots, the lowest pressure was 999.9 hPa , cloud amount varied between 6-8 Oktas these changes are concurrent with the intense active phase of the cyclonic storm. Table 2 shows heavy rainfall recorded at the coastal stations along Andhra Pradesh coast, Bapatla received 21 (cm) on 24 September, and Kakinada received 40 (cm) on 25 September. Table 3 shows the daily 00UCT computed Vorticity and Divergence along the cyclone track at 850,700, 500 hPa The analysis of surface meteorological parameters, upper air wind data and INSAT1D imagery is useful in better understanding the synoptic scale circulations, which can help the synoptic forecaster in improved weather predictions.

Conclusions

Vorticity, Divergence, associated cloud cover and rainfall of a cyclonic storm of 23-26 September 1997 over Bay of Bengal, which has developed close to the Andhra coast (within 1° from coastline) at 15°N, 84°E and moved parallel to the east coast of India has been examined briefly, using NCEP u, v fields. Intense cyclonic active phases are associated with high positive vorticity ranging from $5*10^{-5}$ s^{-1} to $7*10^{-5}$ s^{-1} at 850 hPa & 700 hPa and $4*10^{-5}$ s^{-1} to $6*10^{-5}$ s^{-1}at 500 hPa during 23-26 September 1997. Similarly divergence has varied from $-2*10^{-6}$ s^{-1} to -8*10-6 s^{-1} for 850 hPa, $4*10^{-6}$ s^{-1} to $-7*10^{-6}$ s^{-1} for 700 hPa and $3*10^{-6}$ s^{-1} to $-8*10^{-6}$ s^{-1} for 500 hPa during 23-26 September 1997. Cloudy areas are associated with positive vorticity, implies upward motion, cloud free areas are associated with negative vorticity and positive divergence imply downward motion, low level horizontal advection. High rainfall 40 cm has been recorded at Kakinada when the system has come close to the coast on 24th September 1997. Other stations rainfall varies between 12-21 cm. The NCEP (National Centres for Environmental Prediction), reanalysis wind data can be used to understand the vorticity and divergence at different levels which can be useful to the forecaster for the decision making process, for better weather forecasting.

Acknowledgements

The authors wish to thank the Director IITM Pune, for his keen interest and support during the course of this study. We acknowledge India Meteorological Department for making available the IDWR (Indian daily weather reports), Report on Cyclonic disturbances over the north Indian ocean during 1997, and NCEP/NCAR for providing the reanalysis wind data at their web site. We also wish to acknowledge Mr. A.R.Dhakate, IITM Pune, for his help during the preparation of the paper.

References

Riehl.H, (1948). "On the formation of west Atlantic hurricanes." Dept. Meteor. Univ. Chicago, Misc Rep No.24, Part I.

Report on cyclonic disturbances over north Indian ocean during 1997: RSMC- Tropical cyclones , India Meteorological Department , New Delhi, January 1998.

Koteshwaram, P. and George C.A. (1958), "On the formation of Monsoon Depressions in the Bay of Bengal." Indian J. Met., Geophys., 9,9-22

Koteshwaram, P, (1960). "Symposium on Monsoon of the world." held at New Delhi, 1958, India Met. Dep., 105-110.

George C.A., (1970). "Interaction between lower and upper troposphères during the southwest monsoon season over India." Indian J, Met., Geophys., 21, 401-414.

Sarker.R.P and A.Chowdary, (1988) "A diagnostic description of monsoon depression." Mausam, 39,9-18.

Pettersen ,S., (1956). " Weather Analysis and forecasting." second edition,1,34

.Sajnani P.P., (1968) "Use of observed winds for computation of Divergence and Vorticity over India." VI 45-52, Proceedings of WMO/IUGG Symposium on Numerical Weather Prediction , Tokyo, Nov. 26- Dec. 1968.

Ranjit Singh., (1984) "On the presence of upper air divergence in relation to pre-monsoon and monsoon weather systems of Monex period 1979." Mausam ,35,4,507-514

Sikka D.R.and Gadgil S., (1978) "Large scale rainfall over India during the summer monsoon and its relation to lower and upper tropospheric vorticity." Indian J, met, Hydrol. Geophys 1&2, 219-231.

Chhabra, B.M, Singh, B.V., Dayal V and Arya A.D., (1982) "Vorticity Patterns vis-à-vis rainfall distribution during July 1979" , Mausam , ,33,4,477-480

Warner C., (1984) "Core structure of the Bay Bengal Monsoon depression" Monthly Weather Review, 112, 137-152.

Dvoark V.F. (1977) "The use of satellite imagery in Tropical cyclone analysis". WMO Technical note No. 153.

Disaster Management
Editors: N.C. Mahanti et al.

Changes in Temperature and Precipitation Over Different Regions of India

S.K. Dash, R.K. Jenamani*, S.R. Kalsi* and S.K. Panda

Centre for Atmospheric Sciences, Indian Institute of Technology, Delhi, Hauz Khas, New Delhi-110 016, India
*India Meteorological Department, Mausam Bhavan, Lodi Road, New Delhi-110 003, India

Abstract

The study of climate changes in India warrants top priority specially when it is known that poor people are very vulnerable to climate changes. The most important meteorological parameters affecting us are the temperature and rainfall. Results of this comprehensive study based on observed data and reanalysis indicate that in the last century, the atmospheric surface temperature in India has enhanced by about 1°C during winter and post-monsoon months. Also decrease in the minimum temperature during summer monsoon and its increase during post monsoon months has created a large seasonal temperature gradient of about 0.6°C which may affect the circulation pattern and associated rainfall. Distinct opposite phases of increase and decrease in the minimum temperatures in the southern and northern regions of India respectively have been noticed. The sea surface temperatures of Arabian Sea and Bay of Bengal also show increasing trend. Also extreme temperature events have increased in the east coast of India in the recent past. Rainfall pattern during different seasons indicate small increase during winter months of January and February, pre-monsoon months of March, April and May and post-monsoon months of October, November and December. In contract the summer monsoon rainfall in the months of June to September shows small decreasing trend.

Introduction

India mainly experiences four types of climate (Oliver and Wilson, 1987). The climate of the whole of peninsula is Tropical Savana and that of the West Coast is basically Tropical Rain Forest. On the other hand, the climate of the northern part of India is Warm with Dry winds and that of western India is Dry Steppe. During the four months from June to September, the southwest summer monsoon is predominant and during October to December, the northeast winter monsoon controls the weather of the country in general. Even during the same month or season, different parts of the country experience different ranges of temperature and rainfall. In winter months of January and February, while the northern part of India shivers with sub zero or nearly zero temperatures, the coastal regions to the south are warm and comfortable. Also during April, May and June when the people of Andhra Pradesh and Orissa suffer from scorching heat, those in Simla and Mussourie enjoy the cool climate. In summer monsoon months, while in most of the northeastern states and coastal regions there may be heavy rainfall and flood, Rajstan in the west may be dry.

The most important climatic events affecting India are heat waves, cold waves and fog, snowfall, floods and droughts, monsoon depressions and cyclones. Peoples' perception is in favour of changes in the occurrence of these weather phenomena. It is very essential to examine the observed data very carefully in order to categorize those as scientific evidences. In the past, many studies have been conducted by the meteorologists (Srivastava et al., 1992; De, 2001; Rupa Kumar et al., 2002; Dash, 2003; Rao et al., 2004) using the observed data as well as model results. Nevertheless, it is essential to identify changes observed in the most important meteorological parameters such as temperature and precipitation in India in the recent years which may eventually be useful for model verifications. For generating future climate scenarios, it is essential to verify those based on the changes occurring in the spatial as well as temporal variations. It is also important to examine the changes in the characteristics of temperature and rainfall over different regions of India during winter, pre-monsoon, monsoon and post-monsoon months. These regional and seasonal trends may be used to verify climate model outputs.

Results based on observed data

Based on past data, it may be inferred that the average surface air temperatures over the Indian subcontinent shows a slight warming trend by 0.2° to 0.4°C per 100 years (Attri, 2003; Rupa Kumar et al., 2002; Srivastava et al., 1992) in the mean annual temperature. Past results, in general, indicate warming during the post-monsoon (October–December) and winter (January – February) and no change in the temperatures during the monsoon season (June – September). Maximum temperatures show positive trends over most parts of the country except the north-west region where the trends are non-significant. Minimum temperatures show very little trend over most regions of the country except the north-west region. There are some differences in results obtained by different researchers because of variations in the length of data record and regions considered. (Rao et al., 2004) examined the effect of urbanization on the meteorological parameters at fifteen Indian cities and found that radiation values, bright sunshine hours, wind speeds and total cloud amounts have a decreasing tendency during the last forty to fifty years whereas relative humidity and rainfall amounts show increasing tendency.

Figures 1 (a) and (b) show the annual temperature anomalies in the maximum and minimum temperatures averaged over India during the last century based on National Oceanic and Atmospheric Administration (NOAA) satellite data (http://lwf.ncdc.noaa.gov/oa/climate/online/doe/doe.htm). The trend lines indicate that the annual maximum temperature has increased by about 0.6°C (Figure 1a). The annual minimum temperature over India does not show any appreciable (Figure 1b) enhancement.

In order to examine the temperature trend over India during different seasons, in this study, the entire year has been divided into four seasons namely, winter (January and February), pre-monsoon (March to May), monsoon (June to September) and post-monsoon (October to December). The time series of maximum and minimum temperatures over India during these four seasons in the last century have been shown in Figures 2 (a) to (d). Figure 2 (a) shows an increase of 0.8°C and 0.4°C in the maximum temperature during winter and pre-monsoon months respectively. Similar increase during monsoon and post-monsoon (Figure 2 b) are about 0.3°C and 0.8°C respectively. On the other hand, the minimum temperatures during winter and pre-monsoon months have negligible changes (Figure 2 c) in the last century. Figure 2 (d) shows decrease in the minimum temperature during summer monsoon months by about 0.2°C and increase of about 0.4°C during post monsoon months of October, November and December.

The impact of climate change may not be same everywhere. Hence India has been divided into six zones such as north west, north central, north east, interior peninsula, east coast and west coast in order to examine the changes in maximum and minimum temperatures over these regions. Figure 3 (a) indicates that the maximum temperature has been increasing during the last century over all the regions of India. However, the increase is not same everywhere. West coast shows maximum increase in the maximum temperature by about 1.1°C. Next to west coast, the maximum temperature has increase of 1°C in north east, 0.7°C in north central, 0.55°C in east coast, 0.45°C in north west and the least amount of 0.2°C in the interior peninsula. Similarly, Figure 3 (b) shows the changes in the minimum temperature over the six regions of India in the last century. Unlike the maximum temperature, there are no trends of increase of minimum temperature all over the century. India has two opposite phases of increase and decrease in the minimum temperature. Interior peninsula along with adjacent east and west coasts indicate increase in the minimum temperature, whereas region to the north consisting of north west, north central and north east indicate decrease in the minimum temperature in the last century. The increase is maximum in the interior peninsula with warming of 0.5°C and the decrease is maximum in the north west with cooling of 0.4°C.

Since the east and west coasts of India showed rise in temperature during the last century, it is logical to examine the sea surface temperature (SST) of the Arabian Sea and the Bay of Bengal. SST data available from National Centers for Environmental Predictions (NCEP)/ National Center for Atmospheric Research (NCAR) reanalyzed data set have been examined over the northern (12.4 to 25.7°N and 63.8 to 73.1°E) and southern (4.8 to 12.8 °N and 63.8 to 75 °E) Arabian Sea and northern (18.1 to 21.9 °N and 84.4 to 91.9 °E) and southern (4.8 to 18.1 °N and 78.8 to 90 °E) Bay of Bengal and the time series have been depicted in Figures 4(a) and (b) respectively.

Figure 4(a) shows that during the last 50 years, northern and southern sectors of the Arabian Sea have experienced rise in SST by 0.4°C and 0.8°C respectively. Similarly Figure 4(b) depicts rise of SST over northern and southern sectors of the Bay of Bengal by 0.3°C and 0.8°C respectively.

From the global warming point of view, the examination of the temperature trend only may not indicate the severity of the situation. People are usually concerned with the excesses in heating and cooling. It is essential to examine such extreme heating/cooling events in detail. The heat waves in Orissa in the year 1998 and subsequently in Andhra Pradesh in 2003 and their impacts on loss of life and property are best examples of negative impacts of climate change. Based on the maximum temperature recorded by India Meteorological Department (IMD) at different observatories all over the country, it is found that during the heat wave period from 19 May 2003 up to 10 June 2003, the highest maximum temperature in the country was confined to 7 stations in the Andhra Pradesh and Orissa. During this heat wave period of 23 days, the highest maximum temperature varied between 45°C to 50°C. The maximum temperature at stations Ongole, Hanumankunda, Machillipatnam and Ganaveram were 47, 48, 48.2 and 49°C respectively against their respective climatological highest in the last 100 years values of 46.7, 46.7, 47.8 and 48°C respectively.

Figures 5 (a) and (b) depict the time series of Indian rainfall during the four seasons mentioned in Section 2. Figure 5(a) shows small increase in the rainfall during winter months of January and February and pre-monsoon months of March, April and May. Summer monsoon rainfall in the months June to September indicates little decreasing trend in the monsoon season (Figure 5 b). The same figure also indicates little increasing trend in rainfall during the post-monsoon season. Some increasing trend in winter and pre-monsoon rainfall needs further examination.

Conclusions

Results of this comprehensive study show that in the last century, during winter and post-monsoon months the maximum temperatures at the surface indicate rise by about 0.8°C. During post-monsoon months the minimum temperature has gone up by about 0.4°C, whereas there is decrease in the minimum temperature during summer monsoon months by about 0.2°C. The decrease in the minimum temperature during summer monsoon and its increase during post monsoon months create a large seasonal temperature gradient of about 0.6°C which may affect the circulation pattern and associated rainfall.

Detailed analysis of observed data clearly indicated that the maximum temperature has been increasing during the last century over all the regions of India. However, the increase is not uniform. West coast shows maximum increase in the maximum temperature by about 1.1°C. Next to west coast, the maximum temperature has increase of 1°C in north east, 0.7°C in north central, 0.55°C in east coast, 0.45°C in north west and the least amount of 0.2°C in the interior peninsula. Similarly, the changes in the minimum temperature over the six regions of India in the last century. Unlike the maximum temperature, there is no trends of increase of minimum temperature all over the century. India has two opposite phases of increase and decrease in the minimum temperature. Interior peninsula along with adjacent east and west coasts indicate increase in the minimum temperature, whereas region to the north consisting of north west, north central and north east indicate decrease in the minimum temperature in the last century. The increase is maximum in the interior peninsula with warming of 0.5°C and the decrease is maximum in the north west with cooling of 0.4°C. The sea surface temperatures of the Arabian Sea and Bay of Bengal also show increasing trend.

Extreme temperature events have increased in the recent past. During the heat wave period from 19 May up to 10 June 2003, the highest maximum temperature varied between 45°C to 50°C. The maximum temperature at four stations in the east coast attained the highest values ever observed in the last 100 years.

Rainfall pattern during different seasons indicate small increase during winter months of January and February, pre-monsoon months of March, April and May and post-monsoon months of October, November and December. In contract summer monsoon rainfall shows small decreasing trend.

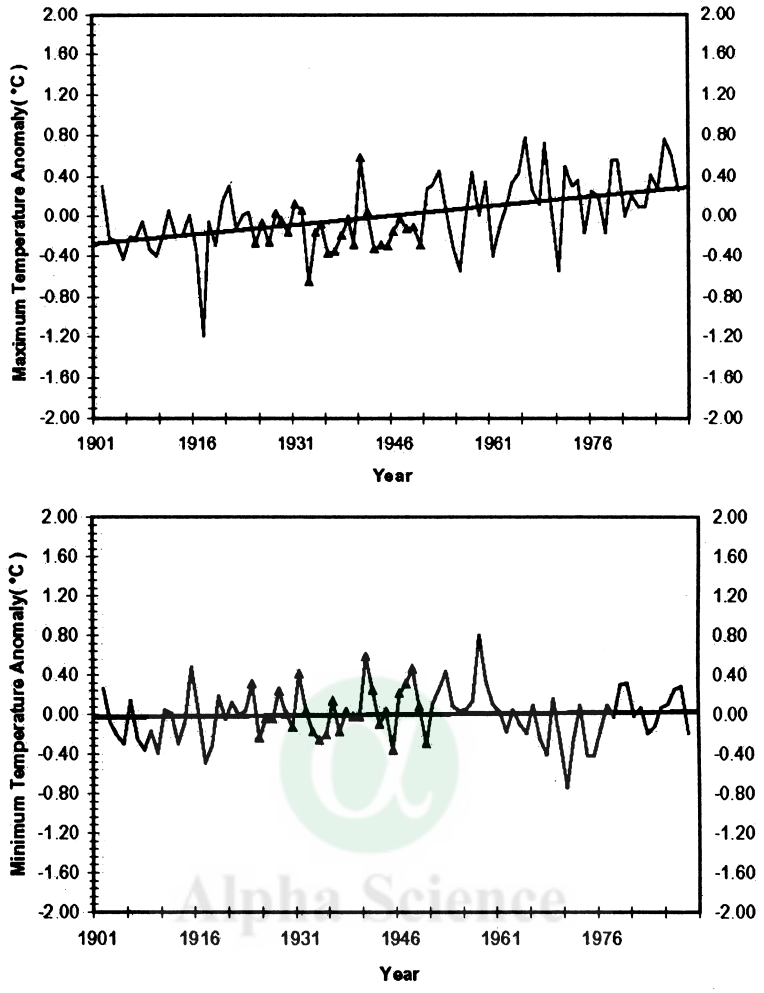

Figure 1 Time series of annual temperature anomalies (°C) over India (a) maximum (b) minimum.

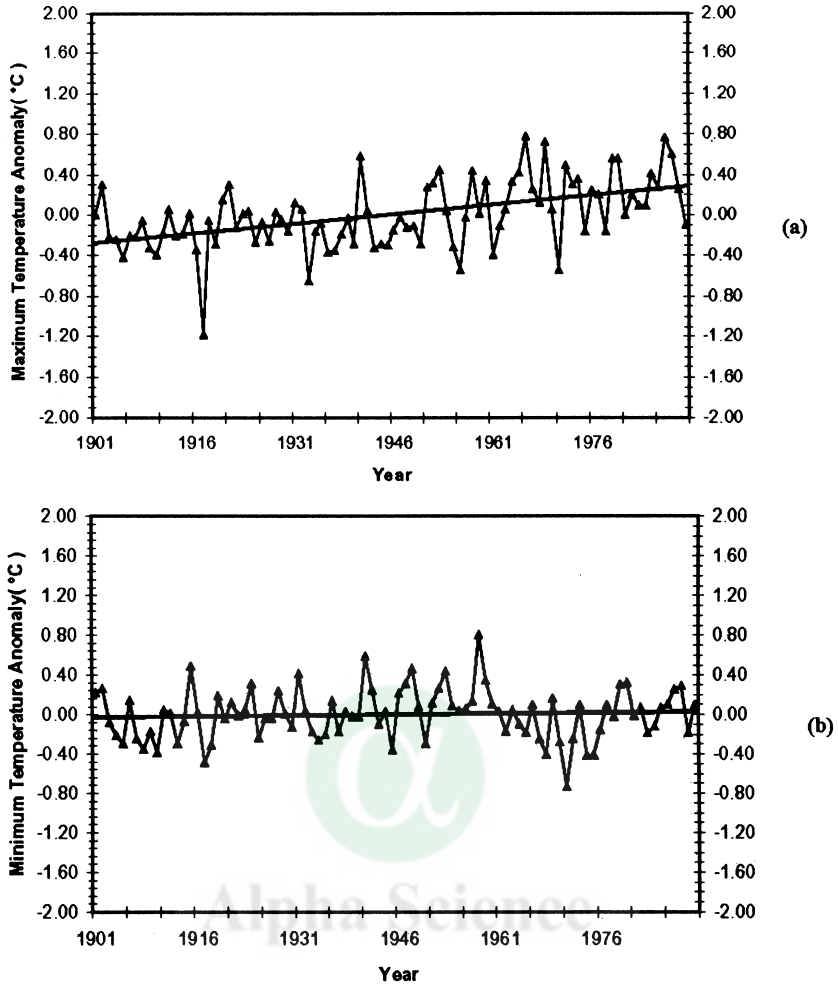

Figure 1 Time series of annual temperature anomalies (°C) over India (a) maximum (b) minimum.

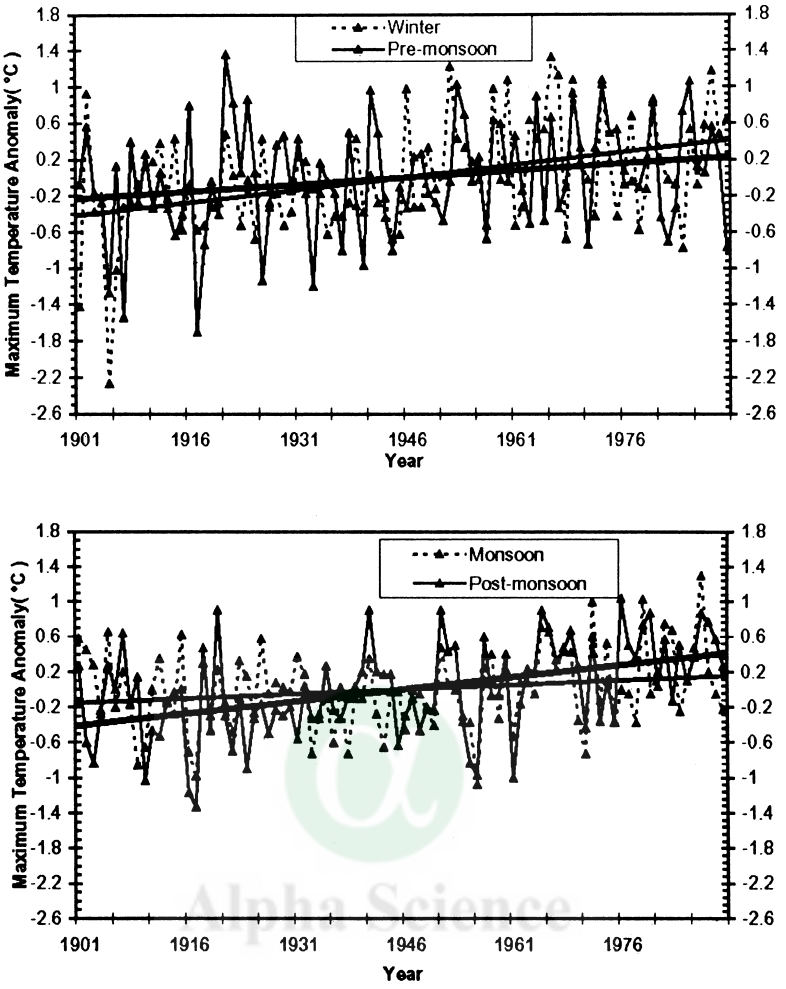

Figure 2 (a) and (b): Time series of anomalies in the maximum temperatures during (a) winter and pre-monsoon and (b) monsoon and post-monsoon months.

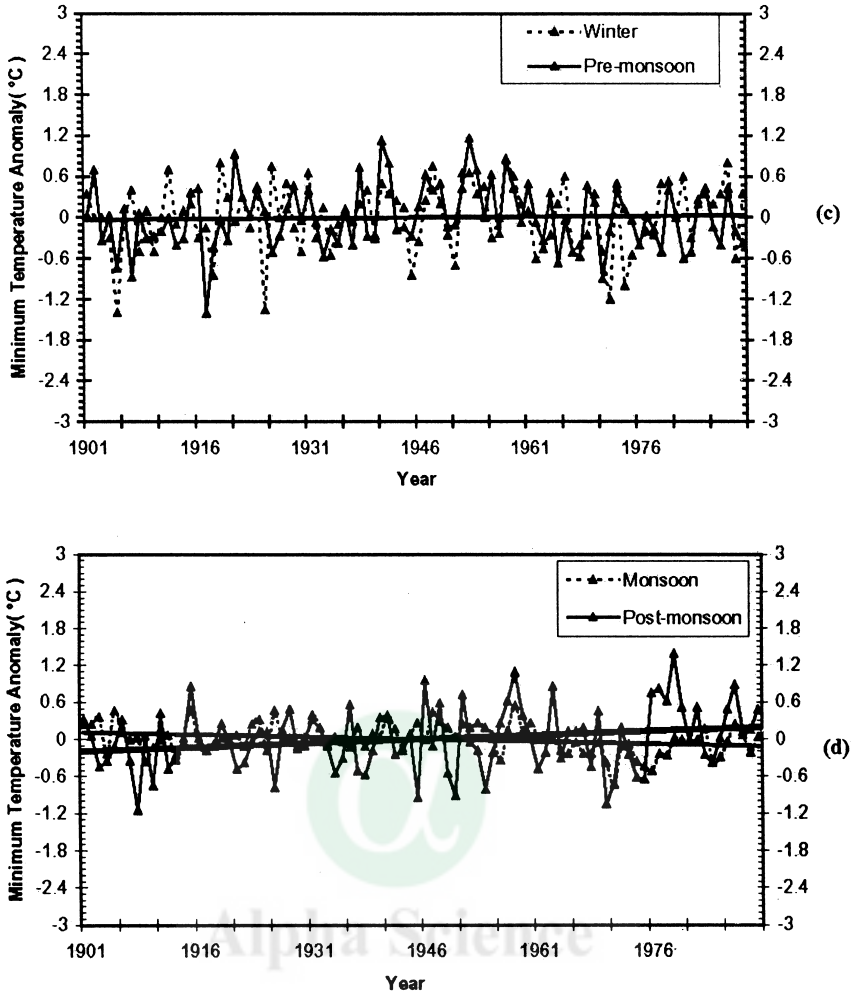

Figure 2 (c) & (d): Same as Figures 2 (a) & (b) except form minimum temperatures.

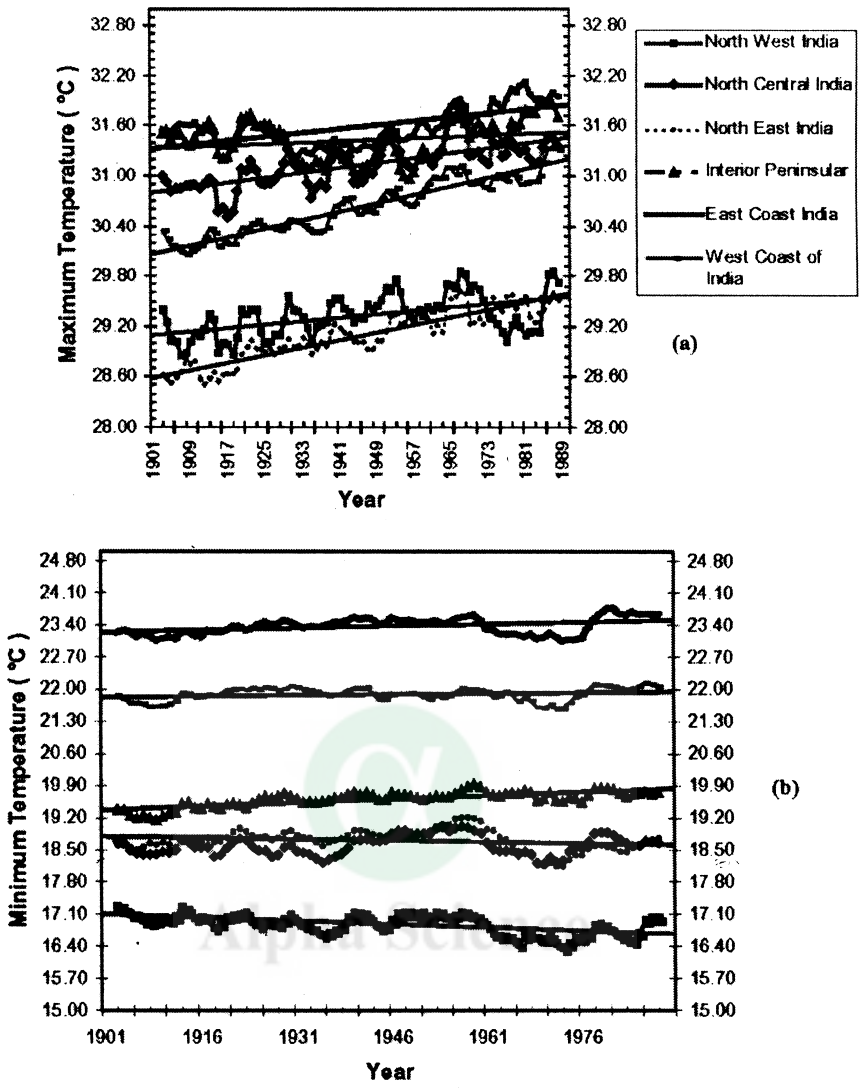

Figure 3 Time series of maximum (a) and minimum (b) temperatures (°C) over six homogeneous regions of India.

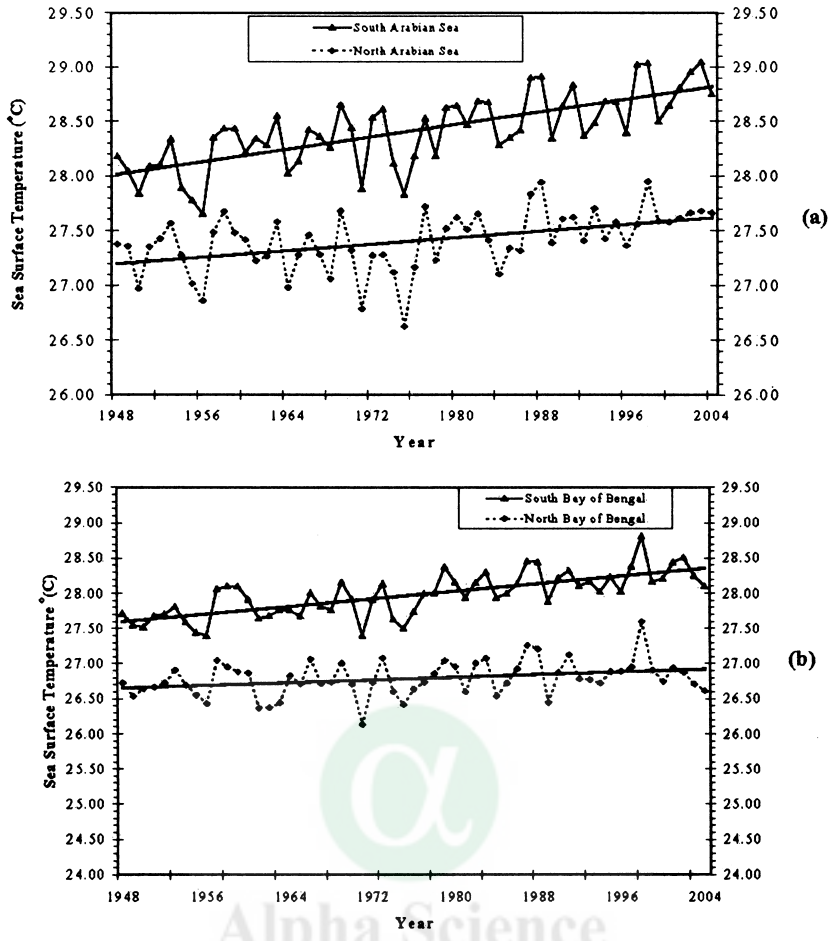

Figure 4 Time series of Sea Surface Temperature (°C) of (a) Arabian Sea and (b) Bay of Bengal.

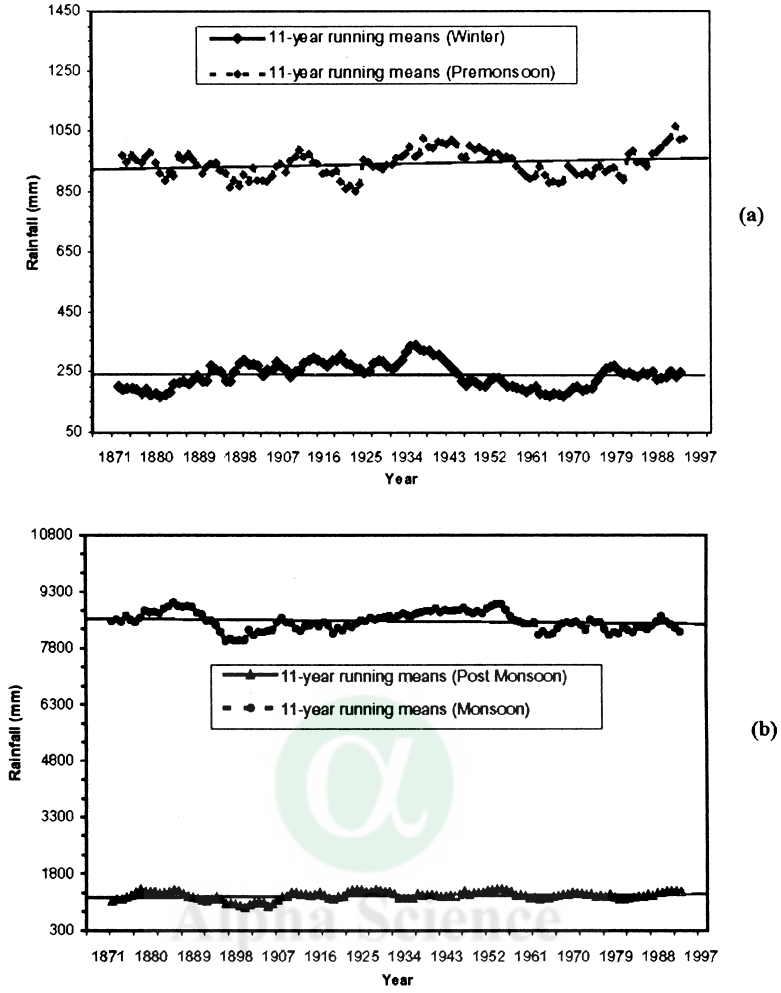

Figure 5 Time series of rainfall in India during (a) winter months of January and February & pre-monsoon months of March, April and May (b) monsoon months of June, July, August and September & post-monsoon months of October, November and December.

Acknowledgements

Data used in this study have been obtained from the archive of India Meteorological Department, NOAA and NCEP/NCAR reanalysis.

References

Attri, S. D.: 2003, 'Status of Climate Change in India' in S. K. Dash and Prakash Rao (eds.), *Assesment of Climate Change in India and Mitigation Policies*, WWF-India, New Delhi, pp. 10-17.

Dash, S. K.: 2003, 'Summary of the Meetings', in S. K. Dash and Prakash Rao (eds.), *Assesment of Climate Change in India and Mitigation Policies,* WWF-India, New Delhi, pp. vii-xii.

De, U. S.: 2001, 'Climate change impact: Regional scenario'. *Mausam*, 52(1), 201-12.

Rao Prakasa, G. S., Jaswal, A. K. and Kumar, M. S.: 2004, 'Effects of urbanization on meteorological parameters'. *Mausam*, 55(3), 429-440.

Rupa Kumar, K., Krishna Kumar, K., Ashrit, R. G., Patwardhan, S. K. and Pant, G. B. 2002, 'Climate Change in India : Observations and model projections', in P. R. Shukla, S. K. Sharma and P. V. Ramana (eds.), *Climate change and India : Issues, Concerns and Opportunities*, Tata McGraw-Hill Publishing Company Limited, New Delhi.

Srivastava, H. N., Dewan, B. N., Dikshit, S. K., Prakash Rao, G. S., Singh, S. S. and Rao, K. R.: 1992, 'Decadal trends in climate over India'. *Mausam,* 43 (1), 7-20.

Oliver, J. E. and Wilson, L.: 1987, 'Climate classification', in J. E. Oliver and R. W Fairbridge (eds), *The Encyclopedia of Climatology,* Van Nostrand Reinhold Company, New Work, pp. 221-236.